THE AUTOMATION OF RESONANT THERMOMETER PROBE MEASUREMENTS

by

ALI ASGHAR FATHIMANI

Submitted for the Degree of Doctor of Philosophy

at

The University of Aston in Birmingham

April 1976

ACKNOWLEDGEMENTS

I wish to thank my project supervisor, Dr. J. F. W. Bell, Reader, for the guidance, fruitful discussions and encouragement throughout the course of the work.

Thanks are also due to the workshop staff and departmental technicians who provided invaluable help and assistance, particularly to Mr. B. Hale, Mr. E. Clenton, Mr. W. Harper and Mr. A. Palmer.

I am indebted to the Tehran University, Institute of Nuclear Science and Technology, for the financial support during the research course. Finally, I gratefully acknowledge the research grant of the Ministry of Science and Higher Education of the Government of Iran for providing funds to travel to the United Kingdom.

CONTENTS

SUMMARY

An ultrasonic thermometer has been developed for high temperature measurement over a wide temperature range. It is particularly suitable for use in measuring nuclear fuel rod centerline temperatures in advanced liquid metal and high flux nuclear reactors.

The thermometer which was designed to determine fuel temperature up to the fuel melting point, utilizes the temperature dependence of the ultrasonic propagation velocity (related to the elastic modulus) in a thin rod sensor as the temperature transducing mechanism.

A pulse excitation technique has been used, where the mechanical resonator at the remote end of the acoustic line is made to vibrate. Its natural frequency is proportional to the ultrasonic velocity in the material. This is measured by the electronic instrumentation and enables a frequency-temperature or period-temperature calibration to be obtained.

A completely digital automatic instrument has been designed, constructed and tested to track the resonance frequency of the temperature sensors. It operates smoothly over a frequency range of about 30%, more than the maximum working range of most probe materials.

The control uses the basic property of a resonator that the stored energy decays exponentially at the natural frequency of the resonator. The operation of the electronic system is based on a digital multichannel transmitter that is capable of operating with a predefined number of cycles in the burst. This overcomes a basic defect in the previous design where the analogue time-delayed circuits failed to hold

synchronization and hence automatic control could be lost.

Development of a particular type of temperature probe, that is small enough to fit into a standard 2 mm reactor tube has made the ultrasonic thermometer a practicable device for measuring fuel temperature. The bulkiness of previous probes has been overcome, the new design consists of a tuning fork, integral with a 1½ mm line, while maintaining a frequency of no more than 100 kHz.

A magnetostrictive rod, acoustically matched to the probe is used to launch and receive the acoustic oscillations. This requires a magnetic bias and the previously used bulky magnets have been replaced by a direct current coil. The probe is supported by terminating the launcher with a short heavy isolating rod which can be secured to the reactor structure. This support, the bias and launching coil and the launcher are made up into a single compact unit.

On the material side an extensive study of a wide range of refractory materials identified molybdenum, iridium, rhenium and tungsten as satisfactory for a number of applications but mostly exhibiting to some degree a calibration drift with thermal cycling. When attention was directed to ceramic materials, Sapphire (single crystal alumina) was found to have numerous advantages, particularly in respect of stability of calibration which remained with $\pm 2^{\circ}C$ after many cycles to $1800^{\circ}C$.

Tungsten and thoriated tungsten (W - 2% ThO_2) were also found to be quite satisfactory to $1600^{\circ}C$, the specification for a Euratom application.

CHAPTER 1

INTRODUCTION

1.1 GENERAL

The concept of temperature has been developed to characterize systems in thermal equilibrium.[1]

When two thermodynamic systems being separated from each other by a dia-thermic wall and isolated from their environment they are said to be in thermal equilibrium and therefore they have the same temperature. A thermometer will therefore read the temperature of its surroundings if this equilibrium is established between the thermometer material and its environment. In another useful definition, temperature can be represented as an intensity factor associated with thermal energy. This plays a central role in the growth of science and technology[2].

The importance of high temperature operation was well established when the science of thermodynamics and particularly the second law or entropy was developed. In the Carnot cycle it was simply shown that the efficiency of a reversible heat engine depends only on the temperature of the two reservoirs between which the engine is operating. It can be shown that the efficiency of a power generator increases with increase in temperature. The more precisely the temperature can be measured, the closer a power generator can be operated to its maximum safe temperature.

Since the limit of high temperature has been increased by development in modern technology, the term "high temperature" became rather arbitrary[3]. Today the temperature range between 700 to 900^{o}C is regarded as quite low, between

900 and 1300°C is intermediate, and above 1300°C is regarded as high.

The temperature limits which apply to high temperature technology are the highest temperature at which some states of matter exist or at which some phenomena reach to their fullest extent, therefore the melting, vaporization, chemical dissociation, and ionization of substances limits the high temperature technology.

The employment of high temperature is involve with enormous number of activities such as material processing, operation, and production. For example petroleum refinement and gas turbines require 1000°C, nuclear reactors operate to 2200°C and refractory carbides require 3300°C.

To extract maximum benefit from above processes and operations, the accurate measurement of temperature is of the utmost importance. Indeed, the primary source of error for measurement of material properties in the 2000 to 3000°C temperature range is almost exclusively the lack of accuracy in temperature measurements.

1.2 TECHNIQUES AND METHODS FOR HIGH TEMPERATURE MEASUREMENT

The number of techniques which have been employed to measure the temperature over 1000°C are few and of these not even all are suitable for measurement of thermophysical properties of materials.

Reviewing the relevant literature very briefly, shows that in the majority of all such measurements, thermocouples or monochromatic optical pyrometry have been used[4]. In nuclear reactors optical methods are automatically excluded and thermocouples suffer various degrees of decalibration

due to radiation damage.

Recently some other new methods and techniques have been established for operation of high temperature measurement. These are suitable for material properties measurement and in particular have been developed on a large scale for the purpose of nuclear reactor fuel rod temperature measurements. Of the new types of thermometer which appear to offer good solutions for nuclear temperature measurement are the ultrasonic thermometer[5] and the Johnson noise thermometer[6,7]. Here an attempt is made to identify typical errors which may occur with each method.

1.2.1 THERMOCOUPLE THERMOMETRY

While a large combination of metals,non-metals, alloys and semiconductors are available only a very few form a practicable thermocouple sensor[8]. Factors governing the choice of thermocouples include calibration characteristics, temperature range of use, diameter of wires and insulator. For a particular case melting point, effect of environment on thermoelectric and mechanical properties, chemical properties, specific heat, density, thermal conductivity, thermal coefficient of expansion, emissivity (spectral and total of bright and oxidized surfaces), electrical resistivity temperature coefficient of resistance, and magnetic properties must all be considered. From the commercial point of view a thermocouple must satisfy requirements such as physical and chemical stability in the working medium, high thermoelectric force (with a reasonably linear dependence on the temperature), reproducibility of working parameters, high mechanical stability and simplicity of production.

Thermocouples can be classified in four major groups[4,8,9].

Group A : Noble metals thermocouples

Group B : Base metals thermocouples

Group C : Refractory metals thermocouples

Group D : Carbon and Carbide thermocouples

Group A:

1-Platinum-Rhodium types.

This type has a wide useful temperature range (up to 1900°C depending upon the alloy combination) and is available commercially for many industrial purposes. They can be used in oxidizing atmospheres but not in reducing conditions. This type of thermocouple after an extended use at high temperature, undergoes grain growth and alloy diffusion at the junction. Wires become brittle and decalibration occurs[10, 11, 12].

The need to minimize grain growth and increase temperature limit and stability, led to substitution of another Pt-Rh alloy for pure platinum leg. All Pt-Rh thermocouples must be annealed before they can produce high accuracy. Typical examples of this type thermocouples are:

Positive Wire	Negative Wire	MP Limit
Pt 10Rh	Pt	1770°C
Pt 13Rh	Pt	1770°C
Pt 13Rh	Pt 1Rh	1790°C
Pt 20Rh	Pt 5Rh	1820°C
Pt 30Rh	Pt 6Rh	1830°C
Pt 40Rh	Pt 10Rh	1880°C
Pt 40Rh	Pt 20Rh	1900°C

2-Platinum - Iridium type. For higher temperature.

The typical example of this type is as follows:

Positive Wire		Negative Wire	MP Limit
Ir	60Rh	Ir	about
Ir	50Rh	Ir	}
Ir	40Rh	Ir	2000°C
Pt	50Ir	Pd	1540°C
Pt	15Ir	Pd	1540°C

A particular thermocouple of this type which was developed as a replacement for Chromel-Alumel in jet engines is Platinel. It has an excellent stability at 1300°C in air

Positive Wire is 3AU-83Pd-14Pt

Negative Wire is 65AU-35Pd

Group B: base metal thermocouples.

This group of thermocouples are limited to those made of metals and alloys whose useful temperature range is considered to be between -190 to 1260°C. They can operate in oxidizing and neutral medium with a very reasonable accuracy but they cannot be used in some atmospheres, such as hydrogen, carbon monoxide, hydrogen sulphide, sulphur dioxide, and other reducing gases even for short periods of time[8]. The most popular thermocouples of this group are, chromel-alumel, iron-constantan, iron-advance, iron copnic, iron-cupron, copper-constantan.

The best solution for thermocouples operating to 1200°C is the chromel-alumel combination with mineral insulation (magnesia) in special steel sheaths. The 1 mm overall version was developed by A.E.A. over a period of 10 years and has a reliability acceptable to safety regulations.

Group C: Refractory metal thermocouples.

The vast amount of effort that has been spent on the

observation of the refractory materials is a direct result of the higher temperatures encountered in the jet, missile and reactor technology[4,8]. The principal materials under this investigation are the so-called refactory materials which are: tungsten m.p. 3420°C, molybdenum m.p. 2620°C, rhenium m.p. 3180°C, tantalum m.p. 2997°C, niobium m.p. 2468°C and iridium m.p. 2454°C.

As tungsten-rhenium thermoelements have potentially acceptable characteristics, the majority of the thermocouples proposed for use at the extremely high temperature are tungsten-rhenium combinations. With neutron irradiation rhenium disintegrates to osmium. In an attempt to overcome this effect tungsten-rhenium alloys for both thermocouple legs have been used. This increases the useful life of the thermocouple but severe decalibration always occurs ultimately [13,14,15, 6].

Extreme care must be taken to select compatible materials and environment for the application of refractory thermocouples. The chemical properties of tungsten and molybdenum prohibit their use in an oxidizing atmosphere and if measurements are to be made under these conditions, protection is of over-riding importance. No degradation of W-Re thermocouples occur in atmospheres of argon, hydrogen, nitrogen and helium even at the highest temperatures, but all react with carbon, oxygen and nitrogen above about 1000°C.

Of the many sources of contaminations, backstreaming of hydrocarbons from pumping systems can occur, causing the formation of tungsten carbide. It is of interest that the helium coolant in the Dragon reactor has an addition of hydrogen to "mop up" these residues.

The most frequently used W-Re thermocouples are:

W	Re
W	W 20 Re
W	W 26 Re
W 3 Re	W 25 Re
W 5 Re	W 26 Re
W 3 Re	W 26 Re
Mo	Re

Group D: Carbon and carbide thermocouples.

Thermocouples of this kind are not widely used in industry and their usefulness has been limited by the bulkiness, fragility and questionable reproducibility. The only point about this type is that they give a fast response[8].

Various types of carbon and carbide thermocouples are listed here:

Thermocouple	Max. Temperature
W/Gr	2400°C
C/NI	1250°C
C/Gr	2400°C
Gr/Gr	2500°C
BGr/Gr	2600°C
B4C/C	2400°C
Gr/SiC	2700°C
Gr/MOC	1050°C
Gr/WC	850°C

1.2.2 RESISTANCE THERMOMETER

In this type of thermometer a platinum resistance wire is used to measure an unknown temperature by determination of

the ratio of its resistance at the unknown temperature to that at the ice point.[1] This thermometer under 1000°C has greater precision than any other thermometer but as the temperature increases the normal type platinum resistance becomes more unstable and above 1000°C has been less reliable than a Pt-PtRh thermocouple.

1.2.3 OPTICAL PYROMETER

When the high temperature region to be measured is visible optical pyrometry is pre-eminent. Operation of optical pyrometers is based on the determination of the brightness temperature of an object through visual comparison of the spectral brightness of the object and the pyrometer lamp. To measure a temperature, the spectral emissivity of the source at the mean effective wavelength of the pyrometer must be known.

For accurate optical pyrometry, a black body should be built into the apparatus, because the accurate spectral emissivity as a function of temperature and surface condition are not available for many substances. Therefore from this method and using proper calibrated pyrometer, temperature can be obtained to about 4 degrees at the gold point 1063°C, 6 degrees at 2000°C and 40 degrees at 4000°C. Only by precise measurement of the current in the pyrometer lamp, these uncertainties can be reduced by a factor of about two.

The temperature measured by pyrometers may be in error because of the use of glass in peep-holes and because of the presence of vapours and gaseous reaction products.

The most common pyrometers are of the disappearing -

filament type and monochromatic hot body brightness. Optical pyrometers are simple and easy to use and special micro-optical pyrometers have been designed for measurement in the case of very small items. There are considerable technological problems in the automation of optical pyrometry and although these difficulties could be overcome by sufficient development effort, in the nature of high temperature systems direct observation is normally impossible.

1.2.4 NOISE THERMOMETER

Noise thermometry is based on application of the Nyquist's theorem in general thermodynamics. According to this theorem, the mean square fluctuation in voltage (arising from thermal agitation) developed across the terminals of an arbitrary passive network is expressed as

$$\bar{V}^2 = 4kTR\Delta f$$

where V is the noise voltage, Δf frequency band, R value of resistance, T absolute temperature and k is the Boltzmann constant[7].

In practice for accurate measurement of temperature the noise voltage of two resistors, one at the unknown temperature, the other at room temperature are compared and processed in a complicated electronic measuring circuit. The ratio of the resistance, where the noise voltage from both resistors are equal, determines the ratio of their absolute temperatures. The noise thermometer is independent of material from which it is made, therefore it can be applied where other measuring methods fail to give exact results. It is also independent of all environmental conditions like radiation or atmosphere

and all previous thermal and mechanical treatment, therefore appears being suitable for temperature measurement in nuclear reactor[6,16]. Technique of noise thermometry is under development and because of its independence of material properties, to a first order, is of considerable interest.

1.2.5 ULTRASONIC THERMOMETER

The ultrasonic thermometer is an alternative, to previous techniques and methods for high temperature technology in certain environmental conditions[17]. It utilizes the temperature dependence of the ultrasonic propagation velocity in a thin rod sensor while it is used as the temperature transducing mechanism[18]. It aimed at meeting present day user demands for reasonable accuracy, high reliability, a wide choice of materials, for a variety of environments and completely automatic operation with interfaces for computer use and data logging[19]. There are various ultrasonic techniques for measuring temperature.

1) Video pulse method or velocity measurement using "time of flight"[20,21].

2) Resonance method or frequency measurement, using continuous or pulse excitation.

For continuous excitation, two separate connecting channels to the resonator are needed,one introduces the exciting energy, the other connectsthe receiver to the resonator (the energy may be applied directly to the resonator, in which case one connection may be electrical). The chief drawback to continuous excitation is the poor sensitivity, the indication of resonance is the frequency of maximum amplitude of the

received signal[22].

With pulsed excitation, the indication of resonance is both characteristic and sharp, resulting in a good reading sensitivity. In resonance method of temperature measurement, there is no great limitation of material for the resonator or line other than that dictated by the environmental and physical properties arising from the maximum temperature requirement.

1.3 COMPARISON BETWEEN DIFFERENT TECHNIQUES OF HIGH TEMPERATURE MEASUREMENTS

Thermocouple offers some clear advantages in terms of physical simplicity, rapid time response and ease of measuring multiple temperatures (axial temperature gradients) but it is susceptible to errors from effects inherent to high temperatures such as insulator shunting and to cumulative effects of irradiation: transmutation, dislocation and metallurgical instabilities all of which combine to produce a sensitivity of output to temperature gradient along the thermocouple's length.

For the Johnson noise thermometry somewhat complicated measuring equipment is necessary. It also requires longer data acquisition time and may be greater in diameter than other sensors (in high temperature reactors instrumentation "holes" are standardised to 2 mm diameter). They appear to be free of transmutation and prompt radiation effects. Potential problems such as the long term effects of radiation - damaged sensor and cable insulator remain to be answered[6,16].

Ultrasonic thermometers can be made small in diameter and

requiring less removal of fuel from the centre than the other sensors. They are independent of axial flux and temperature gradients in lead wires, are free of insulator electrical problems and they can be made from a wide choice of materials. They are however, subject to mechanical damage to loss of signal due to attenuation at high temperature, and are sensitive to the effect of radiation on the elastic modulus and hence the velocity of sound in the sensor material.

The decalibration associated with damage to the material structure must be significant. However, at the high temperature used, above the recrystallisation point of sensor material, defects are mobile and annealing takes place. Work on the AERE (Harwell) Pluto reactor[17] showed that at about 1200°C negligible decalibration of molybdenum sensors occured. The ultrasonic thermometer properly used, is a most versatile, robust and widely applied temperature sensing element. They demonstrated a practical device for nuclear rod thermometry. Tasman and Schmidt[23] present a comparative study of different methods. Table 1.1 gives the merits and limitations of each method. Above 2000°C optical pyrometer appears still to be the best choice where the object is optically accessible and its emissivity is known. The noise thermometer fails above about 1500°C due to the difficulties of measuring electrical resistivity accurately enough at high temperatures. The gas thermometer is relatively bulky and presents severe mechanical problems. Thermocouples fail for mechanical and electrical reasons. In a nuclear environment (gamma radiation) optical pyrometry is impossible, but ultrasonic thermometry looks promising[24].

Table 1.1 Comparison of different methods of high-temperature thermometry (unfavourable conditions are indicated by black areas).

Error sources	Absolute methods			Secondary methods	
	Optical pyrometer	Noise therm.	Gas therm.	Thermo-couple	Ultrasonic therm.
Non black-body conditions					
Sensor contam-ination					
T-gradient in transm.-line					
Electrical leakage					
Mechanical instability					
Radiation damage					
Sensor γ-heating					
Nuclear trans-mutations					
Cost and complexity					

CHAPTER 2

ULTRASONIC TECHNIQUES FOR TEMPERATURE MEASUREMENTS

2.1 INTRODUCTION

Plane sound waves can be propagated at a number of velocities given by a wave equation of the form

$$\frac{\partial^2 U}{\partial x^2} = \frac{1}{C^2} \frac{\partial^2 U}{\partial t^2} \qquad (2.1)$$

where U is a potential function, C is the phase velocity and t is time. The velocity is highly dependent on the state of the matter (solid, liquid or gas), the type of wave (longitudinal or transverse displacements), and boundary conditions.

Sound wave velocity is determined by the stiffness and density of the medium and can be written in the functional form

$$C^2 = (\text{stiffness term/density term}).$$

Two types of sound waves could be used for this application:

First is a longitudinal wave in a thin rod or tube where the material diameter is much smaller than wave length. These waves, which are of the most promising for the work under investigation have a full radial contraction, the radial strain being less than the longitudinal strain by the Poisson's ratio σ. This is the condition for propagation at rod velocity where the appropriate modulus is E, Young's Modulus.

Second, is a torsional wave in a similar line which

is a pure shear stress, the partial motion being circumferential and the corresponding stiffness term is the shear stiffness Modulus G.

For longitudinal waves the velocity C_ℓ is related to the Young's Modulus E, and the density ρ by

$$C_\ell^2 = E/\rho \tag{2.2}$$

while for torsional waves the velocity C_t is related to the Rigidity Modulus G, and the density ρ by

$$C_t^2 = G/\rho \tag{2.3}$$

E, Young's Modulus is independent of Poisson's ratio (σ) but G is related to it by

$$G = E/2(1 + \sigma) \tag{2.4}$$

Torsional waves have the property that the energy is carried mainly near the outside of the rod while in longitudinal propagation it is spread uniformly throughout the area.

A consequence of this is the relatively higher loss which occurs at any contact for torsional waves. This feature is over riding and longitudinal propagation only is used in the instrument.

N.B. Extensional velocity could be in the three forms as following:

1) Rod Velocity $C_L^2 = E/\rho$ (2.5)

2) Plate Velocity $C_P^2 = \left(\frac{E}{1-\sigma^2}\right)/\rho$ (2.6)

3) Bulk Velocity $C_B^2 = \left(\frac{E}{3(1-2\sigma)}\right)/\rho$ (2.7)

2.2 TEMPERATURE DEPENDENCE OF ULTRASONIC RESONANCE FREQUENCIES

Ultrasonic thermometry is based upon the fact that the velocity of acoustic waves in solids depends upon temperature. The frequency of a mechanical resonator has a temperature coefficient arising from the coefficients of wave velocity and linear expansion of the resonator material.

In the most general case of a resonator Rayleigh's Principle of similitude leads to the equation

$$\frac{f.a}{C} = \text{Constant}$$

where f is the frequency, a is a dimension and C an appropriate velocity.

Consider a mechanical bar resonating in a longitudinal half wavelength mode. There will be a node (a region of no movement but maximum stress) at the centre and antinodes at the ends.

For resonance $\ell = \frac{\lambda}{2}$ and $f = \frac{C}{\lambda} = \frac{C}{2\ell}$ (2.8)

The variation with temperature θ, can be obtained by differentiating this equation.

$$\frac{1}{f}\frac{df}{d\theta} = \frac{1}{C}\frac{dC}{d\theta} - \frac{1}{\ell}\frac{d\ell}{d\theta} \qquad (2.9)$$

C is given by equation (2.2), hence the dependence of C on temperature is

$$\frac{1}{C}\frac{dC}{d\theta} = \frac{1}{2}\left(\frac{1}{E}\frac{dE}{d\theta} - \frac{1}{\rho}\frac{d\rho}{d\theta}\right) \qquad (2.10)$$

Substitution of

$$\frac{1}{\rho}\frac{d\rho}{d\theta} = -3\,\frac{1}{\ell}\frac{d\ell}{d\theta}$$

in equation (2.10) gives

$$\frac{1}{C}\frac{dC}{d\theta} = \frac{1}{2}\left(\frac{1}{E}\frac{dE}{d\theta} + 3\,\frac{1}{\ell}\frac{d\ell}{d\theta}\right) \qquad (2.11)$$

By replacement of the value of $\frac{1}{C}\frac{dC}{d\theta}$ from equation (2.11) into the equation (2.9) gives

$$\frac{1}{f}\frac{df}{d\theta} = \frac{1}{2}\left(\frac{1}{E}\frac{dE}{d\theta} + \frac{1}{\ell}\frac{d\ell}{d\theta}\right) \qquad (2.12)$$

or

$$\frac{1}{f}\frac{df}{d\theta} = \frac{1}{2}\left(\alpha_E + \alpha_\ell\right) \qquad (2.13)$$

where $\alpha_E = \frac{1}{E}\frac{dE}{d\theta}$ and $\alpha_\ell = \frac{1}{\ell}\frac{d\ell}{d\theta}$.

These conclusions could be drawn from equation (2.13). Any type of vibration can be used, the frequency coefficient is primarily a function of the material only. The choice of a particular mode is made on purely practical considerations.

In this work the fundamental "tuning fork" flexural resonance is used. Earlier designsused longitudinal resonance. These would have identical calibrations if the materials were identical.

In general, α_E is negative and α_ℓ is positive but the rate of change in the modulus is usually at least ten times as great as the thermal expansion, so for most materials acoustic velocities decrease as temperatures increase. In practice $\alpha_f = \frac{1}{f}\frac{df}{d\theta}$ is 500 ppm per kelvin for molybdenum at 1500^{o}C and 40 ppm per kelvin for alumina at the same temperature.

2.3 TECHNIQUES OF ULTRASONIC VELOCITY AND FREQUENCY MEASUREMENT

Various methods of ultrasonic velocity and frequency measurement have been reported by many investigators.

McSkimin [28] (1961) has classified most of these techniques for measurement of the elastic moduli, but only two methods have been widely used for temperature measurement.

First, those methods involving the propagation of pulses in the material, the velocity of propagation being timed directly. The second are those methods in which the specimen is excited in a resonance mode of vibration, the velocity of elastic waves in the material being determined indirectly by measurement of the resonance frequency. Here an attempt is made to discuss both methods briefly.

2.4 PULSE TECHNIQUES INVOLVING TIME-DELAY MEASUREMENT

Repetitive short ultrasonic pulses are introduced by coupling to a transducer, and after travelling across the specimen are detected by a receiver. The transmitted and detected pulses being displayed on the oscilloscope. The time interval between these, gives the velocity of transit, whilst the amplitude ratio gives a measure of the internal friction and scattering.

Maintaining a wide frequency band pass for the transducer, enables short pulses to be used.

To measure time of flight accurately, great care

must be taken with specimen preparation and crystal transducer surfaces which should be ground flat. The reflection effect at the transducer-specimen interface which causes pulse distortion and hence error in delay time measurement must be considered. Methods of pulse propagation in the case of highly dispersive materials such as polymers are not suitable.

Two wellknown methods for time of flight measurement, the Notched-Bar technique and the Shoulder-End or Thin Wire technique have been widely used in ultrasonic thermometry.

2.4.1 NOTCHED BAR TECHNIQUE

Essentially a burst of ultrasonics in the MHz region is used. Frederick[29] in 1948 developed this technique. He used longitudinal and transverse ultrasonic vibrations for determination of the elastic moduli of different metals at temperature range of -195°C to 850°C. See Fig. 2.1.

In this method a suitable quartz crystal (X cut for longitudinal waves, and Y cut for shear waves) is used as a transducer which is cemented to one end of the transmission line. Thus the velocities of both types of waves are measured simply by observation of the echoes from the notched point and the end. The transducer is kept at room temperature irrespective of the region of the specimen under test.

2.4.2 SHOULDER END AND THIN WIRE TECHNIQUES

This involves transmission of a single pulse of about 5 μsec duration. Both of these techniques were first established by

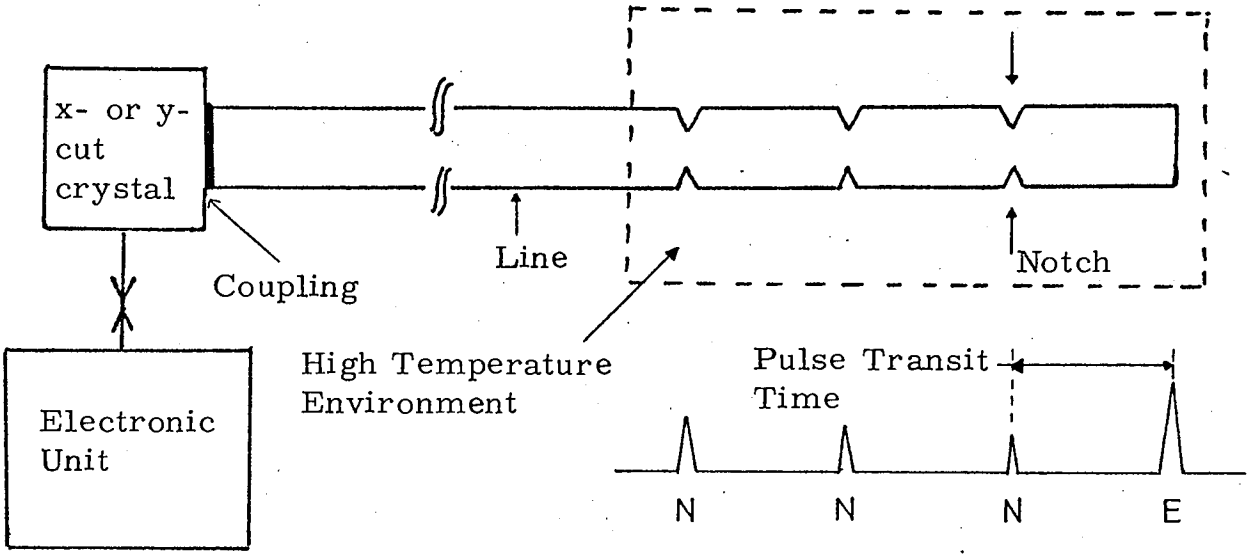

Fig. 2.1 Elastic constants measurement at high temperatures by Notch Bar technique, based on transit time measurements
N : Notch echo, E : End echo

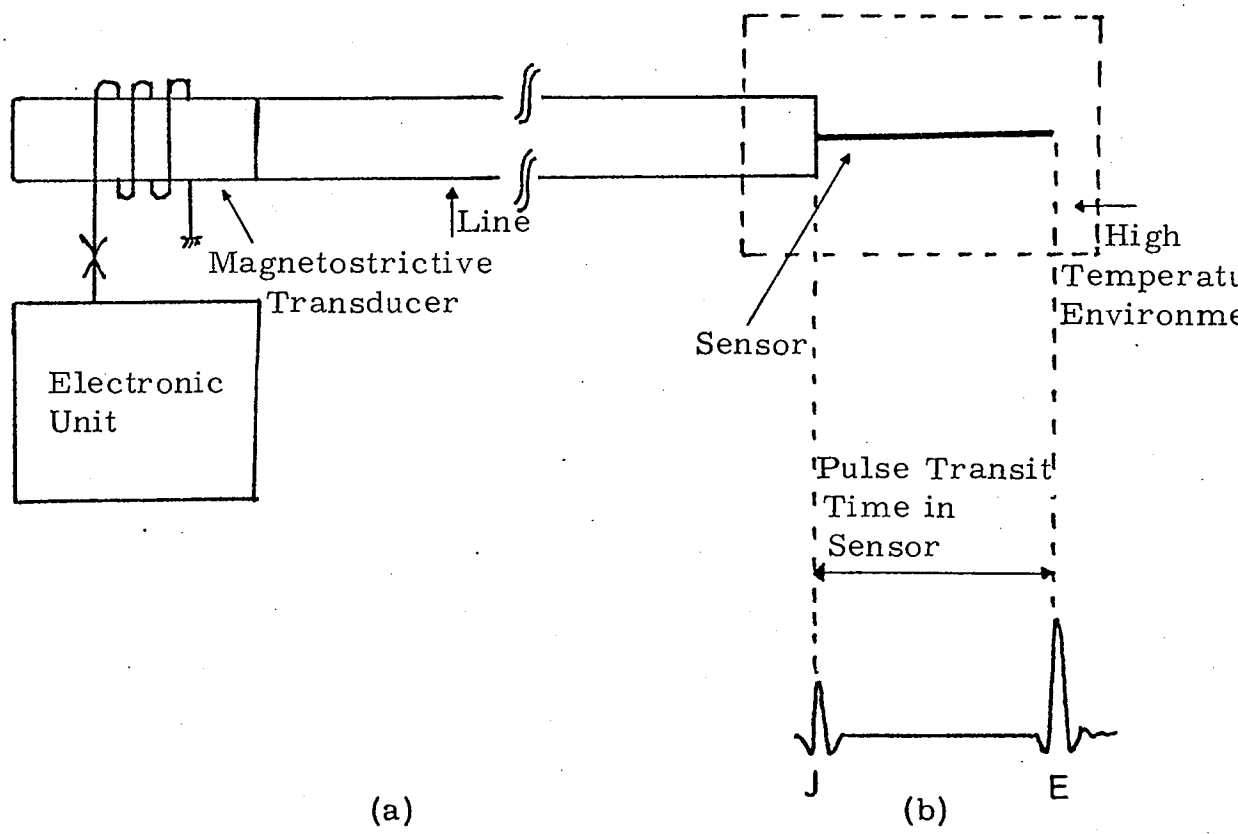

Fig. 2.2 Ultrasonic Thin Wire thermometer, based on transit time measurements
J : Junction echo, E : End echo

Bell[30,31] in 1958. Video pulses of longitudinal or torsional strain (pulse length is very much greater than the specimen diameter) were used to measure the velocity of sound in thin rods over a wide temperature range. The transducer is a polarized nickel tube around which is placed a transmitting coil and a receiving coil, for longitudinal pulses the polarisation must be longitudinal and for torsion it must be circumferential. Electrical pulses fed to the former, causes sound waves to travel along the tube and be received on the latter.

The probe, a rod of 1 or 2 mm diameter, has a shoulder or notch cut into it at a suitable point and it is joined to the nickel tube via an impedance matching piece (Fig. 2.2a). By transmitting a single pulse to the line, two main echoes are obtained from the specimen. The first one from a specially machined shoulder (because of mass discontinuity a portion of the transmitted waves will be reflected back), and the second echo from the end of the probe. There are several other echoes present, such as those from the junction of the matching piece and the probe etc., but by careful matching these are small in comparison with the shoulder and end echoes.

As the acoustic discontinuities are both of high to low impedance, the echoes are of the same polarity. The energy of a pulse in the other direction is damped out by soft pads held in contact with the nickel tube. A typical display is shown in Fig.2.2b.

If a pair of pulses are launched, correctly spaced, the first pulse of the pair will travel to the end of the probe and be echoed back, meeting the echo from the

shoulder of the second pulse of the pair, combining with it and giving rise to a large combined signal. A high degree of sensitivity has been achieved by transmitting alternate pairs of pulses with intervals slightly greater than and slightly less than the correct frequency. Both these combined signals are displayed on the oscilloscope and when, by adjusting the frequency, the two amplitudes are equal, the frequency is correct. Then the time interval between these two echoes enables the velocity to be calculated.

Thorn[32] and Bell in 1962 applied this technique for nuclear thermometry and they measured fuel temperature up to the 1500°C in a gas cooled reactor.

Thin wire technique which is quite similar to the notched bar has shown more successful results in the nuclear environment. Bell[33,34] et.al. in 1966, described the ultrasonic attentuation of solid temperature probe material and investigated the reliability of different refractory metals for dragon project. See Fig.(2.2). Lynnworth[35] et.al. have further developed the thin wire technique particularly for liquid sodium reactor application . They designed the Pana-Therm electronic equipment for measuring of the round-trip time in temperature sensors. A resolution time of 0.1 μsec, which is corresponding to a temperature precision of 1% at 2400°C, for a 50 mm temperature sensor,has been reported.

Panametrics Inc.[21] U.S.A. have extensively expanded this method for temperature measurement in their research projects, such as nuclear rocket engine and liquid metal

fast breeder reactor thermometry. Schmidt and Tasman[24] of Karlsruhe (Germany) have applied the Pana-Therm successfully to nuclear temperature measurements. Pulse echo techniques have also been widely investigated in detail by many authors using different methods. For example, Eros and Reitz[36] by using a short pulse burst of oscillations observed the instantaneous amplitude of waves and studied the transient effect, due to coupling to the transducer. They modified their electronic apparatus to allow only the individual pulse echoes to be observed in their entirety rather than their rectified envelope.

This method made an attempt to eliminate the error in transient time. First they believed by measuring the leading edge of the echo there would be no error in the time of flight, but they found the leading edge,in some cases,strongly attenuated. Then they described how the partial reflection and transmission of the ultrasonic pulses at the crystal-quartz interface,can gradually change the shape of the pulse with successive echoes, and how this distortion can lead to a measured transit time which differs from the true transit time. They also suggested that this error will be maximum when the acoustic impedance of the specimen is close to that of the quartz.

Bernstein [37] in 1962, and Lowrie and Gonas[38] in 1965,studied the temperature dependence of the elastic properties of polycrystalline tungsten up to 1800^{o}C by pulse-echo technique. The velocities were calculated from the difference in the transit times for sonic waves reflected from the end of the specimen, and from a shoulder

machined on to it in a technique similar to that described by Frederick[29] and Bell [30,31]. Fig. 2.3 shows the circuit for pulse-echo measurement.

Other pulse methods for ultrasonic velocity measurement which have been reported by many investigators are such as:

a) pulse superposition technique by McSkimin[39] in 1961.
b) Sing around and coincidence techniques by Holbrook[40] in 1948, and also by Myers et. al.[41] in 1959.
c) methods involving phase comparison by McSkimin[42] in 1959 and also by Williams and Lamb[43] in 1958.
d) optical methods using transparent specimens by many authors.

But all these methods are not applicable for high temperature and therefore, are not of our interest.

2.5 RESONANCE TECHNIQUES OR FREQUENCY MEASUREMENT

One of the first dynamic methods to be widely used for measuring elastic moduli, makes use of the fact that the resonance frequencies of systems vibrating in normal modes are governed by the moduli involved. Thus , if independent measurements are made, all of the moduli can be determined.

Specimens may be in the form of a thin wire or rod or plate vibrating in any type of longitudinal, torsional or flexural. For isotropic materials, the relation between elastic moduli and resonance frequencies are fairly simple for the limiting cases. For example, the half-wave longitudinal resonance frequency for a long,

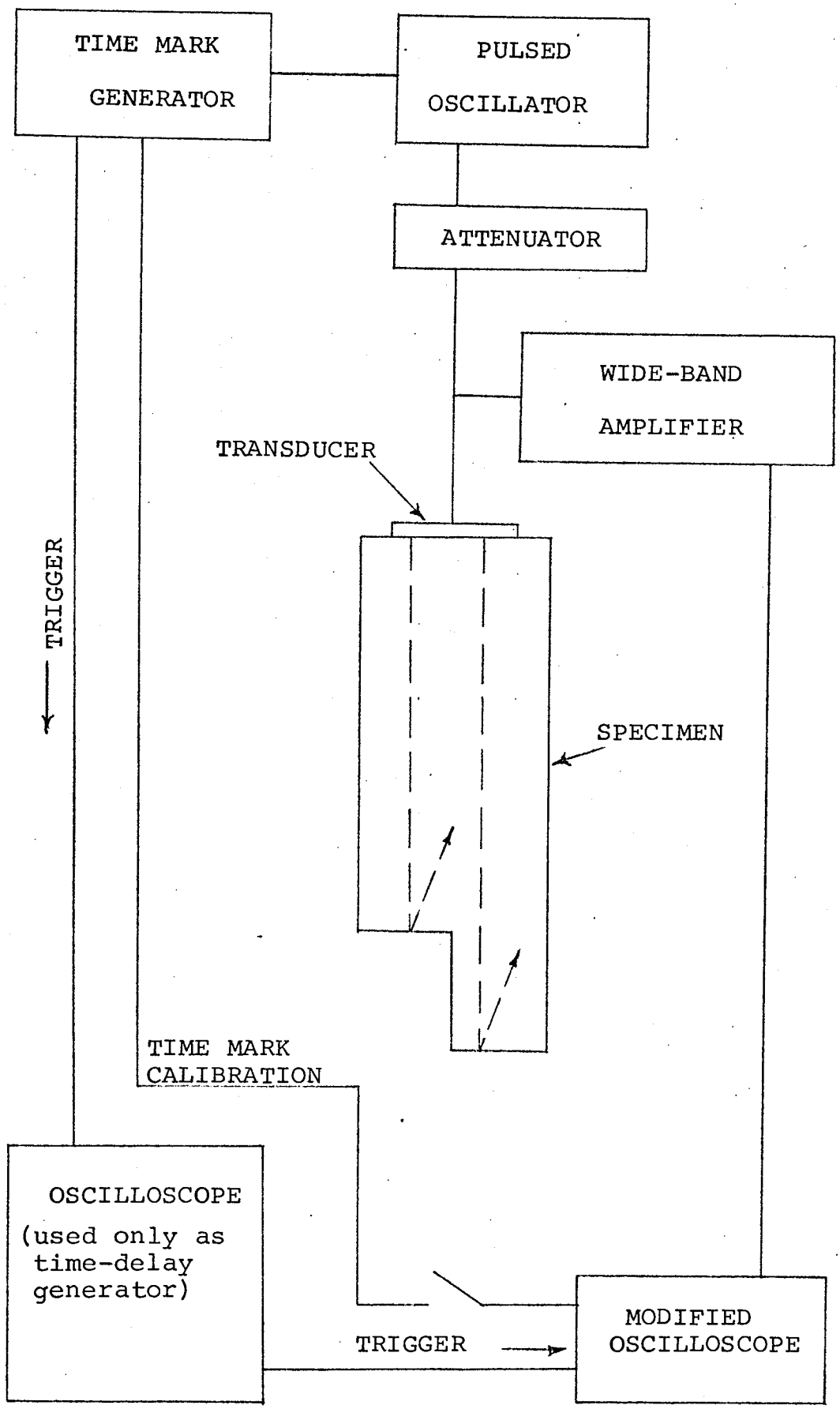

Fig.2.3 Circuit for pulse-echo measurements.

slender rod of negligible dissipation, when the rod's length ℓ is large compared with diameter is given by

$$fr = \left(\frac{E}{\rho}\right)^{\frac{1}{2}} \frac{n}{2\ell} \qquad (2.14)$$

where n is the harmonic number.

In this equation

$$\frac{\omega}{2\pi} \frac{2\ell}{n} = C_o$$

therefore

$$\frac{\omega\ell}{C_o} = \pi n$$ which is similar to the general expression

of Rayleigh $\frac{\omega a}{C}$ = Constant.

From the equation (2.14) appears the successful application of resonance technique at elevated temperature requires a satisfactory means of exciting the sample to resonance and detecting the frequency of resonance. As mentioned before there are two possible ways of exciting the resonator: continuous excitation and pulse excitation, both of which have been described very briefly in Chapter One.

Two resonance techniques are described in the following passage.

2.5.1 RESONANCE BEAM TECHNIQUE

This method apparently was first developed by Forster and Koster[44] in 1938, where they studied the elasticity and damping in relation to the state of the material in temperature range of 0 to 900°C.

In this method, if a metal bar, supported by two wires is stuck, transverse vibration is set up in the way shown in Fig. 2.4(a). Each end of the wires used to suspend the specimen leads to a leaf spring F, Fig. 2.4(b), connected with an electrodynamic system. Mechanical vibrations are excited in the system S by an electrical buzzer, while the system E converts the mechanical vibrations of the test bar into fluctuating current, which are amplified and then read on the instrument I.

When the system S has been excited by the buzzer, the test bar usually remains at rest, but as the exciting frequency approaches its natural frequency of vibration the bar will vibrate.

The maximum amplitude occurs at the natural frequency of the bar. With a test bar of 200 mm in length and 10 mm in diameter, the order of magnitude of the transverse natural frequency is 2 kHz. From the natural frequency determined in this way the modulus of elasticity of the material can be calculated.

Roberts and Nortcliffe [45] in 1947, improved the technology of this method, using a small loudspeaker driven by a beat-frequency oscillator to supply the exciting energy. A standard piezoelectric crystal gramophone pick up was used as the detector of vibrations, which were displayed on an oscilloscope. To find the natural frequency of the bar, the oscillator was tuned until a large maximum deflection appeared on the C.R.O. When this occurred, the position of the nodes were determined by resting a thin steel needle lightly at various points on

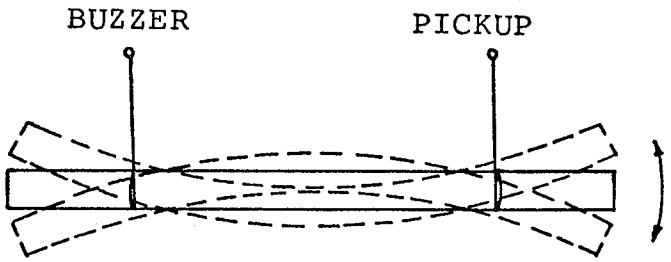

Fig.a. Suspending bar vibrating in flexure

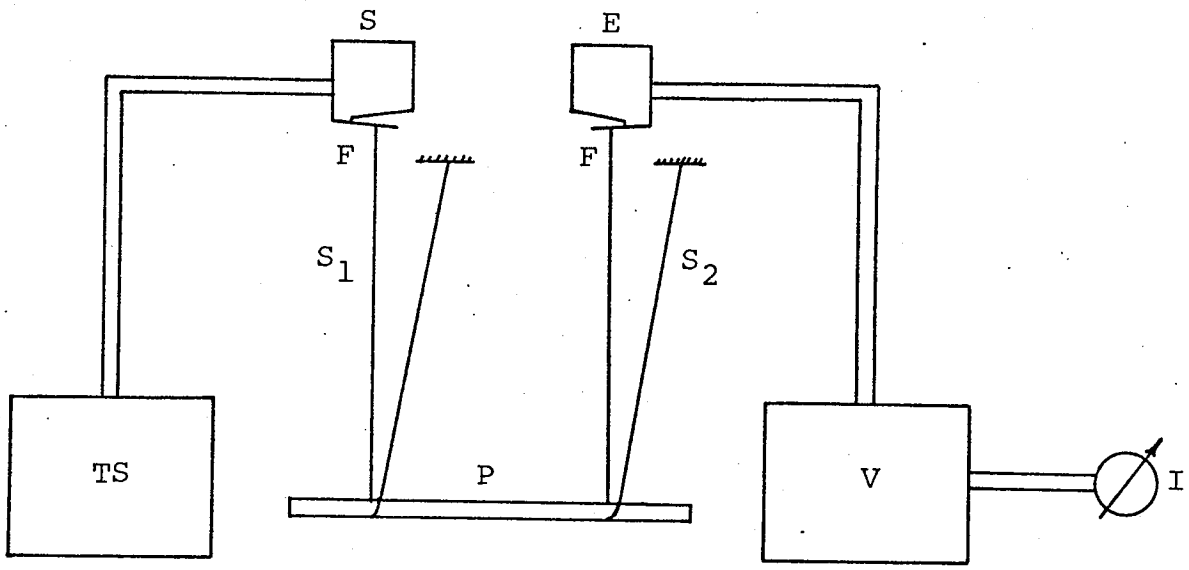

Fig.b. Block diagram of apparatus for dynamic measurement of modulus of elasticity of the material.

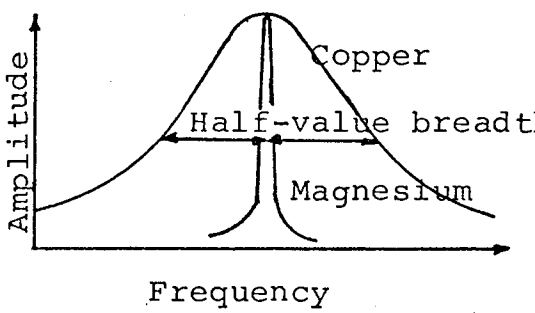

Fig.c. Striking difference between the resonance curves of copper and magnesium.

Fig. 2.4

the bar, with the oscillator still driving the speaker. The deflection on the C.R.O. varied from zero to the maximum according to where the needle was placed at the antinodes or the nodes. With the bar resonating in its fundamental frequency there are two nodes, situated at a distance of about one quarter of the length of the bar from the ends.

The sensitivity in this case depends on eliminating, as far as possible, cross talk between the loudspeaker and the pick-up. The support for the loudspeaker and the pick up must be entirely independent, which is achieved by mounting a thick rubber or felt. This effect does not exist in the pulse-echo system.

Wachtman and Lam[46] in 1959 used Forster's method for Young's Modulus measurement of various refractory materials as a function of temperature. In this work one of the supporting wires attached to a magnetic record cutting head which was driven through a power amplifier by an oscillator. The frequency of the oscillator was measured by a crystal controlled frequency counter with an accuracy of ±0.1 Hz and the flexural vibration of the specimen was transmitted through the other supporting wire to a crystal pick-up. Fig. 2.5 illustrates the block diagram of the apparatus.

This technique has also been used by Brown and Armstrong[47] in 1963 to measure Young's Modulus above 2000^{o}C. In this system a beam or rod as a whole is made to resonate by exciting it from a remote transducer, using continuous wave (CW) excitation. Thin supporting tungsten

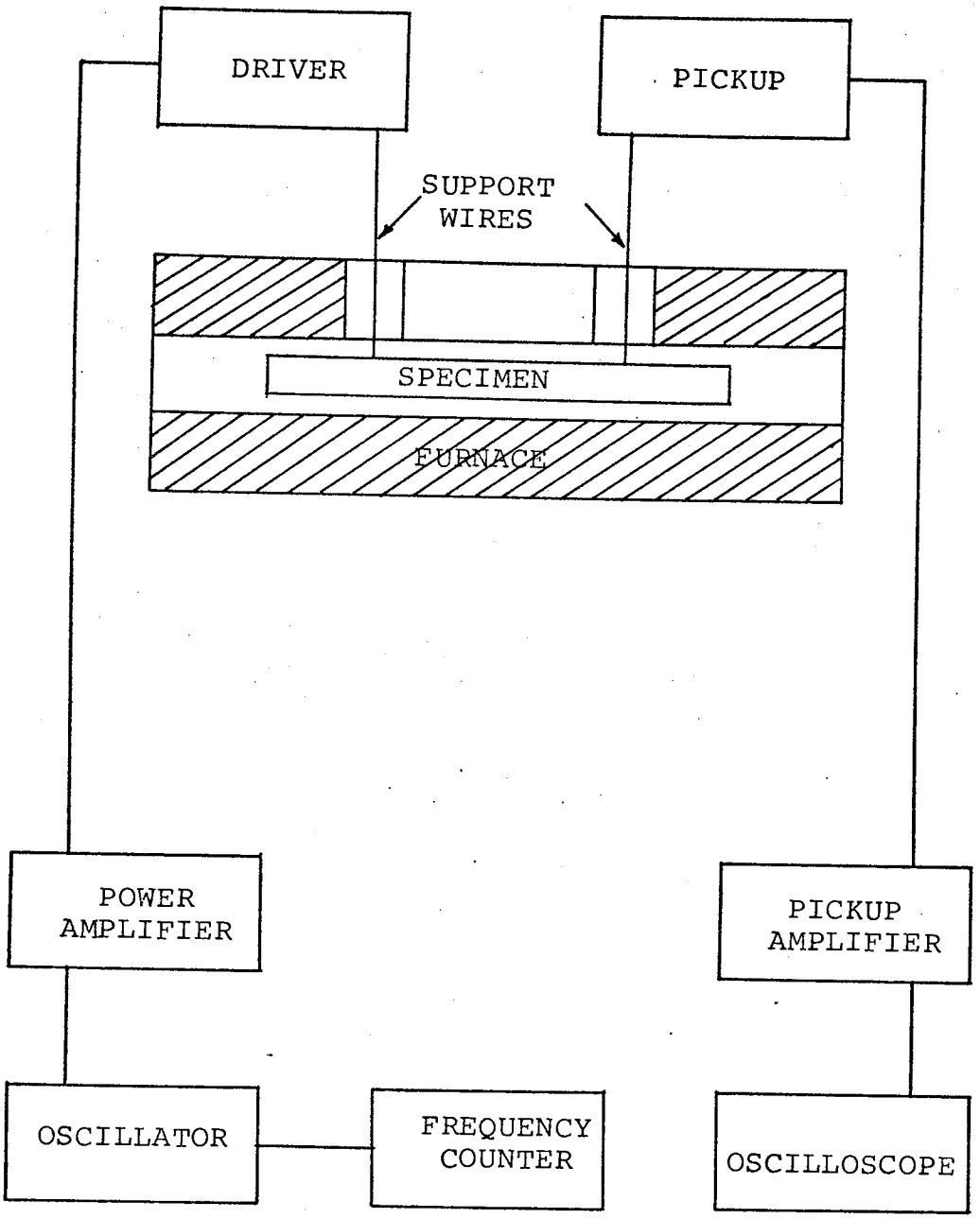

Fig.2.5 Block diagram of apparatus for dynamic measurement of Young's modulus of a "free-free" bar vibrating in flexure.

wires are long enough to enable the transducer to operate at ambient temperatures, while the sample is maintained at high temperature. Spinner[48] in 1954, used a particular apparatus shown in Fig. 2.6 for measuring the sonic modulus of materials at elevated temperatures. The mechanical resonant frequency of the specimen is excited in some modes of vibration by the electromagnetic driver. The increased amplitude of vibration of the specimen is detected by the crystal pick-up which, together with an audio signal of the same frequency, produces a Lissajou pattern on the oscilloscope.

For each specimen, the fundamental frequency of the following modes of vibration were determined:

1) longditudinal

2) flexural, driven on the wide side,

3) flexural, driven on the thin side, and

4) torsional.

Two methods of driving the specimen were tried. In one the specimen was in direct contact with the driver; in the other the specimen was driven through air as shown in Fig.2.6.

The highest reproducibility of these frequencies were obtained where the specimens were driven through air, this considered to be the best way to drive a specimen to get its true natural frequency; since the coupling with the driver is reduced as much as possible, loading and other spurious effects are minimized.

In the system used by the author the long line which couples the energy to the resonator, presents a pure

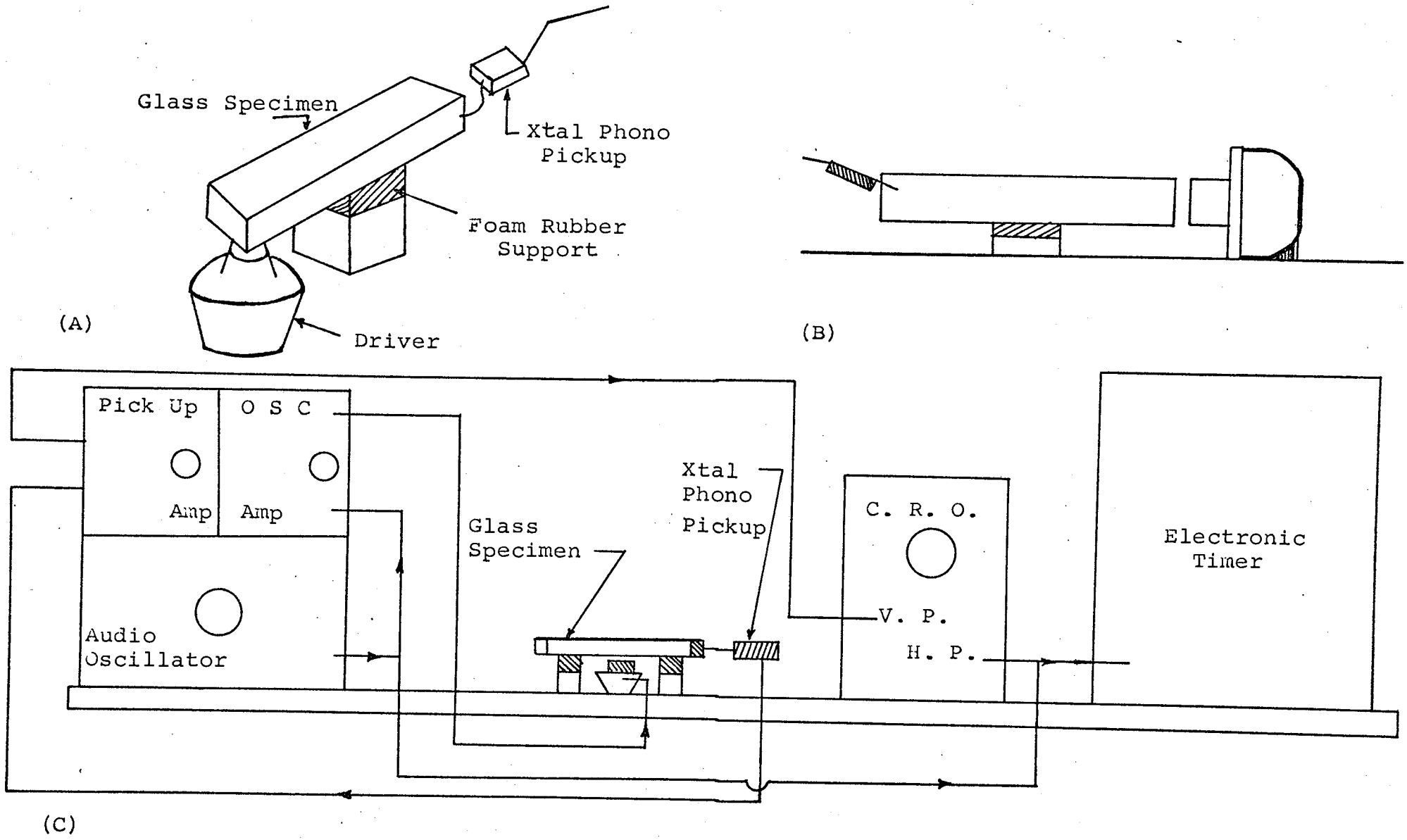

Fig.2.6 Diagrammatic sketch of apparatus used for dynamic measurement. Position of driver and specimen (A) for torsional vibrations, (B) for longitudinal vibrations, and (C) for flexural vibrations

resistance load and whilst reducing the Q factor has no effect on the frequency.

2.5.2 REMOTE RESONATOR OR LINE RESONATOR TECHNIQUE[5,19,22]

This technique as has been described in the detail by Seth[17], is due to Bell[19,5], where an acoustical transmission line is terminated by a resonator, which acts as a temperature sensor. Fig.2.7 shows a functional diagram of the system .

Pulses of ultrasonic oscillations which are generated and received in a magnetostrictive transducer, travel up and down the line as mechanical strain with the velocity of sound. At the end of the probe, coupled to the line, is a resonator which is dealt with in detail later in the thesis. The resonator takes up energy from the burst of oscillation, stores it and finally re-radiates it in proportion to the amount stored.

The echo consists of the signal from the coupling mismatch and the re-radiated signal. Theoretical considerations will show that whatever the nature of the coupling and the resonator, the two signals are in antiphase, and the echo return is therefore the difference between these two signals.

There are two possible modes of excitation of the resonator[22], continuous wave (CW) excitation and pulse excitation. As described before, CW excitation requries two separate channels for driver and receiver. Pulse excitation requires just one channel for both and gives a characteristic and sharp indication of resonance.

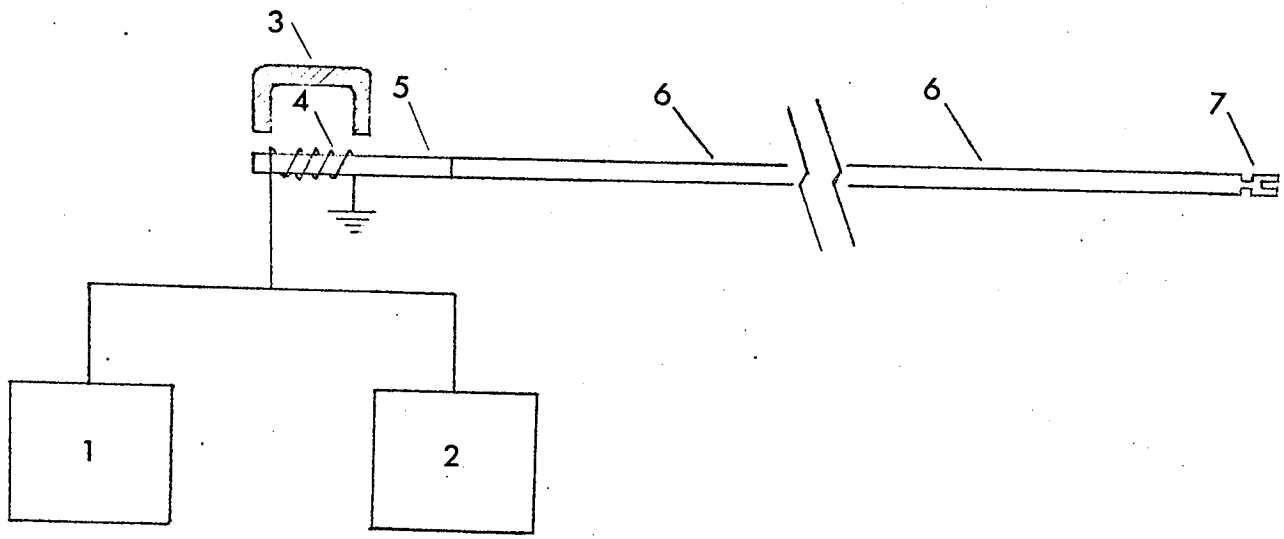

fig. 2.7 General diagram of the pulse apparatus

1 – Electronic Box 2 – CRO 3 – Magnet 4 – Coil 5 – Transducer Rod

6 – Lead-in rod (Acoustic Transmission Line) 7 – Resonator

A burst of n oscillations are transmitted at an interval long enough to avoid intereference by multiple echoes. Fig. 2.8 (a) represents the tranmit signal, (b) the way energy in the resonator builds up during the transmission period and then falls away, (c) the resultant echo, which is the difference between (a) and (b)[19].

By displaying the first echo return, the oscillator can be tuned manually to the resonant frequency of the sensor. The cross over, which is a phase effect, is the most sensitive criterion of resonance.

2.6 RESONATOR

A resonator is described by its frequency and the "Q"factor, which is the sharpness of the resonance. The frequency is proportional to the velocity of sound in the material and is a function of the shape of the resonator. For any resonator there is an almost infinite number of resonances but the lowest modes are well spaced and can be excited separately.

In the resonator design a frequency of the order of the 100 kHz was selected as being the most convenient for TTL signal processing. The diameter of the resonator (and line) is dictated by the hole size, provided by the user. The length of the line dictates the number of oscillations in the burst and hence, to some extent the degree of coupling to the resonator.

Losses in the resonator, due to the internal friction in the material and attenuation in the transmission line

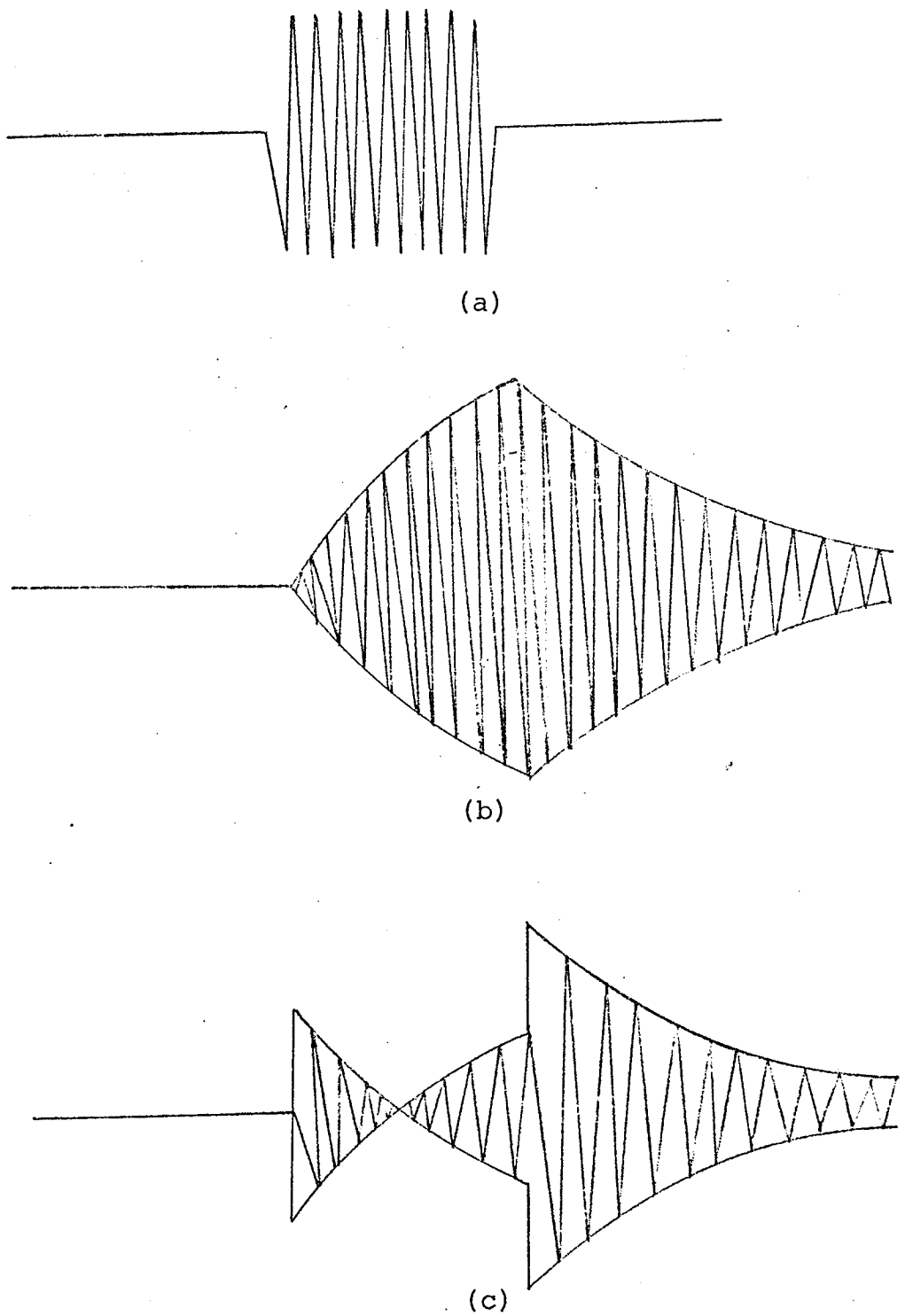

Fig. 2.8 Energy waveforms in a resonator

(a) Incidence pulse
(b) Energy stored in resonator
(c) Resultant echo

are all increasing functions of frequency, thus favouring lower frequencies . The 100 kHz chosen is a convenient compromise.

For a given number of oscillations in the burst, the line length required would be smaller for higher frequency. A compromise design of the resonator is obtained to achieve small resonators at low frequencies. If the size of the resonator and the line length is not a major factor in a particular application then the frequency is kept low, extending the temperature range of the material.

In general, a compromise is made between the various factors and the frequency is kept in the range of 30 to 150 kHz.

The sensitivity of the resonator is proportional to the "Q" factor which is another important design parameter, and determined by the following factors:

a) Tuning sensitivity

In terms of the resonator Q is given by

$$fr \frac{d\phi}{df} = 2Q \qquad (2.15)$$

where fr = resonance frequency

df = frequency deviation from resonance

$d\phi$ = corresponding phase deviation from 180^{o} across the null.

Therefore a high value of Q is desirable for better sensitivity. The cross over, as mentioned before, is a most sensitive criterion of resonance, and the number of oscillations from the start of the echo to the cross over is proportional to resonator Q.

For a lossless material it is given by

$$Pm = \frac{Q}{\pi} \log_e 2 = Q \,/\, 4.55 \qquad (2.16)$$

b) Burst Length

For a large value of Q, the Pm will be large, thus requiring a long burst length and hence a long line. It will be shown later that the increase in material loss, i.e. drop in the material Q, at high temperature results in an increase in Pm. Therefore a compromise is made between the sensitivity desired and the burst length available. A value of Q in the range of 50 to 70, corresponding to Pm of 11 to 15 is generally taken. This gives a setting accuracy of 1 part in 10^4.
A higher Q, while improving the sensitivity will reduce the operating temperature range.

2.7 RELATIVE MERITS OF THE RESONANCE AND VIDEO TECHNIQUES

1. Higher sensitivity of resonance over time measurement for given sensor dimensions.
2. Narrow band discriminates against extraneous noise.
3. Variety and size of the resonator.
4. Video technique is less sensitive to material loss. For example, in platinum the video technique works to nearly its melting point, 1750^{o}C. Resonance technique to 1300^{o}C.

   The high measuring accuracy of 0.01% obtained in the resonance technique compared to 0.1% in the video technique is an overiding factor.

CHAPTER 3

ULTRASONIC THERMOMETER USING RESONANCE TECHNIQUE

3.1 INTRODUCTION

The basic principles of the ultrasonic resonance technique for temperature measurement has been described at the 5th Symposium on temperature (Bell, Washington D.C. 1971), and since then has been further developed, simplifying the acoustic probe and improving the electronics and automatic control.

Further work on probe materials has been carried out and the advantage of ceramic materials, in particular sapphire, over the refractory materials has been quantified. (Bell, Fathimani,Seth)[49], Petten, Dec. 1974.

Acoustically the probe can be considered as an acoustic transmission line terminated by a resonator (the temperature sensor). It has been analysed extensively as a single resonator (Bell)[5,19], a distributed body with an arbitrary spectrum of resonances(Sharp)[50], and from the point of view of internal friction (Pelmore)[51].

A feature of the previous probe design (Seth)[17], was that the resonator is integral with the line, being machined in the form of a tuning fork on the line itself. But this was not suitable for nuclear centre line thermometry, where the instrumentation holes provided in the standard nuclear fuel rods have 2 mm diameter. Therefore, the main problem was reducing the previous probe diameter from 3.1 mm to at least 1.5 mm, which means increasing the resonance frequency of the sensor by a factor of 2. This is because the resonance frequency and the probe diameter are reciprocally

proportion, due to the similitude principle of Rayleigh.

The problem was to redesign the tuning fork resonator on the 1.5 mm line to have a frequency of 100 kHz as before, while maintaining adequate coupling between the line and the resonator. The original design known as "Seth's fork" has been superseded by the new design "Asghar's fork".

Further details of the recent fork design will be discussed in the Chapter 5 of this thesis.

3.2 THE ECHO SPECIFICATIONS

The principles of the echo technique for high temperature measurement have been described in the previous chapter. In this chapter mathematical analysis of the echo with some experimental results and their interpretation will be discuss in detail.

Fig.3.1 shows a theoretical computer plot of an echo for the resonance condition. The echo signal changes exponentially starting with an amplitude E_o, falling to zero after Pm oscillations. See Fig.3.2. At the same time the phase of the echo signal reverses as it goes through the null value and then its amplitude rising towards a steady state value E_∞, when all the incident signal is reflected, and the junction of resonator and line is an antinode. The initial amplitude is determined by the reflection coefficient, R. At the end of the signal the energy stored in the resonator leaks back down the line giving the decrement signal. It is a fundamental feature that the decrement of a resonator is at the natural frequency of the resonator, irrespective of the drive frequency. The amplitude of the decrement, of course, falls off as the

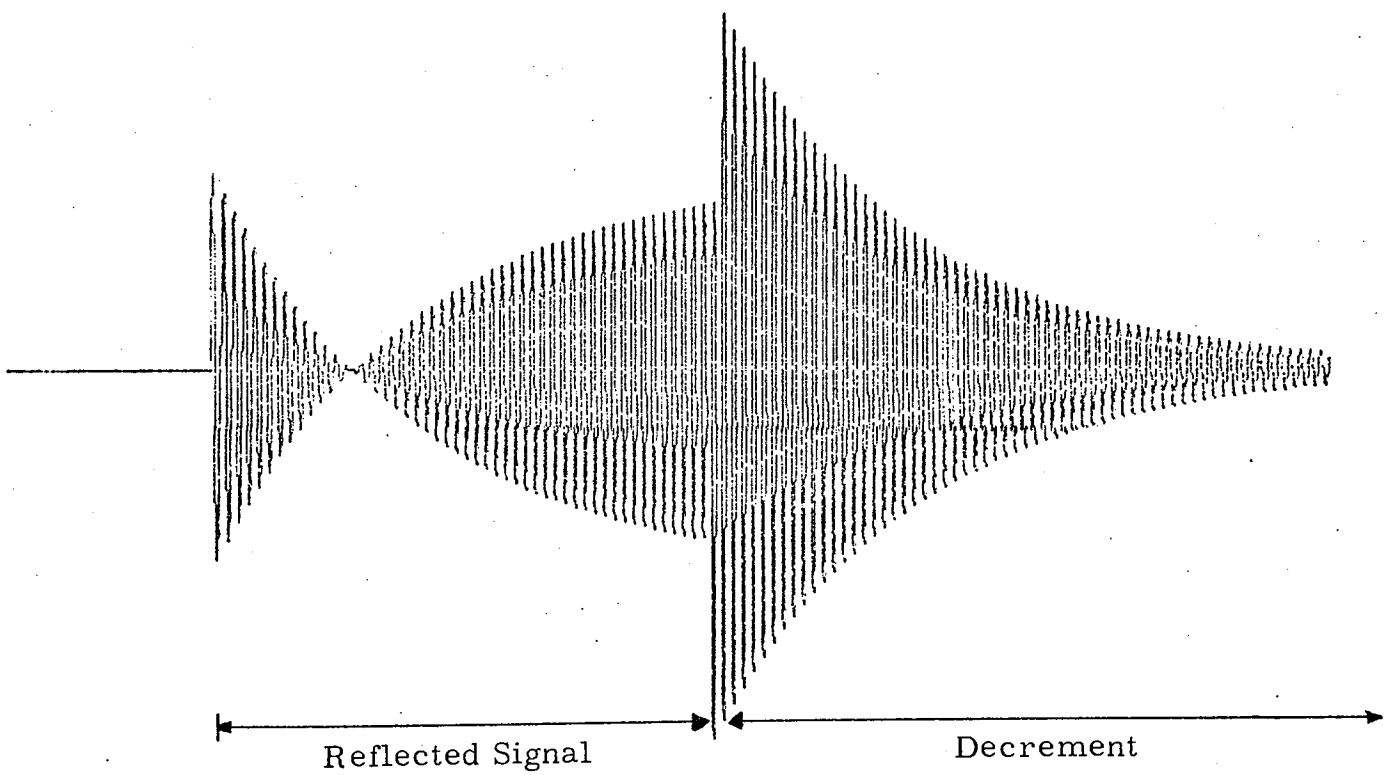

Fig. 3.1 Echo signal at resonance for a lossless material

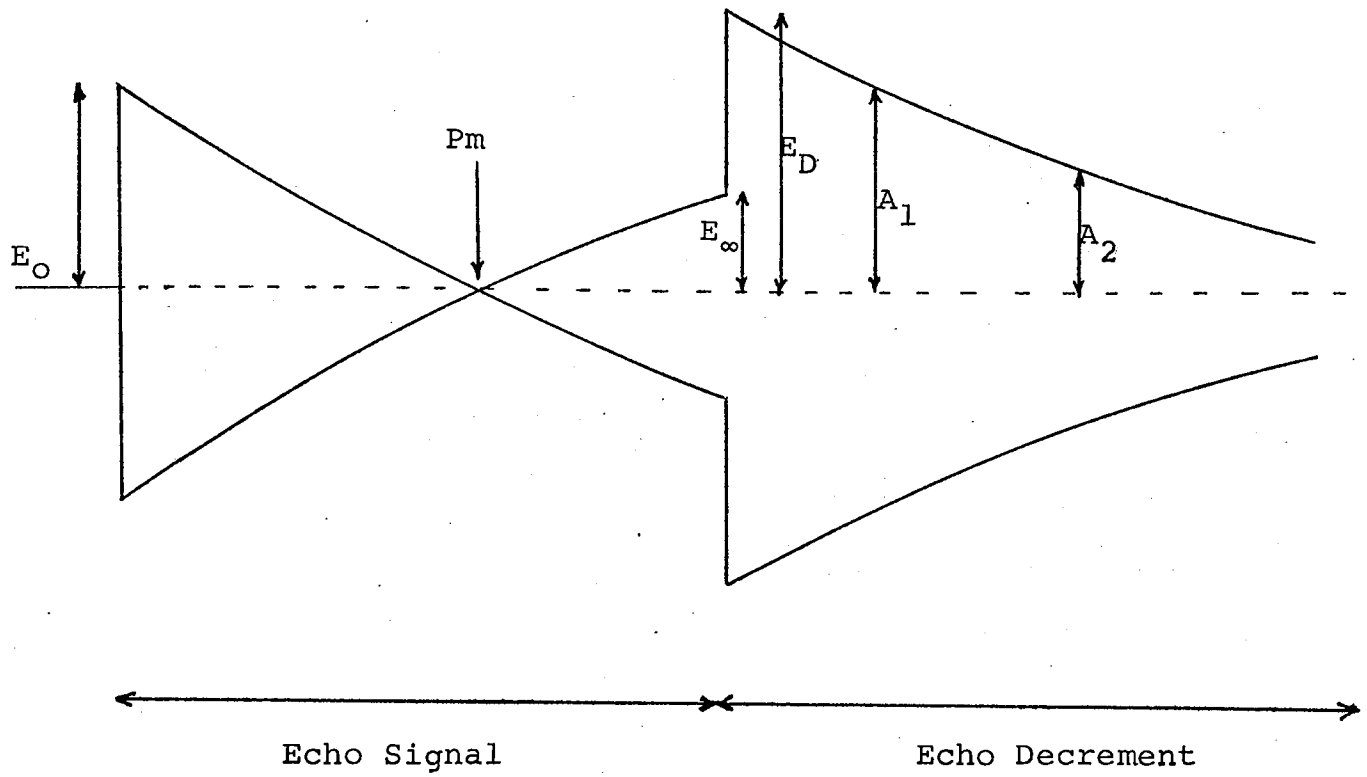

Fig. 3.2 Specifications of a returned echo.

drive frequency is tuned away from the resonator frequency and hence null or cross-over is lost. With still further detuning (see Fig.3.3) the echo decrement disappears, and the echo becomes an image of the incident signal. The decrement frequency is measured with high accuracy in the signal processing for automatic control.

The exponent of the decrement is the same as that of the signal. The form being given by equation (3.1)

$$A_n = A_o \mathrm{Exp}\left(\frac{-\pi n}{Q}\right) \qquad (3.1)$$

where A_n is the amplitude after n oscillations and is expressed in terms of "Q" factor.

The amplitude E_∞ in Fig. 3.2 is to some extent a reliable criterion of the material internal friction, as described later, the higher the internal friction the smaller the amplitude E_∞.

3.3 THE ECHO EQUATION

Mathematical analysis of the echo is given by Sharp[50], where he used a Laplace transform technique to solve the basic equation of motion for the resonator coupled to the transmission line. Detailed comparison of experimentally observed echoes with the graphical computer output confirmed the rigour of the solutions. This mathematical approach is complicated but some of the echo phenomena can not be explained by less rigourous methods.

The following is a theoretical and mathematical consideration of the waves propagated in the line and resonator in the same way which Bell[19] and Seth[17] achieved an equation describing the echo in terms of the

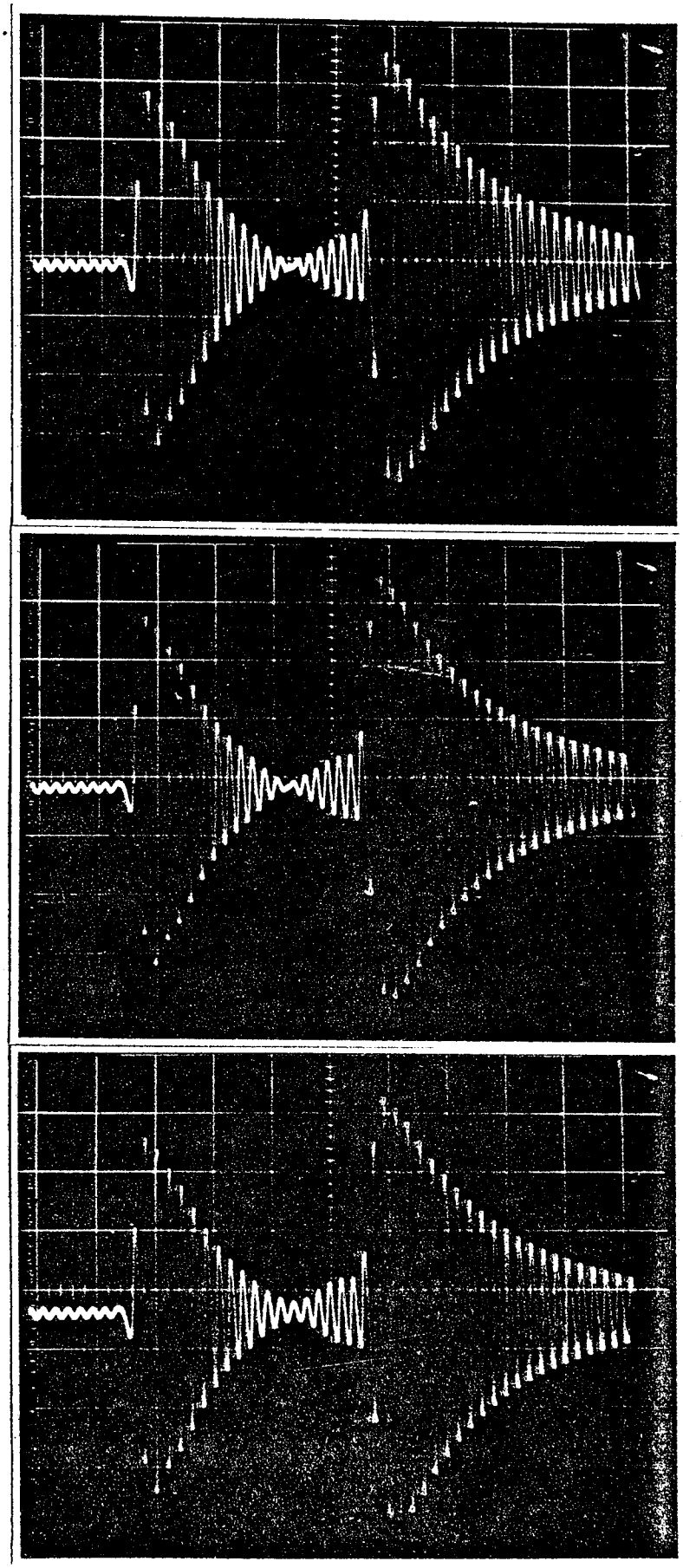

a) At resonance
Period=10.210μsec

b = 0.02%

c = 0.1%

Fig. 3.3 The echo is shown with successive amount of detuning.

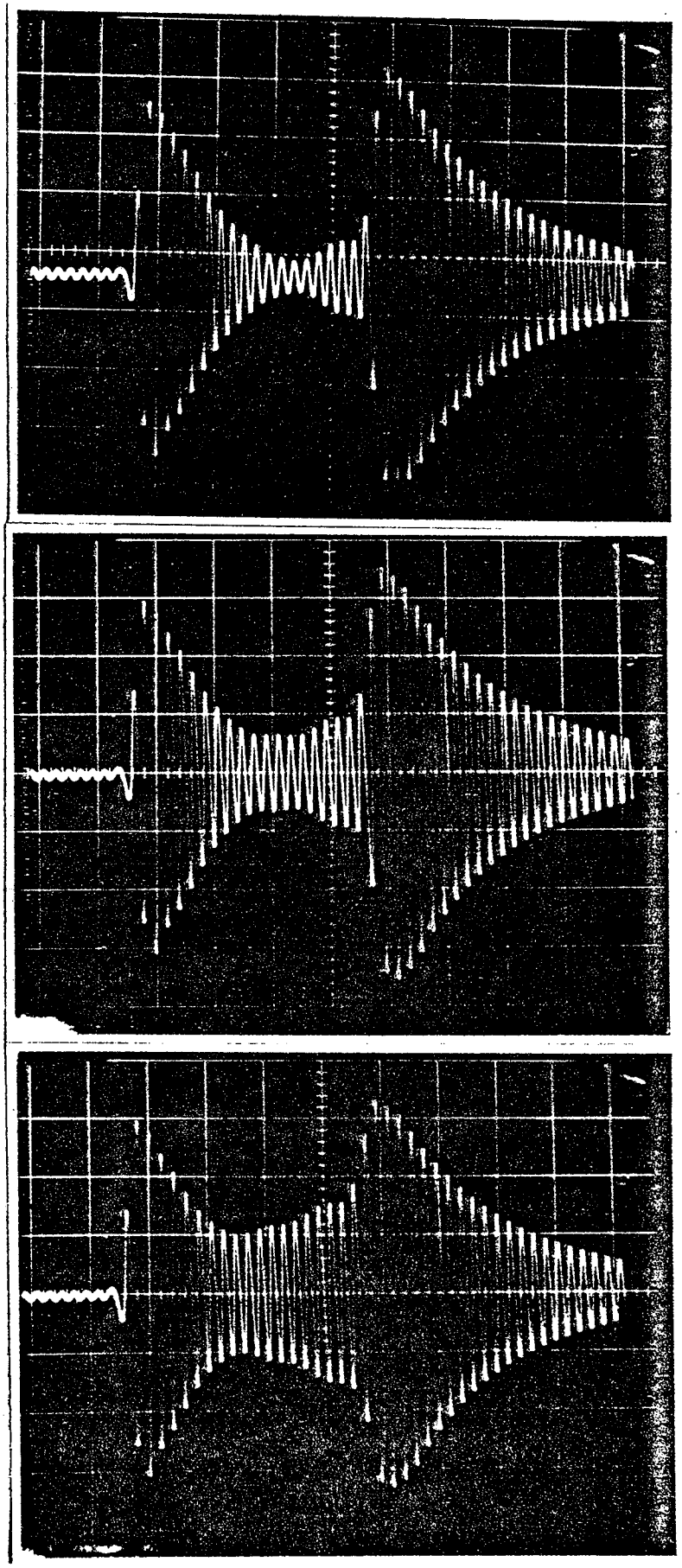

d = 0.2%

e = 0.5%

f = 1%

Fig. 3.3 The echo is shown with successive amount of detuning.

corresponding parameters and factors. The argument can then be extended to obtain the desired information such as internal friction and Young's modulus of elasticity.

Consider a burst of oscillations incident on the junction between specimen and the transmission line. These waves are mainly reflected (R→1) but those transmitted oscillate up and down the resonator and leak back into the line via the junction. Fig.3.4 represents the reflected and transmitted terms, where the specimen is taken to be a half wave resonator, having antinodes at the ends, and vibrating in a longitudinal mode.

A signal entering the resonator travels up and down, experiencing a phase reversal at the free end of the resonator. It is also attenuated by the losses in the resonator material and will have an additional phase difference due to the passage in the resonator. If the attenuation per traverse is given by $e^{-\delta}$ and the phase difference relative to the signal by $3\pi-\phi$. Then

$$\phi = \frac{fi-fr}{fi} = 2\pi \frac{\delta f}{fi} \qquad (3.2)$$

where

fi = incident signal frequency

fr = resonance frequency and also note that at resonance fr=fi, which gives $\phi = 0$.

Then an equation expressing the build up of the echo can be written as follows:

$$E = R-T^2e^{-\delta+j\phi} -T^2R(e^{-\delta+j\phi})^2 -T^2R^2(e^{-\delta+j\phi})^3 \ldots (3.3)$$

As the resonance condition is always desired which implies $\phi = 0$, equation (3.3) becomes

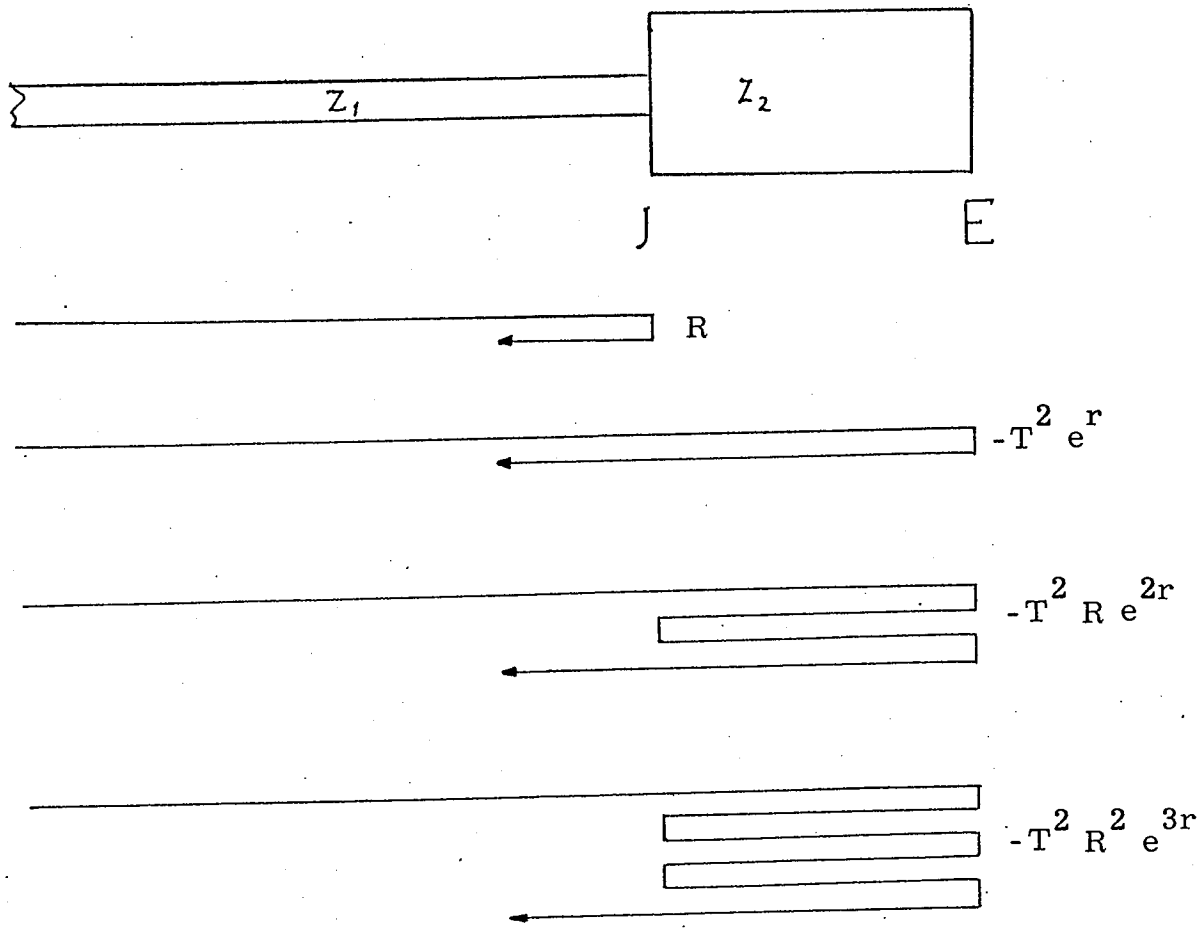

Fig. 3.4 Reflection and transmission at the junction of line and resonator

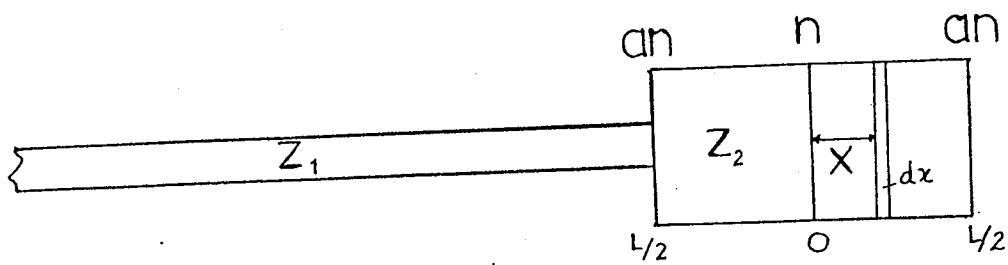

L : length of the resonator

n : node

an : antinode

Fig. 3.5 Half wave resonator vibrating in longitudinal mode

$$E = R-T^2e^{-\delta}[1+(Re^{-\delta}) + (Re^{-\delta})^2 + ...+(Re^{-\delta})^n + ...] \qquad (3.4)$$

This gives the amplitude of the echo signal. Its value at infinity being of great importance as mentioned before is denoted by E_∞.

If we make $x = (Re^{-\delta})$

then the value inside the bracket in equation (3.4) becomes

$$[1 + x + x^2 + ...+ x^n] = \frac{1-x^n}{1-x} \qquad (3.5)$$

If $n = \infty$ then $\frac{1-x^n}{1-x} = \frac{1}{1-x}$

therefore equation (3.4) becomes

$$E_\infty = \left[R-T^2e^{-\delta}\left(\frac{1}{1-Re^{-\delta}}\right)\right] = \left[R - \frac{T^2e^{-\delta}}{1-Re^{-\delta}}\right] \qquad (3.6)$$

in the absence of attenuation $\delta = 0$ therefore

$$E_\infty = \left[R- \frac{T^2}{1-R}\right] \qquad (3.7)$$

By substitution of $T^2 = 1-R^2$ in equation (3.7)

$$E_\infty = \left[R- \frac{1-R^2}{1-R}\right] = [R-(1+R)] = -1$$

and finally $E_\infty = -1$ (3.8)

If coming back again to the equation (3.4), the amplitude of the first reflection E_o, is given by

$$E_o = R \qquad (3.9)$$

Having obtained the echo equation one can measure internal friction and other elastic properties provided the values of R and T, the reflection and transmission coefficient and δ are known in terms of the resonator and line parameters and their coupling "Q" factor.

3.3.1 "Q" Factor

This is an important characteristic property of any resonator and is defined as:

$$Q = 2\pi \frac{\text{Energy stored}}{\text{Energy lost per cycle}} \qquad (3.10)$$

The following definition relates Q to the echo (Sharp[50]):

Q_{Cm} is coupling Q for mode m when the only loss is due to coupling.

Q_{Mm} is material Q for mode m when energy is merely lost in resonator material.

Q_{Tm} is total Q for mode m.

Using only the first order of vibrations, the following formula relates the three Q factors:

$$\frac{1}{Q_T} = \frac{1}{Q_M} + \frac{1}{Q_C} \qquad (3.11)$$

3.3.1.1 Coupling Q Factor for a lossless resonator

Considering a half wave resonator(length L) coupled to a transmission line is vibrating with a node in the centre and antinode at the ends, as shown in Fig.(3.5).

The end is vibrating with a velocity amplitude as

$$\dot{\xi} = \dot{\xi}_o \sin \omega t$$

and at any distance x from the node

$$\dot{\xi} = \dot{\xi}_o \sin \omega t \sin \frac{\pi x}{L}$$

calling A_r the area of cross section and ρ_r density of resonator then stored energy can be given as:

$$E = \frac{1}{2} \int_{-\frac{L}{2}}^{+\frac{L}{2}} \rho_r A_r \dot{\xi}_o^2 \sin^2 \omega t \sin^2 \frac{\pi x}{L} \, dx$$

and

$$E_{max} = \frac{1}{2} \int_{-\frac{L}{2}}^{+\frac{L}{2}} \rho_r A_r \dot{\xi}_o^2 \sin^2 \frac{\pi x}{L} \, dx$$

$$E_{max} = \frac{1}{2}\left(\frac{1}{2} \rho_r A_r L\right) . \dot{\xi}_o^2 \qquad (3.12)$$

$$E_{max} = \frac{1}{2}\left(\frac{1}{2} M\right) . \dot{\xi}_o^2 \qquad (3.13)$$

Equation (3.13) is derived in standard text books.

$$\text{Energy lost along the line} = \frac{1}{2} \rho_\ell C_\ell A_\ell \dot{\xi}_o^2 \qquad (3.14)$$

Where $\rho_\ell C_\ell A_\ell = Z_\ell$ = specific acoustic impedance of the line (3.15)

and $\rho_r C_r A_r = Z_r$ = specific acoustic impedance of the resonator (3.16)

where ρ_ℓ and ρ_r are the densities of line and resonator respectively,

C_ℓ and C_r are the velocities of longitudinal waves in the line and resonator,

and A_ℓ and A_r are cross-section areas of the line and resonator.

Therefore coupling "Q" is

$$Q_C = \frac{2\pi . \frac{1}{2}\left(\frac{1}{2} \rho_r A_r L\right) \dot{\xi}_o^2}{\frac{1}{2}\left(\rho_\ell A_\ell C_\ell\right) \dot{\xi}_o^2 / f} \qquad (3.17)$$

and also $L = \frac{\lambda}{2} = \frac{C_r}{2f}$

therefore $Q_C = \frac{\pi \rho_r A_r C_r}{2 \rho_\ell A_\ell C_\ell} = \frac{\pi}{2} \frac{Z_r}{Z_\ell}$

or $$Q_C = \frac{\pi}{2r} \qquad (3.18)$$

where $$r = \frac{Z_\ell}{Z_r} \tag{3.19}$$

3.3.1.2 "Q" Factor for a resonator with losses

If ξ_o is the displacement amplitude at one end of the line, then displacement amplitude at any point with distance x from the origin can be written as

$$\xi = \xi_o e^{-\alpha x} \tag{3.20}$$

where α is an attenuation constant of the line.

The corresponding energy relations are

$$E = Eo\ e^{-2\alpha x} \tag{3.21}$$

In a line, energy loss per cycle is equivalent to the energy loss per wave length, then

$$dE = -2E\alpha dx$$

or $$E = -2E\alpha\lambda \tag{3.22}$$

where E = stored energy,

therefore

$$Q_M = \frac{2\pi \text{ Energy stored}}{\text{Energy loss per wave length}}$$

$$= \frac{2\pi . E}{2\alpha\lambda E} = \frac{\pi}{\alpha\lambda}$$

or $$Q_M = \frac{\pi}{\alpha\lambda} = \frac{\pi}{\delta} \tag{3.23}$$

or $$\delta = \frac{\pi}{Q_M} = \alpha\lambda \tag{3.24}$$

where δ is attenuation constant per wave length.

3.3.1.3 Total Q factor of a resonator with losses

By equation (3.12) the energy stored in a half wave

resonator is given by

$$E = \frac{1}{2}(\frac{1}{2}\ \rho_r A_r L).\dot{\xi}_o^2$$

Energy loss due to coupling by equation (3.14) $= \frac{1}{2f}(\rho_\ell C_\ell A_\ell).\dot{\xi}_o^2$, and energy loss in the resonator by equation (3.22) $= 2E\alpha\lambda$, composite Q can be written as

$$Q_T = \frac{2\pi \text{ stored energy}}{\text{total energy loss per cycle}}$$

$$= \frac{2\pi.\frac{1}{2}(\frac{1}{2}\ \rho_r A_r L)\dot{\xi}_o^2}{\frac{1}{2}f(\rho_\ell C_\ell A_\ell)\dot{\xi}_o^2 + 2E}$$

or $$\frac{1}{Q_T} = \frac{\frac{1}{2}f\rho_\ell C_\ell A_\ell \dot{\xi}_o^2}{2\pi(\frac{1}{2}\rho_r A_r L)\dot{\xi}_o^2} + \frac{2E\alpha\lambda}{2\pi E}$$

or $$= \frac{2r}{\pi} + \frac{\alpha\lambda}{\pi} \qquad (3.25)$$

or $$\frac{1}{Q_T} = \frac{1}{Q_C} + \frac{1}{Q_M} \qquad (3.26)$$

By designing for a Q_C of 50, Q_T is virtually unchanged over a wide temperature range.

The next step in the derivation of the echo equation is to find the expression for the junction reflection and transmission coefficients in terms of Q_C.

3.3.2 Reflection Coefficient R

If a line of impedance Z_1 is terminated by an impedance Z_2, signals are echoed from the junction because of the impedance discontinuity The ratio between the incident signal and echo can be written as

$$\frac{\xi-}{\xi+} = \frac{Z_2-Z_1}{Z_2+Z_1} = \frac{1-r}{1+r} \qquad (3.27)$$

where $\xi+$ is the displacement amplitude of the incident signal and $\xi-$ is the displacement amplitude of the echo, and

$$r = \frac{Z_1}{Z_2} \tag{3.28}$$

If $\xi+ = 1$ and $\xi-$ is denoted by R, the reflection coefficient is a fraction of the incident signal reflected. Therefore

$$R = \frac{1-r}{1+r} \tag{3.29}$$

Expanding the geometric series $\frac{1}{1-(-r)}$ then

$$R = (1-r)(1-r+r^2-r^2+.....)$$

and if $r<<1$, then $R=1-2r$ (3.30)

Writing r in terms of coupling Q factor, expression obtained before by equation (3.18)

$$r = \frac{\pi}{2Q_C}$$

then

$$R = 1- \frac{\pi}{Q_C} = [1 - 0.69\ Pm] \tag{3.31}$$

3.3.3 Transmission Coefficient T

For a line of impedance Z_1 terminated by an impedance Z_2, the signal transmitted through the junction for unity amplitude of incident signal is given by

$$T_{1\to2} = \frac{2Z_1}{Z_1+Z_2} = \frac{2r}{1+r} \tag{3.32}$$

Similarly transmission from Z_2 to Z_1 may be written as

$$T_{2\to1} = \frac{2Z_2}{Z_1+Z_2} = \frac{2r}{1+r} \tag{3.33}$$

signal received at the sending end due to two transmissions

$$T^2 = T_{12} \cdot T_{21} = \frac{4Z_1Z_2}{(Z_1+Z_2)^2} = \frac{4r}{(1+r)^2} \qquad (3.34)$$

If $r<<1$ then T^2 can be written as

$$T^2 = \frac{4r}{(1+2r)} = 4r(1+2r)^{-1} = 4r(1-2r+4r^2- \ldots.)$$

or

$$T^2 = 4r-8r^2 \qquad (3.35)$$

Expressing T^2 in terms of coupling Q factor

$$T^2 = 4\,\frac{\pi}{2Q_C} - 8\,\frac{\pi^2}{4Q_C^2}$$

or

$$T^2 = \frac{2\pi}{Q_C}(1-\frac{\pi}{Q_C}) \qquad (3.36)$$

And finally for reflection and transmission coefficients in terms of coupling Q_C one can write,

$$R^2+T^2 = (1-\frac{\pi}{Q_C})^2 + \frac{2\pi}{Q_C}(1-\frac{\pi}{Q_C}) \qquad (3.37)$$

and neglecting the terms $\frac{\pi^2}{Q_C^2}$

this is consistent with

$$R^2 + T^2 = 1 \qquad (3.38)$$

3.3.4 Internal Friction

Consider the steady state amplitude of the echo equation for resonance derived earlier (equation 3.6).

$$E_\infty = (R-\frac{T^2e^{-\delta}}{1-Re^{-\delta}}) \qquad (3.6)$$

As $T^2 = 1-R^2$

therefore

$$E_\infty = \frac{R-e^{-\delta}}{1-Re^{-\delta}} \qquad (3.39)$$

Substituting for the values of δ and R from equations (3.24) and (3.31) respectively, $\delta = \frac{\pi}{Q_M}$ and $R = 1 - \frac{\pi}{Q_C}$ in the equation (3.39) therefore

$$E_\infty = \frac{1 - \frac{\pi}{Q_C} - e^{-\pi/Q_M}}{1-(1-\frac{\pi}{Q_C})e^{-\pi/Q_M}} \qquad (3.40)$$

Expanding the exponential term $e^{-\pi/Q_M}$ and neglecting high powers of $\frac{\pi}{Q_M}$ the above equation becomes

$$E_\infty = \frac{(1-\frac{\pi}{Q_C}) - (1-\frac{\pi}{Q_M})}{1-(1-\frac{\pi}{Q_C})(1-\frac{\pi}{Q_M})}$$

or

$$E_\infty = \frac{\pi/Q_M - \pi/Q_C}{\pi/Q_M + \pi/Q_C - \pi^2/Q_M Q_C}$$

Neglecting the term $\pi^2/Q_M Q_C$ therefore

$$E_\infty = \frac{Q_C - Q_M}{Q_C + Q_M} \qquad (3.41)$$

Recall the amplitude of the first reflection E_o, given by equation (3.9) and replace reflection coefficient R from equation (3.31)

$$E_o = (1-\frac{\pi}{Q_C}) \qquad (3.42)$$

For a typical probe $Q_C \tilde{=} 100$ and therefore an error of only 3% will occur if the π/Q_C is neglected. Thus equation (3.42) becomes

$$E_o = +1 \qquad (3.43)$$

In the case of lossless material as it said before,

$Q_M = \infty$. The echo amplitude in infinity as given by equation (3.41) becomes

$$E_\infty = -1 \tag{3.44}$$

By comparing equations (3.44) and (3.43) it will be seen that the two signals are of opposite polarities, the phase reversal occurring at cross-over.

Coming back to the equation (3.41) and considering equation (3.43)

$$\frac{E_\infty}{E_o} = \frac{Q_C - Q_M}{Q_C + Q_M}$$

rearranging

$$\frac{Q_C}{Q_M} = \frac{E_o + E_\infty}{E_o - E_\infty}$$

or

$$Q_M^{-1} = \frac{E_o + E_\infty}{E_o - E_\infty} Q_C^{-1} \tag{3.45}$$

This is the formula which is used to determine internal friction Q_M^{-1}. For this purpose the value of E_o and E_∞ could be measured directly on the oscilloscope. To complete the required data, the method described below could be used to give the value of the coupling loss Q_C^{-1}.

The formula governing the relation between the number of oscillations to cross-over point and the Q factor has been given to be (ref. 50 and 17).

$$Pm = \frac{Q_C}{\pi(1+Q_C/Q_M)} \ln \frac{2}{1-Q_C/Q_M} \tag{3.46}$$

Now consider the case where the material internal friction

is negligible, i.e. $Q_M >> Q_C$. Then the equation (3.46) changes form to:

$$Pm = \frac{Q_C}{\pi} \ln 2$$

or

$$Q_C = 4.55Pm \qquad (3.47)$$

Hence the value of Q_C can be calculated by counting the number of oscillations to cross-over point "Pm" and replacing in equation (3.47). The amplitude E_o is in this case equal to E_∞ and the expected pattern of the echo is shown in Fig. 3.6a.

Another special case is when the material internal friction is relatively high and the amplitude E_∞ is very small, say zero, Q_C then is equal to Q_M. Thus in the steady state there will be no signal, all the energy going into the resonator is absorbed. There will, of course, be a transmitted signal at the beginning and end of the echo, see Fig. 3.6b.

Further details of materials internal friction and different methods of its measurement is given by Pelmore[51] (1975) and Sadollah[52] (1974).

3.3.5 Echo-Decrement

The echo-decrement follows the echo-signal and is the exponential re-radiation of the stored energy. The cessation of the signal removes the R term of the equation (3.4) and leaves $-\frac{T^2}{1-R}$ (for the lossless case) which become 1+R and is approximately equal 2. This resolves the paradox of the large increase in amplitude which occurs when the signal ceases.

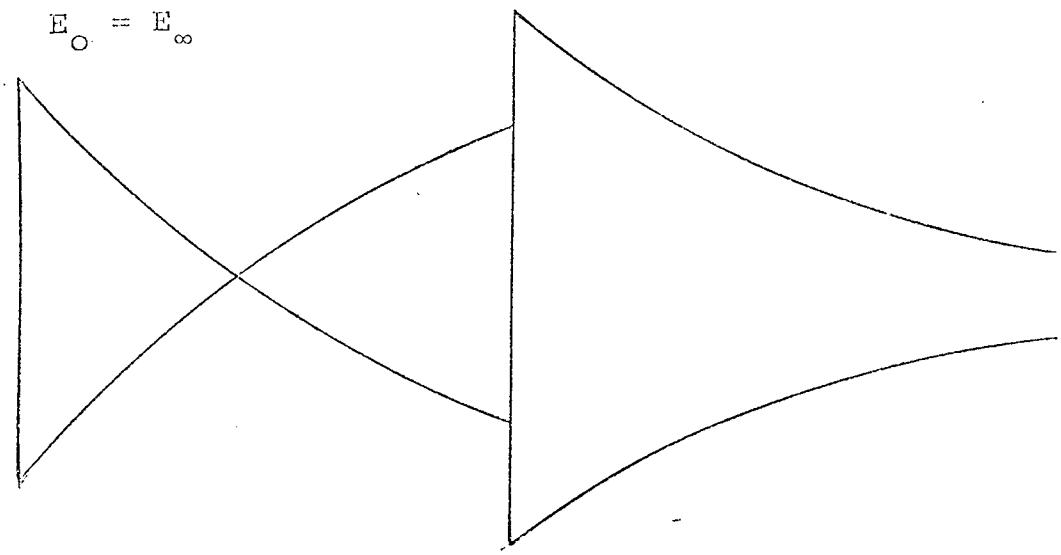

Fig. a

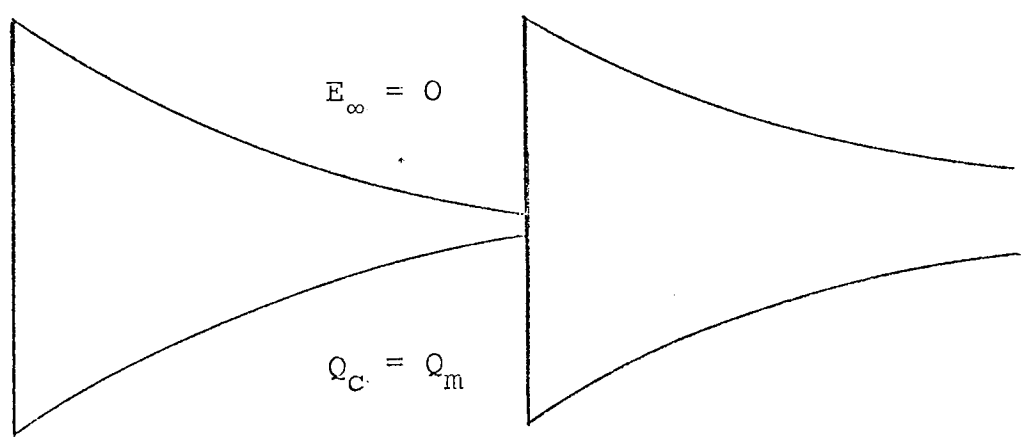

Fig. b

Fig. 3.6 Echo pattern for a material with negligible internal friction (fig.a) and for a material with relatively high internal friction (fig.b).

Diagrammatically Fig. 3.7 shows (a) the reflected signal, (b) the re-radiated signal and (c) the sum of the two signals.

A simple case of echo-decrement at the resonance frequency will be analysed. The echo amplitude for any number of oscillations n in the burst is given by equation (3.48) ref.[17].

$$E_n = (1- \frac{\pi}{Q_C}) - \frac{2Q_T}{Q_C}(1- \frac{\pi}{Q_T}) [1-e^{- \frac{\pi n}{Q_T}}] \qquad (3.48)$$

Considering the special case where $\frac{\pi}{Q_C}$ and $\frac{\pi}{Q_T}$ are much less then unity then

$$E_n = 1- \frac{2Q_T}{Q_C}(1-e^{- \frac{\pi n}{Q_T}}) \qquad (3.49)$$

This equation gives the reflected signal. The re-radiated signal is identical to the reflected signal but delayed in time and opposite in phase, adding to two signals gives the echo as shown in Fig.3.7.

Therefore the decrement amplitude ((m-n) oscillations after the end of the signal burst on n oscillations) is

$$E_d = [1-\frac{2Q_T}{Q_C}(1-e^{- \frac{\pi n}{Q_T}})]-[1- \frac{2Q_T}{Q_C} (1-e^{- \frac{\pi m}{Q_T}})] \qquad (3.50)$$

or $$E_d = \frac{2Q_T}{Q_C} [+e^{- \frac{\pi n}{Q_T}} -e^{- \frac{\pi m}{Q_T}}] \qquad (3.51)$$

where m> n.

For a lossless material $Q_T = Q_C$

therefore $$E_d = 2e^{- \frac{\pi n}{Q_C}} -2e^{- \frac{\pi m}{Q_C}} \qquad (3.52)$$

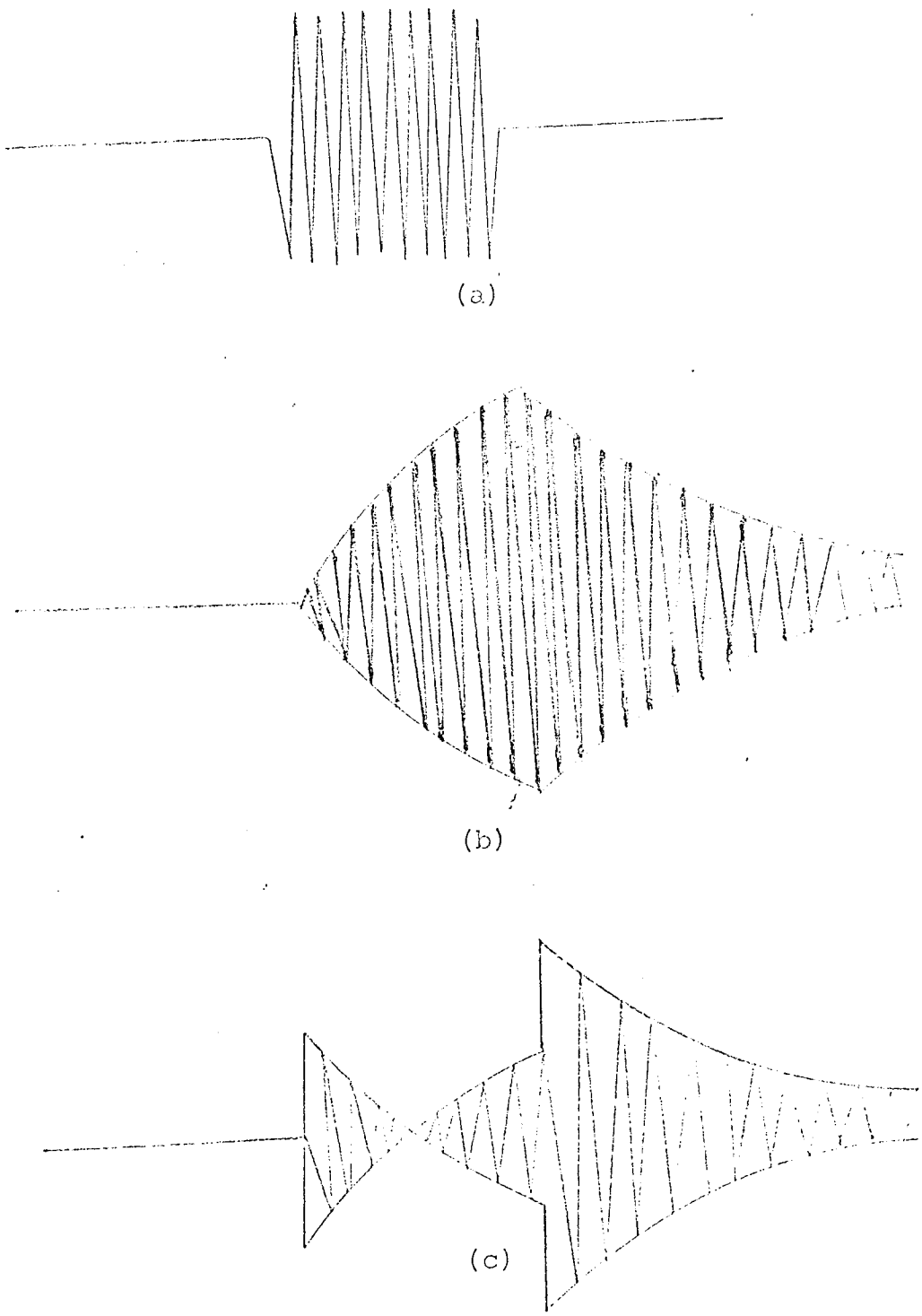

Fig. 3.7 The echo envelope (c) as the sum of the reflected signal and the decrement
(a) The reflected signal without decrement
(b) The reradiated signal starting at the end of the reflected signal and opposite in phase.
(c) Sum of (a) and (b), the echo signal with decrement.

In practice n and Q_C are chosen so that $e^{-\frac{\pi n}{Q_C}}$ is small ($E_\infty \to 1$), the decrement therefore approximates to $-2e^{-\frac{\pi m}{Q_C}}$ and decays from an initial value of 2. This large amplitude allows a good signal to noise ratio for the electronic processing.

3.4 SUMMARY

The envelope of the reflected signal component is exponential having the same time constant as the envelope of the echo-decrement. The phase of the reflected signal component reverses as it goes through the null value and the amplitude rises to steady state unity, when all the incident signal is reflected, and the junction of the resonator and the line is an antinode. The initial amplitude is determined by the reflection coefficient R, which is almost unity.

The effect of the materials losses results is an increase in the number of oscillations to cross-over and a drop in steady state amplitude. The effect of detuning is a loss of the null and a fall in stored energy, resulting in a decrease of the echo-decrement amplitude.

A computer plot of the echo at resonance for materials with losses is shown in Fig.3.8 and an echo for considerable detuning in Fig.3.9. This full mathematical description of the echo is used in the automation of the system. The control signal can be derived from a variety of the features of the echo. In the case of complex resonators such as tuning forks etc ,the echo pattern is that of a single resonance and all the parameters defined for a half wave resonator apply

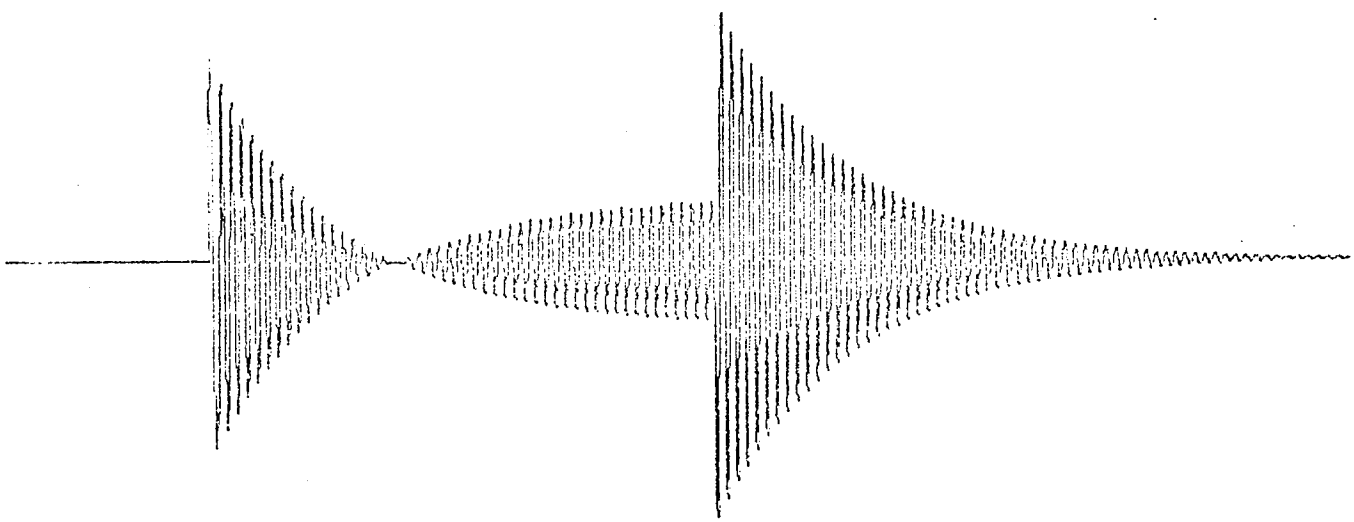

Fig. 3.8 Echo signal at resonance for a material with losses $Q_c = 50$ and $Q_m = 250$

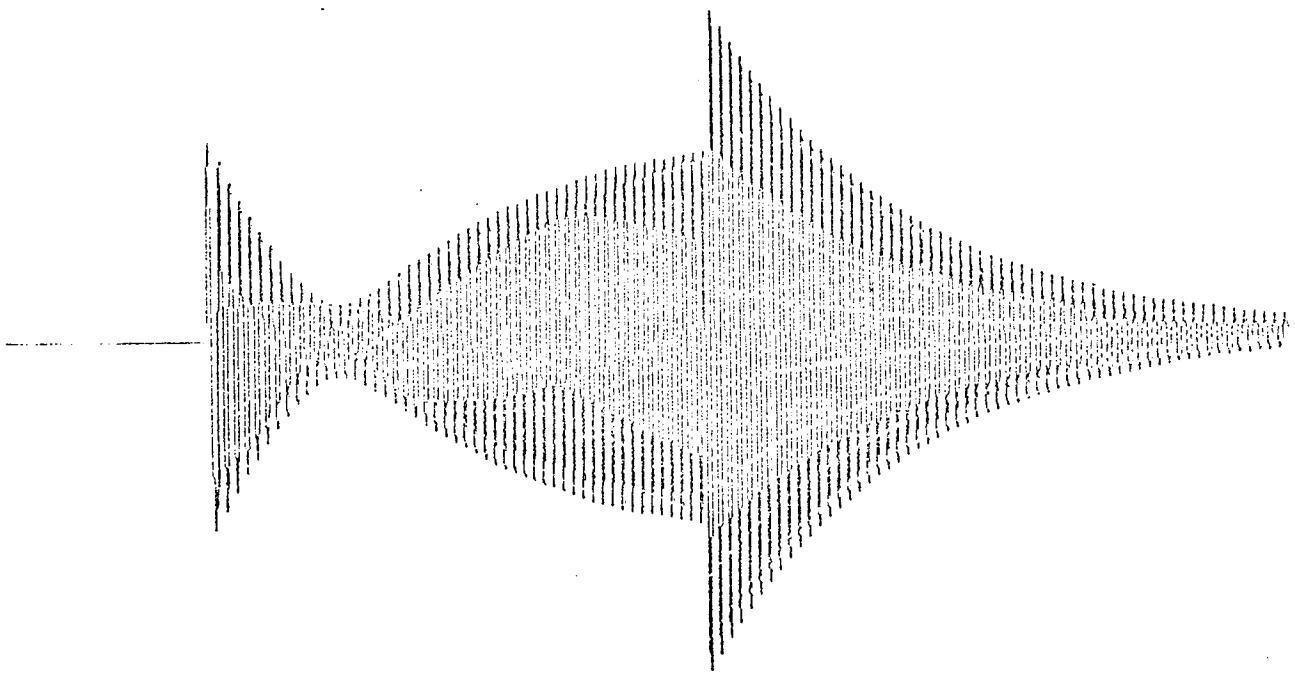

Fig. 3.9 Echo signal at off resonance for a lossless material
$f_{Tx} = f_R(1 + 0.05)$

to the case. The coupling Q factor which is a complex function of the design parameters is not directly calculable.

3.5 RELATIVE MERITS OF THE METHOD

A comparison of the echo resonance and the time of flight techniques is summarised as follows:

1. Higher sensitivity of resonance technique over time of flight measurement for a given sensor dimensions.
2. Variety of size of resonator.
3. Narrow band discrimination against extraneous noise.
4. Small size of resonator for most of applications, particularly for temperature measurement in the nuclear fuel rods which lead to less removal of the fuel from the centerline.
5. Both methods allow a wide choice of probe and sensor materials.
6. The resonance technique has been applied to other measurements such as:
   a) Elastic constant measurements, Sharp[50](1974).
   b) Internal friction measurements, Pelmore[51] and Sadollah[52](1974).
   c) Investigation of fluid properties; particular, density, viscosity and pressure. Mahil[53](1975).
   d) Investigation of resonant modes in many structures.
7. The resonance method is the more sensitive to internal friction. Thus for a given material the time of flight method operates to a higher temperature. It is however, much less accurate.
8. The echo resonance technique is very suitable for

automation. This has been done by author and the apparatus is called "Ultrasonic Resonance Tracking Instrument" which was exhibited in the "8th International Congress on Acoustics", London, 23-31 July, 1974.

Subsequently a copy of this instrument has been constructed for the AWRE (Aldermaston). It is being used for the measurement of the high temperature properties of materials such as graphite and other refractories.

CHAPTER 4

ACOUSTIC PROBE REQUIREMENT FOR HIGH TEMPERATURE MEASUREMENTS

4.1 INTRODUCTION

In this chapter the types of resonators which are available for high temperature applications and their limitations will be reviewed.

Essentially what is required is a resonator which is as small as possible, can be effectively coupled to the transmission line part of the probe and is integral with the line. The latter feature is highly desirable as it avoids the problems of making a high temperature joint.

As described in the previous chapter, the echo pattern is completely characterised by the resonator frequency and it's coupling to the line. Thus any geometrical form is acceptable as long as the design gives control of these two factors.

Mobsby [22] has considered the operational modes for the case of solid resonators. He makes two classifications where the vibrations are extensional and flexural respectively. Of the former are half and quarter wave line resonators and "in plane" disk resonators. Of the latter are rings, clamped-clamped and clamped-free bars and variations of these such as the tuning fork. The frequency of flexural vibrations dependson the thickness as well as the length and resonators of this form would be much more difficult to manufacture to a standard frequency than the others where the length is the only controlling dimension . On the credit side a feature is that very small resonators of low frequencies can

be made by using the flxural modes of vibrations. Fig.(4.1) shows a variety of resonators from the both types where the vibrations are extensional or flexural.

4.2 CHOICE OF RESONATORS

The detailed factors governing the choice of resonators for the ultrasonic temperature probe are:

a) Frequency of the resonator.

The most convenient frequency for the TTL operation must be considered. In the resonator design a frequency of the order of 100kHz was selected as being a suitable range for the TTL signal processing. Losses in the resonator, due to the internal friction in the material and attenuation in the transmission line are also of the important factors controlling the frequency of the resonator.

b) Coupling "Q" factor of the resonator and the line.

Of the most important parameters governing the degree of coupling are the tuning sensitivity, equation (2.15), and the burst length. The latter is also proportional to the length of the line, therefore the longer the burst length, the higher the Q, and hence the longer the line.

Coupling Q controls the sensor sensitivity and dictates the number of oscillation to the cross-over, equation (2.16).

c) Shape and size of the resonator.

Generally, the size of the resonator decreases with the increasing frequency but, the choice depends on the type of application and environment. In the nuclear case the size of resonator is dictated by the hole size provided by the user. In considering a very small resonator such as the integral

Extensional

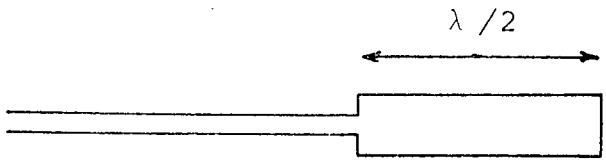

a) Half wave resonator(extensional)

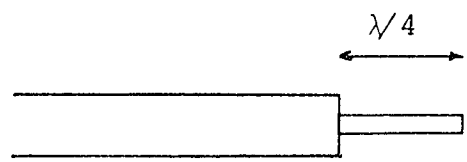

b) Quarter wave resonator

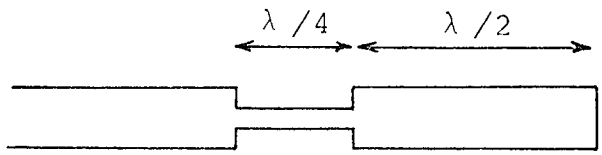

c) Integral half wave with λ/4 coupling transformer

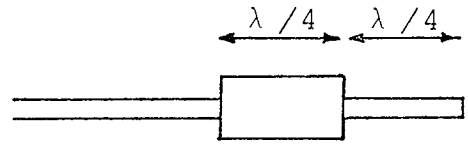

d) "Bell" λ/4 resonator with λ/4 coupling transformer

Flex ural

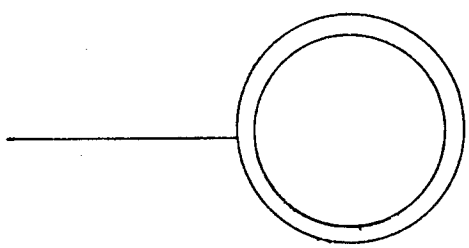

e) In plane ring

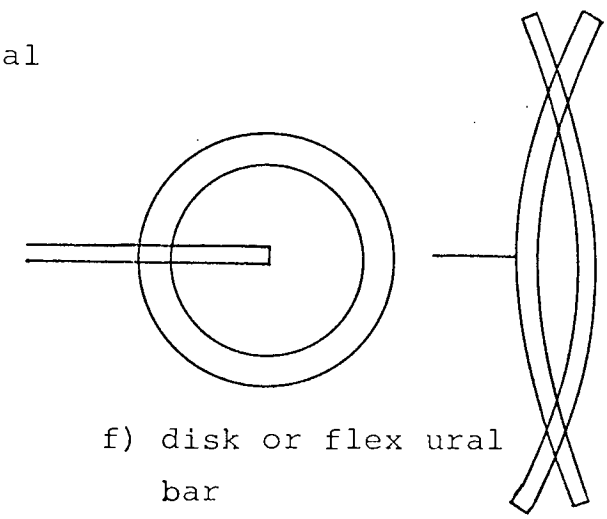

f) disk or flex ural bar

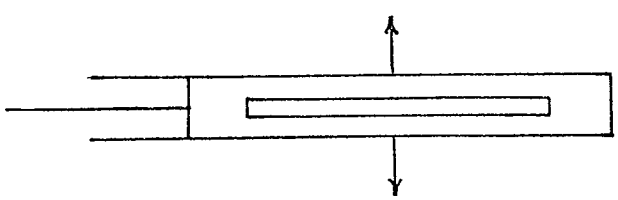

g) Clamped-clamped bar giving dynamic balance

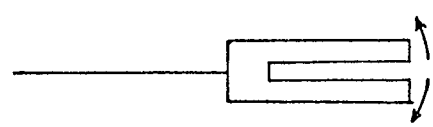

h) Double clamped-free bar as tuning fork

Fig.4.1 Variety of resonators vibrating in extensional or flex ural modes.

tuning fork its advantage over a bulky resonator would be less radiation absorbed, because the absorption of radiation is proportional to the size.

d) Position and nature of the junction between resonator and line

The position of the joint is one of the limiting factors for selection of the temperature sensors. To overcome this problem, the junction must be placed out of the hot region. If this is not convenient, high temperature brazing and soldering materials such as the ceramic solder must be considered. An integral line resonator would be ideal as it avoids making a high temperature joint. Acoustic matching of the joint is also important as a spurious echo may be superposed on the end echo. A small mismatch on the joint simply effects the efficiency at certain frequencies.

e) Types of materials used for the resonator.

There is no limitation on the choice of material for the resonator or line other than dictated by the environment and physical properties associated with the acoustic requirements. Basically low velocity material such as tungsten, presents proportionally a lower frequency, therefore, providing more degrees of freedom to chose convenient dimensions for the resonator. Sufficient high melting point, low material losses, machinability and high thermal shock resistance are of the important factors which must be considered for the physical properties of the sensor materials.

A classification of the typical resonators which can be used as a sensor in temperature measurement applications could be as follows:

1. (a) Half wave length resonator and its variation.

(b) Quarter wave length resonator and its various, e.g. Bell resonator.

2. Disk resonator
3. Ring resonator
4. Bar resonator
5. Tuning fork resonator,
   (a) Based on the rectangular bar,
   (b) Based on the circular bar.

4.3 HALF WAVE LENGTH AND QUARTER WAVE LENGTH RESONATORS

These are the simplest type of all the mechanical resonators and the design parameters can be easily controlled and analysed mathematically. The coupling "Q"factor is proportional to the ratio of the cross-sectional areas of the line and the resonator, while the resonant frequency is a simple function of the resonator's length. The fabrication of the resonator is very simple and the joint between the line and the resonator can be made relatively easily although it must operate at the temperature to be measured. The characteristics of resonators are given in Fig. 4.2 as was reported by Bell[5].

Consider the four resonators separately:

4.3.1 Half Wave Length Resonator

This type of resonator is shown inf Fig. 4.2(a). Considering a typical case of a resonator of frequency 100 KHz and Q-factor of 50 (Pm = 11,number of oscillations to cross-over). The required length of a steel resonator will be 25 mm and if using a 1.5 mm line diameter, the resonator's diameter will be 8.5 mm. These relative size are inconvenient

Table 4.2 Characteristics of half wave length and quarter wave length resonators

No.	Resonator	Frequency	Q	Diameter ratio for Q = 50	Features
a	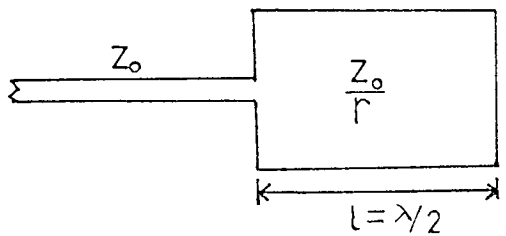	$\frac{m}{2L} \cdot C$	$\frac{\pi}{2r} \cdot m$	5.66	Requires a high temperatur joint
b	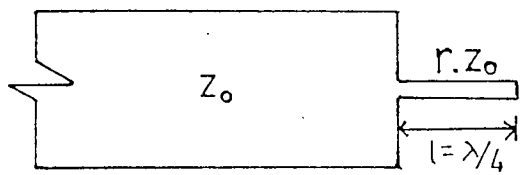	$\frac{(2m-1)}{4L} \cdot C$	$\frac{\pi}{4r} \cdot (2m-1)$	8	Can be made integral with the line
c	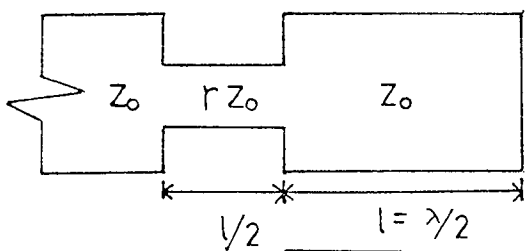	$\frac{m}{2L} \cdot C$	$\frac{\pi}{2r^2} \cdot (2m-1)$	2.4	Requires minim machining and integral with the line
d	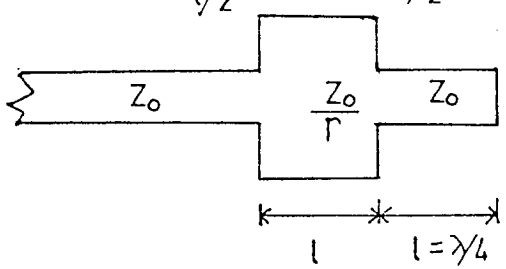	$\frac{(2m-1)}{4L} \cdot C$	$\frac{\pi}{4r^2} \cdot (1+r)(2m-1)$	2.8	Can be supported on a large diameter section

where $r = Z_o/Z_L$ and m is the order of resonance

for many applications and supporting difficulties arises practically.

4.3.2 Quarter Wave Length Resonator

This length of the resonator would be half that of the half wave resonator (12.5 mm), but the diameters ratio (8) is even greater for the same coupling "Q", presenting machining difficulties. As the resonator can be machined from a length of line, the joint can be outside the high temperature region. This type of resonator is suitable to joint with a thick line and hence there would be no supporting problem as the resonator is light and short, Fig. 4.2(b). Only the smallness and consequent machining difficulties prevent the adoption of this design.

4.3.3 Modified Half Wave Length Resonator

Resonator (c) Fig. 4.2 is integral with the line, requires only the minimum of machining and can be joined to the line at any point, ideally at some distance from the high temperature zone. While it is suitable for a thick line, it is still rather fragile. The diameters ratio is much better (2.4), less than the simple half wave resonator, but the length is the same (25 mm).

4.3.4 Modified Quarter Wave Length Resonator - Bell Resonator

This resonator, (d) in Fig. 4.2 consists of a $\lambda/4$ or $3\lambda/4$ length of the tip of the transmission line which is isolated from the rest by a $\lambda/4$ coupling transformer, both machined from the same specimen. This isolator serves as

the coupling unit and presents a serious mismatch except at the resonance frequency. The high impedance coupling section has a low vibration amplitude and may be used to mount the resonator to its supports. The resonator section can be joined to the line at any point but still is in the high temperature region. It is suitable for a thin line. Mechanically it is stronger than the quarter wave length resonator but the resonator's diameter diminishes its practicability. Diameters ratio for the same coupling Q of 50 is 2.8, much less than quarter wave resonator.

4.3.5 Limitations of λ/2 and λ/4 Resonators

The limiting features in all the above resonators are their size, both length and diameters. The thermal response time increases with the size of the resonator. When using a ceramic as a sensor material, the thermal shock resistance is an important parameter which increases as the size is reduced. This aspect is treated in detail in Chapter 8.

These resonators require considerable machining from solid materials and such a procedure is difficult to control. In the case of refractory metals, for example Re can not be machined, only ground, and the grinding away of a relatively large amount of Re would be very uneconomic. Experience with tungsten shows that while the pure material is also difficult to work, the thoriated form is readily machinable.

4.4 DISK RESONATOR

The complex pattern of vibrations in disks and plates

has been known and studied for about two centuries. Their analysis has been attempted by many mathematicians, and while the differential equations are readily derived, the boundary conditions can make certain solutions extremely difficult. In the case of thin disks with planer isotropy , two basic types of vibration can be considered. Flexural and contour extensional (in plane) mode. The simplest case is that of the disk clamped at its edge under no tension. The values of the flexural vibration frequencies are given by Morse[54].

$$f_n = \frac{\pi}{2\sqrt{3}}\left(\frac{h}{a^2}\right) C_p \beta_n^2 \qquad (4.1)$$

where $\beta_1 = 1.015$ and $\beta_2 = 2.007$, etc.

The fundamental frequency is:

$$fo = \frac{\pi}{2\sqrt{3}}\left(\frac{h}{a^2}\right) Cp \qquad (4.2)$$

and the first overtone is four times the resonant frequency ($f_1 = 4fo$).

The constant value from the similitude principle of Rayleigh $\left(\frac{\omega . a}{C}\right)$ is equal to:

$$\omega = 2\pi fo = \frac{2\pi^2}{2\sqrt{3}}\left(\frac{h}{a^2}\right) Cp$$

therefore

$$\frac{\omega\left(\frac{a^2}{h}\right)}{Cp} = \frac{\pi^2}{\sqrt{3}} = 5.7 \qquad (4.3)$$

Where $2h$ = thickness of the disk,

a = radius of the disk,

Cp = the plate velocity = $\sqrt{\frac{E}{\rho(1-\sigma^2)}}$,

E = Young's modulus of elasticity,

σ = Poisson's ratio,

ρ = density.

The second case which was analysed by Kirchoff is a disk free at the edge[55].

The lowest frequency has two nodal diameters and is given by:

$$fo = 0.522\left(\frac{h}{a^2}\right)Cp \qquad (4.4)$$

therefore

$$\frac{\omega\left(\frac{a^2}{h}\right)}{Cp} = 0.522 \times 2\pi = 3.27 \qquad (4.5)$$

The next resonance has one nodal circle and is 1.57 fo. The radius of the nodal circle is given by

$$r = 0.678a \qquad (4.6)$$

4.4.1 The Feature of a Disk Resonator for Temperature Measurement

1) Convenient frequencies and coupling coefficients can be obtained.
2) The joint between the line and the resonator is in the high temperature region.
3) The disk is subjected to higher damping if placed in any fluid due to its shape and flexural vibrations which launch acoustic waves on the fluid.
4) Overtones are close to each other in certain cases, (for example, the free edge disk) and are difficult to discriminate. This effect may be temperature sensitive.
5) The geometrical form alone makes such a temperature probe

impractical for many applications.
However, the disks have been extensively studied by my colleagues Mr. Sharp[50] as a distributed resonator with an arbitrary spectrum of resonances, and Mr. Mahil[53] as a potential transducer for fluid applications.

4.5 RING RESONATOR

Ring and shell resonators have the same practical difficulties similar to those of the disk, therefore are not applicable to high temperature uses. But the only credit point about them is that with a very small size of ring, very low frequencies can be obtained.

4.6 BAR RESONATOR

The vibration of a solid bar or rod are of three kinds, longitudinal, torsional and lateral or flexural. The latter are the most important for this application being the basis of the tuning fork resonator. To analyse the flexural vibration of a bar, it is normally assumed that the vibrating bar is straight and uniform in cross-section. It is also assumed that the amplitude of vibration is so small that the rotary effects can be neglected. With these initial conditions imposed, the analysis of the vibrating bar is well known. Three boundary conditions, clamped-free, free-free, and clamped-clamped are considered.

4.6.1 Clamped-Free Bar (The Vibrating Reed)

The frequencies are given by Morse[54].

$$fn = \frac{\pi}{2}\left(\frac{k}{\ell^2}\right) C_L \beta_n^2 \qquad (4.7)$$

where ℓ = length of the bar,

k = the radius of gyration which is $\frac{2h}{\sqrt{12}}$ for a bar of rectangular cross-section of thickness 2h.

C_L = rod velocity $= \sqrt{\frac{E}{\rho}}$

β_n = factor determining the overtones, the values are given as $\beta_1 = 0.6$, $\beta_2 = 1.5$, $\beta_3 = 2.5$, etc.

Therefore, the fundamental frequency is

$$fo = \frac{\pi x 0.36}{\sqrt{12}} \left(\frac{h}{\ell^2}\right) C_L \qquad (4.8)$$

The first overtone is 6.2 time the fundamental. The fundamental frequency is thus very well isolated.

The expression $\frac{\omega . a}{C}$ for the fundamental frequency is

$$\frac{\omega\left(\frac{\ell^2}{h}\right)}{C_L} = \frac{2\pi^2 x 0.36}{\sqrt{12}} = 2.0 \qquad (4.9)$$

shapes of the first three characteristics functions for a vibrating bar are shown in Fig.4.3.

4.6.2 Free-Free and Clamped-Clamped Bar

The frequencies are the same in both cases, and are given by Morse[54] as equation (4.7). The symbols have the same meaning as before except β_n whose values for the two cases are given by

$$\beta_1 = 1.5, \quad \beta_2 = 2.5, \quad \beta_3 = n+\tfrac{1}{2}.$$

Therefore the fundamental frequency is

$$fo = \frac{\pi x 2.25}{\sqrt{12}} \left(\frac{h}{\ell^2}\right) C_L \qquad (4.10)$$

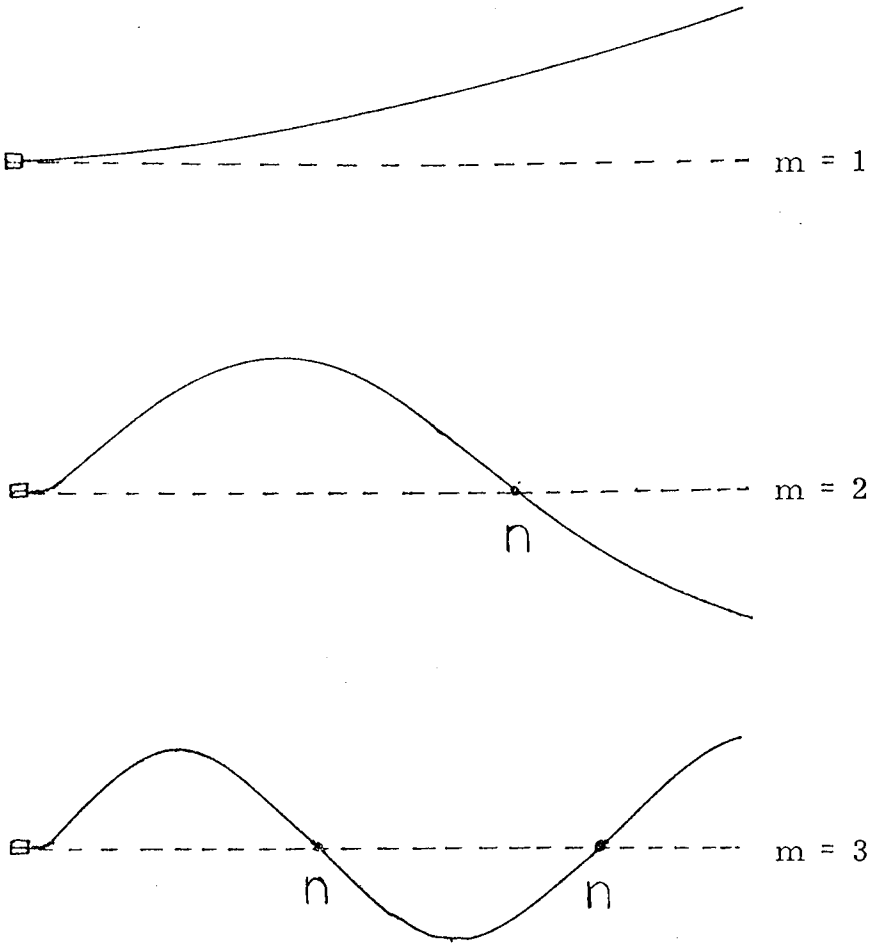

Fig. 4.3 Shapes of the first three characteristic functions for a vibrating Reed
n : node

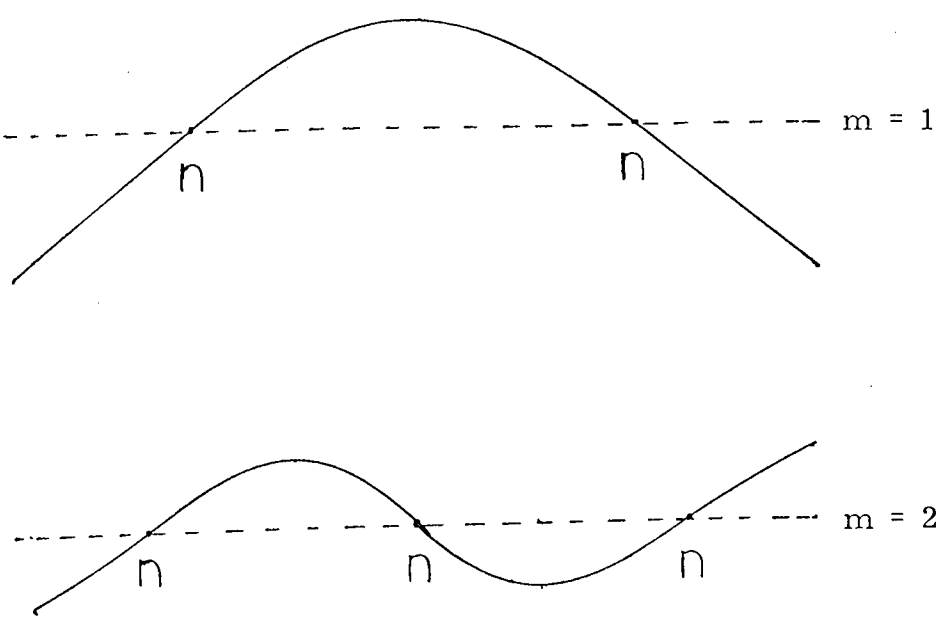

Fig. 4.4 Shapes of the first two characteristic functions for a Free-free Bar
n : node

The first overtone is 2.8 times the fundamental. In this case too, the fundamental is well isolated from the overtones.

The expression $\frac{\omega.a}{C}$ for the fundamental frequency is

$$\frac{\omega\left(\frac{\ell}{h}\right)^2}{C_L} = \frac{2\pi^2 x 2.25}{\sqrt{12}} = 12.8 \qquad (4.11)$$

forms of the characteristic function for a bar free at both ends and for a bar clamped at both ends are shown in Fig. 4.4. The disadvantages of a bar resonator as the temperature sensor are the same as those for disk, namely the size, geometry and the jointing problem.

To summarises, all the flexural vibrators considered are comparatively small for their lowest resonant frequency and with the exception of the free disk there are no adjacent resonances. The clamped-free bar in the form of the tuning fork was chosen for development. The first overtone is particularly remote and the dynamic balance of the tines enable the longitudinal vibrations in the line to be coupled to their flexural vibrations.

4.7 TUNING FORK

4.7.1 Introduction

As the tuning fork is the basis of the integral line temperature sensor its development will be considered in detail.

According to the Rayleigh's[56] description, the later development of tuning fork was due to Koning (1870), who made many forks of a wide range of frequencies. Various concept for the working principle of a tuning fork has been

given by many authors. Rayleigh[56] regards the fork as consisting of "clamped-free" bars mounted on a heavy stiff block of metal. A.B.Wood[55], Lamb[57] and Kinsler and Frey[59] are presenting two views saying Chaldni regarded it as developed from a "free-free" bar by bending in the form of an elongated "U". In this case the nodes are very close to each other and amplitude of vibration at the centre of the bend will be small compared with that at the end of the tines. The circumstances are somewhat modified by the attachment of the stem, but the transmission of energy is comparatively slow, and the vibrations have considerable persistance. "Morse[54] writes" a tuning fork can be considered to be two vibrating bars both clamped at their lower ends. "Stephens and Bate[58] described it as " it is preferable to regard the tine as being equivalent to a straight bar fixed at the stem-end but free at the other end.

4.7.2 Free-Free Bar Concept[55]

Fig.4.5 illustrated forming of a tuning fork from a free-free bar. Bending of a bar is to cause the two nodes of the fundamental tone to approach each other and lower the frequency of vibration.In Fig.4.5(a,b), n, n denotes the nodes and Fig.b shows the form of vibration of such a U shape bar. The addition of stem at the bend has the double effect of adding mass at the antinode and increasing the stiffness of that portion of the fork. This results in a further approach of the nodes towards the stem and a reduction in the amplitude of vibration at this point. If the tip of one tine is lightly touched, the vibration stop in both tines indicating the essential coupling between

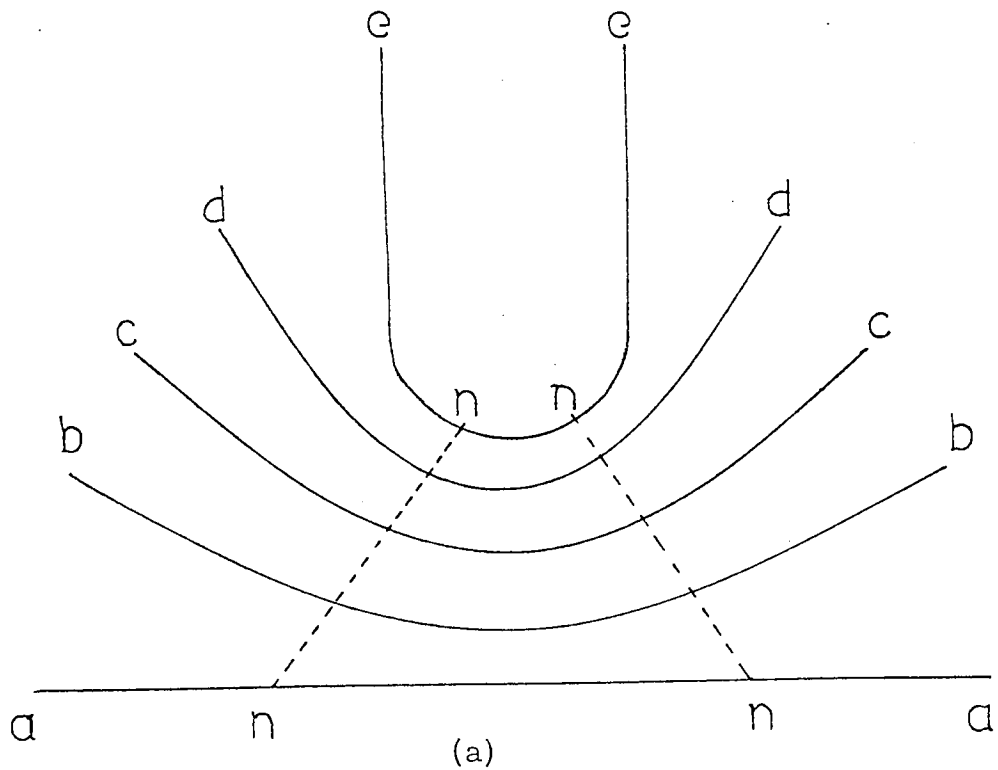

(a)

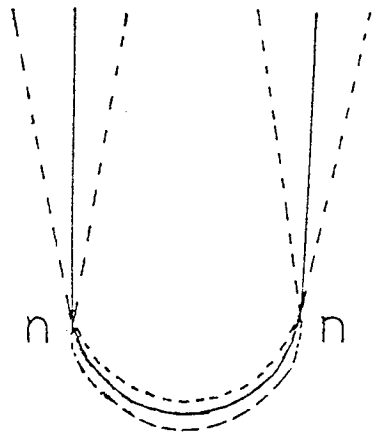

(b)

Fig. 4.5 (a) Successive shapes of a bar bending to a U-shape, n, n the nodes approaching towards centre

(b) Vibration of a U-shaped bar, n, n the nodes

them. This concept gives a good physical picture of the coupling to the longitudinal vibrations at the root of the fork.

4.7.3 Clamped-Free Bar Concept[55]

Regarding the fork as consisting of a pair of symmetrical calmped-free bars, somewhat similar conclusions may be reached in a different manner.

First of all consider a single bar (or tine) clamped to a block of metal. As a consequence of the vibration of its centre of gravity there will be a communication of vibration to the block. To reduce the amplitude of such vibration the block must be firm and massive. If a second exactly similar bar is now attached symmetrically to the block and arranged to vibrate with exactly the same amplitude as the first bar, but in opposite phase, the two reactions on the block will exactly compensate each other and the centre of gravity will be unmoved in the direction in which the tines vibrate. In practice it was found that this essential nature of the fork vibration was present even when the tines were of slightly different dimensions. The frequency of a fork of this construction will be approximate to that of a single reed, the fundamental frequency with fair accuracy is given by equation (4.9).

$$\frac{\omega\left(\frac{\ell^2}{h}\right)}{C_L} = 2.0$$

The parameters are defined in equation (4.7) and the first overtone is given by

$$f_1 = 6.27\ f_o$$

The frequencies of vibration of the tuning forks made in the laboratory correspond closely to that of a reed. Therefore in subsequent discussions the clamped-free bar concept of the tuning fork will be used when considering frequency.

4.8 Development of Tuning Fork as a Temperature Sensing Element

The original tuning fork based on rectangular bar is the simplest type of all the tuning forks and has a familiar feature for many acoustic investigators. The construction of the conventional forks are easy but their resonance frequencies are below 30 kHz and hence their employment has been limited. Fig.4.6 shows a typical geometry of the original tuning fork,

(a) based on rectangular bar and (b) based on circular rod.

It can be seen that they are similar to a conventional fork with the exception that there is no stem attached at the base. An acoustic transmission line from the transducer to the base of the fork acts as an stem for both delivering and extracting the energy.

To increase the fundamental frequency of these tuning forks to above 30 kHz, the dimensions must be proportionally smaller than the previous forks. To overcome this problem, enormous number of these tuning forks has been made from the mild steel bars or rods, by my colleague Dr. Seth[17]. He aimed to find an empirical relationship between the frequencies observed and the effective tine length of the forks. For this purpose, a low frequency fork is taken and its frequency and coupling is measured, the tines are

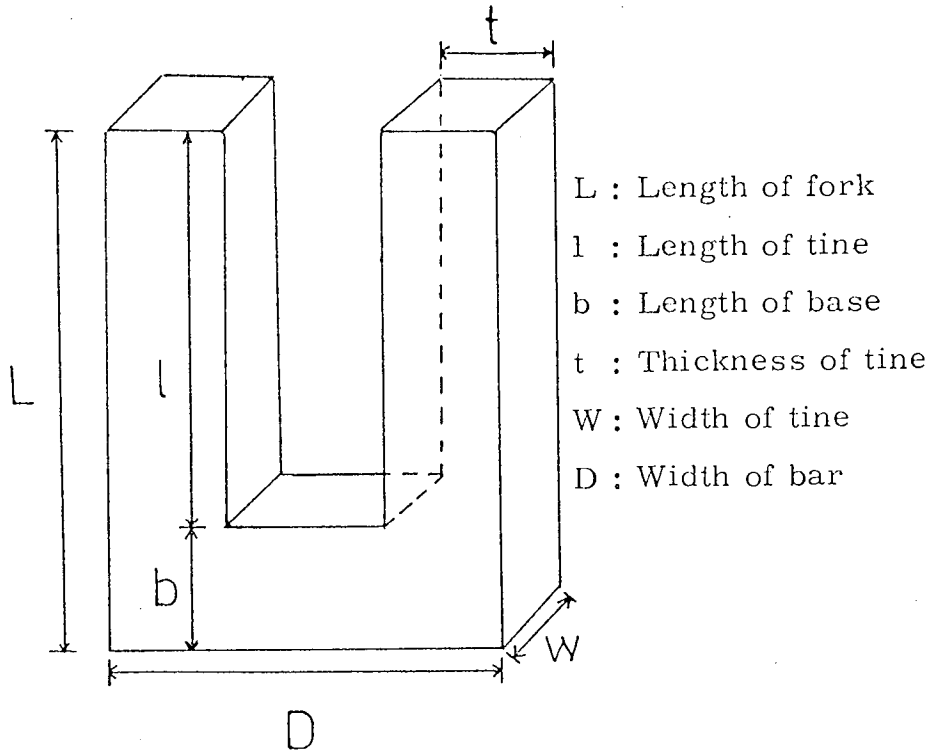

Fig. 4. 6(a)Geometrical form of a Rectangular Tuning Fork

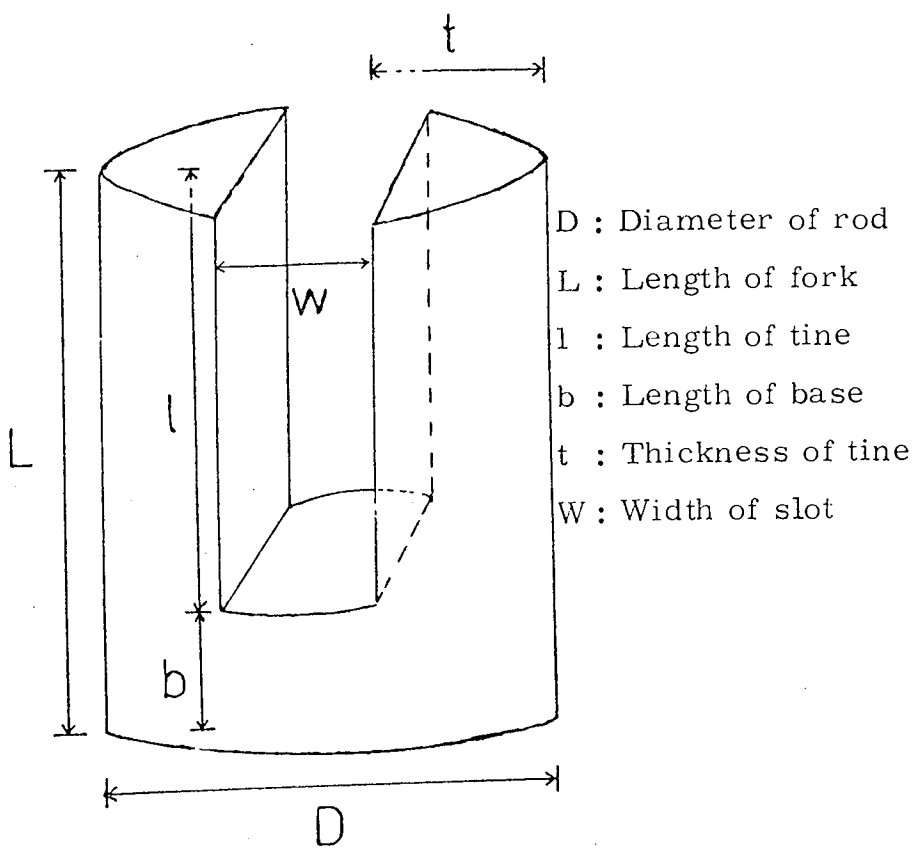

Fig. 4. 6(b)Geometrical form of a Circular Tuning Fork

filed down to give higher frequencies. A plot of L vs $\frac{1}{\sqrt{f}}$ gave a straight line and the intercept on the x-axis gives the effective base length. The frequencies calculated from these dimensions gives only approximate values.

The development of tuning fork of small dimensions was a great success but still the joint between the line and the resonator poses the same problem as in other cases. This was ultimately resolved by the development of a fork which is integral with the line, i.e. it is machined at the end of the line.

4.9 Integral Line Resonator (Seth's Tuning Fork)

After a number of empirical tests a satisfactory integral line resonator was produced by Seth[17]. It was based on a 6.4 mm diameter steel rod or the same width of a strip. The tines vibrate by the transformation of longitudinal to flexural vibrations at the root. A sectional diagram of the probe on a line is shown in Fig.4.7. The mechanism can be visualised by considering the alternating longitudinal force on the axis of the fork. This exerts a mechanical moment on each tine driving them into clamped-free flexural vibration. The characteristic dynamic balance of the fork occurs because of the reverse phase vibration of the tines. Once a geometrical form is obtained, a decrease or increase of the scale raises or lowers the frequency proportionately but the coupling is unchanged. An integral line resonator can be divided into three sections a) Resonator R, b) Coupling section C and c) Lead in line LL.

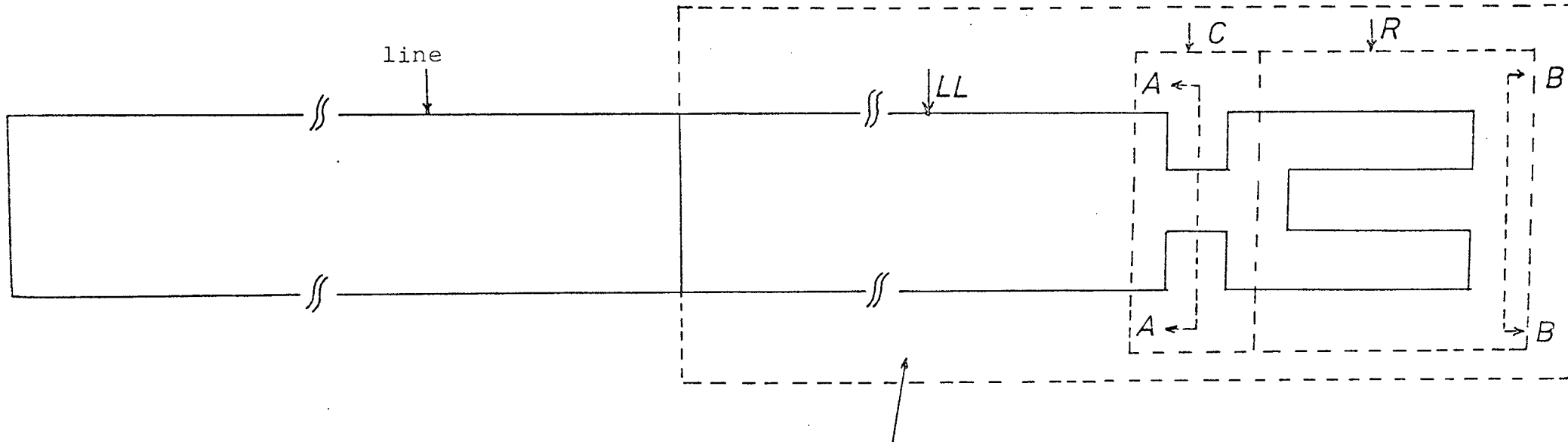

LL: Lead-in line

C : Coupling section(circular cross-section)

R : Resonator

Fig. 4.7 Sectional diagram of an Integral Line Probe on a line

4.9.1 The Resonator

The resonator section, machined at the end of the lead in line, is a circular or strip tuning fork. The frequency is a function of the length of the tuning fork, base length, slot width or tine thickness and also position and the depth of the lateral slots.

4.9.2 The Coupling Section C

In the conventional form the resonator is joined to the end to the lead in line. The coupling Q of the system is a function of the impedance ratio of the lead in line and the resonator. In the integral line probe, however, where the resonator is on the line itself, the coupling is provided by introducing an impedance discontinuity between the lead in line and the resonator. This is achieved by cutting the lateral slots on the lead in line at the end of the resonator section as shown in Fig. 4.7. This coupling section, called the neck of the integral probe, gives a similar coupling as a thin line. The effect of the coupling section on the performance of the integral probe is of the most important and will be discussed later.

4.9.3 Lead-in Line LL

This has the resonator machined at one end and is joined to the main acoustic line at the other end. This joint must be as good match as possible. The joint is kept out of the hot zone and preferably in a water cooled region. The length of the lead-in line is determined by the cost and availability of the probe material discussed in Chapter 8.

Ideally, as in the case of the tungsten probe prepared for the "Petten" experiment, (1.5 mm diameter) the whole line (2 metre length) is of one material.

4.10. Conclusions

The main advantages of the integral line probe over other probes are:

a) small size,

b) no high temperature joint,

c) ease of machining.

The integral line (rod) probe has a few limitations compared with the strip line probe, as following:

1) An integral probe to operate at low frequency with a low coupling "Q" and good mechanical strength cannot be obtained on a small diameter line. Whereas a strip line probe can be designed to achieve a low frequency, a tight coupling along with good mechanical strength.

2) Thermal time constant is a scale phenomenon, the larger the diameter, the longer it takes to reach isothermal conditions. Due to machining difficulties it was not practicable to go much below 3 mm diameter. In the case of the strip probe the thickness controls the time constant and this form gives the best thermal performance.

3) Thermal shock is associated with the thermal time constant, the longer the time constant, the greater will be the thermal gradients and the greater the mechanical stress resulting in low thermal shock resistance. But thin strip

line probe have very high thermal shock resistance, essential if high rates of change of temperature are expected.

4) Most resonators cease to vibrate in a liquid medium because of the acoustic loading. This point became significant when a demand arose for liquid metal measurements. The main advantage of the strip line lies in the maintenance of its "Q" factor when immersed in liquid. A thin molybdenum probe has been used satisfactory in molten lead. Being more flexible it can negotiate bends in the lead in path more easily. Acoustic matching between the strip line and a circular line presents a problem which is dealt with in Appendix (A_1).

Fig.4.8 This photograph shows an Integral Line Probe on 3mm tungsten rod and a Strip Line Probe on 3mm tungsten strip.

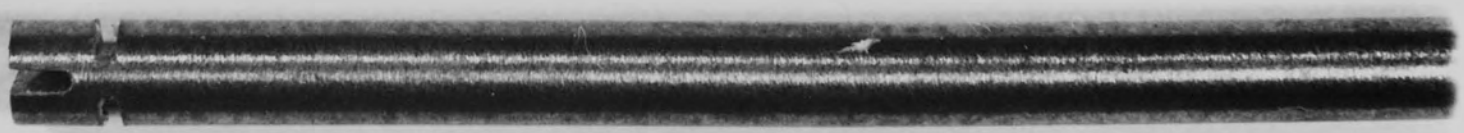

CHAPTER 5

ACOUSTIC PROBE DEVELOPMENT FOR NUCLEAR FUEL ROD THERMOMETRY

5.1 INTRODUCTION

In the previous chapter various types of resonators available to date have been described and their merits and limitations discussed. It was concluded that the integral line tuning fork (circular in cross section area) and the strip line tuning fork (rectangular in cross section area) are the best suited for high temperature applications.

As mentioned before, by development of the integral line probes the joining problem of the line and the resonator was automatically solved and apart from some particular applications such as the nuclear fuel rod thermometry they were extremely reliable without any limitations.

Facilities for an experiment in the Euratom (Petten) reactor were offered. A major problem was the 2 mm standard instrumentation holes available, our probes being based on 3 mm rods. Simply to reduce the size to 1½ mm without further fork design would double the frequency and drastically reduce the performance of the electronics.

It was therefore decided to redesign the resonator, attempting to obtain the 100 kHz frequency and adequate coupling.

This problem was ultimately solved when the recent temperature sensor was developed. It is a tuning fork integral with a 1½ mm line maintaining a frequency of no more than 100 kHz and achieving tight coupling by a new design of coupling section.

To discuss this development, it is essential that the effects of all the geometrical dimensions of the previous integral line on its preformance be known. For this purpose in the early part of this chapter the characteristics of the former resonators will be considered in detail.

5.2 INTEGRAL LINE RESONATOR

The development of the integral line and strip line resonators (Seth's Tuning Fork) were described in the Chapter 4. They were regarded to be formed by combinations of the three main sections as: The resonator section, the coupling section and the lead-in line section which are shown in Fig. 5.1.

To study about the effective parameters which controlling the performances of the frequency and coupling Q, a large number of integral line probes, named TI-X and strip line probes, named TIS-X were made of various materials and the results will classify below.

5.3 EXPERIMENTAL WORK

As it is shown in Fig.5.1 the resonator's parameters governing the frequency and coupling of the integral line and strip line probes are:

1 - ℓ : length of tine,

2 - b : length of base,

3 - t : thickness of tine,

4 - W_s: width of longitudinal slot,

5 - N_t: thickness of neck,

6 - W_n: width of neck or width of transverse slot.

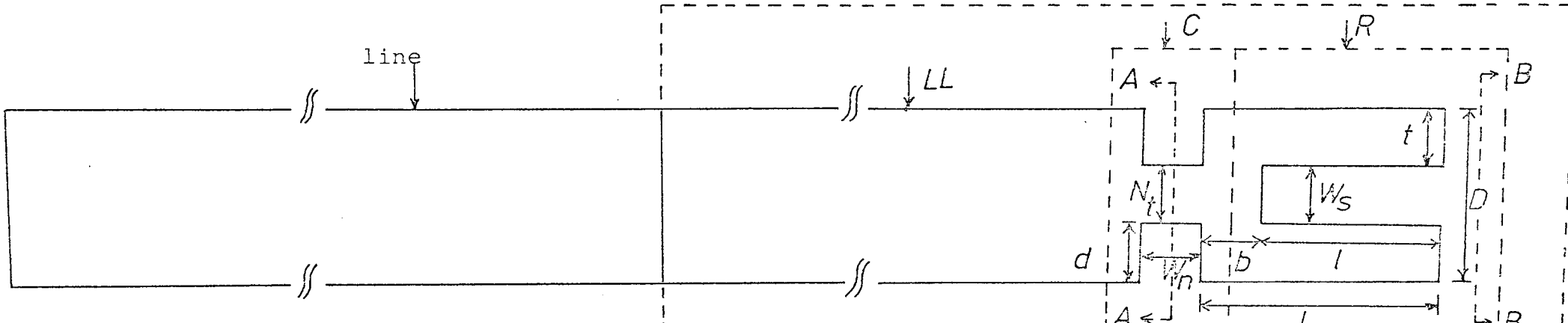

LL: Lead-in line

C : Coupling section(circular cross-section)

R :Resonator

D :Diameter of the rod

L :Length of the fork

l :Length of the tine

b :Length of the base

t :Thickness of the tine

W_s :Width of the longitudinal slot

W_n :Width of the neck

N_t :Neck thickness

d :Depth of the neck

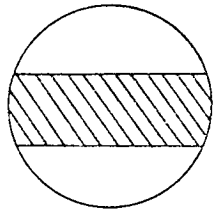
Section-AA

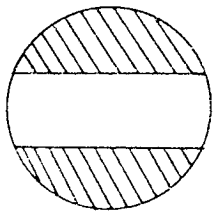
Section-BB

Fig.5.1 Sectional diagram of an Integral Line Probe on a line

Items 1, 2, 3 and 4 are major factors in determining the frequency and items 2, 4, 5 and 6 determine the degree of coupling. To investigate the effect of these parameters separately, following experiments have been done.

5.3.1. Effect of Tine Length on Frequency and Coupling

Precision measurements were carried out on a 3.10 mm thick molybdenum strip, to investigate the effect of tine length and hence the fork length on frequency and coupling. The results were expressed in two forms f and Pm as a function of ℓ and Pm against f as shown in Fig.5.2(a) and (b).

The intial dimensions of this probe (TIS-1) were: ℓ = 2.60 mm, b = 1.0 mm, W_s = 0.9 mm, N_t = 1.10 mm, W_n = 1.0 mm, t = 1.10 mm. See Fig. 5.3. The results are given in Table 5.1.

Table 5.1

ℓ	f	Pm	Q
2.60 mm	67 kHz	15	68
2.45	71.5	14	64
2.30	76.0	12	55
2.0	89.8	8	36
1.80	102.7	6	27
1.60	112.6	5	23

5.3.2 Effect of Base Length on Frequency and Coupling

Observations were made for various base length b, resulting in change of tine length ℓ, keeping other parameters the same.

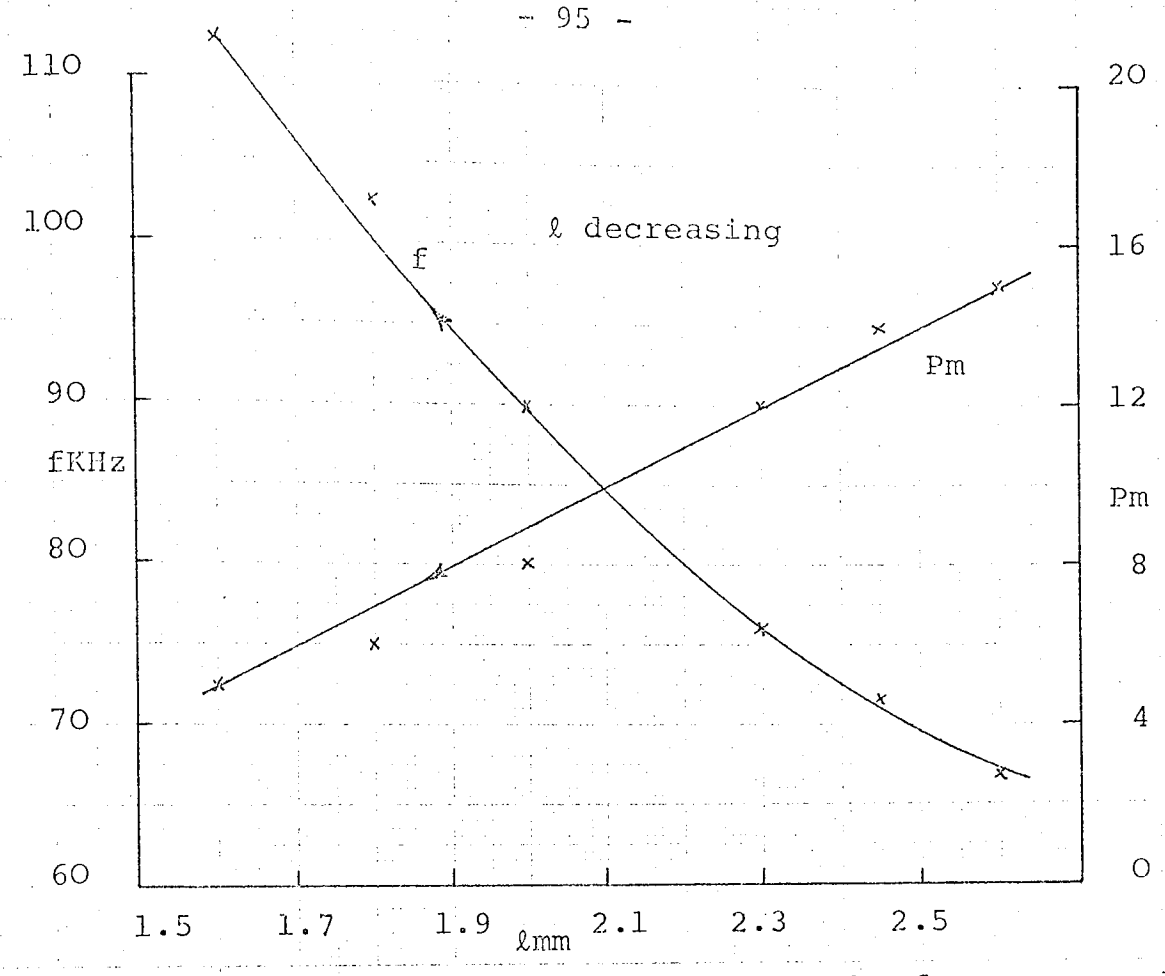

Fig.5.2(a) Effect of the tine length on the frequency and Q-factor, in terms of Pm of an integral line resonator.

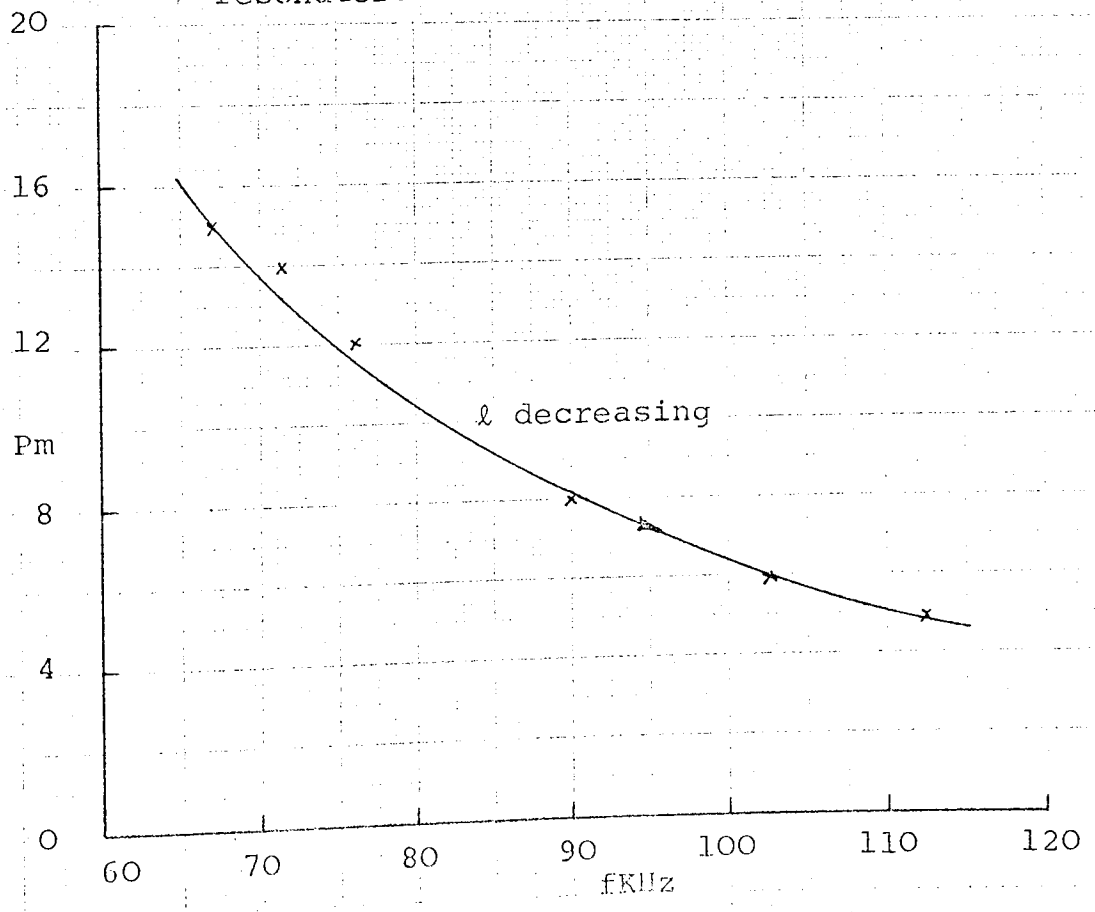

Fig.5.2(b) Variation of Q-factor with frequency of the resonator for decreasing tine length.

The variation of f and Pm with base length and Pm against f are shown in Fig.5.4 (a) and (b). From the latter curve the difficulty of achieving low Pm at low frequency is very apparent, all values of b however gives acceptable values of Pm.

The initial dimensions of the probe (TIS-2) were:

ℓ = 1.40 mm, b = 1.0 mm, W_s = 0.9 mm, N_t = 1.10 mm, W_n = 1.0 mm, t = 1.10 mm.

The results are given in Table 5.2.

Table 5.2

b	f	Pm	Q
1.0 mm	122.0 KHz	2	9
0.9	105.8	3	14
0.8	87.5	3	14
0.65	81.3	4	19
0.55	69.5	5	22
0.40	66.5	8	36
0.30	61.0	10	45

5.3.3 Effect of Slot Width (W_s) on Frequency and Coupling

Another set of experiments were performed to investigate the effect of longitudinal slot width on the probe performance. The results are given in Table 5.3.A variation of f and Pm with W_s and Pm against f is shown in Fig. 5.5 (a) and (b).

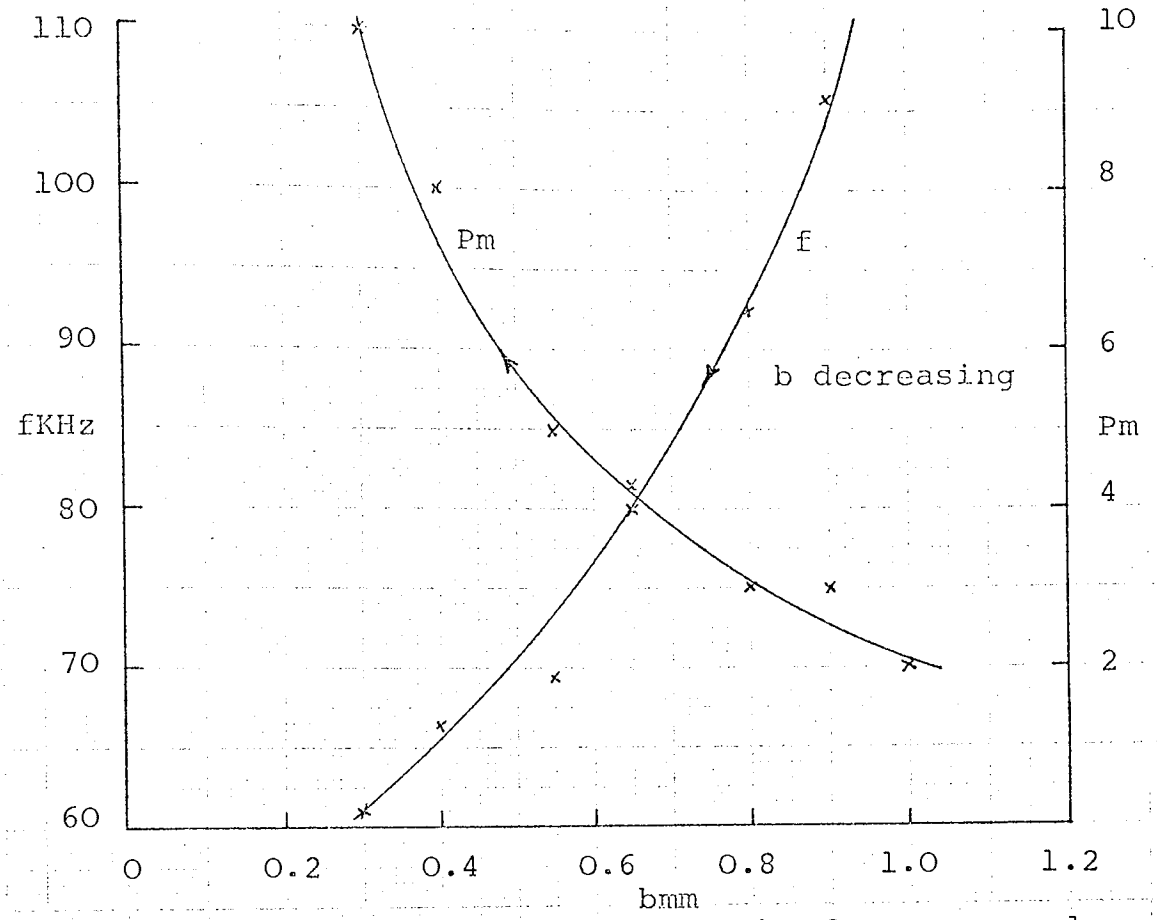

Fig.5.4(a) Effect of base length on the frequency and Q-factor of an integral line resonator.

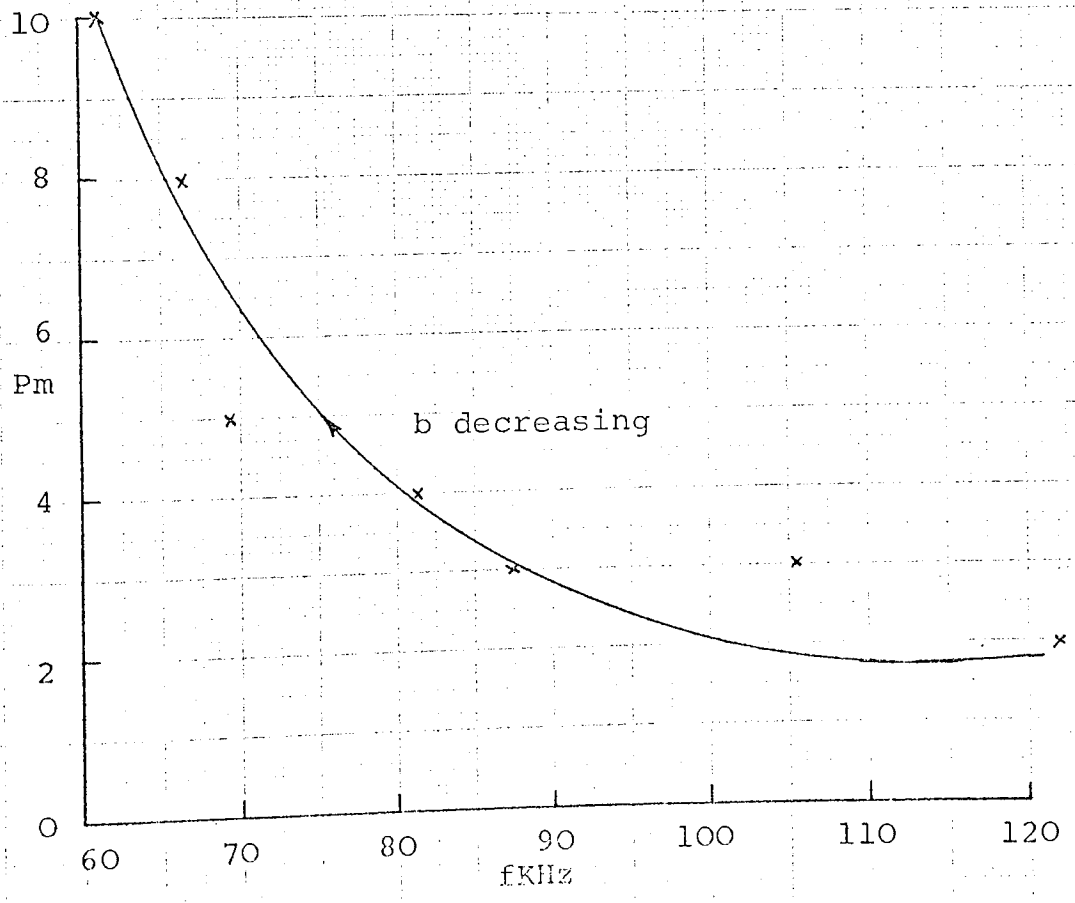

Fig.5.4(b) Variation of Q-factor with frequency for decreasing base length.

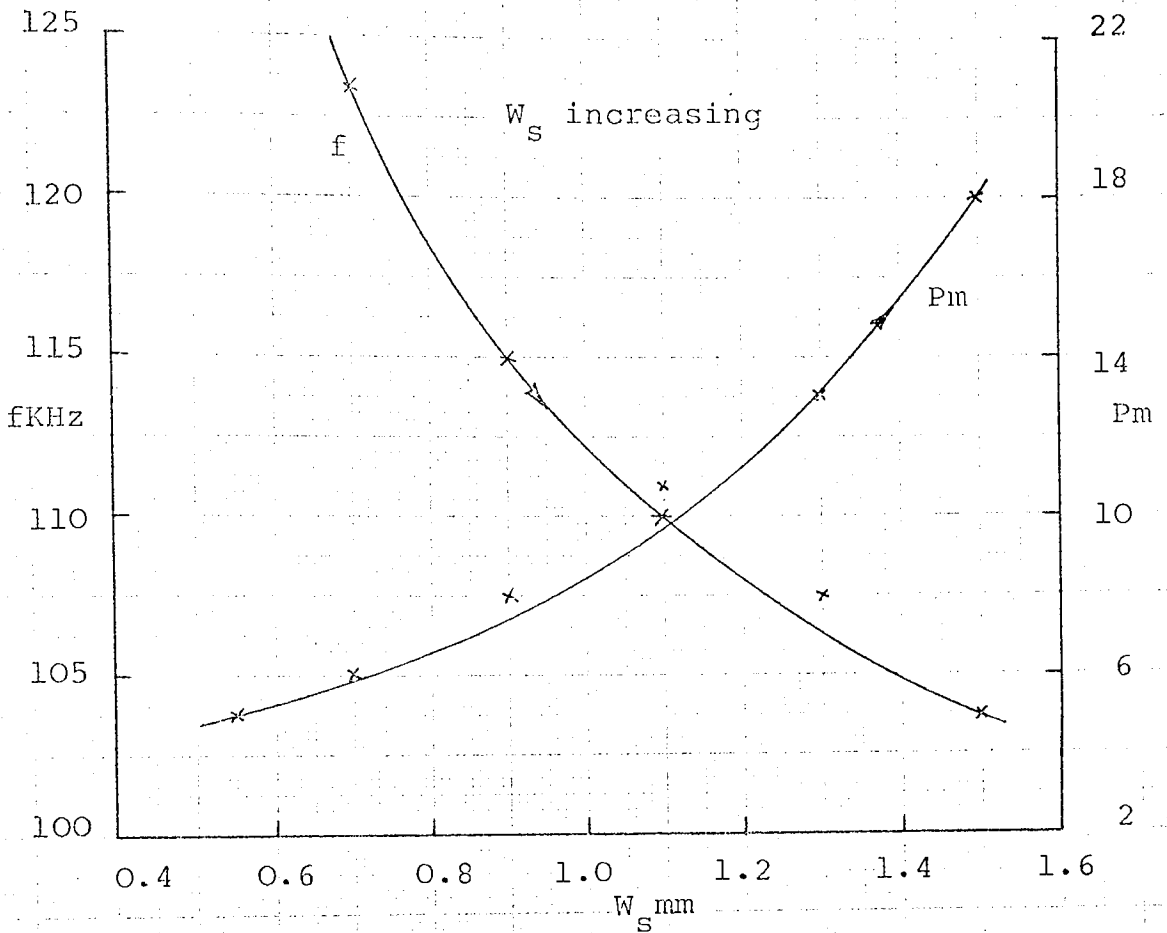

Fig.5.5(a) Effect of a longitudinal slot width on the frequency and Q-factor of an integral line resonator.

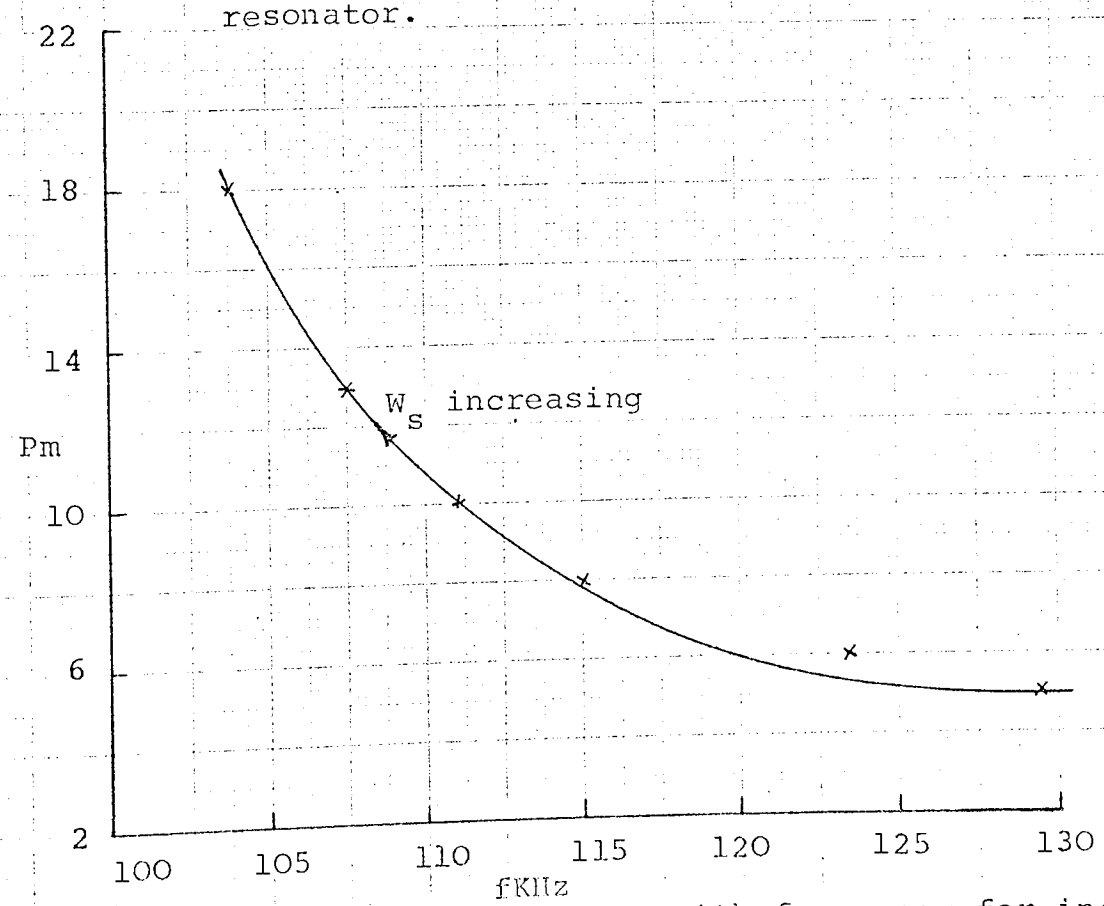

Fig.5.5(b) Variation of Q-factor with frequency for increasing longitudinal slot width.

Table 5.3

W_s	f	Pm	Q
0.55 mm	129.5 KHz	5	23
0.70	123.5	6	27
0.90	115.0	8	36
1.10	111.0	10	45
1.30	107.5	13	59
1.50	103.7	18	82

The intial dimensions of the probe (TIS-3), as shown in Fig. 5.6 were:

ℓ = 1.80 mm, b = 1.20 mm, W_s = 0.55 mm, N_t = 1.40 mm, W_n = 1.20 mm, t = 1.30 mm.

Large value of W_s are not acceptable from the point of view of both coupling and mechanical strength. These results all show the difficulty of obtaining low frequency and good coupling.

5.3.4 Effect of Neck Depth or Neck Thickness (N_t) on the Probe Performance

An experiment was performed by increasing the neck depth d,i.e. decreasing the neck thickness N_t. Results are given in Table 5.4. A variation of f and Pm with N_t and Pm against f is shown in Fig. 5.7 (a) and (b).

The table shows that the effect is very complex. Understandably, the coupling is loose for very thick and very thin necks. Unexpected effects occurred at intermediate values where there were indications of internal friction. There is also a decrease in the frequency as the thickness N_t is

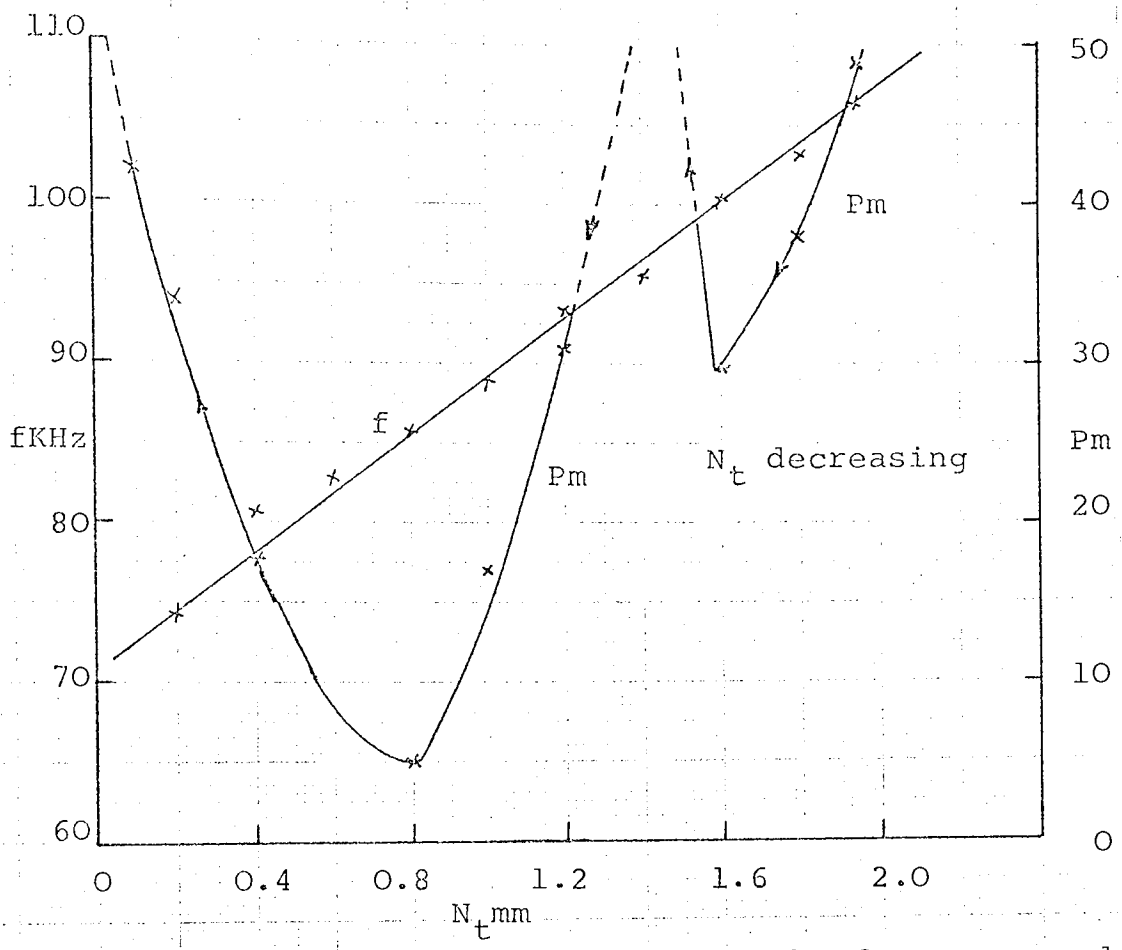

Fig.5.7(a) Effect of neck thickness on the frequency and Q-factor of an integral line resonator.

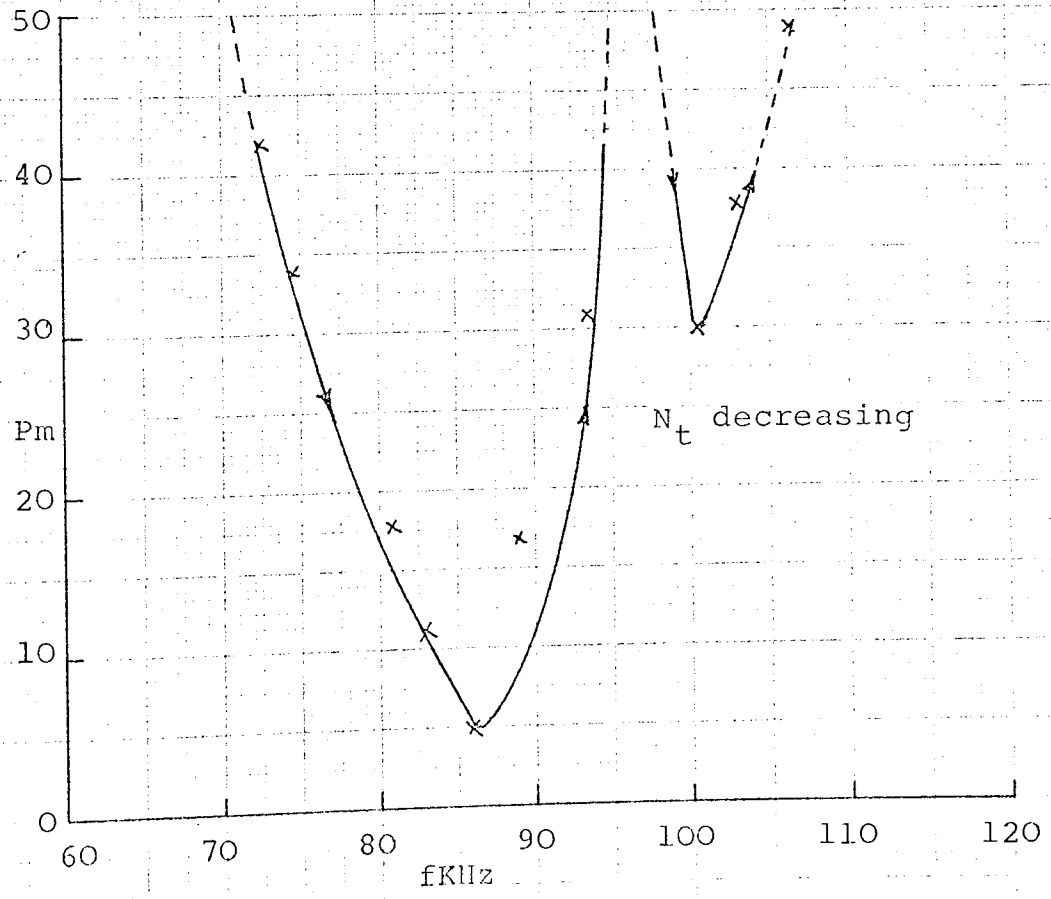

Fig.5.7(b) Variation of Q-factor with frequency for decreasing neck thickness.

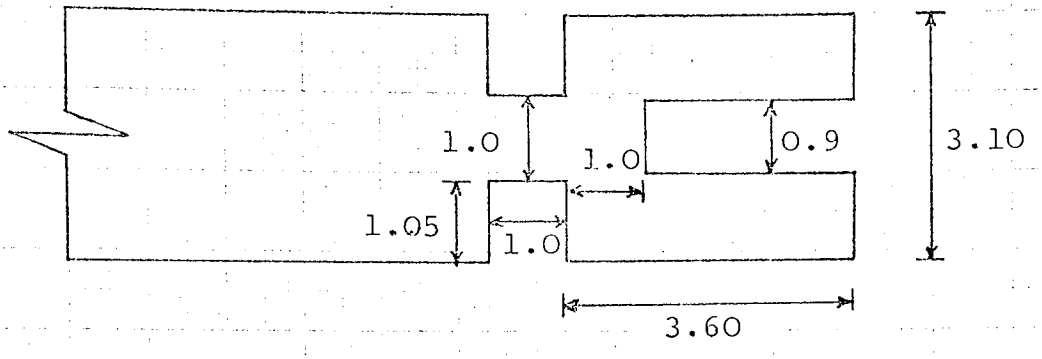

Fig. 5.3 Type (TIS-1)

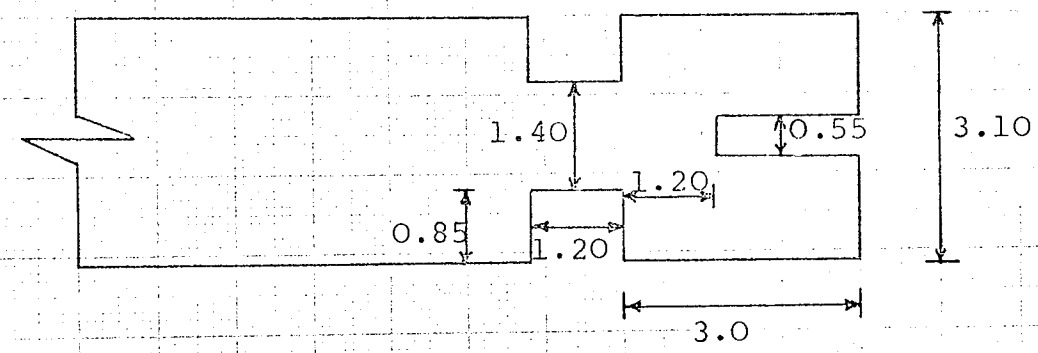

Fig. 5.6 Type (TIS-3)

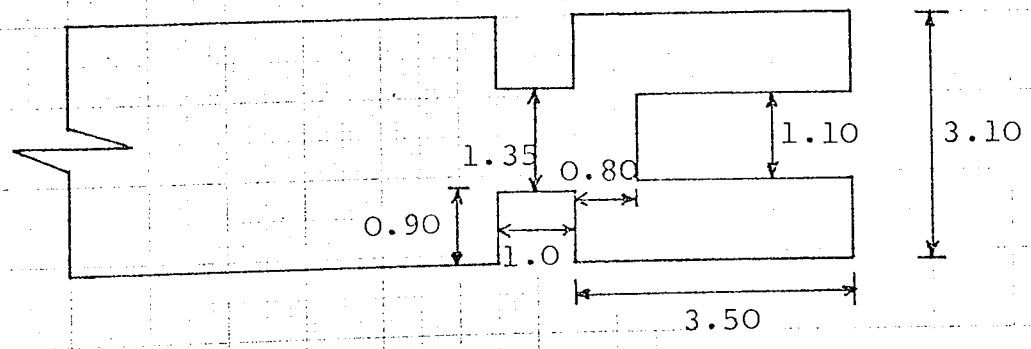

Fig. 5.8 Type (TIS-5)

Dimensional diagram of the three strip line probes on 3.10 mm molybdenum.

reduced, this is attributed to the reduction in the stiffness at the stem of the resonators. The initial dimensions of the probe (TIS-4) were:

ℓ = 2.0 mm, b = 0.75 mm, W_s = 0.9 mm, N_t = 1.95 mm, W_n = 1.0 mm, t = 1.10 mm.

Table 5.4

N_t	f	Pm	Q
1.95 mm	106.5 KHz	49	223
1.80	103.0	38	173
1.60	100.6	30	136
1.40	95.7	large	large
1.20	93.5	31	141
1.0	89.0	17	77
0.80	85.8	5	23
0.60	83	11	50
0.40	80.8	18	82
0.20	74.5	34	155
0.10	72.5	42	191

If considering the results of all the sets of experiments, it will be apparent that the frequency and coupling are dependent to various degrees on all the design parameters. There is a strong interaction between the frequency and coupling for all the cases and achievment of resonators having low frequencies and tight coupling is not possible. The only design parameter still to be tested, proved to be overridingly effective on the coupling. This is the Width of Neck (W_n). Variation of this parameter showed a very encouraging result.

The investigation finally led to the development of the new tuning fork which presents low frequency and tight coupling together.

5.3.5. Effect of Neck Width (W_n) on Frequency and Coupling

Experiments were performed to investigate the effect of the Neck Width (W_n) on the performance of the resonator. A 3.10 mm thick molybdenum strip line resonator (TIS-5) of Fig. 5.8 was used and the results expressed in form of f and Pm as function of W_n as shown in Fig.5.9.

The initial dimensions were:

ℓ = 2.70 mm, b = 0.8 mm, W_s = 1.10 mm, N_t = 1.35 mm, W_n = 1.0 mm, t = 1.10 mm.

and the results are given in Table 5.5.

Table 5.5

W_n	f	Pm	Q
1.0 mm	63.7 KHz	20	90
1.30	63.9	18	82
1.60	63.9	16	73
2.50	63.9	14	64
3.25	63.7	12	55
4.10	63.6	12	55
4.65	63.4	11	50
5.50	63.2	10	45
6.40	63.1	9	41
7.40	63.0	8	36
8.70	62.9	7	32
9.80	62.6	5	23

Table 5.5 contd.

W_n	f	Pm	Q
11.35 mm	62.5 KHz	4	18
12.20	62.1	3	13
13.10	60.8	3	13
14.50	63.1	3	13
16.0	63.9	3	13
17.35	64.9	3	13
18.80	65.8	4	18
20.30	65.8	5	23
21.60	65.5	6	27
22.50	65.2	7	32
23.70	64.9	8	36
25.40	64.9	10	45
26.70	64.7	13	59
28.0	64.7	14	64
29.4	64.5	15	68
30.0	64.2	16	73
30.7	64.1	18	82

The results give a very effective control of coupling with little effect on frequency. By increasing the value of the Neck Width (W_n), the amount of the stiffness is reduced and hence tighter coupling is achieved. When the value of the Neck Width approaches a quarter wave length, the coupling Q reaches to its lowest value. As the Neck Width is further increased the coupling becomes looser and presumably is a minimum at $\lambda/2$. The fluctuatuion of the frequency in whole range of the Neck Width is very small, therefore at quarter wave length of the Neck Width the best

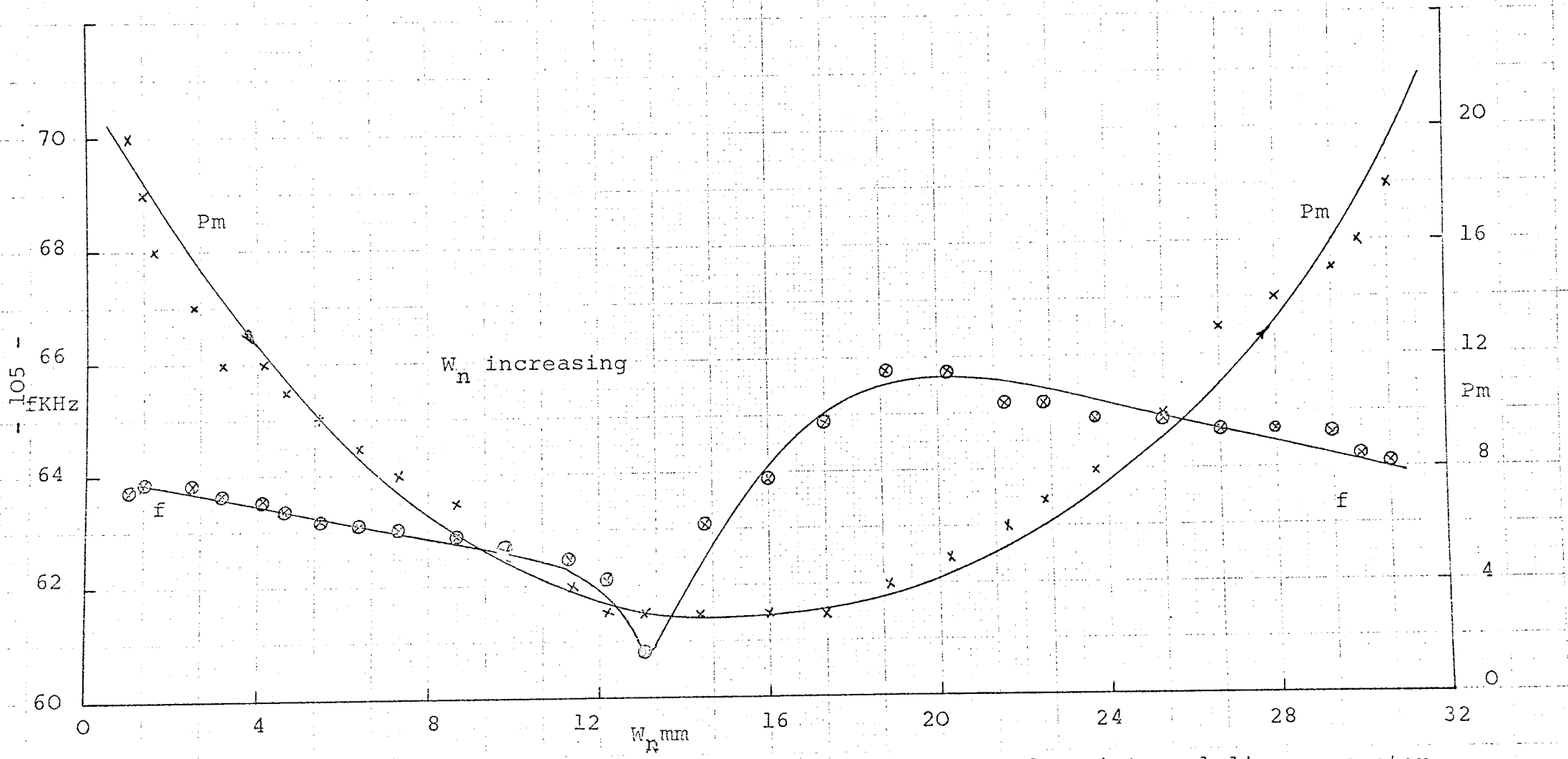

Fig.5.9 Effect of the neck width on the frequency and Q-factor of an integral line resonator.

values of frequency and coupling can be obtained.

5.4 DEVELOPMENT OF NEW INTEGRAL LINE RESONATOR

After a number of empirical tests a satisfactory integral line resonator was produced. It was based on a 1.5 mm diameter steel rod. A sectional diagram of the probe on a line is shown in Fig. 5.10.

From the figure it is apparent that it is a development from the circular rod tuning fork. The integral line resonator could be divided in to three sections as: 1) Resonator Section R, 2) Coupling Section C, 3) Lead-in Line LL.

5.4.1 Resonator Section R

The resonator is machined at the end of the lead-in line having a semi circular cross section (*BB*); shown in Fig. 5.10.

The frequency of the resonator is, as before, a function of the length of the tuning fork, base length, slot width or tine thickness, and finally the neck width.

5.4.2 Coupling Section C

The coupling Q of the system is a function of the impedance ratio of the lead-in line and the resonator. In the integral line probe, where the resonator is on the line itself, the coupling is provided by introducing an impedance discontinuity between the lead-in line and the resonator.

In the recent design this was achieved by taking two semi-circular sections off the lead-in line, at the end of the resonator section and making a rectangular cross

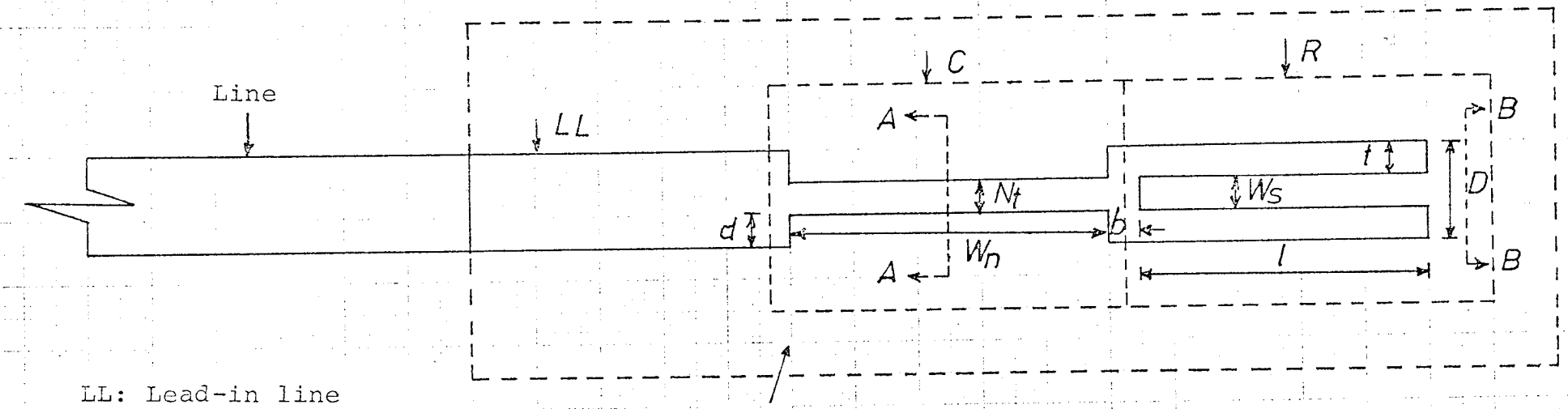

LL: Lead-in line

C : Coupling section
(Rectangular cross-section)

R : Resonator

D : Diameter of the rod

l : Length of the tine

b : Length of the base

t : Thickness of the tine

W_S: Width of the longitudinal slot

W_n: Width of the neck = Quarter wave length

d : Depth of the neck

N_t: Neck thickness.

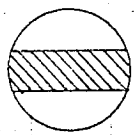

Section -AA

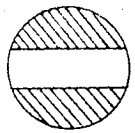

Section - BB

Fig. 5.10 Sectional diagram of an Integral Line Probe on a Line.

section (AA), as shown in Fig. 5.10. This coupling section, called the neck of the integral line probe, is the most effective design parameter and is highly dependent on the neck width of the resonator. If the neck width is properly calculated and machined, resonators of very low frequencies and tight coupling can be obtained as will be discussed later in this chapter.

5.4.3 Lead-in Line LL

This has the resonator machined at one end and is joined to the main acoustic line at the other end. The joint must be as good a match as possible and also far from the hot region. In the recent probe design, where a 2 m long tungsten line is used, the problem of impedance matching with the launcher unit was overcome and no problem arising from the hot region occurred. The type of suitable materials for the integral line resonator and also their physical and metallurgical properties will be discussed in Chapter 8 of this thesis.

5.5 EXPERIMENTAL WORK

After satisfactory results which were obtained from the experiments on 3.1 mm molybdenum strip line and attainment of the new integral line resonator, a large number of experiments were continued particularly on 2 mm and 1.5 mm diameter steel rod, where the attention was drawn to find the best dimensions for the resonator performance.

In the following the experiments are described in the

details.

5.5.1 Effect of the Neck Width (W_n) on 3 mm Steel Integral Line Resonator

An experiment was performed to ascertain the effect of the Neck Width (W_n) on a 3 mm diameter steel integral line resonator (TI-1).

The results are in the form of Pm as a function of W_n as shown in Fig. 5.11.

The initial dimensions of the probe as shown in Fig. 5.12 were:

ℓ = 3.0 mm, b = 0.75 mm, W_s = 0.60 mm, W_n = 8.20 mm, N_t = 0.90 mm, t = 1.25 mm.

The results are given in Table 5.6.

Table 5.6

W_n	f	Pm	Q
8.20 mm	53.7 kHz	16	73
9.0	53.5	15	68
9.80	53.4	13	59
10.70	53.1	11	50
11.30	52.9	9	41
12.10	52.8	8	36
12.40	52.88	8	36
13.30	52.91	7	32
14.35	53.0	6	27
15.0	53.1	6	27
16.20	53.4	6	27
16.80	53.70	8	36
17.90	53.80	11	50

Table 5.6 contd.

W_n	f	Pm	Q
18.60 mm	53.88 kHz	13	59
19.20	53.85	15	68
20	53.80	16	73

This result was proved the previous discussions of the similar experiment for 3.1 mm molybdenum strip. Again, the coupling Q between the resonator and the line presents its lowest value at the quarter wave length and gets loose for the values beyond that.

5.5.2 Effect of the Neck Width (W_n) on 2.0 mm Steel Integral Line Resonator

The results of the 3 mm steel rod series being satisfactory, it was decided to proceed to resonators of the smaller diameter. For this purpose, another set of experiments were arranged to confirm the effect of the Neck Width on the frequency and coupling of 2.0 mm steel integral line resonator.

The results, as before, are shown in the form of Pm as a function of W_n and shown in Fig. 5.13.

The initial dimensions of the probe (TI-2) as shown in Fig. 5.14 were:

ℓ = 6.0 mm, b = 0.15 mm, W_s = 0.85 mm, N_t = 0.9 mm, W_n = 7.5 mm, t = 0.55 mm.

The results are given in Table 5.7.

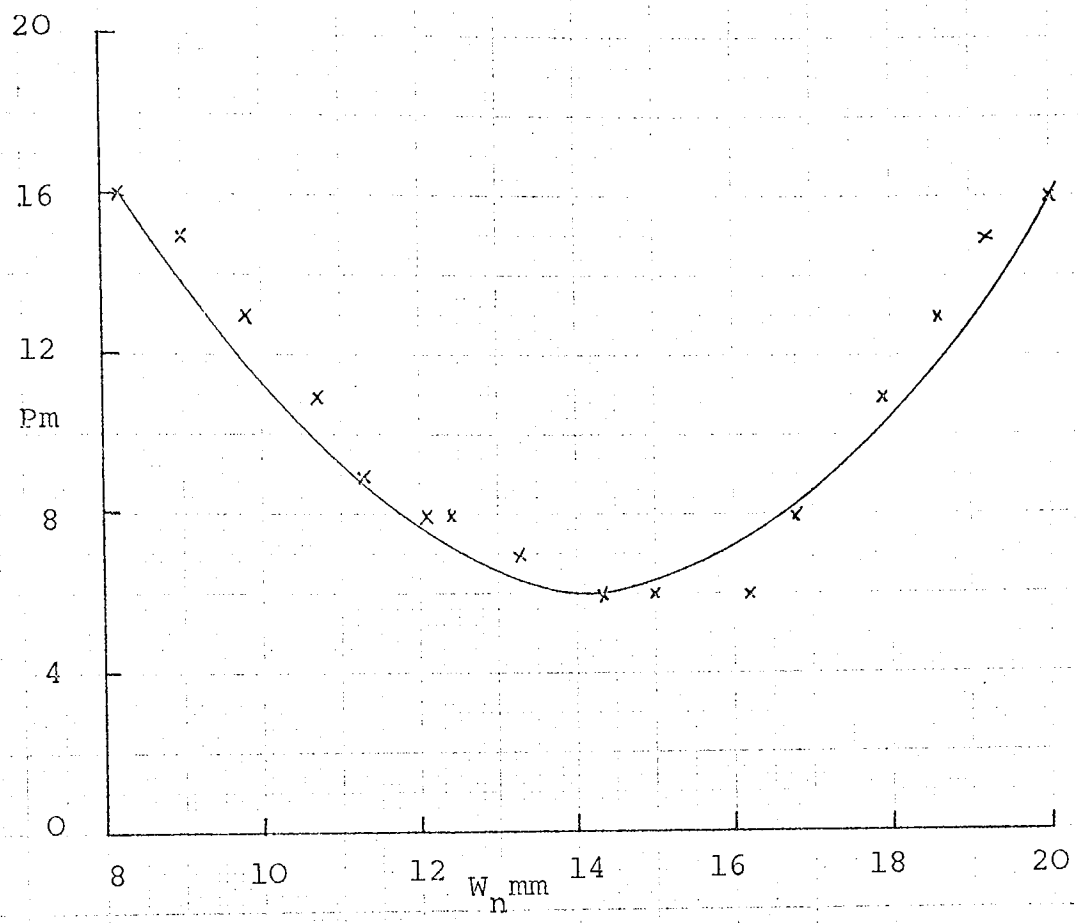

Fig.5.11 Effect of the neck width on Q-factor of an 3mm integral line resonator.

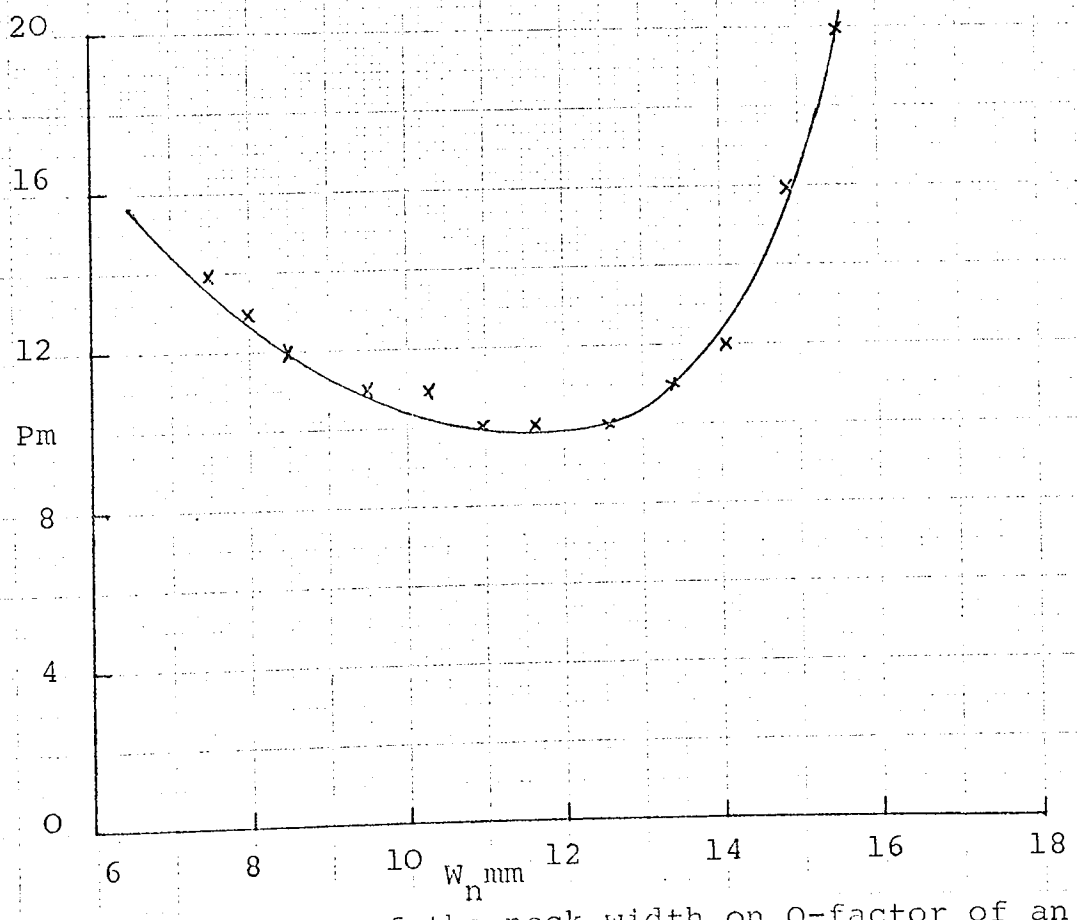

Fig.5.13 Effect of the neck width on Q-factor of an 2mm line resonator.

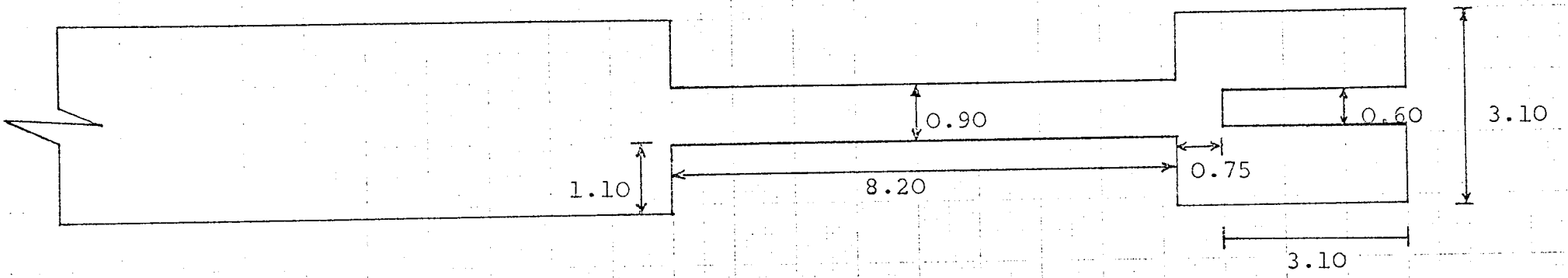

Fig. 5.12 Dimensional diagram of an integral line resonator type (TI-1) on 3 mm steel rod.

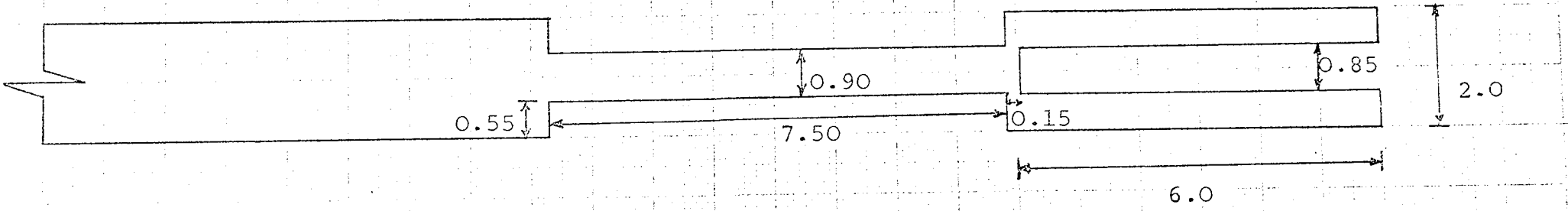

Fig. 5.14 Dimensional diagram of an integral line resonator type (TI-2) on 2 mm steel rod.

Table 5.7

W_n	f	Pm	Q
7.50 mm	67.0 kHz	14	64
8.0	66.8	13	59
8.50	66.7	12	55
9.50	66.7	11	50
10.30	66.8	11	50
11.0	67.1	10	45
11.60	67.1	10	45
12.60	67.3	10	45
13.40	67.4	11	50
14.10	67.3	12	55
14.90	67.2	16	73
15.50	67.1	20	91

comparison of the results of the two recent experiments, the effect of the neck width on 3 mm and 2 mm steel integral line resonator (Figs. 5.11 and 5.13), showed that this design parameter has identical effects on both resonators performances irrespective to the probe diameter.

As a consequence, minimum coupling Q between the resonator and the lead-in line will be achieved at the quarter wave length of the neck width of the resonator.

5.5.3 Effect of the Neck Thickness (N_t) on 2.0 mm steel Integral Line Resonator

In this stage, to complete the development of the new coupling section and to take full advantage of the design, the thickness of this section was considered. The neck thickness (N_t) is a sensitive design parameter for both mechanical

strength and coupling factor, therefore its investigation is very important.

For this purpose, two sets of experiments were performed to study the effect of Neck Thickness (N_t) on the frequency and coupling of the two integral line resonators, made on 2 mm steel rods.

Resonators have different dimensions, hence different performances. The results were expressed in the form of the Pm as a function of N_t and were shown in Fig. 5.15 for both resonators.

The initial values as shown in Fig. 5.16 (a) and (b) were:

Resonator a) (TI-3) ℓ = 5.50 mm, b = 0.1 mm, W_s = 0.80 mm, W_n = 8.40 mm, N_t = 0.85 mm,

Resonator b) (TI-4) ℓ = 5.10 mm, b = 0.3 mm, W_s = 0.75 mm, W_n = 3.50 mm, N_t = 0.75 mm,

The results are given in Table 5.8 (a) and (b)

Table 5.8(a)

N_t	f	Pm
0.85 mm	68.1 kHz	12
0.82	67.7	11
0.77	67.6	10
0.68	67.1	8
0.63	65.6	6
0.53	66.6	5
0.45	66.6	3

Table 5.8(b)

N_t	f	Pm
0.75 mm	85.7 kHz	14
0.70	85.2	13
0.60	84.8	11
0.50	84.7	10
0.45	84.3	8
0.40	84.1	6
0.35	84.0	5
0.30	83.6	4
0.25	83.6	3

The results for both resonators (Fig. 5.15) are quite identical and showed that reducing the neck thickness of

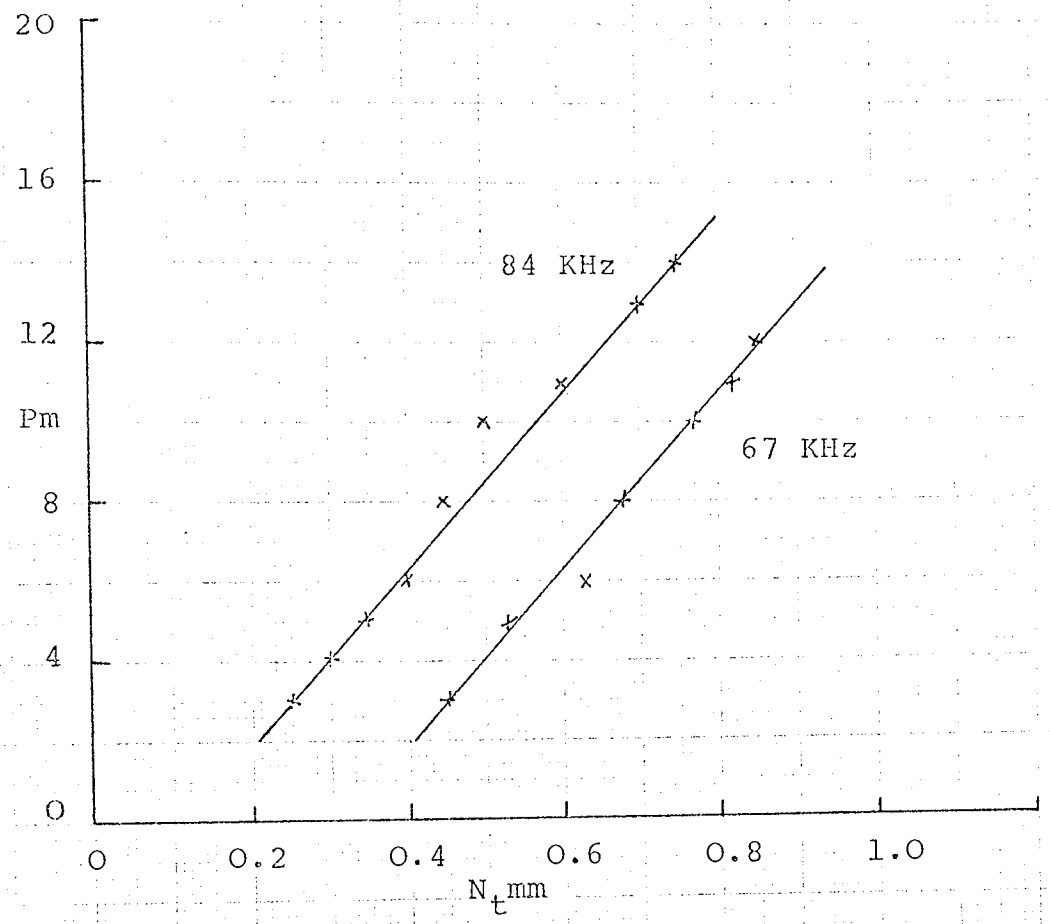

Fig. 5.15 Effect of the neck thickness on Q-factor of 2mm integral line resonators.

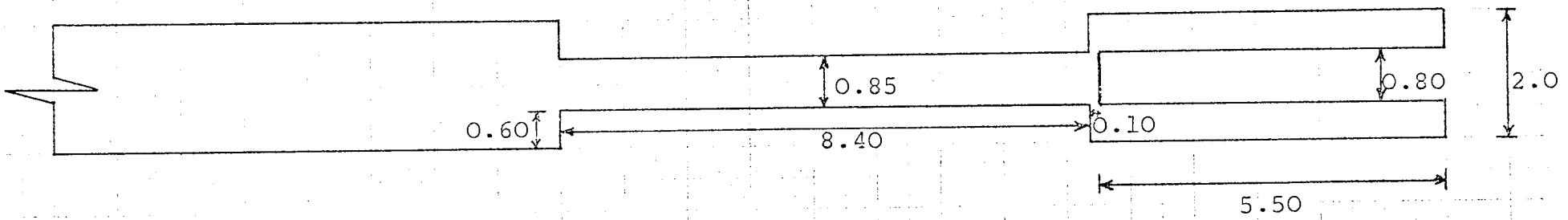

Fig. 5.16(a) Dimensional diagram of an integral line resonator type (TI-3) on 2 mm steel rod.

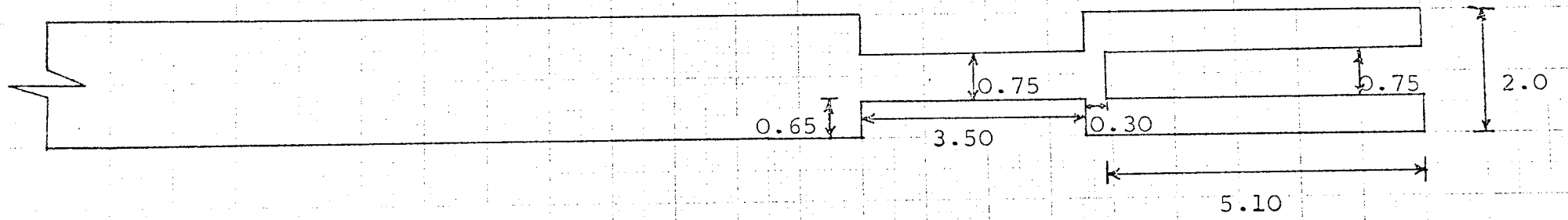

Fig. 5.16(b) Dimensional diagram of an integral line resonator type (TI-4) on 2 mm steel rod.

the coupling section has no major effect on the frequency but it produces a tighter coupling factor. Meanwhile the mechanical strength of this part will reduced, therefore a compromise should be made between a reasonable mechanical strength and a coupling factor which is desired.

5.5.4 Development of 1.5 mm Integral Line Resonator

Approaching the 2 mm integral line resonator and maintaining the best designs of the 3 mm probe disclosed no problems. An attempt was therefore made to proceed to resonators of 1.5 mm. For this observation a sets of three similar integral line resonators were made on 1.5 mm steel rod and the effects of the neck width were investigated for each resonator separately.

The results, as before, were expressed in the form of Pm as a function of the W_n and are shown in Figs. 5.17(a) and (b) and (c) respectively. The initial values as shown in Figs.5.18 (a), (b) and (c) were:

Resonator a: (TI-5) ℓ = 4.65 mm. b = 0.2 mm, W_s = 0.35 mm, W_n = 2.7 mm, N_t = 0.50 mm.

Resonator b: (TI-6) ℓ = 4.65 mm, b = 0.15 mm, W_s = 0.40 mm, W_n = 2.6 mm, N_t = 0.60 mm.

Resonator c: (TI-7) ℓ = 4.70 mm, b = 0.40 mm, W_s = 0.40 mm, W_n = 3.0 mm, N_t = 0.50 mm.

The results are given in Tables 5.9(a),(b) and (c).

Table 5.9(a)

W_n	f	Pm	Q
2.70 mm	101.62 kHz	14	64
3.20	102.10	12	55

Table 5.9(a)
contd.

W_n	f	Pm	Q
3.70	102.53	10	45
4.0	102.73	9	41
4.70	102.95	8	36
5.20	103.00	10	45
5.70	102.78	13	59
6.0	102.70	16	73

Table 5.9(b)

2.60	100.88	20	90
3.0	100.23	19	86
3.50	100.11	17	77
4.50	100.25	14	64
4.80	100.36	14	64
5.40	100.47	13	59
6.0	100.54	13	59
6.50	100.54	14	64
7.20	100.64	17	77
8.0	100.81	19	86

Table 5.9(c)

3.0	99.00	20	90
3.40	100.50	17	77
4.0	102.25	14	64
4.60	102.07	14	64
5.0	101.83	16	72
5.20	101.58	18	81
5.50	100.80	20	90

The following conclusions can be attained from comparison of the above tables and relative curves of Fig. 5.17(a),(b)

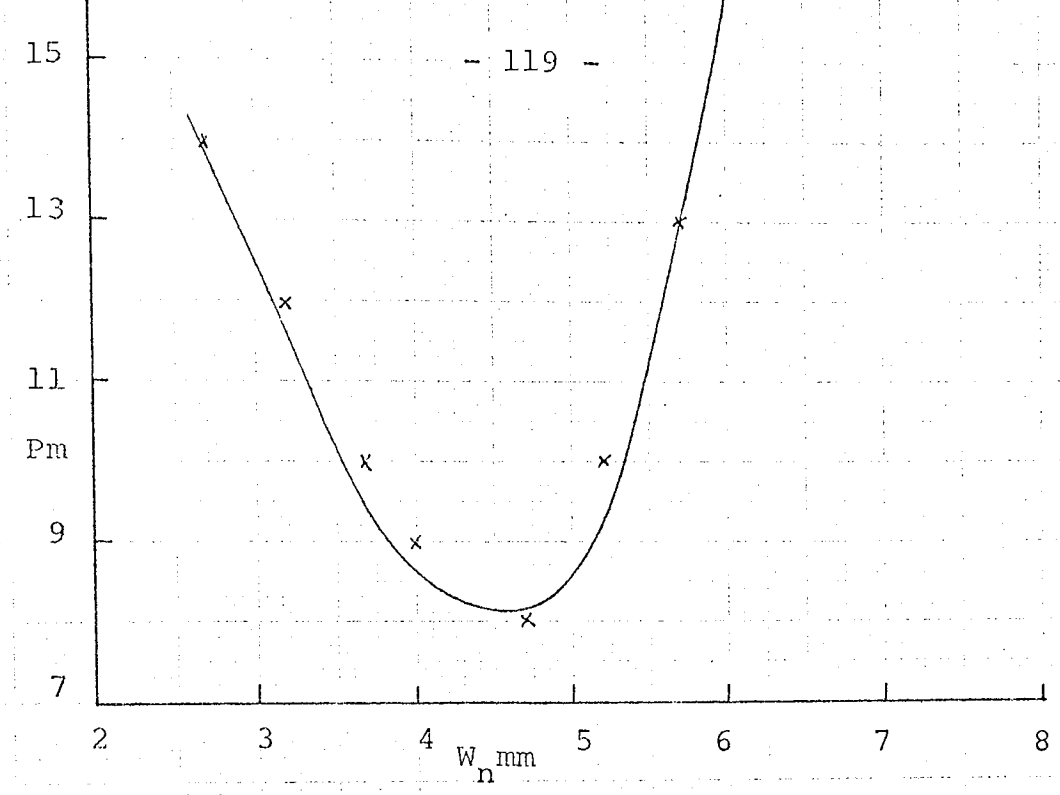

Fig.5.17(a)

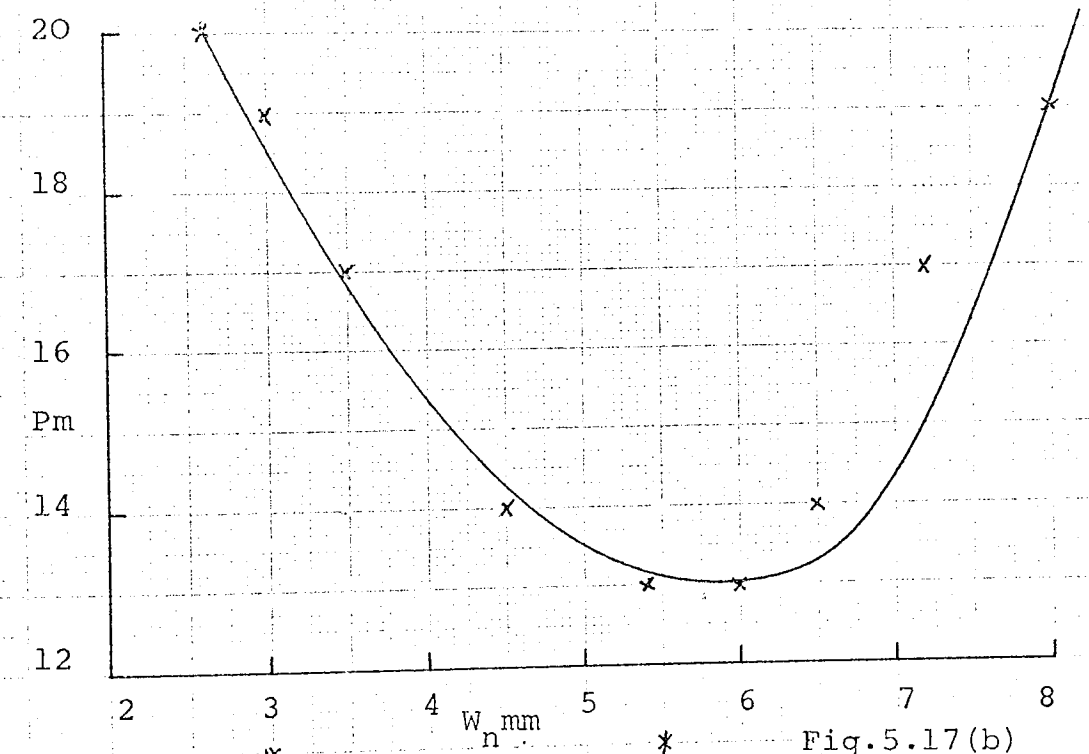

Fig.5.17(b)

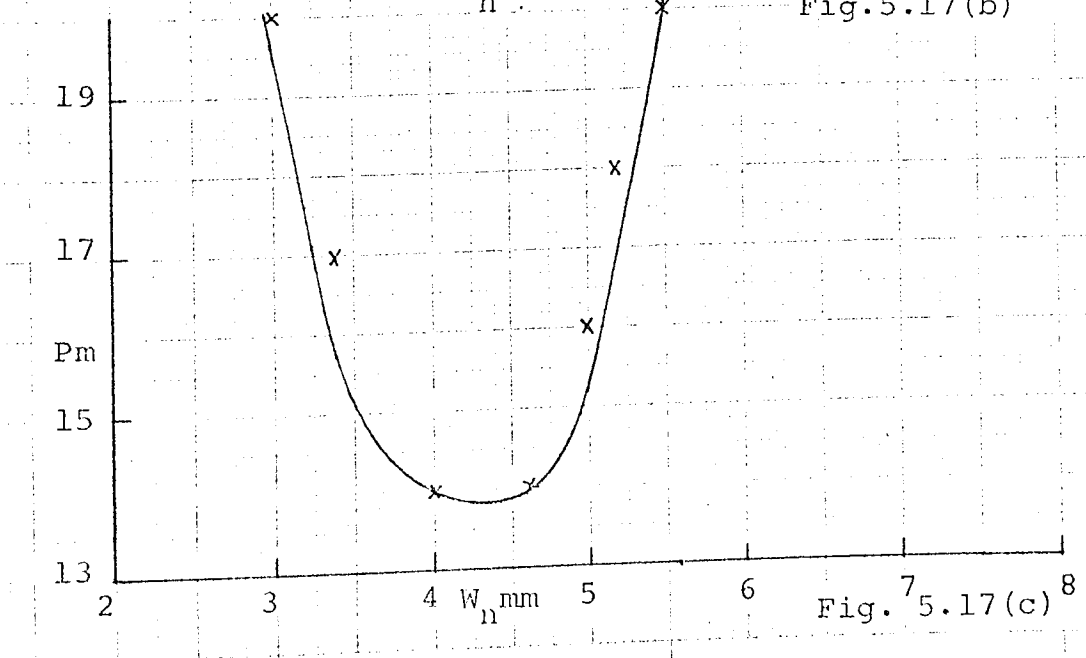

Fig.5.17(c)

Fig.5.17 Effect of the neck width on Q-factor of three similar 1.5 mm integral line resonator.

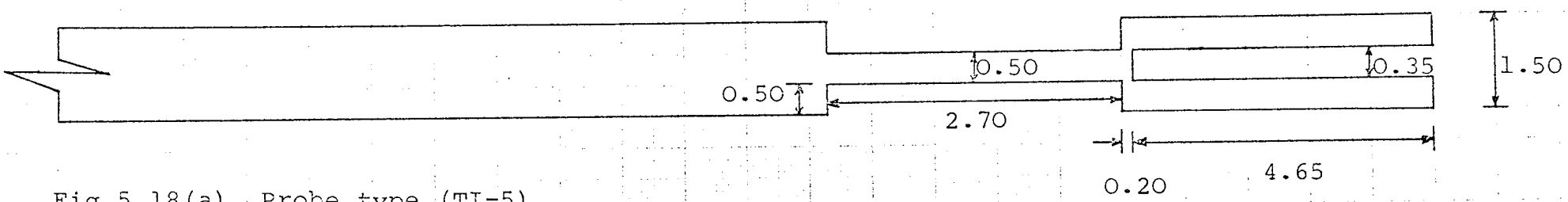

Fig.5.18(a) Probe type (TI-5)

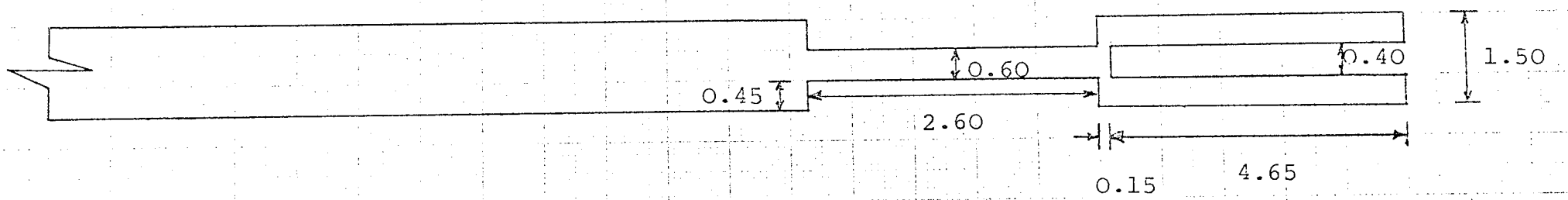

Fig. 5.18(b) Probe type (TI-6)

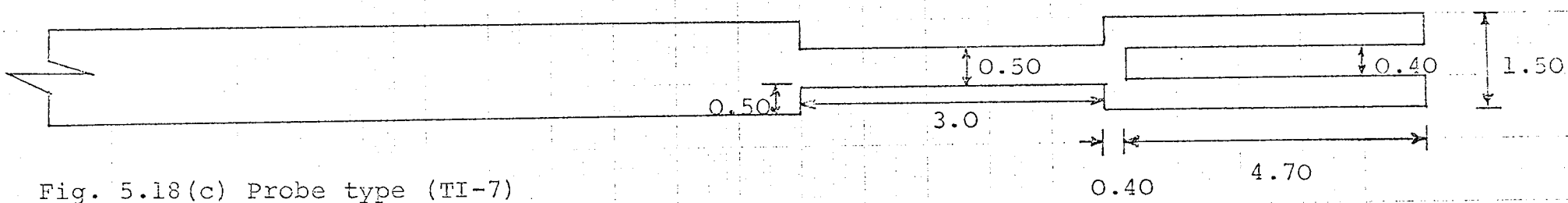

Fig. 5.18(c) Probe type (TI-7)

Fig.5.18 Dimensional diagram of three integral line resonators on 1.5 mm steel rod.

and (c).

1. The effect of the neck width (W_n) on the coupling Q of a 1.5 mm integral line resonator is exactly the same as 2 mm and 3 mm integral ine and strip probes. The value of the coupling Q, as before, approached to the minimum at the quarter wave length of the neck width.

2. Inspection of the above tables confirmed the previous discussion of the independence of the neck width on the frequency. Therefore, by altering the parameters controlling frequency, such as the tine length, base length and slot width, the desired 100 kHz frequency was obtained on a 1.5 mm line.

3. Considering the results of the Figs. 5.17 showed the similarity of the effects on all three resonators. This is a confirmation to the previous discussions about the coupling section and hence development of 1.5 mm integral line resonator.

5.6 FURTHER EXPERIMENTAL WORK

Accordingly a large number of the new 1.5 mm and 2 mm integral line resonators were made with great precision in order to be a model for tungsten and thoriated tungsten high temperature probes. The frequencies will be in the ratio of the velocities but the coupling Q will remain the same.

5.7 SUMMARY

The summary of the design data along with the observed frequency and coupling is given in Table 5.10 for all the

probes studied.

The table shows that for maintaining the frequency of the 1.5 mm probe in the same order of the 3 mm, resulting is increasing the tine length (ℓ) together with reduction of the base length (b) and slot width (W_s). For maintaining the coupling in the same order of the 3 mm, resulting is increasing the neck width (W_n) to a quarter wave length and reducing the neck thickness.

5.8 CONCLUSION

Integral line probes, made on a 1.5 mm diameter and 200 cm long tungsten rod, joined to the main acoustic transmission line by silver brazing were tested upto 1800^{o}C and gave satisfactory results. The main advantages of the integral probe over other probes are:

(a) Small size

(b) No high temperature joint,

(c) Ease of machining,once a geometrical form is obtained an increase of scale lowers the frequency proportionately but the coupling is unchanged.

(d) Low frequency probe with a low coupling Q can be obtained together on a small diameter line. This was the object of the new design of probe.

Table 5.10 Summary of the design data and observed parameters.

Probe No.	Material	Velocity of sound in material	Diameter of probe	Dimensions					Observed		
				ℓ	b	W_s	W_n	N_t	f	Pm	Q
TIS-1	Molybdenum	5.6 mm/μsec	3.10 mm	2.60 mm	1.0 mm	0.9 mm	1.0 mm	1.10 mm	67 KHz	15	64
TIS-2	Molybdenum	5.6	3.10	1.40	1.0	0.9	1.0	1.10	122	2	9
TIS-3	Molybdenum	5.6	3.10	1.80	1.20	0.55	1.20	1.40	129.5	5	23
TIS-4	Molybdenum	5.6	3.10	2.0	0.75	0.90	1.0	1.95	106.5	49	223
TIS-5	Molybdenum	5.6	3.10	2.70	0.80	1.10	1.0	1.35	63.7	20	90
TI-1	Steel	5.0	3.10	3.0	0.75	0.60	8.20	0.90	53.7	16	73
TI-2	Steel	5.0	2.0	6.0	0.15	0.85	7.50	0.90	67.0	14	64
TI-3	Steel	5.0	2.0	5.50	0.10	0.80	8.40	0.85	68.1	12	55
TI-4	Steel	5.0	2.0	5.10	0.30	0.75	3.50	0.75	85.5	14	64
TI-5	Steel	5.0	1.50	4.65	0.20	0.35	2.70	0.50	101.62	14	64
TI-6	Steel	5.0	1.50	4.65	0.15	0.40	2.60	0.60	100.88	20	90
TI-7	Steel	5.0	1.50	4.70	0.40	0.40	3.0	0.50	99.0	20	90
TI-8	Steel	5.0	2.0	5.60	0.30	0.85	6.15	0.38	51.64	5	23
TI-9	Steel	5.0	2.0	6.05	0.15	0.85	8.0	0.85	50.62	15	68
TI-10	Steel	5.0	2.0	5.0	0.30	0.70	3.50	0.50	77.82	4	18
TI-11	Steel	5.0	1.50	4.70	0.20	0.45	4.70	0.50	86.0	8	36
TI-12	Steel	5.0	1.50	4.70	0.15	0.40	4.70	0.50	87.33	6	27
TI-13	Steel	5.0	1.50	4.70	0.40	0.50	4.70	0.60	93.0	12	55

Fig. 5.19 This photograph shows the new design of integral line probe on a 2 mm steel rod.

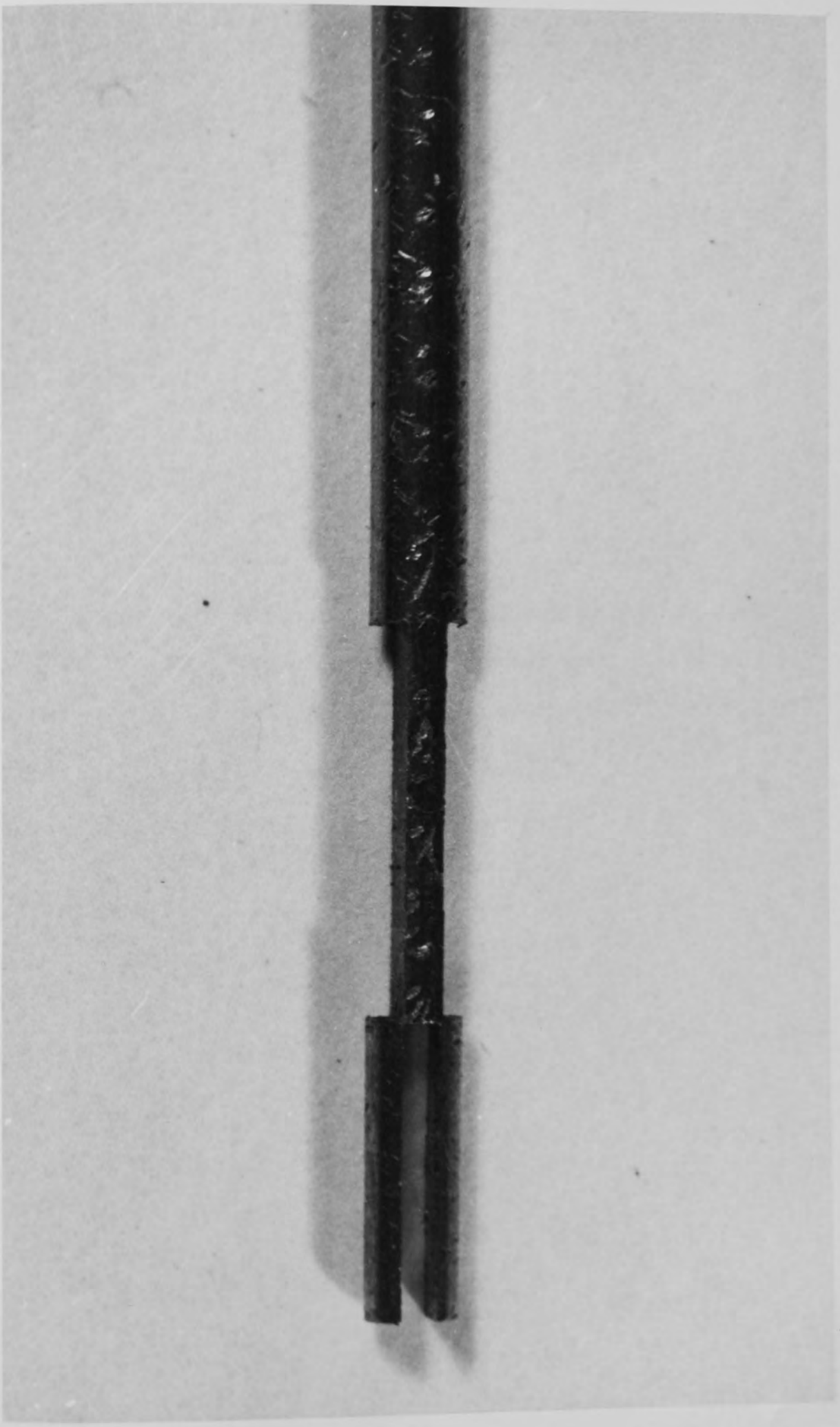

Fig. 5.20 This photograph shows the new design of integral line probe on a 1.5 mm steel rod.

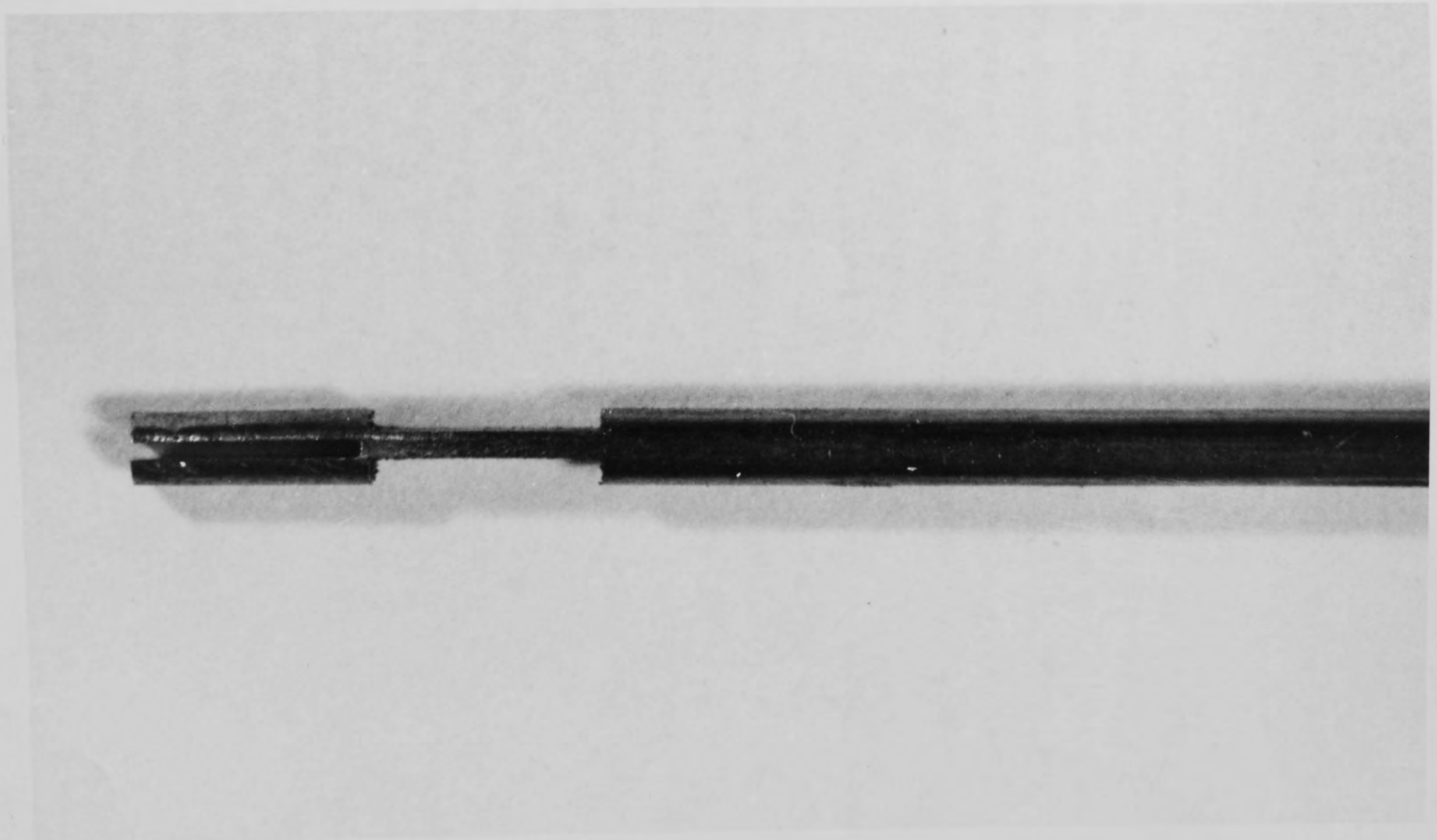

CHAPTER 6

ELECTRONIC DESIGN REQUIREMENT FOR AUTOMATING THE MEASUREMENTS

6.1 INTRODUCTION

The electronic system is an essential part of the ultrasonic thermometer, it's function being to maintain a signal generator at the same frequency as that of the sensor. The essence of the problem is that the sensor is at the remote end of the probe, a large number of wavelengths away and this excludes the use of a conventional resonator maintained oscillator.

For this purpose a digital multichannel signal generator that is capable of being switched on and off for a predefined number of cycles was constructed. In one phase of operation it produces bursts of ultrasonic oscillations in the probe via the magnetostrictive transducer and is then processed to compare the resonator and the oscillator frequencies. The resultant error signal is reduced to the zero by the control loop, making the two frequencies equal. The control uses the basic property of a resonator that the energy stored during the transmit period decays exponentially at the natural frequency of the resonator,independent of the transmitted frequency. Therefore a comparison of the periods of an equal number of the transmitter and the decrement oscillations provides the error signal. Being completely automatic the system must find resonance even when there is considerable detuning. The transmitter frequency measured in a separate burst is available for display, data logging and computer access and also in the analogue form for chart

recorder applications. The electronic system required to perform these functions can be divided into the following subsystems:

(a) Transmitter - for producing the transmitted burst of oscillations from a voltage variable signal generator.

(b) Receiver - for identifying the returned echo signal and decrement and any necessary amplification.

(c) Error measurement - for generating of an error signal which is the difference between the decrement period and that of the signal generator.

(d) Display system, digital to analogue converter and data transfer unit.

The functional block diagram of the electronic system is shown in Fig. 6.1. Digital techniques were used as extensively as possible and the technology is based on TTL integrated circuits making minimal use of discrete components and analogue devices.[60,61,62].

Also when required, signal delays are obtained in terms of number of pulses rather than a fixed time interval. This avoids a basic defect where the analogue time-delayed circuits might fail to hold synchronization and hence automatic control could be lost.

6.2 TRANSMITTER

The function of the transmitter is to drive the magnetostrictive transducer with a high powered burst of oscillations, the number being preselected. To do this the voltage variable signal generator has the characteristics:

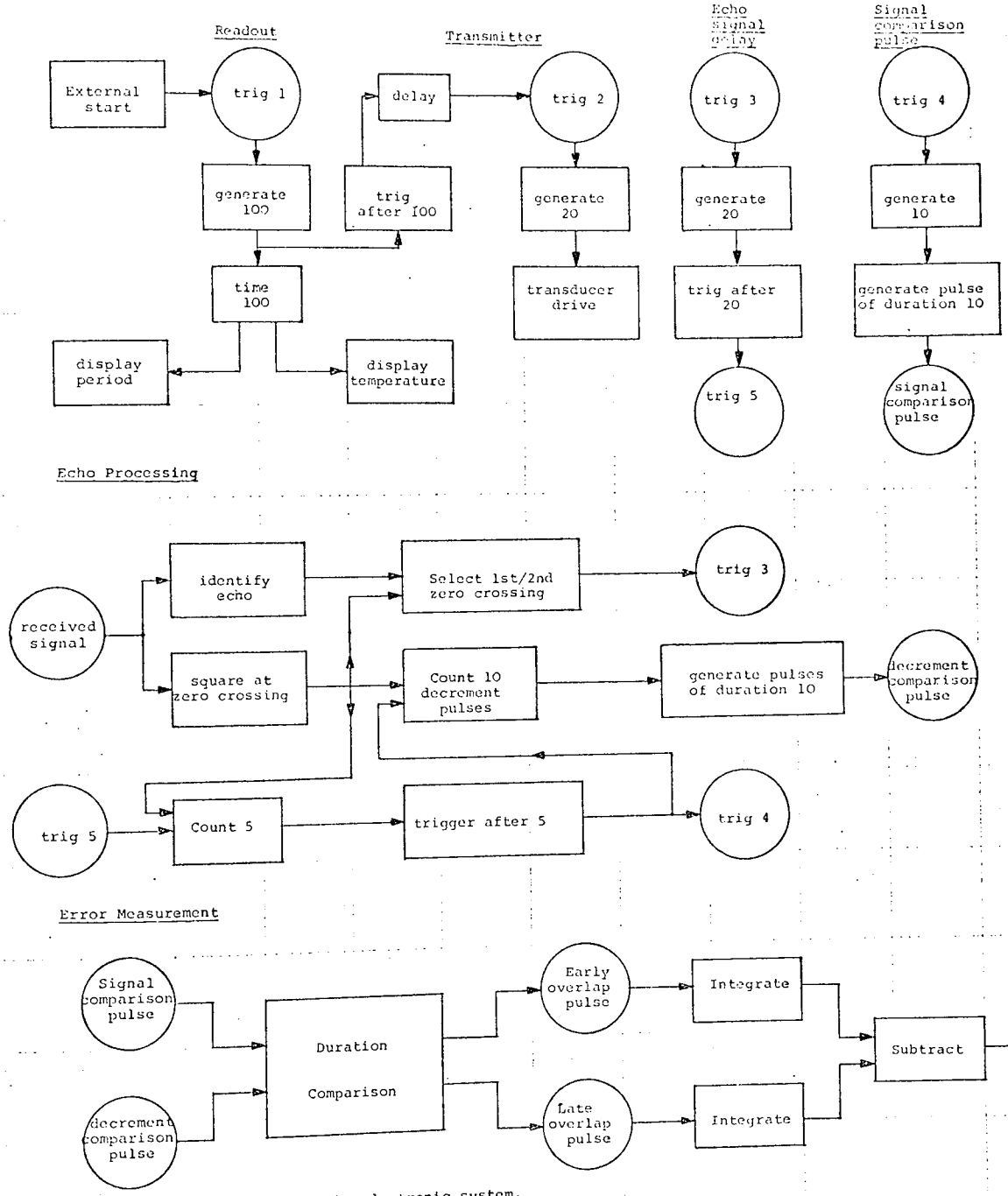

Fig. 6.1 Block diagram of the electronic system.

a) The range of the manual frequency variation, coarse and fine, is about 30 to 520 kHz which is suitable for the ultrasonic aspect of the system.

b) The oscillations in the burst and repetition rate are selected to be suitable for the particular ultrasonic probe. These variables must be independent of each other. The number of oscillations can be as low as 5 to 10, but for most practical probes it may be as many as 30 or 40.

6.2.1 PRF Generator

The pulse recurrence frequency (PRF) generator produces repetition periods between 3 m sec. to 60 m sec., preselected manually for different length of transmission lines and different probes. For this case, a low frequency oscillator was designed as describing in the following paragraph.

A cross-coupled monostable multivibrator mono (M_1 and M_2) type SN74121 TTL integrated circuit was used. Fig. 6.2. A simple potentiometer enables the base voltage on the transistors (T_1 and T_2) and hence the charging current changes the period from 3 m sec. to 60 m sec. The RC network on the B input of the monostable delays the rise to the +5 volt value,making sure that when the power supply is switched on the monostable will be in the correct mode for the start of oacillation.

6.2.2. Transmitter Signal Generator

The signal generator which has four functions to perform every PRF cycle is shown in full circuit detail in Fig.6.3. It is essentially a free-running multivibrator which with

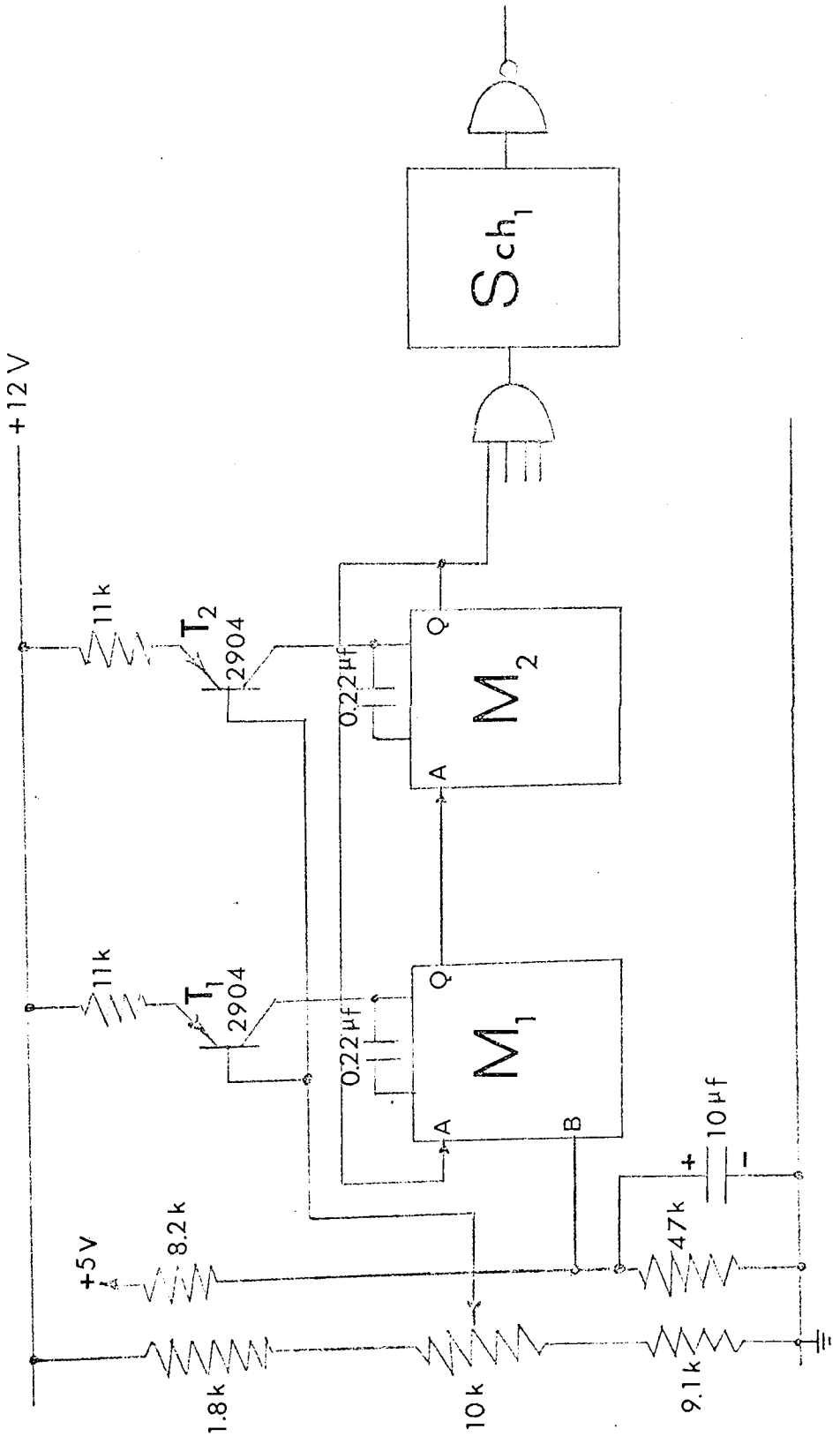

fig.6.2 PRF Generator

associated multiplexing circuits can be switched on and off via four independent channels, each having an input and an output (Fig.6.4).

On receipt of a trigger pulse, the multivibrator will run for the number of cycles, which must not vary with the oscillator frequency, designated by the channel, the signal appearing only at the one channel output.

By operating the multivibrator at twice the required signal frequency and dividing by two, two phases are available, each of equal mark space ratio, enabling delay steps of half cycle to be obtained as required.

The multivibrator consists of two cross-coupled monstable (M_3 and M_4), similar to the PRF generator, using external timing resistors. Being an aperiodic oscillator it can be switched on and off very precisely without time delay or transient. This feature is used extensively.

Voltage control of frequency is obtained by additional timing resistors driven from the output of a d.c. amplifier A_1, type SN72741. The values were chosen to give a frequency coverage of ±50% about a centre value. The random frequency changes from second to second are of order of 1 in 10^5. This stability is well within the target performance of the instrument, (1 in 10^4), where the control loop and readout acts in a fraction of a second. On open loop operation long term drift arises from the 0.6% per kelvin, temperature coefficient and the 0.05% change per millivolt of chip voltage. In the oscillator circuit F.g 6.3, the 0.1 μF capacitorprevents the monostable oscillations feeding back into the system. The frequency is variable in four ranges

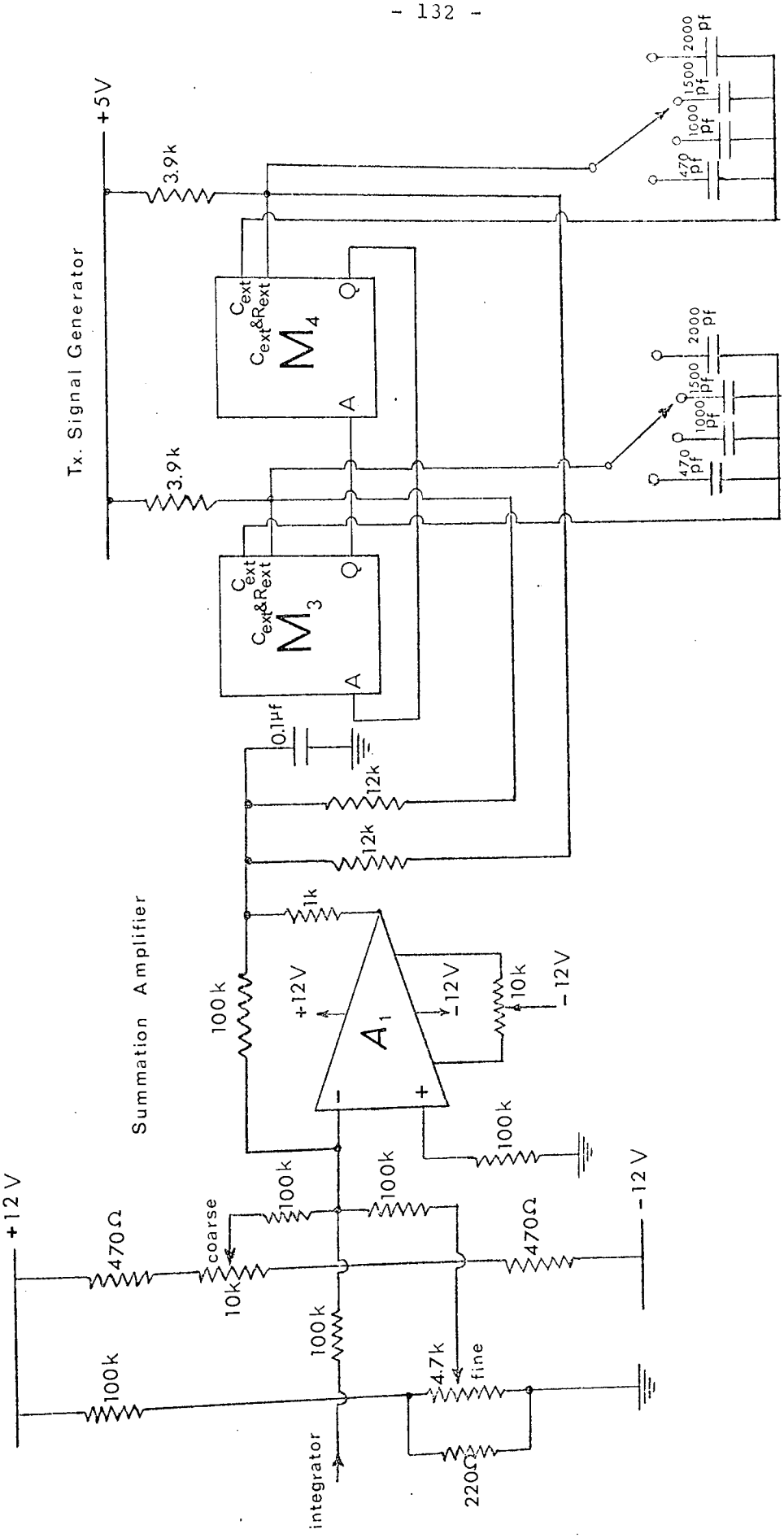

fig.6.3 Voltage Controlled Signal Generator

and coarse and fine control facilities are provided for manual adjustment. Fig.6.5 shows a calibration curve of control voltage and frequency. The excellent linearity of the characteristic will be noted.

6.2.3 Operating Cycle

In the cycle of operation Fig. 6.4 a starting pulse (trigger 1 on the receipt of the positive edge of the PRF pulse) operated the readout channel. This enables the time for 100 oscillations to be measured. A 20 MHz crystal clock gives an accuracy of ±1 in 10^4 at 100 kHz and better than this for lower frequencies. Other circuits, pre-set for a particular probe calibration, give an direct readout of temperature.

The readout is followed (trigger 2 on the receipt of the negative edge of the PRF pulse) by a burst of 5 or 10 or 20 oscillations which operate a complementary pair of power transistors driving the magnetostrictive transducer which is described in detail later.

The next signal initiated by trigger 3, occurs at a zero crossing near the beginning of the returned echo signal. The signal generator operates for a burst of 20 or 10 or 5 oscillations which will be described later in this chapter. This channel which is called delay processing and decrement identifying, produces a trigger pulse (trigger 5) to start the decrement sampling operation.

Trigger 5 is produced 20 periods later. It is after the beginning of the decrement but because of the finite bandwidth of the transducer there is a transient of a few

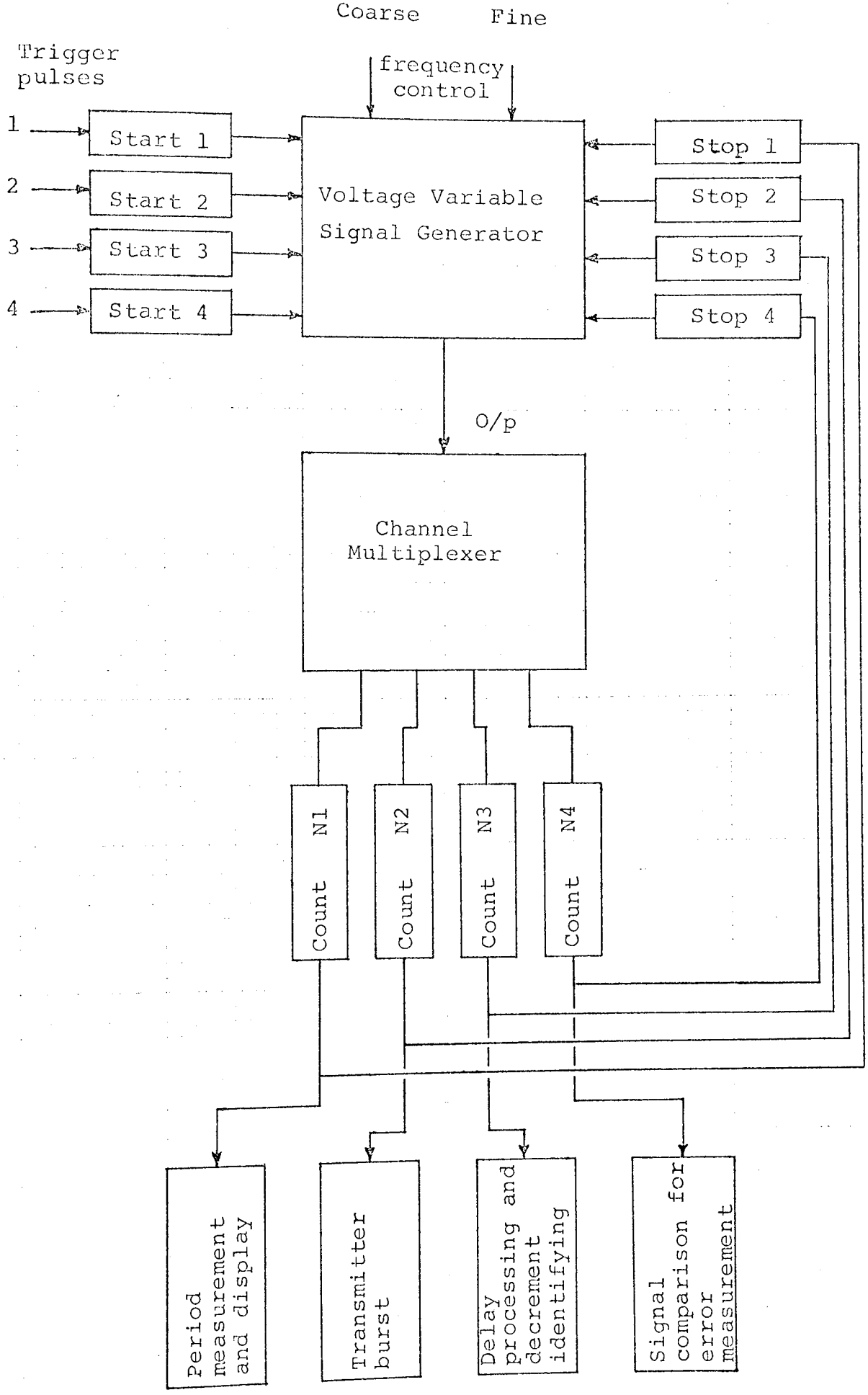

Fig. 6.4.
Channel Multiplexer and operating cycles of the electronic system.

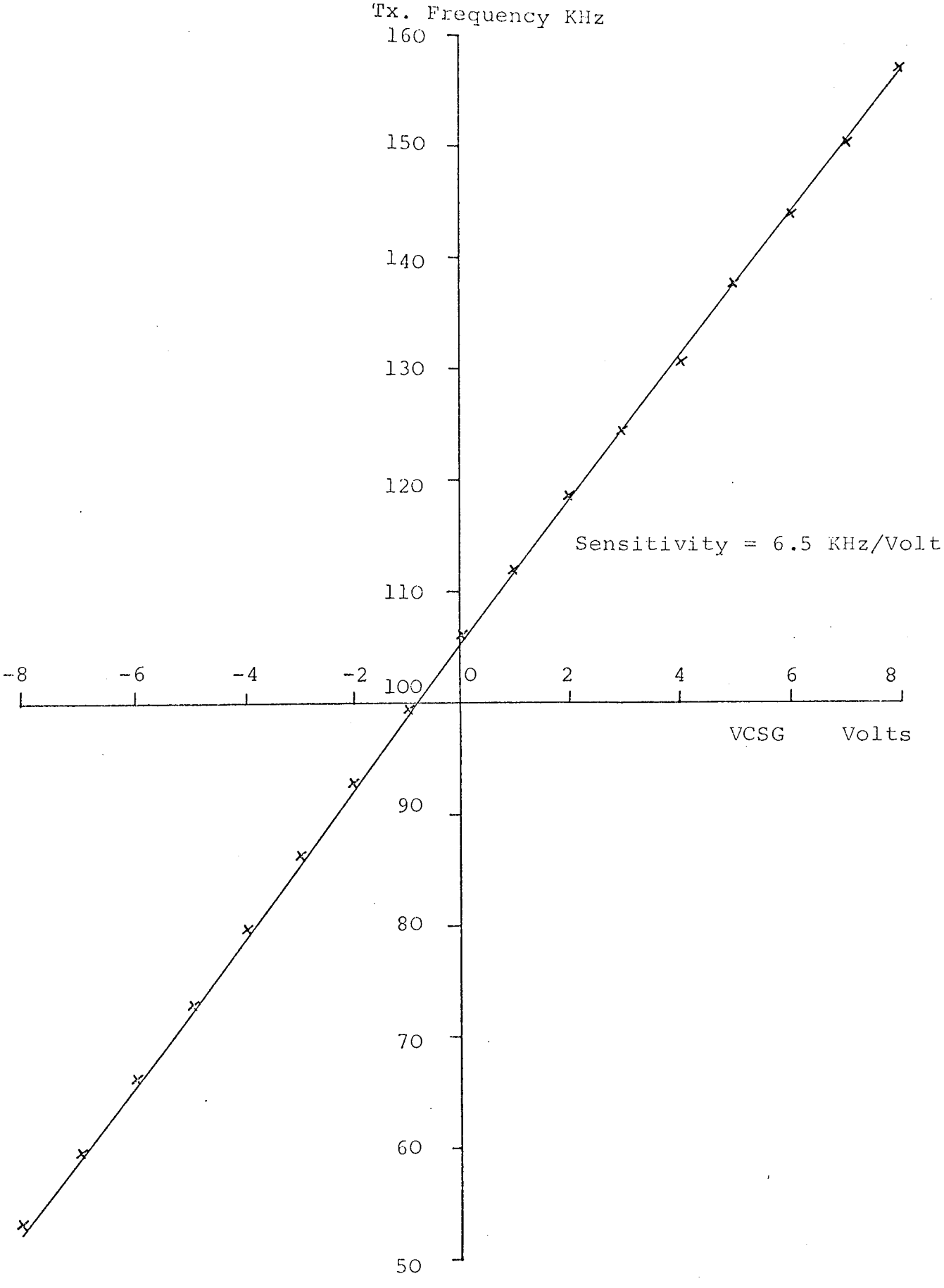

Fig. 6.5 The voltage shown here is the output of the summing amplifier, the input of which is the sum of the voltage fed back, the manually controlled voltage and any test voltage that may be applied. The excellent linearity is obtained because the frequency of transmitter is proportional to the current charging capacitors.

oscillations before the decrement is effectively established. There is therefore a further delay of 5 echo cycles before trigger 4, which again is synchronous with a zero crossing, initiates the signal comparison circuit. The comparison pulse generated lasts precisely 10 signal periods but is delayed by half a period, as will be discussed in detail in the error measurement section.

The operating cycle is now complete, the signal generator awaits the arrival of the next trigger 1. This interval (PRF period) is made just sufficiently long to allow reverberations on the probe to die down. Of course, the shorter the interval the more efficient will be the control loop. The returned echo is of the order of one volt peak to peak and has no significant acoustic or electronic noise.

6.2.4 Readout Channel (N_1) and Burst Channel (N_2)

The functional block diagram and the waveforms of the first and the second channels are shown in Fig.6.6 and Fig. 6.7 respectively and are described briefly here.

The positive edge of the PRF pulse, trigger 1 as before, switches mono M_5 to produce a very short and negative pulse at the output which in turn clears the input of a 7474 D type flip flop (D_1) , changing its output level from logic 1 to the logic 0. This pulse after passing through a four input NAND gate (G_1), type 7420, produces a positive pulse at the B input of the mono M_3 and hence commands the transmitter oscillator to start.

After counting 100 of these oscillations (channel N_1),

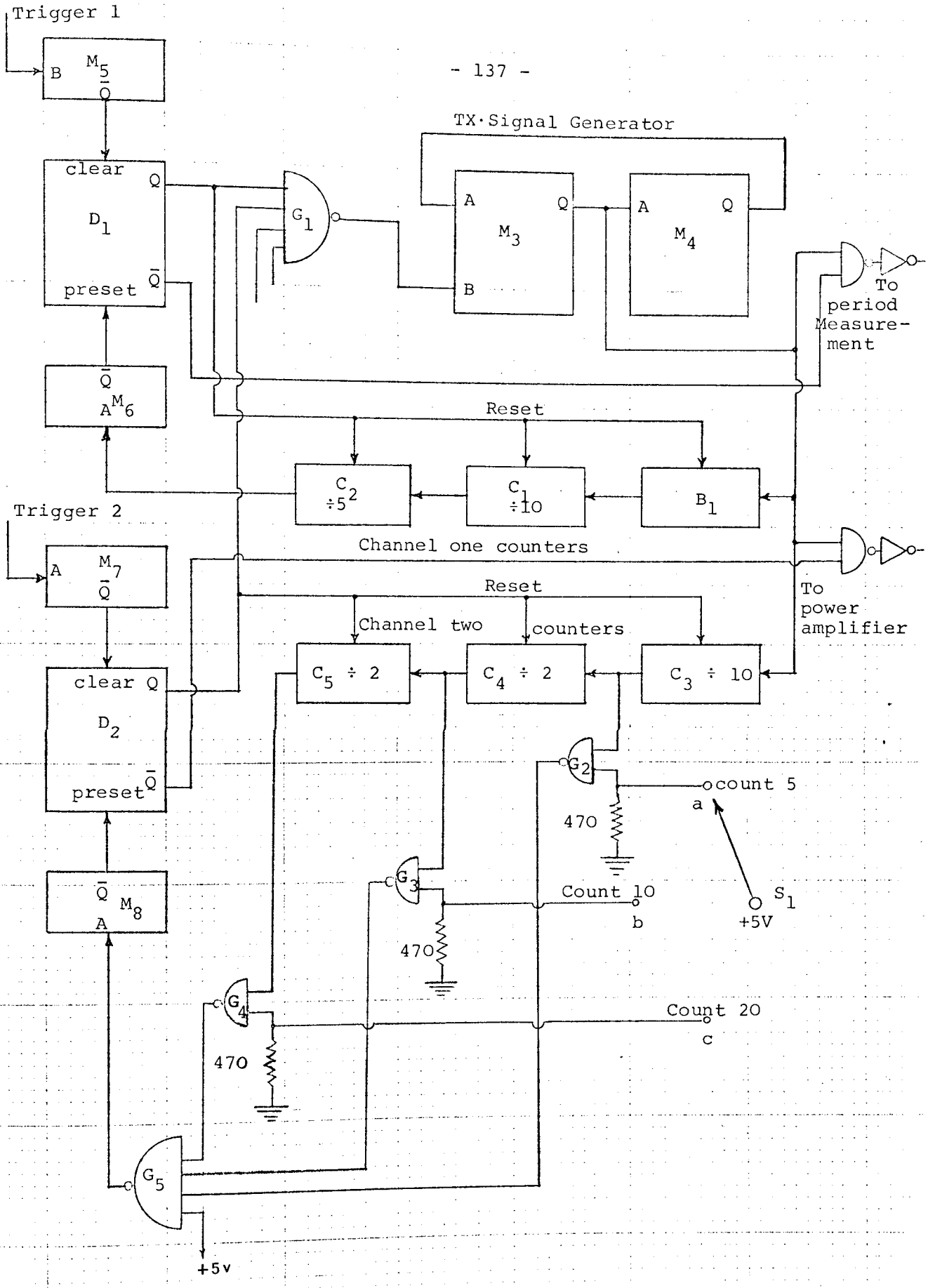

fig.6.6 Block diagram of the first and second channel of the system.

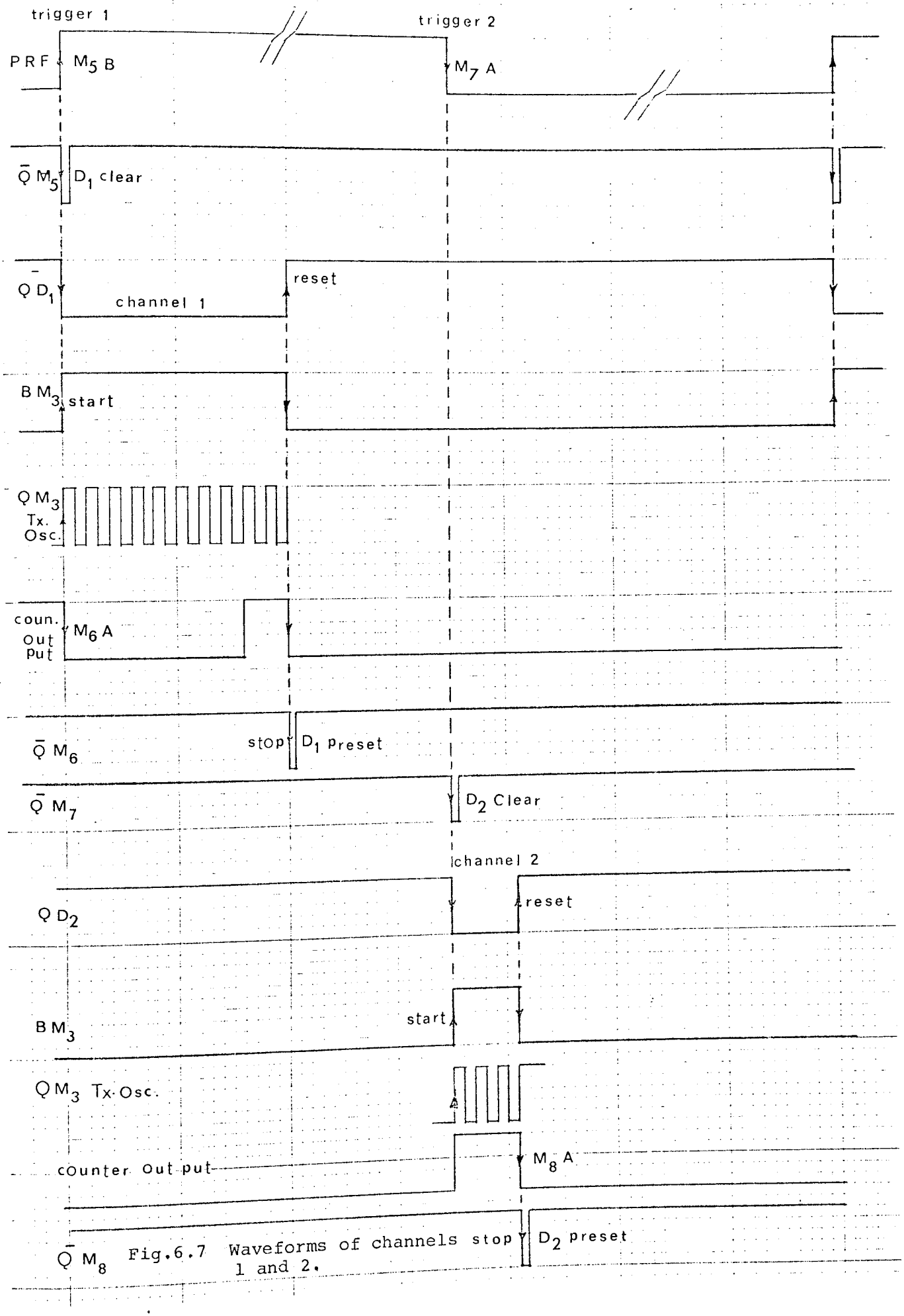

Fig.6.7 Waveforms of channels stop 1 and 2.

using decade counters (C_1,C_2) and JK flip flop (B_1) type 7490 and 7476 respectively, the counting stops automatically using another mono (M_6) for restting the output level of the D_1 to logic 1. Therefore with this positive edge the transmitter oscillator will stop. The duration of these 100 oscillations will be measured, using a 20 MHz crystal clock and the period will then be displayed for readout access, as will be discussed later in this chapter.

The second channel N_2, which is basically quite similar to the first channel, operates with the negative going edge of the PRF pulse and monos M_7, M_8 and flip flop D_2, have the same performances of the M_5, M_6 and D_1 as before.

In this channel the serial counters C_3, C_4 and C_5 will count 40, 20 or 10 oscillations of the Tx oscillator (depending upon the probe's length and the transmission line). The associated gating system ($G_2 \rightarrow G_5$) and the relative switch S_1, allowed any of the above number of oscillations which are desired to be selected.

6.2.5 Transmitter Amplifier

A push pull transformerless output stage amplifier is used to drive the probe from channel 2 of the signal generator. Fig. 6.8, shows the amplifier. The transducer is fed from the collectors rather than emitters of the transistors to avoid loading the receiver, the output transistors being cut off except when transmitting, and there is negligible loading of the transducer. The drive transistors required signals as shown in Fig. 6.9.

While a sinusoidal drive is ideal, the final waveform

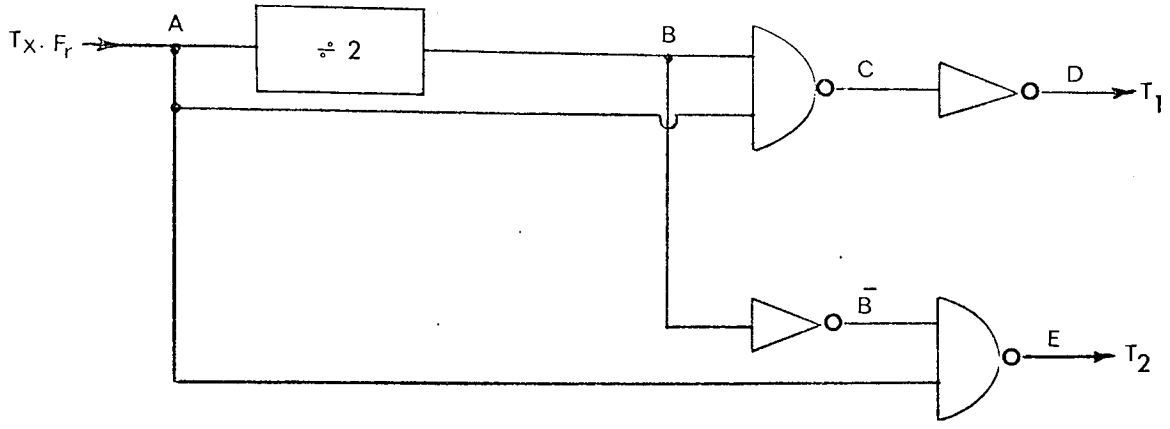

Gating Circuit

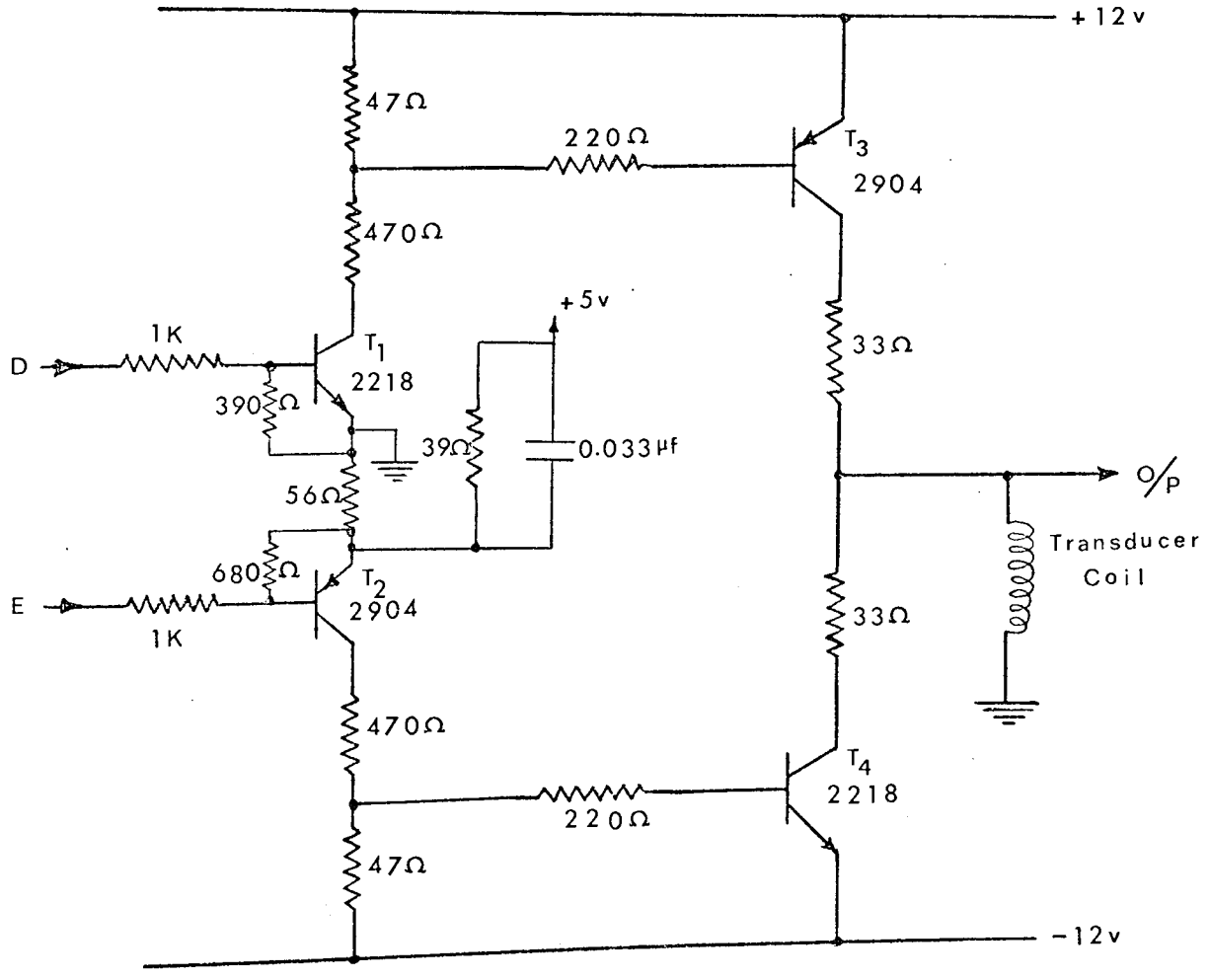

Power Amplifier

fig. 6.8

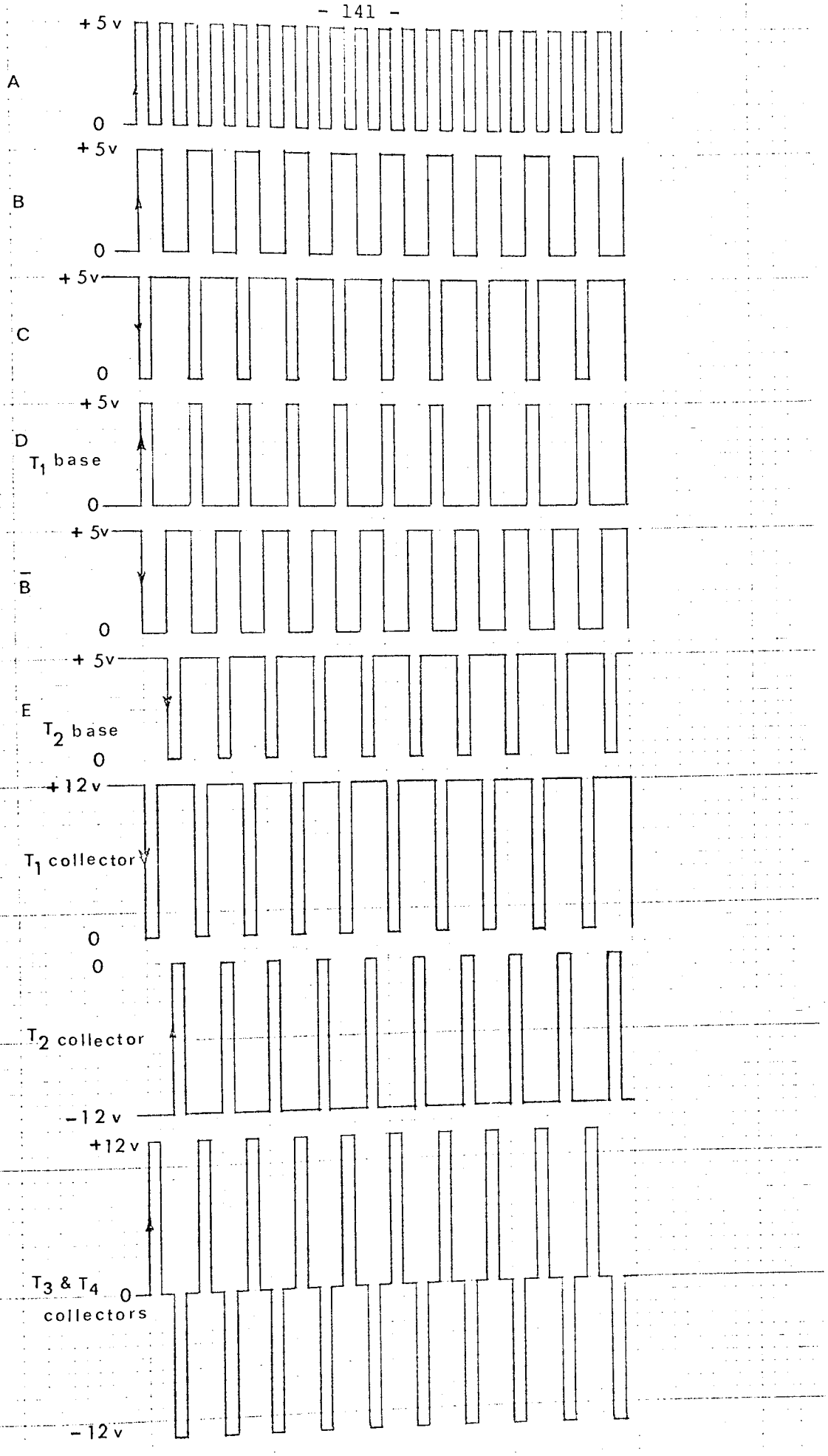

fig.6.9 Required waveforms for the transmitter burst.

shown in Fig. 6.9 is sufficiently free from harmonics due to an element of tuning in the transducer. This maintains digital design throughout.

The gating circuit of Fig. 6.8 produces the required signals for complementary pairs of transistors which generate pulses going from -12V to +12V for the transmitter/ receiver transducer.

The transducer is a magnetostrictive material (rod, tube, etc.) inserted in a coil wound on a thin walled former. The required magnetic bias is normally provided by a ring or horse-shoe magnet but for this particular application D.C. bias are employed as will be described later in the thesis. The transducer coils is tuned to further reduce harmonics in the transmitted signal which would distort the echo decrement.

The 33Ω resistors limits the output current to a safety level.

6.3 RECEIVER AND DECREMENT SIGNAL PROCESSING

The receiver, which is connected directly across the transducer coil, must amplify the returned echo to an amplitude suitable for the efficient operation of the comparators. The control depends on the fact that the decrement is always at the natural frequency of the resonator and the drive frequency must of course be sufficiently close to the resonator frequency to give a measurable decrement.

A few pulses of the decrement are sampled and the period are compared with the burst of the same number of the

transmitted signals, producing an error signal to control the transmitted frequency. These are discussed in details in the error measurement section.

A block diagram of the receiver and subsequent signal processing are shown in Fig. 6.10 and the circuit details, together with the waveforms, are shown in Figs. 6.11 and 6.12 respectively.

6.3.1 Input Voltage Follower (Buffer)

The received signal is clamped to ±0.7V for protection against the transmitted signals Fig. 6.11. It drives the voltage follower which is an integrated circuit type LM310 connected internally as a unity-gain non-inverting amplifier. This device has internal frequency compensation and provision for offset balancing. The output impedance is sufficiently low to drive the low input impedance comparators. The 4.7kΩ series input resistor in conjunction with the "back to back" diodes limits signals reaching the voltage follower to ±0.7V and giving a fast recovery time.

6.3.2 Echo Detector Comparator

An integrated circuit voltage comparator type LM306 giving a TTL compatible pulse output with a sensitivity of a fraction of a millivolt is used to interface the analogue to digital signals. The echo signal drives the comparator and the threshold level is adjusted to identify the start of the echo and must be quite clear from the background noise.

The comparator is switched to the operating mode by

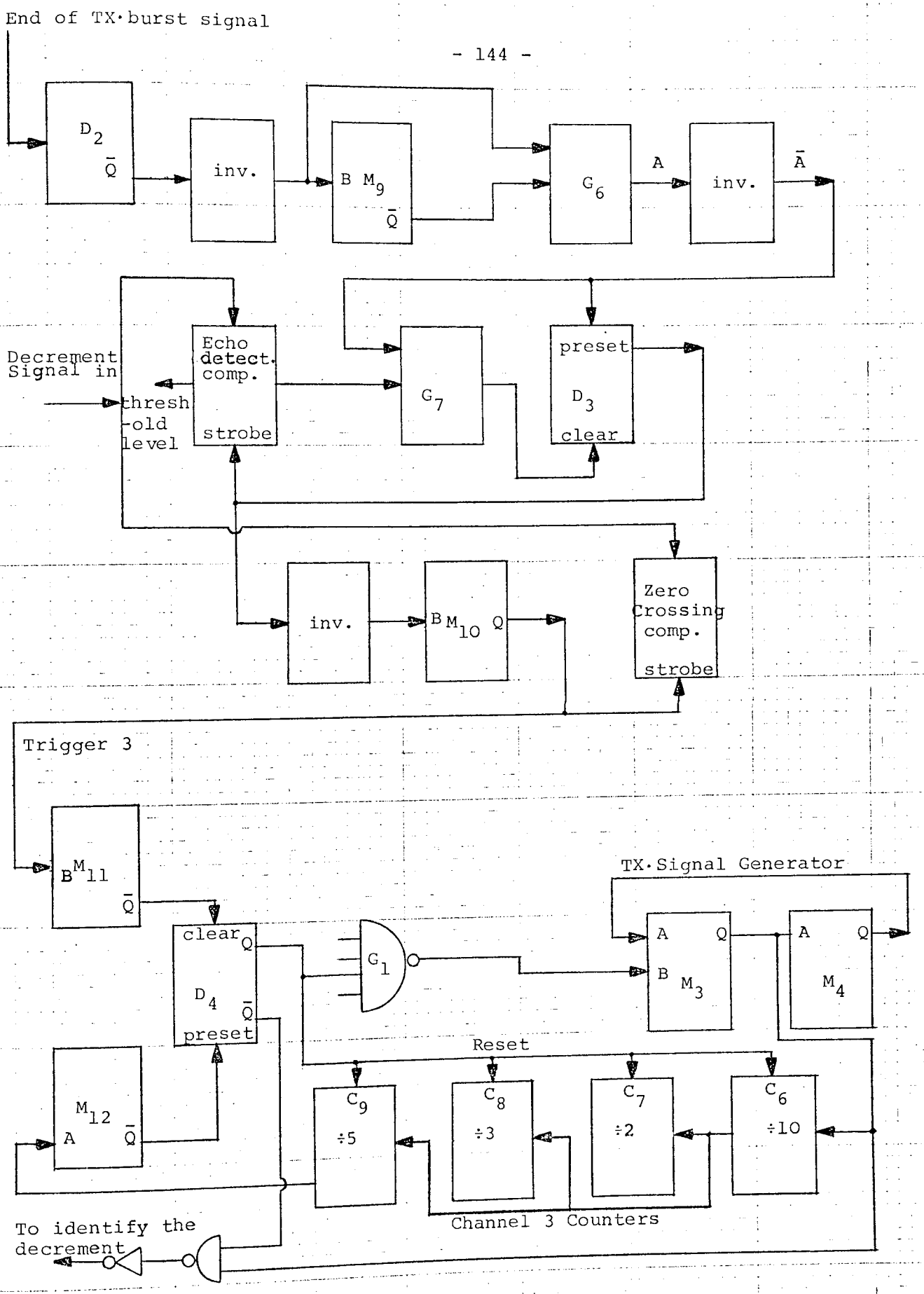

fig. 6.10 Functional block diagram of the receiver and signal processing.

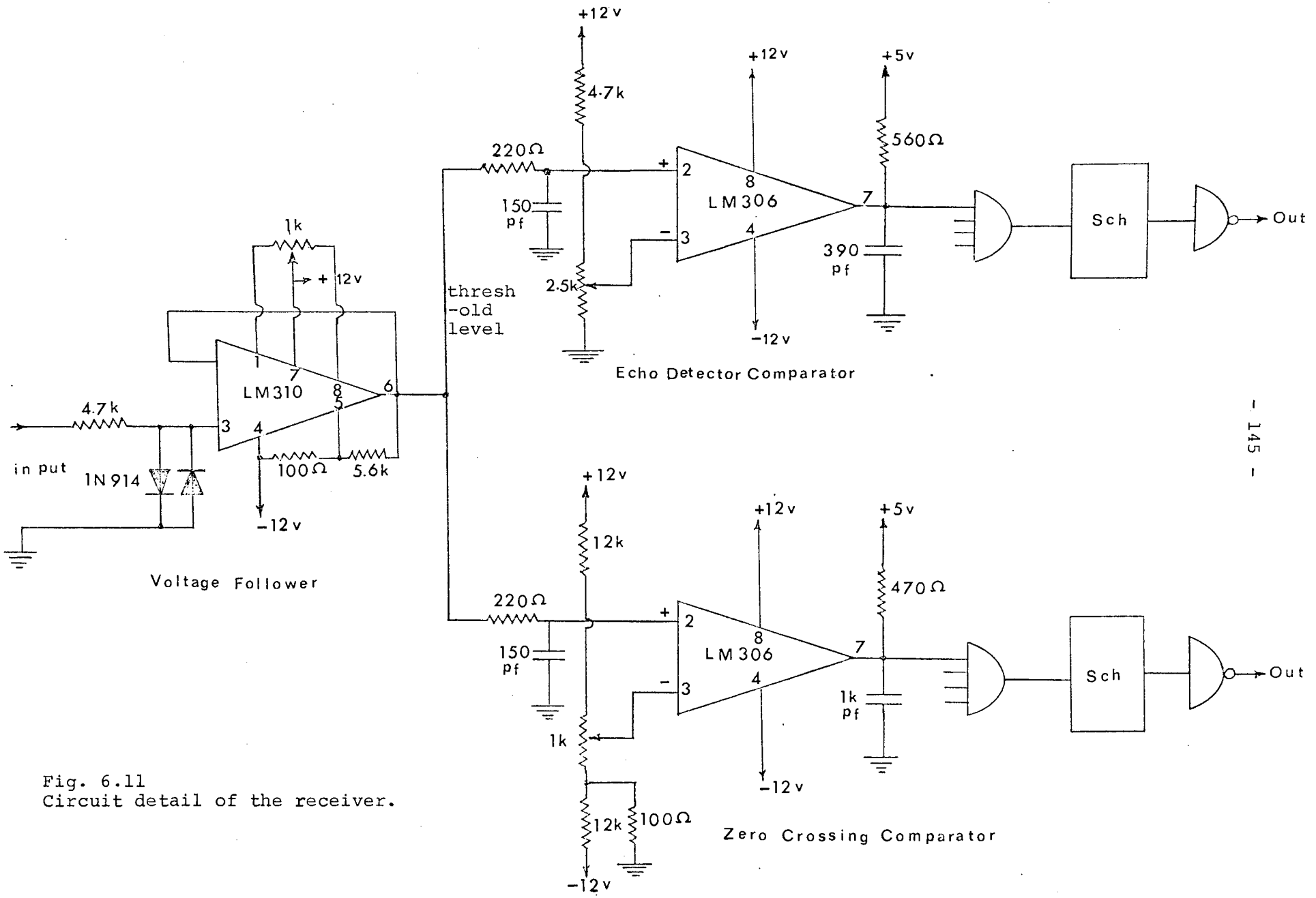

Fig. 6.11
Circuit detail of the receiver.

a TTL strobe. The strobe, waveform D_3 Q in Fig. 6.12, switches the comparator to operate from the beginning of the transmitted burst, but the output signals are suppressed in the gate G_7 by waveform $\bar{A}$ and the comparator output, will therefore be from the echo. This signal itself will switch the strobe off, hence the comparator will stop operating. The bias must be selected to cover the same part of the echo signal over the full temperature range of the probe.

6.3.3 Zero Crossing Comparator

The comparator is also a high-speed integrated circuit type LM306 which is used to detect the zero crossing of the (analogue) decrement very accurately and drive a TTL digital load. The echo signal drives the comparator which is unbiased and therefore, acting as a zero crossing detector, produces square waves. The strobe, however, is arranged to give the comparator output from the start of the echo to a period extending well into the decrement. During the rest of the period, the comparator is off (waveform M_{10}Q Fig. 6.12).

6.3.4 Strobe Generator for Echo Detector and Zero Crossing Comparators

As shown in Figs 6.10 and 6.12, the echo comparator output is gated with the waveform $\bar{A}$, which is stretched form of the D_2 Q (channel 2).

The output of this gate is a negative going edge, identifying the echo. This signal then clears the D_3 flip flop to the logic 0, which has previously been preset by

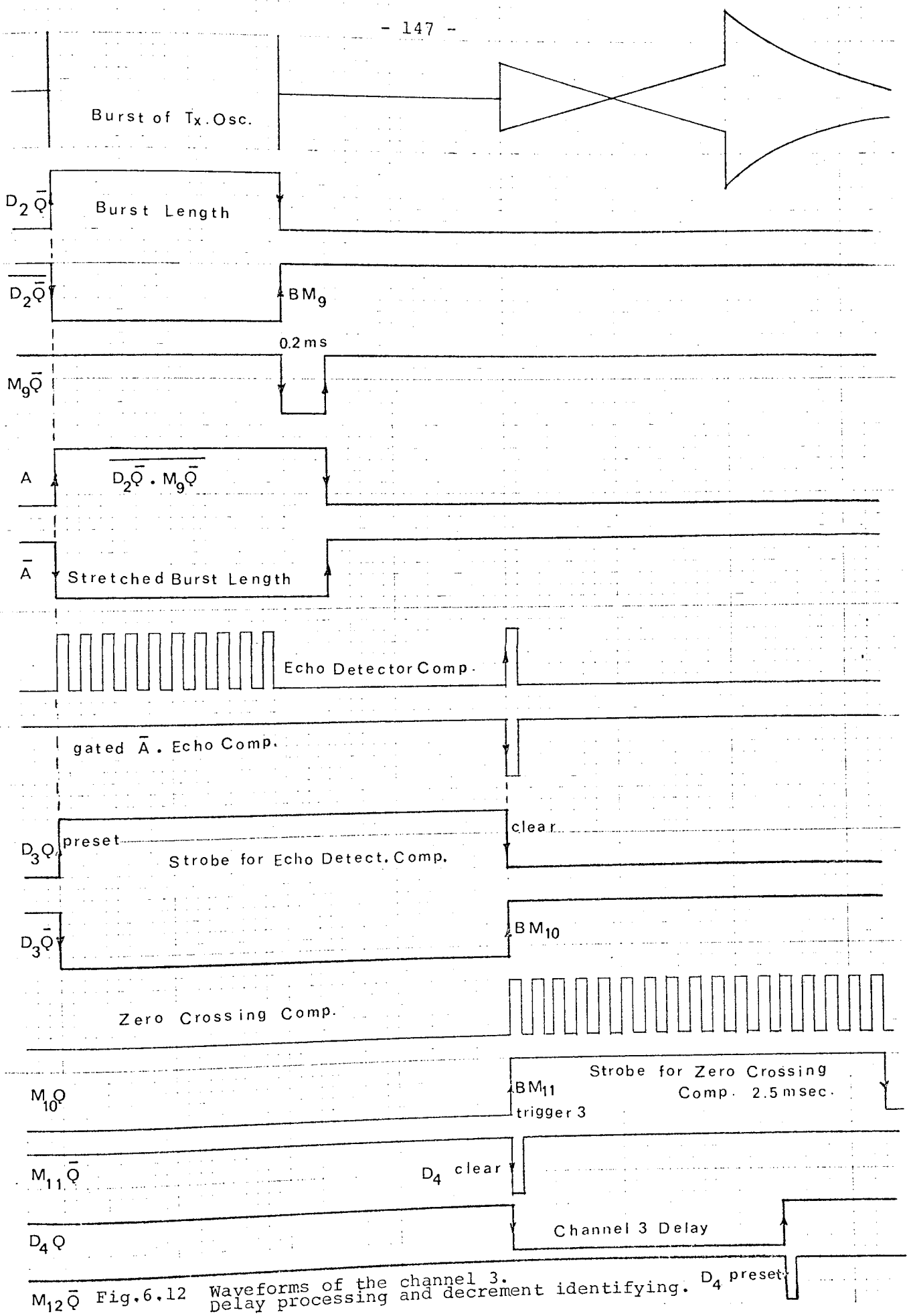

Fig.6.12 Waveforms of the channel 3. Delay processing and decrement identifying.

the signal $\bar{A}$. The D_3 Q is therefore used for the echo detector comparator strobe signal, starting before the arrival of the echo and ending after the first identifying pulse.

At the next step, this strobe (D_3 Q) signal, after inversion, triggers mono M_{10} giving a 2.5 m sec. gate, to strobe the zero crossing comparator (M_{10} Q) giving a long burst of decrement square waves.

6.3.5 Channel 3 of the Multiplexer

The function of the channel 3 is to identify the start of the decrement signal and provide a signal (trigger 5) for the decrement sampling.

The circuit for the channel 3 is basically the same as the channels 1 and 2 but it starts operating with the trigger pulse 3 (M_{10} Q) which occurs at a zero crossing near the beginning of the returned echo signal and extending well into the decrement. Figs. 6.10 and 6.12 show the block diagram and the waveforms of this channel. The same output pulse from M_{10} which was used to strobe the zero crossing comparator, will trigger mono M_{11} which opens the channel 3.

Fifty oscillations of the signal generator are counted, equally to 25 transmitter pulses [50 = (20 + 5) x 2], the extra five pulses are to ensure that the decrement is well established before sampling begins. The output of the counters (C_6, C_7, C_8, C_9) will then trigger M_{12} to switch the channel 3 off. Therefore the waveform D_4 Q (Fig. 6.12) is the channel 3 duration which corresponds to a burst of 50 oscillations of the signal generator.

In practice the electronics is required to operate with probes of a variety of lengths, resonant frequencies and coupling Q factors. For this reason channel 3 was provided with three manually selected modes of operation as in channel 2. The selector switch S_1 has three positions.

In position 1 (a_1) channel 2 produces a burst of 5 transmitted oscillations, channel 3 producing a delay of 10. In position 2 (b_1) the numbers are 10 and 15 and for position 3 (c_1) they are 20 and 25.

In general (c_1) would be used for high Q probes and (a_1) for those with a low Q. Fig. 6.13 shows the associated gating circuit to perform the above functions.

As in some particular cases the decrement was rapid at high temperatures and decrement sampling was difficult, it was decided in such cases to initiate the sampling at the start of the decrement. For this purpose another gating circuit was added to the apparatus, where a simple switch (S_2) enabled the decrement sampling started with or without the extra five delay pulses. Fig. 6.13 shows the relative gating circuit.

6.3.6 Decrement Sampling (Duration n x D)

The inverted form of D_4 Q (channel 3), was used for the D input of the D_5 flip flop and the decrement oscillations for the clock pulse, to preform synchronization between the transmitter oscillations and the decrement oscillations. Thus, D_5 Q is a waveform of similar duration to D_4 Q but the edges defining the begining and the end are precisely synchronous with the decrement square waves.

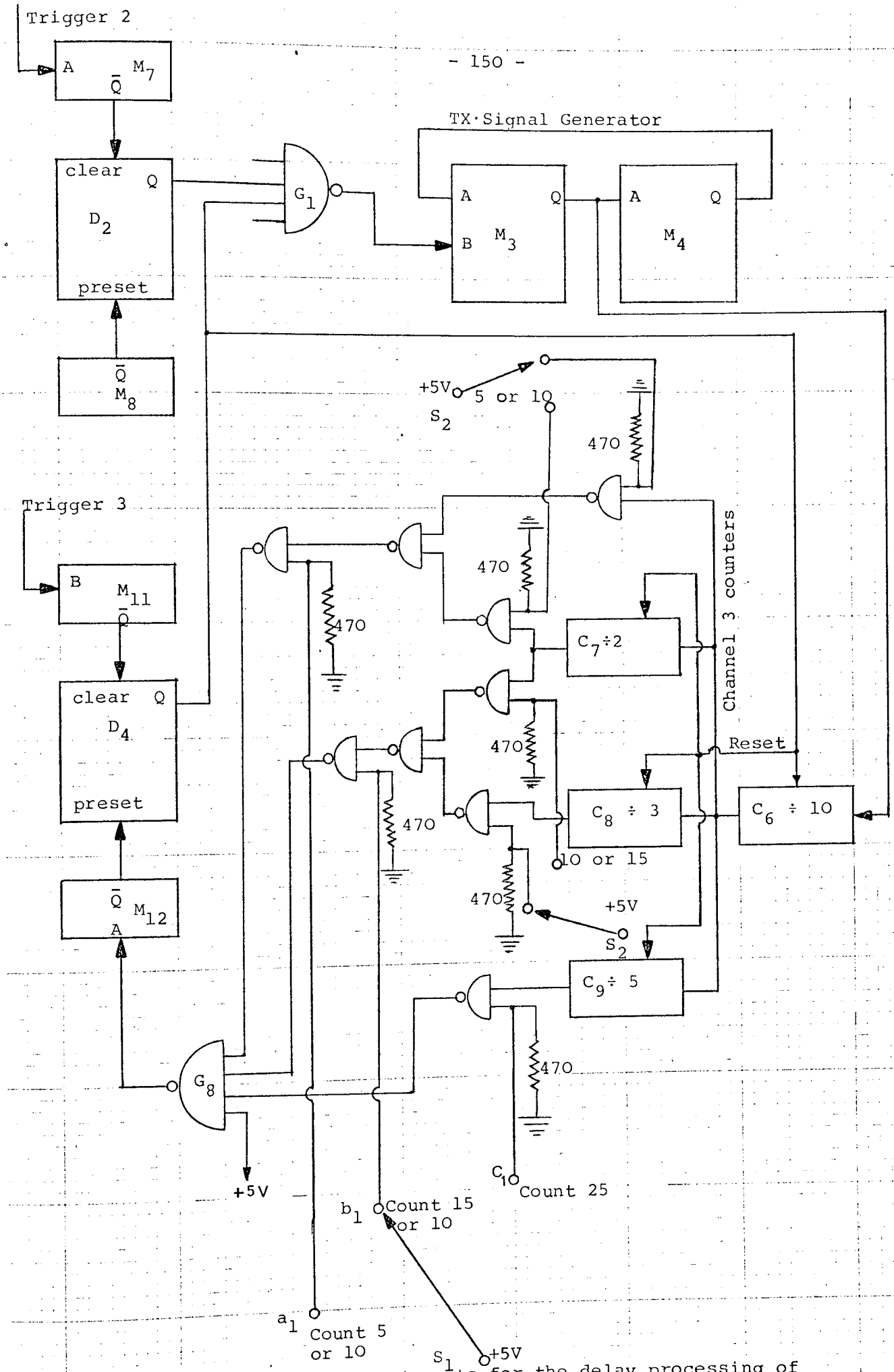

Fig. 6.13 Associated gating circuits for the delay processing of Channel 3.

The positive edge of D_5 $\bar{Q}$ triggers M_{13}, and M_{13} $\bar{Q}$ clears D_6 to start the decrement counter (C_{10}). The output of the counter after passing through M_{14} resets D_6, producing a waveform of duration n x D, equal to the number of decrement pulses counted.

In this part of the system a facility was prepared to take 5 or 10 pulses of decrement for sampling (switch S_3, Fig. 6.14), the selection depending upon the type of the probe material and its physical properties at high temperatures.

6.3.7 Channel 4 of the Multiplexer (Sample duration n x S)

This signal generator waveform is compared to the decrement waveform (n x D) to produce the error signal.

Fig. 6.15 shows the block diagram and Fig. 6.16 the waveforms of the channel 4 of the multiplexer.

The output of the D_5 flip flop (the inverse of waveform D_5 $\bar{Q}$), was used as the D input for D_7 and the inverted of the decrement oscillations as the clock pulse. The output of D_7 (D_7 $\bar{Q}$) is therefore a waveform which has a half-period of decrement delay compared with the decrement sampling (D_6 Q). The positive edge of this waveform (trigger 4), which occurs at the fifth oscillation of the decrement, starts channel 4 of the multiplexer to produce a burst of reference oscillations of the transmitter. Monostables M_{15} and M_{16} produced start and stop pulses for this channel, where D_8 and two counters (C_{11} and C_{12}) were used to perform the function of this channel as before. The resultant waveform (Duration n x S) of Fig. 6.16, is used in conjunction

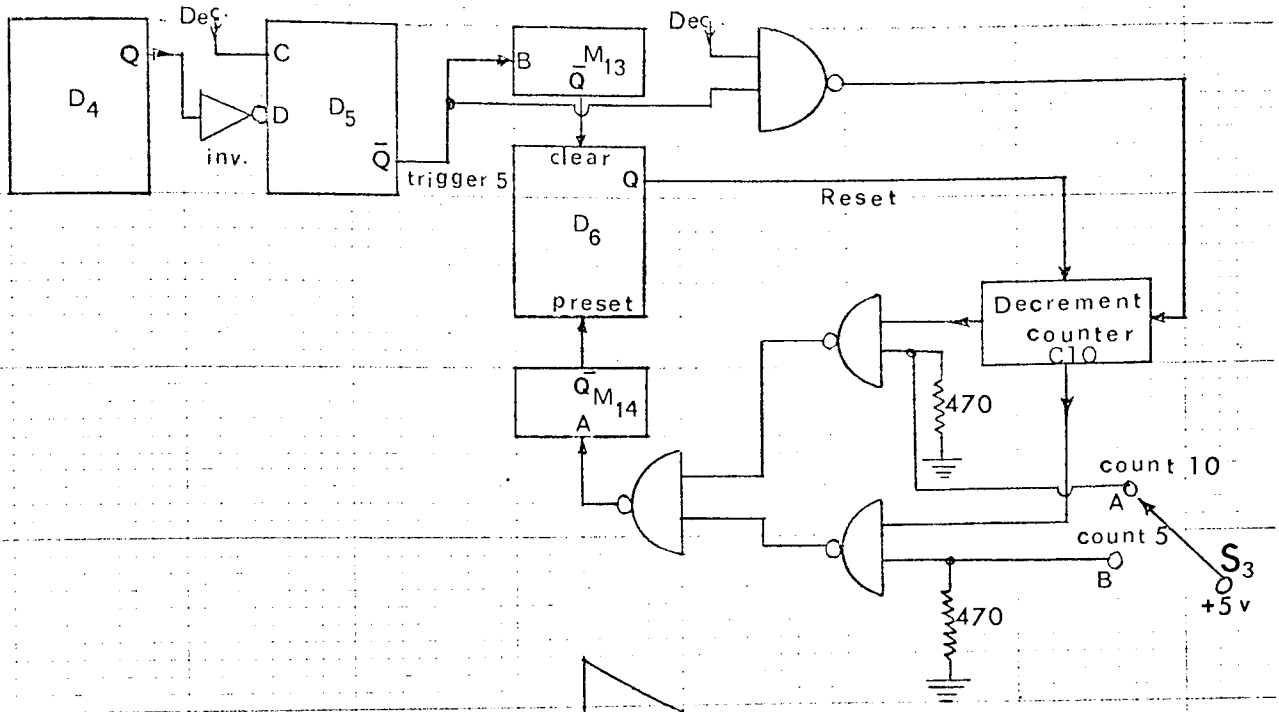

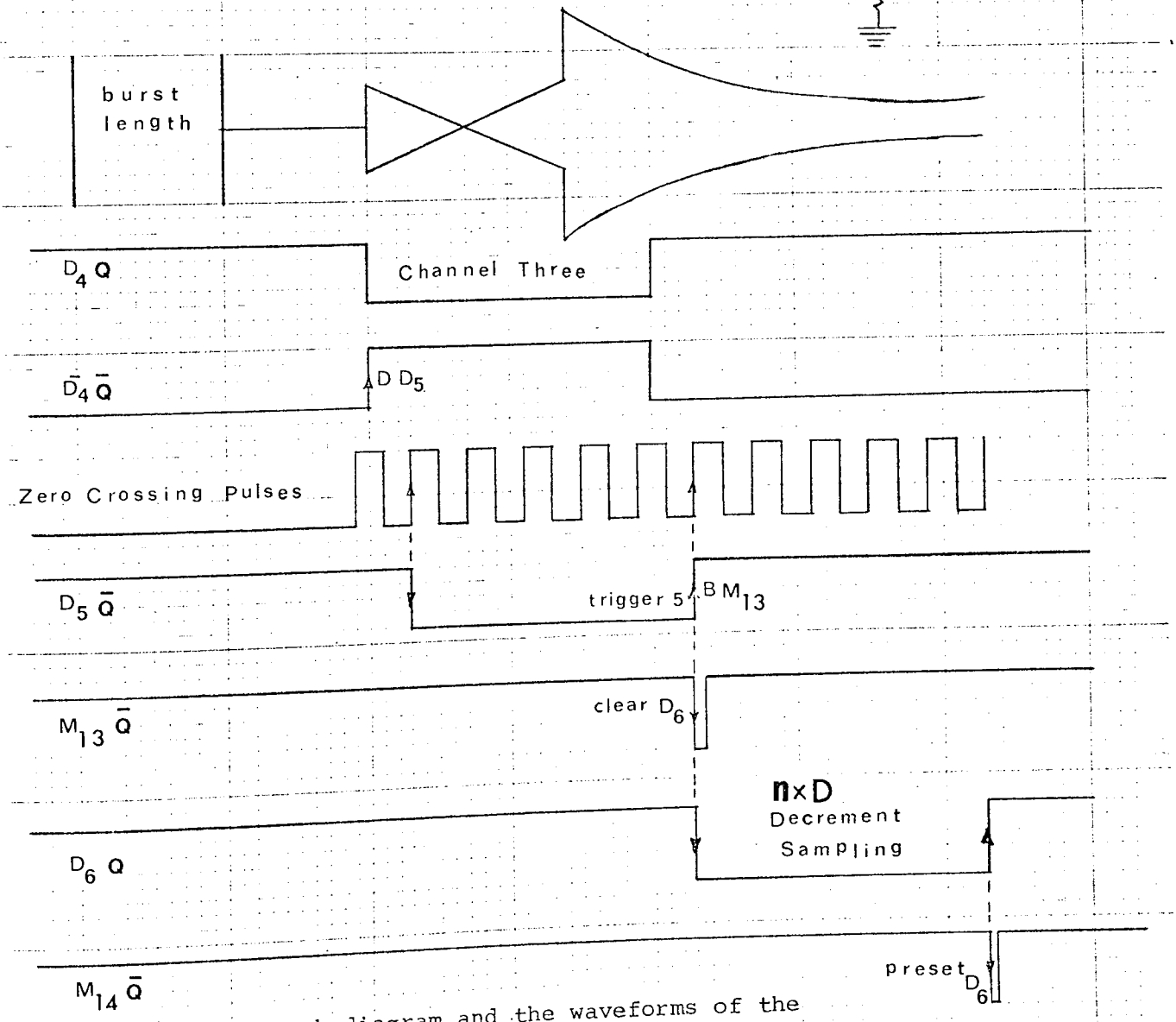

Fig. 6.14 Block diagram and the waveforms of the decrement sampling.

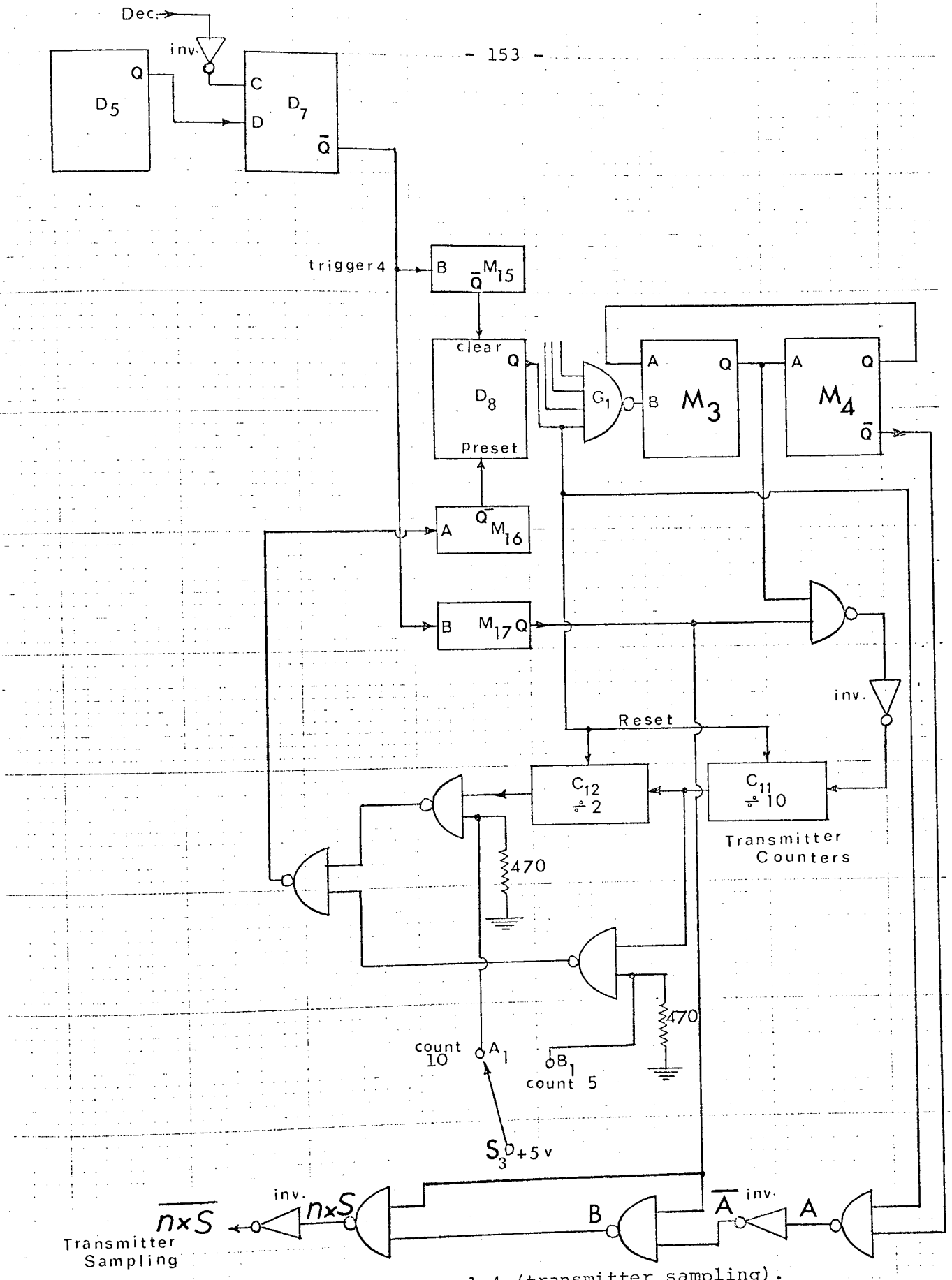

Fig. 6.15 Block diagram of Channel 4 (transmitter sampling).

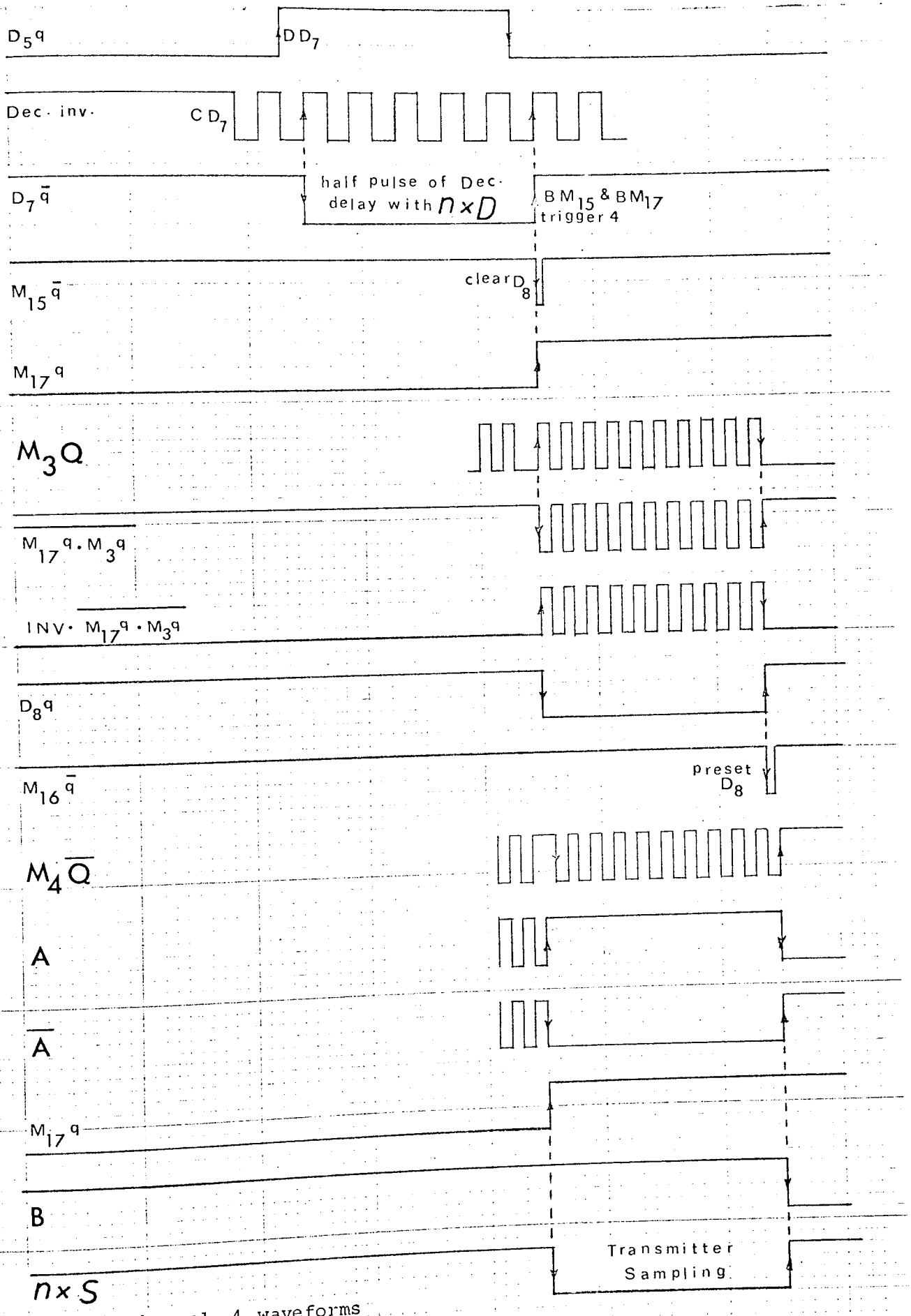

Fig 6.16 Channel 4 waveforms

with (n x D) to produce the error signal.

6.4 THE ERROR MEASUREMENT

In the error measurement the difference in time between n decrement signals (n x D) and the same number of transmitter oscillations (n x S) is obtained. The digital difference attained by gating the two waveforms, contains the error signal in the form of an "Early" pulse and a "Late" pulse (Fig. 6.17).

As previously stated the transmitter signal (n x S) starts half a decrement period after the decrement sample (n x D), this makes the early pulse of D/2 duration which is always constant. The late pulse changes duration with transmitter frequency, being equal to the early pulse when the periods are equal. The error signal is then obtained by generating a voltage equal to the difference in duration between the early and the late pulses.

6.4.1 Circuit Details

Both the early and the late pulses are applied to high level logic gates (as buffer and interface gates with open collector output). At the output of these gates pulses from 0 to 12V are obtained without any significant change in their widths. These pulses are applied to separate integrators which act as time to voltage converters (Fig. 6.18). The values of R and C in both integrators are exactly equal, presenting 20 μsec. charging time and 160 msec. discharge time. The difference between these two voltages gives the error signal.

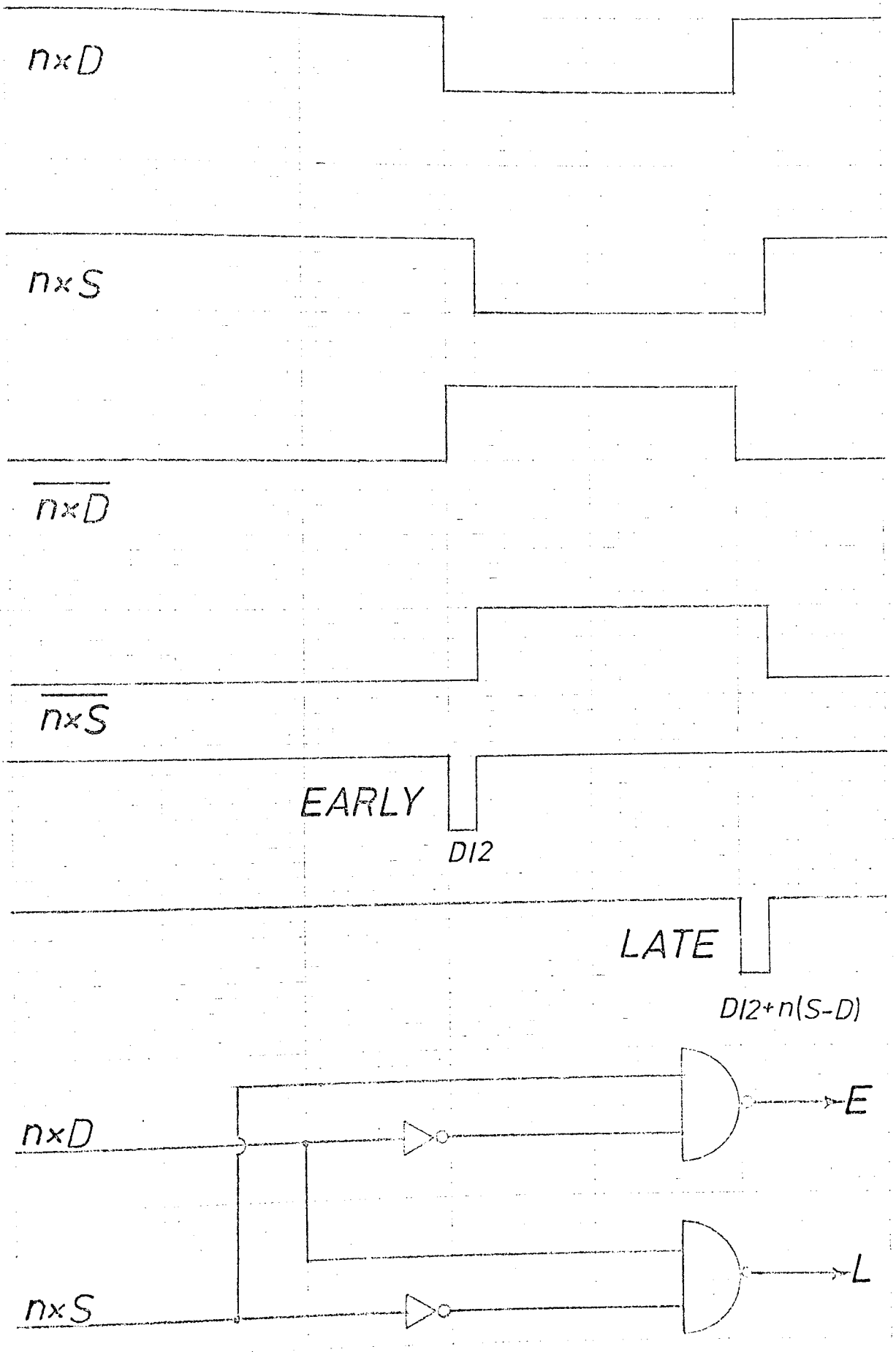

fig. 6.17 Waveforms of the Sampling Comparison.

The high level logic was needed to make pulses sufficiently large for application to the voltage followers. Fig. 6.18 shows the diagram of the error measurement circuit and Fig. 6.19 the relative waveforms.

The voltage followers used are I.C. type LM310, which have certain advantages over the conventional capacitors feedback type integrator. They are more sensitive, more stable and unlike the feedback integrator, low frequency noise is not present. The output of the voltage followers are then applied to the inputs of a difference amplifier which acts as a discriminator and produces the error signal. The error signal is then integrated over a number of the PRF cycles to give an average error voltage which in turn controls the voltage controlled signal generator. The integrator which is the essential part of the control loop operates in two different modes. In proportional control a resistor is put in parallel with the feedback capacitor giving a gain of 3.4 and in integral control the error(because it is integrated)is reduced to zero by the control system. The control loop is discussed in detail in Chapter 7. The response of the discriminator to the transmitter signal generator is shown in Fig. 6.20.

6.4.2 Analysis of the Error Measurement

The error measurement is a determining factor in the overall accuracy of the instrument. It is obtained from the transmitter signal and the decrement comparison pulses. Let each be of n cycles duration and the signal pulse being delayed by D/2. Two short pulses are derived from them, the early and the late overlap pulses of duration D/2 and

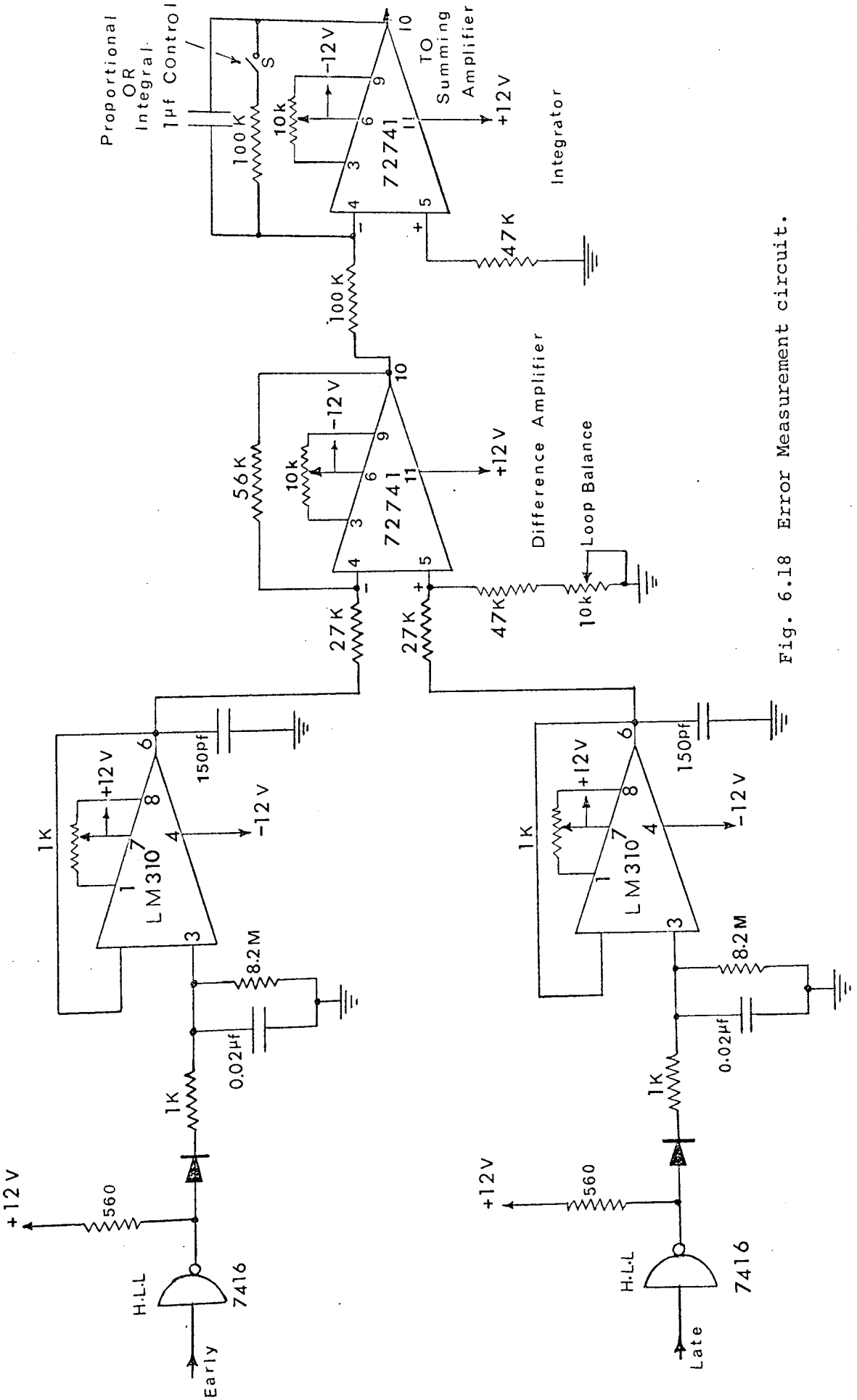

Fig. 6.18 Error Measurement circuit.

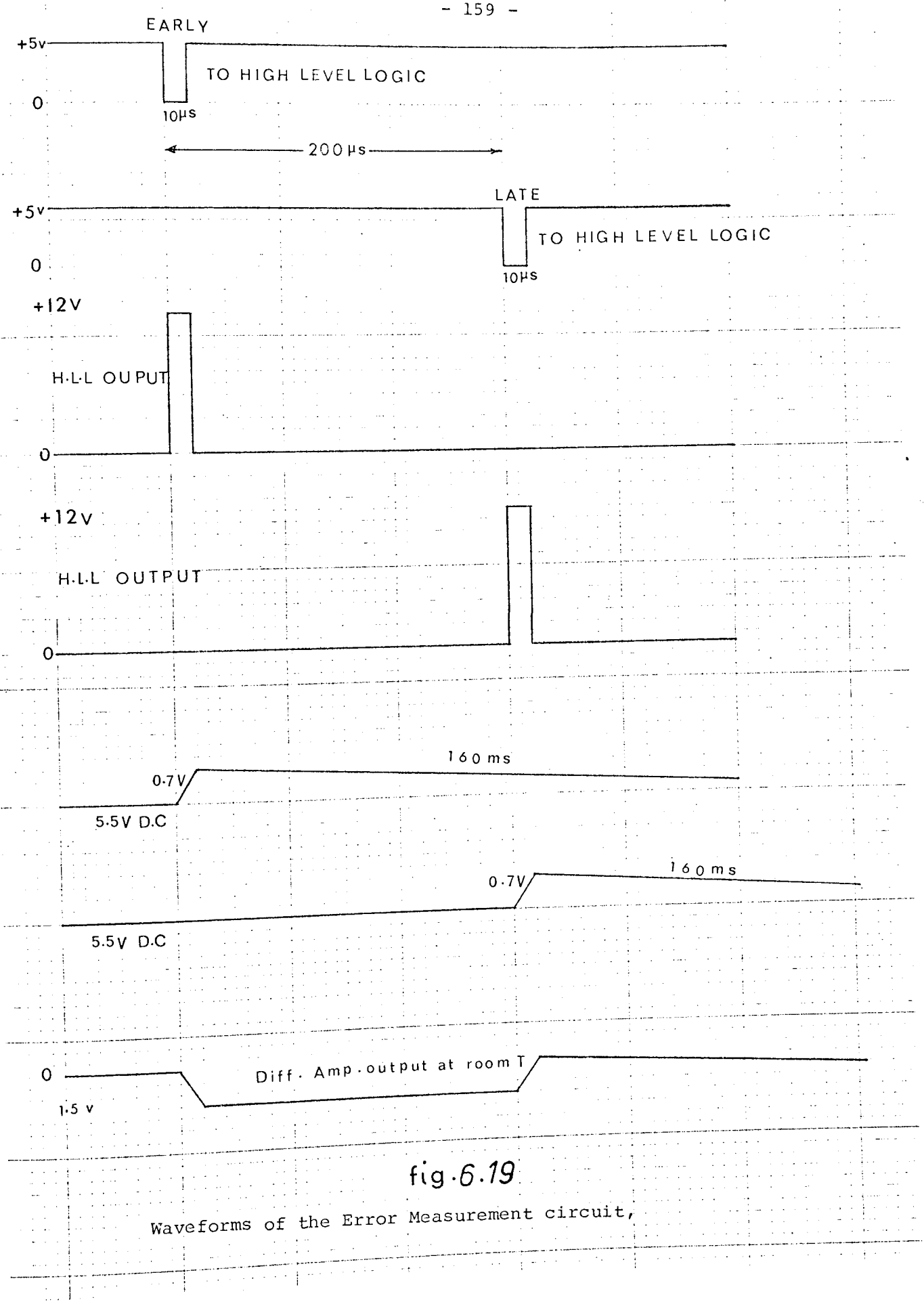

fig.6.19

Waveforms of the Error Measurement circuit,

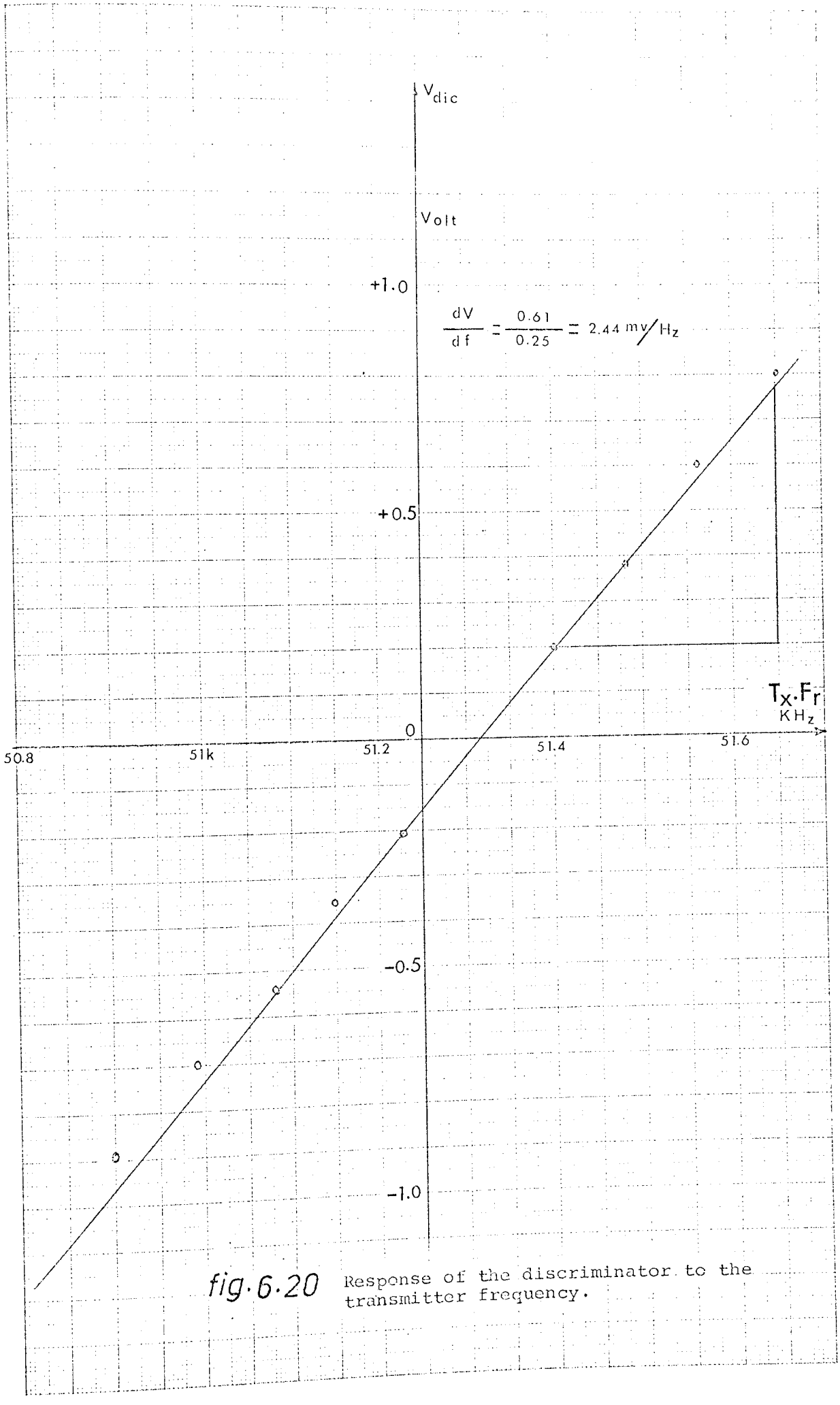

fig. 6.20 Response of the discriminator to the transmitter frequency.

$D/2 + n(S-D)$ respectively. The late pulse can be numerically negative when $S<D/(1 - \frac{1}{2n})$ but no pulse is generated for this condition. Thus as S is increased from a small value the late pulse width remains at zero until $S = D/(1 - \frac{1}{2n})$ after which it increases linearly with (S-D), the pulses being equal when S=D and the erro is zero. This is shown in Fig. 6.21.

The pulse durations are converted to voltage by two integrators and subtracted to give the error signal Fig. 6.18. The storage time constant of the integrators are four or five times the cycle time of the instrument and constitute the major signal delay in the control loop. So long as there is a detectable decrement, the polarity of the error signal will give the true sense of (S-D).

In the absence of a decrement the control, which is second order and consequently incorporates an integrator, will drive the signal generator to a high or low frequency extreme. In practice, once established, control is not lost even with very rapid temperature cycling. An alarm could however, be incorporated by monitoring the decrement signal.

The error measurement is a determining component of the sensitivity of the control system. In terms of a decrement period of 10μsec a measuring accuracy of 1 in 10^4 and a sample of 10 oscillations requires a 10 nsec resolution. The initial sample of 5 μsec. gives 5 volts output and the measuring accuracy required is therefore 5 m volt.

Noise in the output originates from intrinsic electronic noise and pulse fluctuations of the sensor. If the early pulse (D/2) is applied to both error measurement channels, only

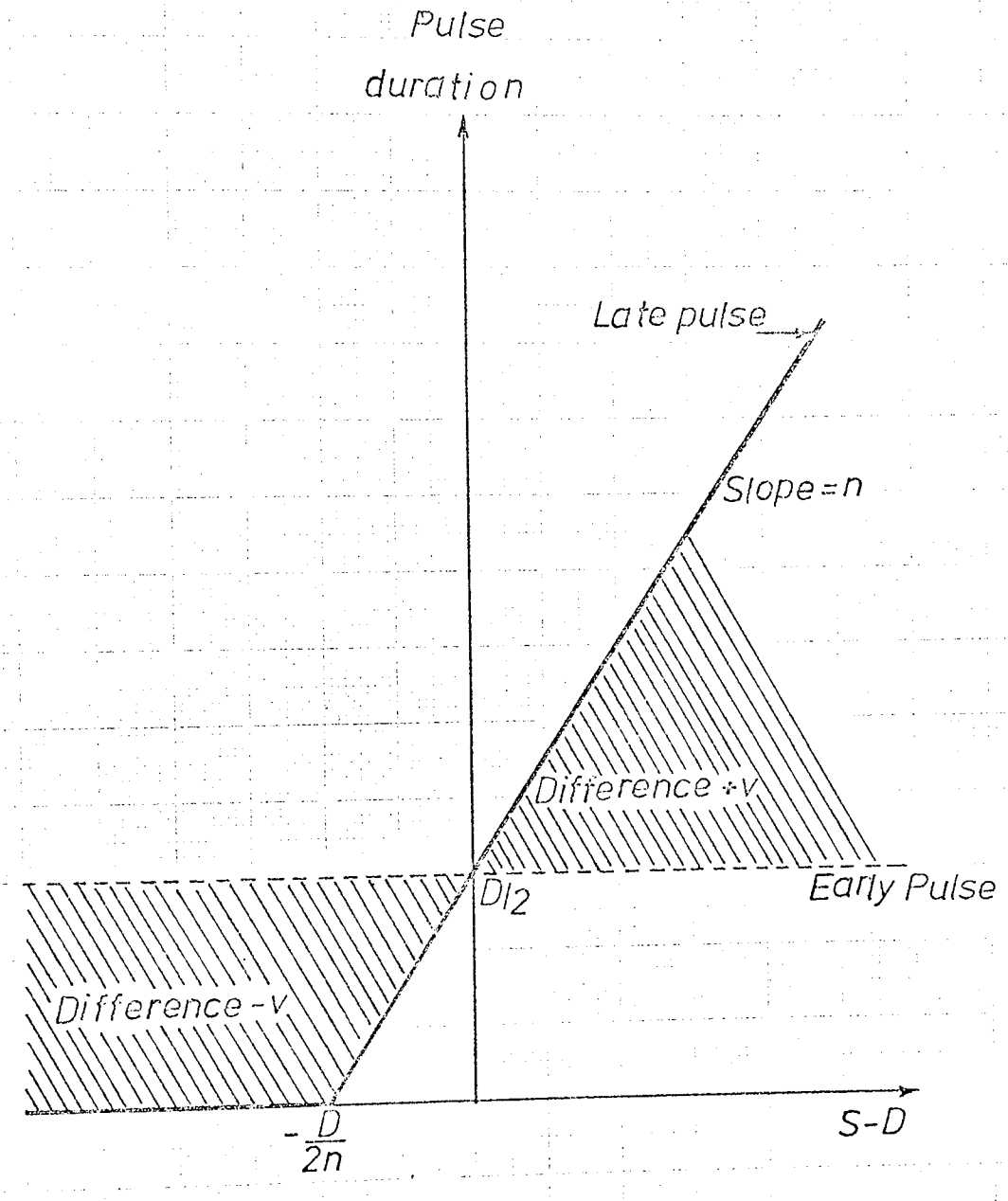
Pulse
duration
Late pulse
Slope = n
Difference +v
Early Pulse
D/2
Difference -v
-D/2n
S-D

fig. 6.21

intrinsic noise will appear at signal generator. Similarly pulse width noise can be identified by keeping the sensor at constant temperature.

6.4.3 Summation Amplifier

As described before and shown in Fig. 6.3, the amplifier A_1 controlling the signal generator has two inputs, one from a manual controlled potentiometer and the other feedback voltage from the integrator. In the closed loop condition the voltage from the manual control and that from the integrator must combine to make the oscillator frequency that of the resonator. While the control operates effectively for integrator outputs between ±9 volts - the full linear range of the operational amplifier - it is desirable during an experiment to avoid excessive voltage on the integrator output and this is effected by initial adjustment of the manual control in the proportional or open loop states.

The summation amplifier being part of the control loop is considered also in the Chapter 7.

6.5 DATA TRANSFER AND DISPLAY

It is generally required to design and provide measuring and displaying facilities for the instrument itself. In this particular case, there are two quantities to be measured in the system, the period of the transmitted signal and the temperature which is derived from the period.

To measure the period, channel 1 which produces 100

oscillations of the signal generator is used (Fig. 6.6). The $\bar{Q}$ output of the start-stop flip flop D_1 [Cf. QD_1 of Fig. 6.7] has duration of 100 oscillator periods [equal to 50 x S as the period actually used in the instrument is half that of the oscillator]. This operates a gate allowing signals from a 20 MHz clock to pass through and be counted. The count will be 50 x S x 20 = 1000S, giving the required 1 in 10^4 accuracy for S = 10 μsec. (See Fig. 6.23).

The clock oscillator was used is a compact unit crystal quartz oscillator type QC1310 which is compatible for direct logic drive applications and no interface was required. A frequency tolerance of ±10 in 10^6 at 25°C is of the specifications of this clock oscillator and this is more than adequate. For the second requirement, the digital values of the probe temperature may be needed to dispaly. In this case, a series of accurate measurements of the period temperature calibrations for the particular probe must be considered. Calculations of the probe sensitivity at the different temperature range is also important for the above purpose.

6.5.1 The Display System

To display the period, a series of the Hewlett Packard solid state numeric indicator type HP7300 were used. It is TTL compatible, includes decoder/driver with memory for 8421 BCD positive logic input and has a decimal logic facility. Logic 0 at the enable input transfers the data from the counter to the indicator. Display is updated at every enable pulse.

6.5.2 The Data Transfer

The content of the counters is transferred to the display by the enable pulse E_2 (Fig. 6.23). At the same time a transfer can be to the other digital units such as the digital to analogue converter or data logger. Data transfer takes place through a 6 x 4 bit latch type 7475. Before displaying the content of the counters on the indicators, a 40 nsec. reset pulse is produced by monostable (reset mono of Fig. 6.23), which resets all the indicators from the previous numbers. When the counting of the oscillations are completed, mono L_1 produces an enable pulse E_1 to transfer the content of the counters to the digital to analogue converter unit andalso to the display system.The repetition of this enable pulse is synchronous with the PRF, updating the information.

Using another mono L_2 with 0.6 sec. pulse width, a 100 nsec. short enable pulse E_2 and long latch pulse of 0.6 sec. is produced to hold the data on the display for vision. Fig. 6.22 shows the block diagram and Fig. 6.23 shows the relative waveforms of the display system and data transfer.

6.6 ANALOGUE DISPLAY OF PERIOD

In most of the real applications of the ultrasonic thermometer it would be necessary to demonstrate the variations of a probe temperature or temperature stability of a particular probe against the time or against any references such as the thermocouple emf and etc. To meet

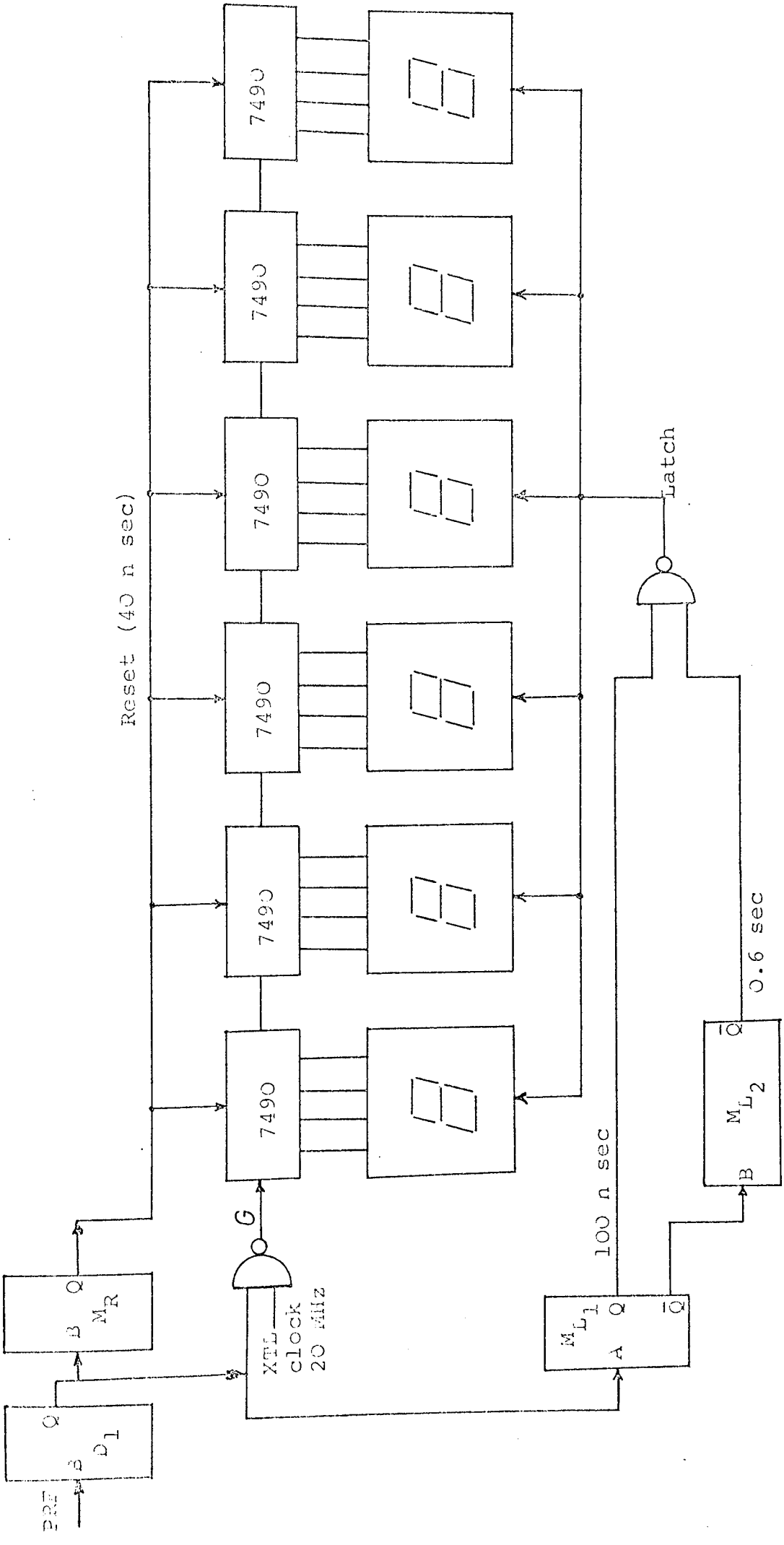

Fig. 6.22 Period Display Circuit.

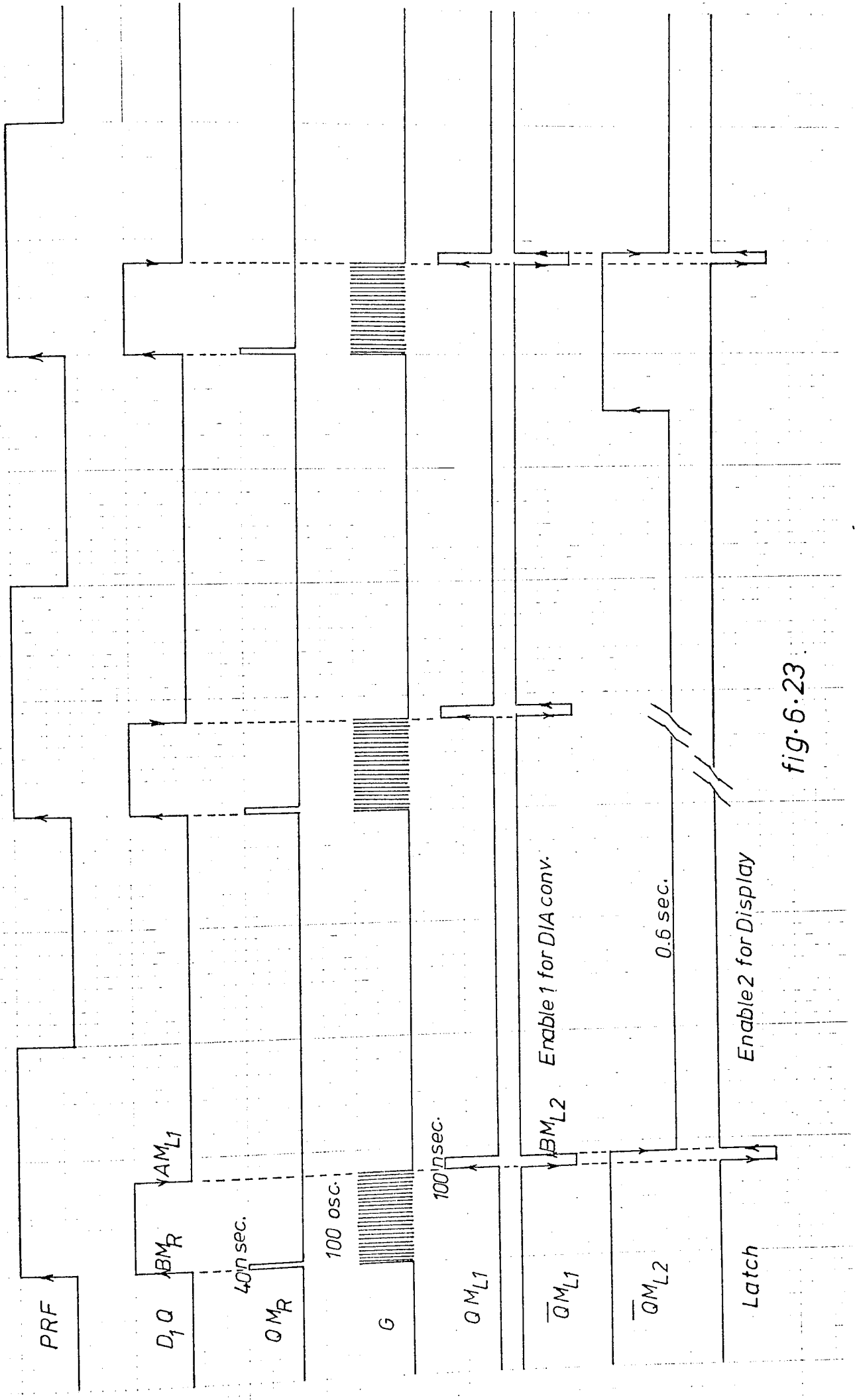
PRF
D1 Q
BMR
AML1
40 n sec.
QMR
100 osc.
G
100 n sec.
QML1
BML2
Enable 1 for DIA conv.
0.6 sec.
Enable 2 for Display
Latch

fig. 6.23

these requirements one of the very useful and precise methods is to convert the digital data to the analogue voltage at the output of the electronic system. To perform this function a monolithic high-speed 12 bit BCD D/A converter type MP1812A (Analogic) is used in the instrument. It is TTL compatible and has a 20 V/μsec. output which provides analogue outputs upto ±10 volts. It has built-in recalibration potentiometers and is short circuit proof to ground. The high precision wire wound resistor network presents an accuracy of 0.01% of full scale reading (FSR), and the isolation facility between the analogue and digital grounds is provided. 5 decades of period are displayed, the least significant digit being 1 nsec. BCD code 8,4,2,1.

6.6.1 D/A Converter Selector Switch

Selection facilities for different resolution of display are required. For calibration a wide digital range is necessary and for watch keeping only the two significant digits are needed. This involves a four position wafer switch which is located at the rear panel of the instrument and enables various D/A combinations to be obtained. As these combinations are complicated therefore are discussed in detail (see Fig. 6.24).

The four positions of the selector switch is as follows.

Position 1 - Looking to the three digits S.R.Q. of the display, if considering the analogue display being $\overset{MSD}{X}$ Y $\overset{LSD}{Z}$ respectively.

therefore in this position

X $\xrightarrow{\text{relates to}}$ S

Y —relates to→ R

Z —relates to→ Q

Position 2 - Looking to the three right hand side digits R, Q, P.

therefore X —relates to→ R

Y —relates to→ Q

Z —relates to→ P

Position 3 - Looking to the two right hand side digits only Q, P.

therefore X —relates to→ Q

Y —relates to→ P

Z —relates to→ O, O, O, O.

Position 4 - Calibration full scale 999.

therefore X —relates to→ 9 = 1001

Y —relates to→ 9 = 1001

Z —relates to→ 9 = 1001

See Fig. 6.24.

A combination of 4 wafer switches each wafer being 3 poles 4 ways, makes a good arrangement between the binary output of the display latches and the BCD input of the D/A converter. To distinguish the binary output of each lach by the letters A, B, C, D for 1, 2, 4, 8 respectively, therefore:

digit S				digit R				digit Q				digit P			
1	2	4	8	1	2	4	8	1	2	4	8	1	2	4	8
A_S	B_S	C_S	D_S	A_R	B_R	C_R	D_R	A_Q	B_Q	C_Q	D_Q	A_P	B_P	C_P	D_P

And considering the following names for the 3 BCD input of the D/A converter.

First Bit				Second Bit				Third Bit			
1	2	4	8	1	2	4	8	1	2	4	8
A_X	B_X	C_X	D_X	A_Y	B_Y	C_Y	D_Y	A_Z	B_Z	C_Z	D_Z

To operate the 4 positioned selector switch, the following combinations must be arranged.

Position 1	A_S	→	A_X	A_R	→	A_Y	A_Q	→	A_Z
	B_S	→	B_X	B_R	→	B_Y	B_Q	→	B_Z
	C_S	→	C_X	C_R	→	C_Y	C_Q	→	C_Z
	D_S	→	D_X	D_R	→	D_Y	D_Q	→	D_Z
Position 2	A_R	→	A_X	A_Q	→	A_Y	A_P	→	A_Z
	B_R	→	B_X	B_Q	→	B_Y	B_P	→	B_Z
	C_R	→	C_X	C_Q	→	C_Y	C_P	→	C_Z
	D_R	→	D_X	D_Q	→	D_Y	D_P	→	D_Z
Position 3	A_Q	→	A_X	A_P	→	A_Y	0	→	A_Z
	B_Q	→	B_X	B_P	→	B_Y	0	→	B_Z
	C_Q	→	C_X	C_P	→	C_Y	0	→	C_Z
	D_Q	→	D_X	D_P	→	D_Y	0	→	D_Z
Position 4	1	→	A_X	1	→	A_Y	1	→	A_Z
	0	→	B_X	0	→	B_Y	0	→	B_Z
	0	→	C_X	0	→	C_Y	0	→	C_Z
	1	→	D_X	1	→	D_Y	1	→	D_Z

Figs. 6.25 shows the way which the wafer switches are adapted for performing the above functions. In this arrangement all A's inputs and outputs are connected on one wafer (e.g. A_X, A_Y, A_Z) and all B's are on one wafer and etc. This method avoids any interconnection between the wafers.The four wafers are identical except for the fourth position (999).

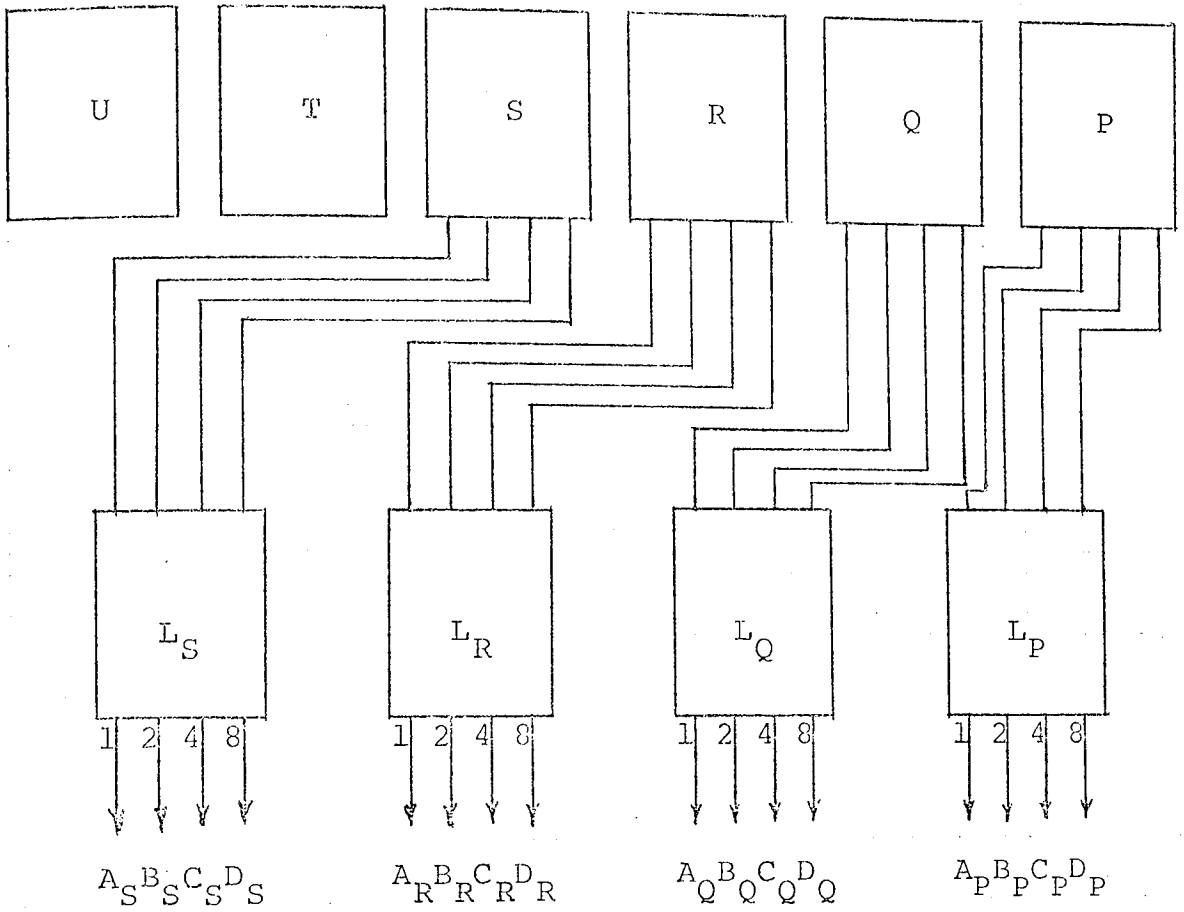

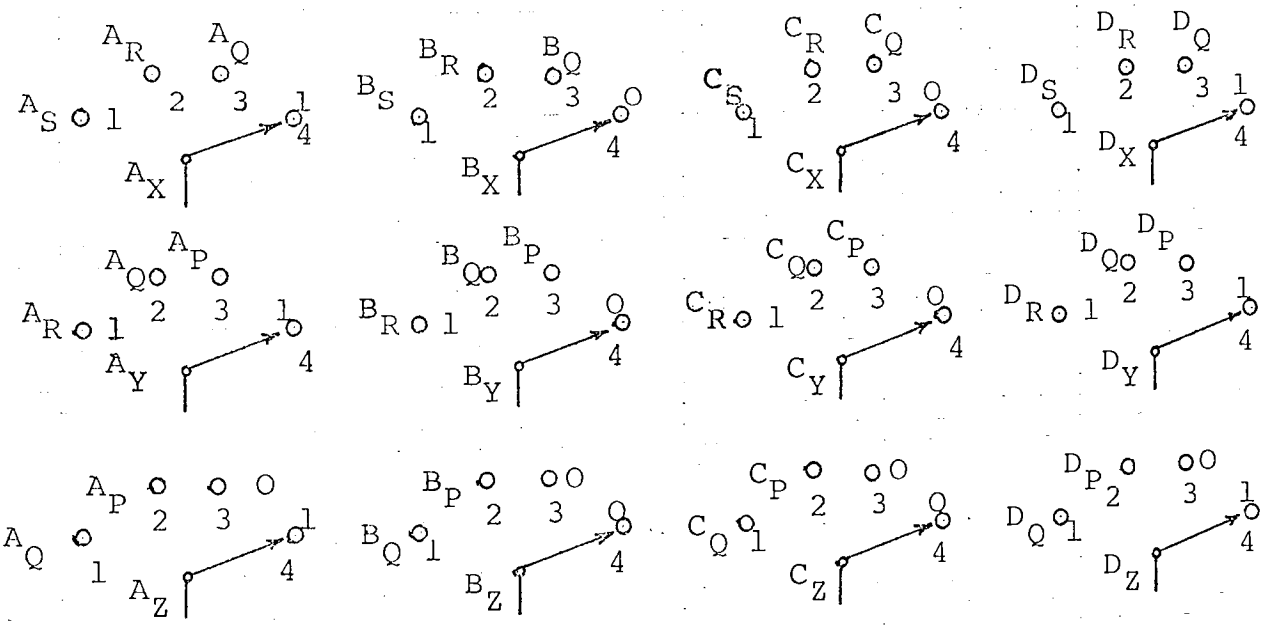

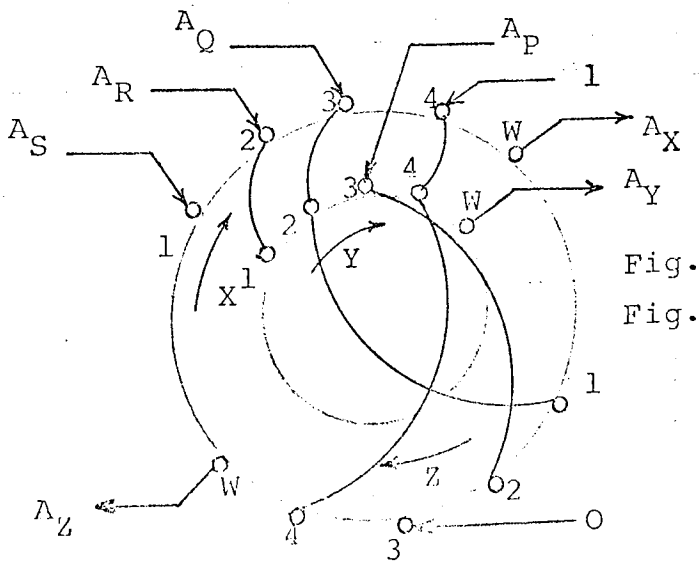

Fig.6.24 Display

Fig.6.25 A's wafer switch.

Fig. 6.26 This photograph shows the electronic circuits design, constructed on the Vero boards.

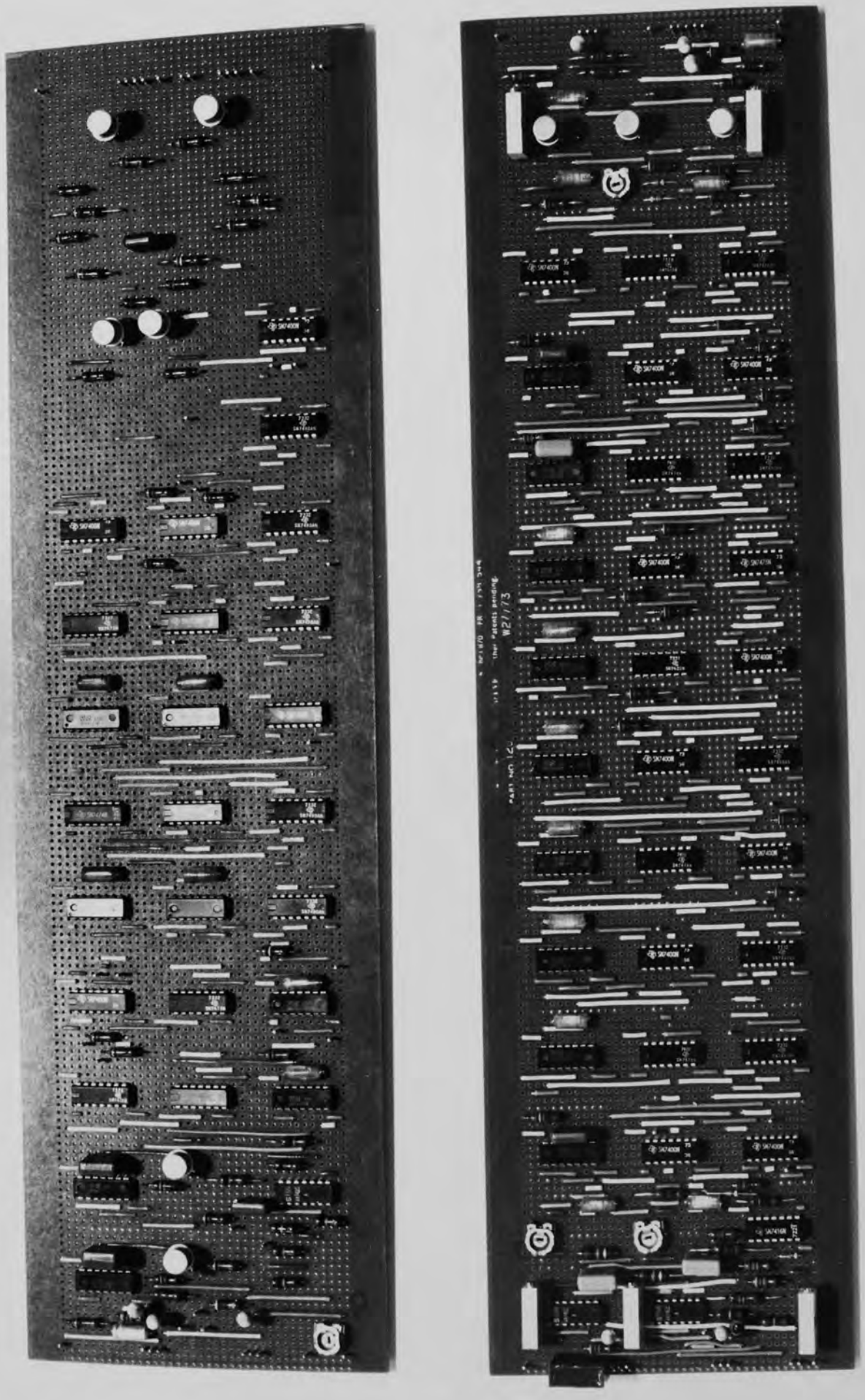

Fig. 6.27 This photograph shows the complete electronic automatic instrument for tracking the resonance frequency of the temperature sensors.


ASTON UNIVERSITY
APRIL 1974 A.A.FATHIMANI
ULTRASONIC RESONANCE TRACKING INSTRUMENT
TYPE F.A.8543
TEMPERATURE °C
PERIOD µs
DISPLAY
P.R.F.
LOOP BALANCE
BURST NUMBER
5 10 20
FREQUENCY
DECREMENT SAMPLE
5 10
SAMPLE DELAY
OFF ON
12V
0V
-12V
PROPORTIONAL
INTEGRAL
CONTROL
MANUAL
AUTOMATIC
TTL
ON
OFF
SOLARTRON 7040
Schlumberger
LAMP LOAD MODIFIED
USER GUIDE

CHAPTER 7

PERFORMANCE OF THE ELECTRONIC SYSTEM

7.1 INTRODUCTION

The function of the electronic system and design requirements for automating the ultrasonic thermometer are described in Chapter 6. To employ the electronic system practically for high temperature measurements, the system must be capable of operating automatically for several hours or days without any failure and the signal generator must always track the resonance frequency of the temperature sensor during the whole period of experiment.

In most of the experimental works with the automatic system for investigation of the thermophysical properties of the probe materials in the 1800^{o}C vacuum furnace, the electronic system operated perfectly in conjunction with the Data Transfer Unit and the teletype machine which used to give simultaneous automatic recording of resonance (period) and temperature. The frequency change might typically be 100 kHz - 80 kHz. To obtain the capability of the electronic system, a series of the standard measurements and tests were prepared to investigate its reliability and performances.

Control loop analysis, open and closed loop static gain calculations, frequency response measurements (using a transfer function analyser), response to the step function and the overall noise investigations are of the major experiments which were performed for the automatic instrument

and will be described in detail in this chapter.

7.2 THE CONTROL SYSTEM

The function of the control system is to make the signal generator period follow the variations in decrement period as it varies with the temperature. The control system as shown in Fig. 7.1(a) makes use of the following sections:

(a) The difference amplifier or discriminator. For comparing the early and late signals to produce the error signal. As described in Chapter 6, the amplitudes are proportional to the respective pulse widths.

(b) The integrator. For integrating the error signal with a time constant of τ_2=0.1sec which is a few times longer then the operating cycle of the instrument. The transfer function is therefore $1/\tau_2 p$.

(c) The summation amplifier. The output controls the signal generator frequency and the input is the sum of signals from three sources. The amplifier has unity gain, inverting the signal, making the overall feedback negative.

7.2.1 Analysis of the Control Loop

The period S of the voltage controlled signal generator has three control inputs, Vm from the manual potentiometer, V_{in} which is zero until the feedback loop is closed and Vx which is available for performance tests, Fig.7.1(b).

The voltages are applied through equal resistors to a summing point. Equation (7.1) gives the relationship.

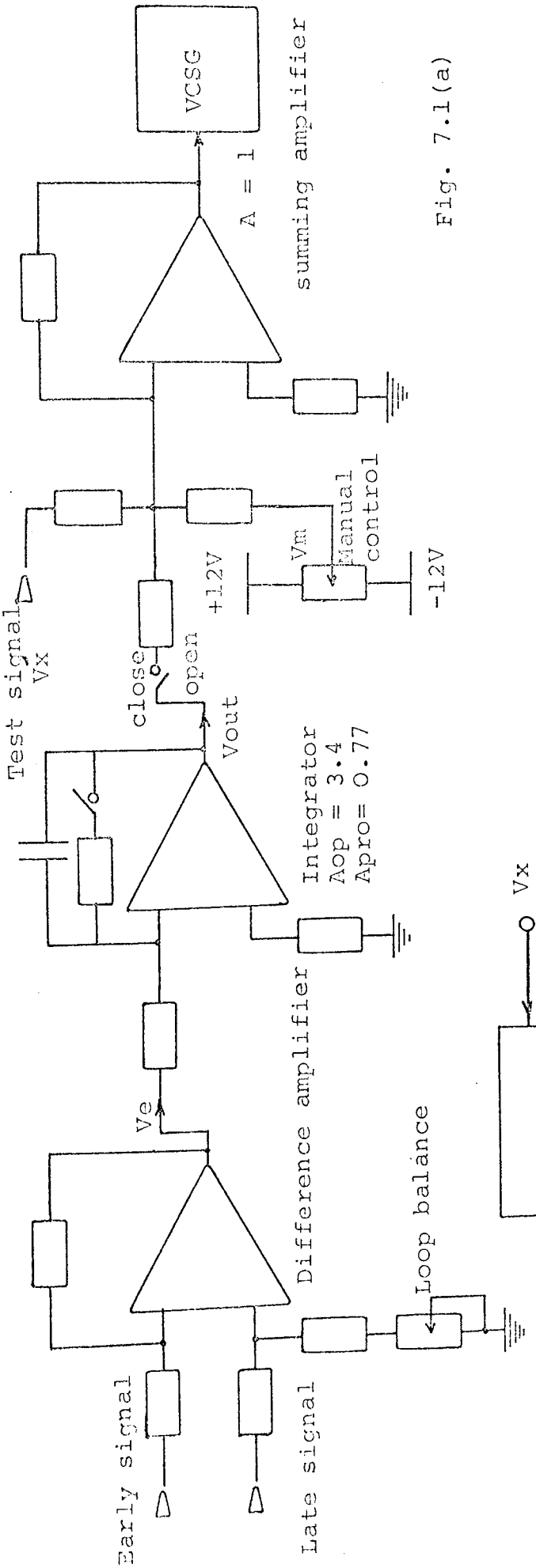

Fig. 7.1(a)

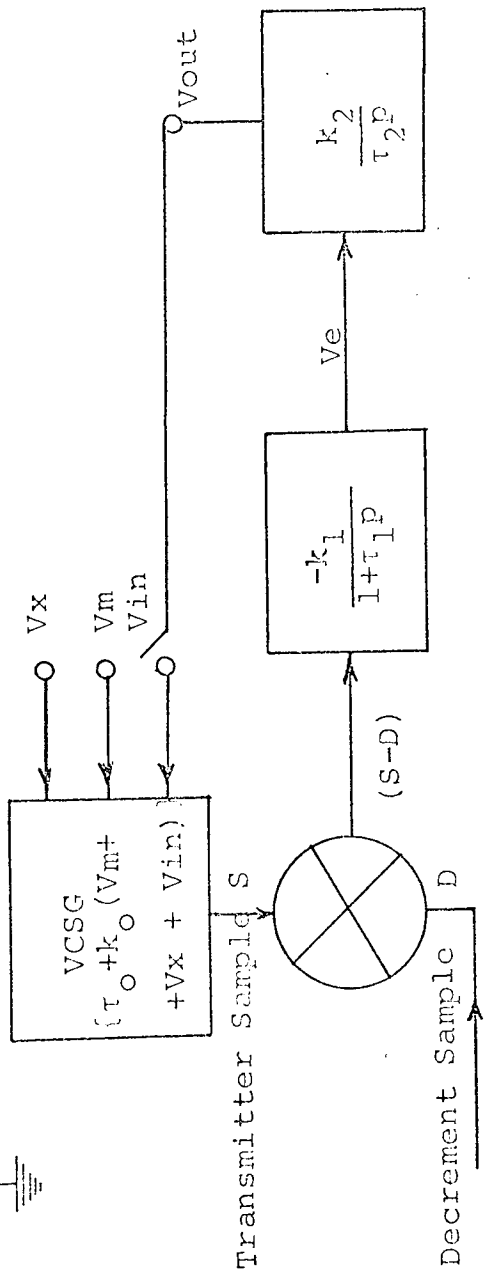

Fig. 7.1(b)

τ_o is preselected to be in the midrange of the probe in use and k_o enables S to be varied over about ±50% for ±9 volt input, the dynamic range of the amplifiers.

$$S = \tau_o + k_o(Vin + Vm + Vx) \qquad (7.1)$$

The error measurement averages the difference between S and D over about five recurrence cycles. This averaging involves a significant delay which is represented by the denominator in the error voltage equation (7.2).

In the steady state the denominator is unity and in the case of a step in S or D, Ve approaches the new steady state value exponentially, following the function $1- \exp (-t/\tau_1)$

$$Ve = \frac{k_1}{1+\tau_1 p} (S - D) \qquad (7.2)$$

On closing the loop the error signal is fed back to the input either via a unity gain amplifier giving proportional control or an integrator giving integral control. The latter is a second order system controlling down to zero error.

The overall open loop transfer function for integral control is given by equation (7.3). On proportional control the Laplace factor becomes $\frac{k_1}{1+\tau_1 p}$

$$V_{out} = \frac{Ve}{\tau_2 p} = \frac{k_1/\tau_2}{p(1+\tau_1 p)} \{\tau_o + k_o(V_{in} + Vm + Vx - D)\} \qquad (7.3)$$

When the loop is closed with negative feedback $V_{in} = -V_{out}$ and the dynamic performance can be found by

differentiating equation (7.3) with respect to Vx, giving equation (7.4)

$$\frac{\partial Vout}{\partial Vx} = \frac{k_o k_1/\tau_2}{p(1+\tau_1 p)} \left(1 - \frac{\partial Vout}{\partial Vx}\right) \qquad (7.4)$$

Equation (7.5) gives the standard form for unity negative feedback where

$$A = \frac{k_o k_1/\tau_1\tau_2}{p(p+\frac{1}{\tau_1})} = \frac{K}{p(1+\frac{1}{\tau_1})}$$

$$\frac{\partial Vout}{\partial Vx} = \frac{1}{1+1/A} = \frac{K}{p^2+\frac{1}{\tau_1}p+K} \qquad (7.5)$$

7.2.2 Static Tests On The Control Loop

Three sets of static tests were performed to obtain the overall loop gain for the three conditions of control, manual, proportional and integral. The resonator was used is a 3.1 mm sapphire integral line probe with S = 5.884 μsec period of the resonance frequency. The classified results are given below.

a - On Manual Control

In this mode of control Vin = 0 and the variations of Vm, the manual input of the summing amplifier, and Vo=Ve from discriminator output and the period S from display were taken. The results are given in Table 7.1 and shows S and Ve to be linear with Vm.

Table 7.1

S	Vm=Vx	Ve=Vo
5.800 µsec	-525 mV	-1212 mV
5.810	-488	-1040
5.820	-450	- 833
5.830	-412	- 730
5.840	-376	- 586
5.850	-337	- 436
5.860	-299	- 294
5.870	-260	- 152
5.880	-224	- 25
5.884 Resonance	-209	+ 30
5.890	-185	117
5.900	-151	229
5.910	-112	357
5.920	- 76	471
5.930	- 38	588
5.940	+ 0.5	704
5.950	36	809
5.960	72	911
5.970	108	1013
5.980	147	1120
5.990	183	1220
6.000	219	1304

b - On Proportional Control

The same tests were performed on the proportional mode of control and variations of output voltage Ve and period S against the input voltage Vx were measured. The results are given in Table 7.2. Again S and Ve are linear functions of Vm but the control greatly reduces the dependence.

Table 7.2

S	Vx	Ve
5.800 µsec	-1760 mV	-1218 mV
5.810	-1555	-1050
5.820	-1351	- 887
5.830	-1155	- 730
5.840	- 962	- 577
5.850	- 786	- 438
5.860	- 595	- 287
5.870	- 414	- 145
5.880	- 243	- 12.6
5.884 Resonance	- 187	+ 31.5
5.890	- 83	112
5.900	+ 85	241
5.910	242	361
5.920	397	478
5.930	554	596
5.940	704	709
5.950	851	818
5.960	994	924
5.970	1141	1033
5.980	1276	1131
5.990	1412	1230
6.000	1524	1309

c - On Integral Control

The above static test were also performed on the integral mode of control and the variations of Vout against Vx were considered (Ve=0). The only point about the integral control is, the error voltage approaches zero and therefore display S always shows the period of the resonance frequency (S = 5.884 µsec), hence only Vx and Vout were taken in the note. The results are given in Table 7.3 and shows S to be sensibly independent of Vm.

Table 7.3

Vx	Vout	Vx	Vout	Vx	Vout
-2000 mV	-1778 mV	-600 mV	-378 mV	800 mV	1022 mV
-1900	-1678	-500	-278	900	1122
-1800	-1578	-400	-178	1000	1222
-1700	-1478	-300	- 78	1100	1322
-1600	-1378	-200	+ 22	1200	1422
-1500	-1278	-100	122	1300	1522
-1400	-1178	0	222	1400	1622
-1300	-1078	100	322	1500	1722
-1200	- 978	200	422	1600	1822
-1100	- 878	300	522	1700	1922
-1000	- 778	400	622	1800	2022
- 900	- 678	500	722	1900	2122
- 800	- 578	600	822	2000	2222
- 700	- 478	700	922		

The graphical results of the three above tables are shown in Figs 7.2 and 7.3. In Fig 7.2 the relationship between Vout and Vx for three conditions, the open loop, the closed loop proportional and the closed loop integral are shown.
On manual control the slope is open loop gain A,

$$\frac{\partial Ve}{\partial Vm} = \frac{\partial Ve}{\partial Vx} = k_o\, k_1 = 3.4 = A \qquad (7.6)$$

On proportional control the slop is $\frac{A}{1+A}$

$$\frac{\partial Ve}{\partial Vm} = \frac{k_o k_1}{1+k_o k_1} = 0.77 = \frac{A}{1+A} \qquad (7.7)$$

$$\text{Therefore } \frac{\partial \text{Vout open loop}}{\partial \text{Vout closed loop}} = 1+k_o k_1 = 4.4 = 1+A \qquad (7.8)$$

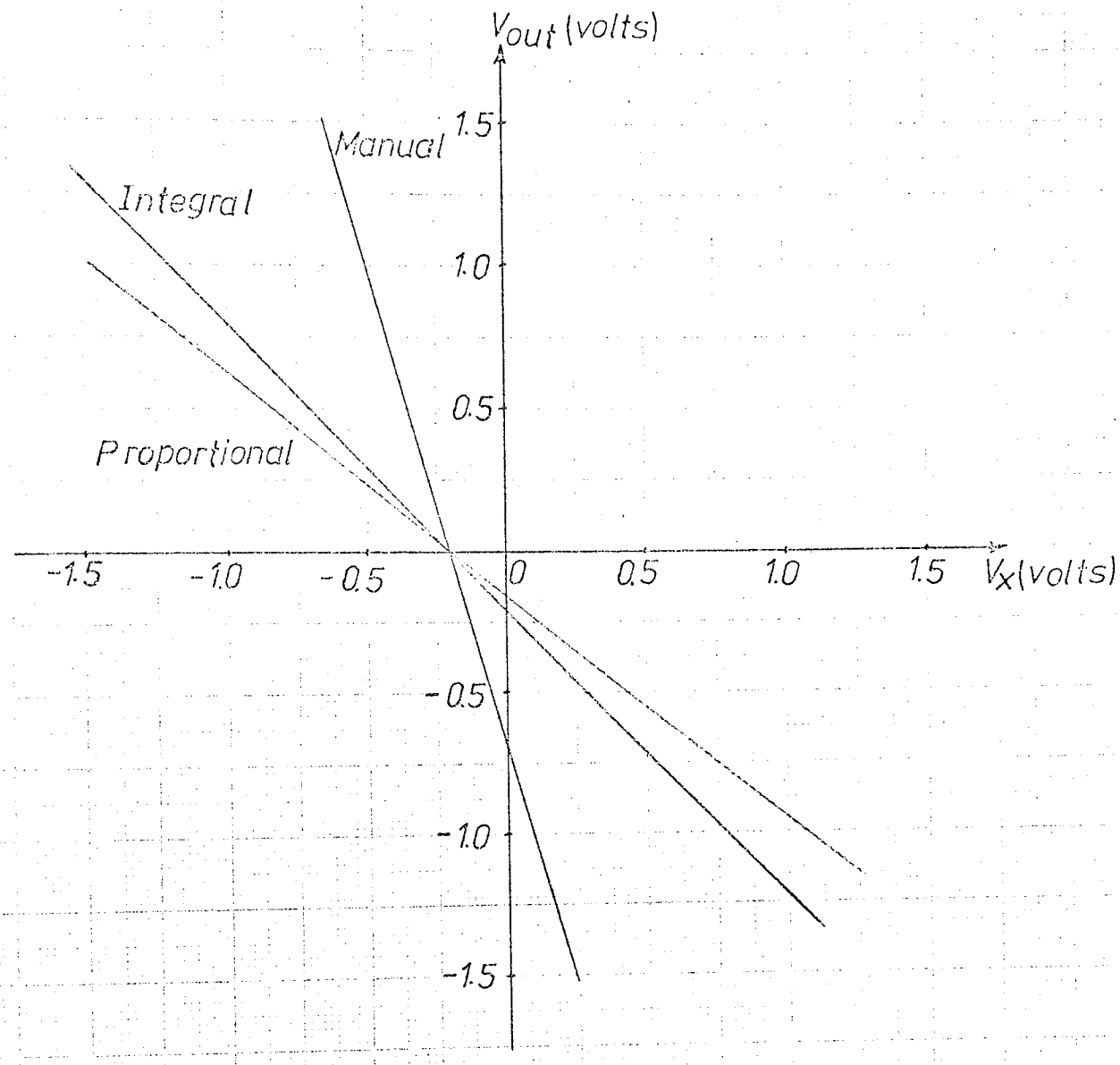

Fig.7.2

This figure shows the relationship between V_{out} and V_x for three conditions, the open loop, the closed loop proportional and the closed loop on integrate. On integrate the slope is unity as the feedback voltage nullifies V_x. The slope on open loop is the open loop gain A (=3.4) and on proportional is $\frac{A}{1+A} = 0.77$. It will be noted that, for a particular value of V_x, V_{out} is zero for all three conditions.

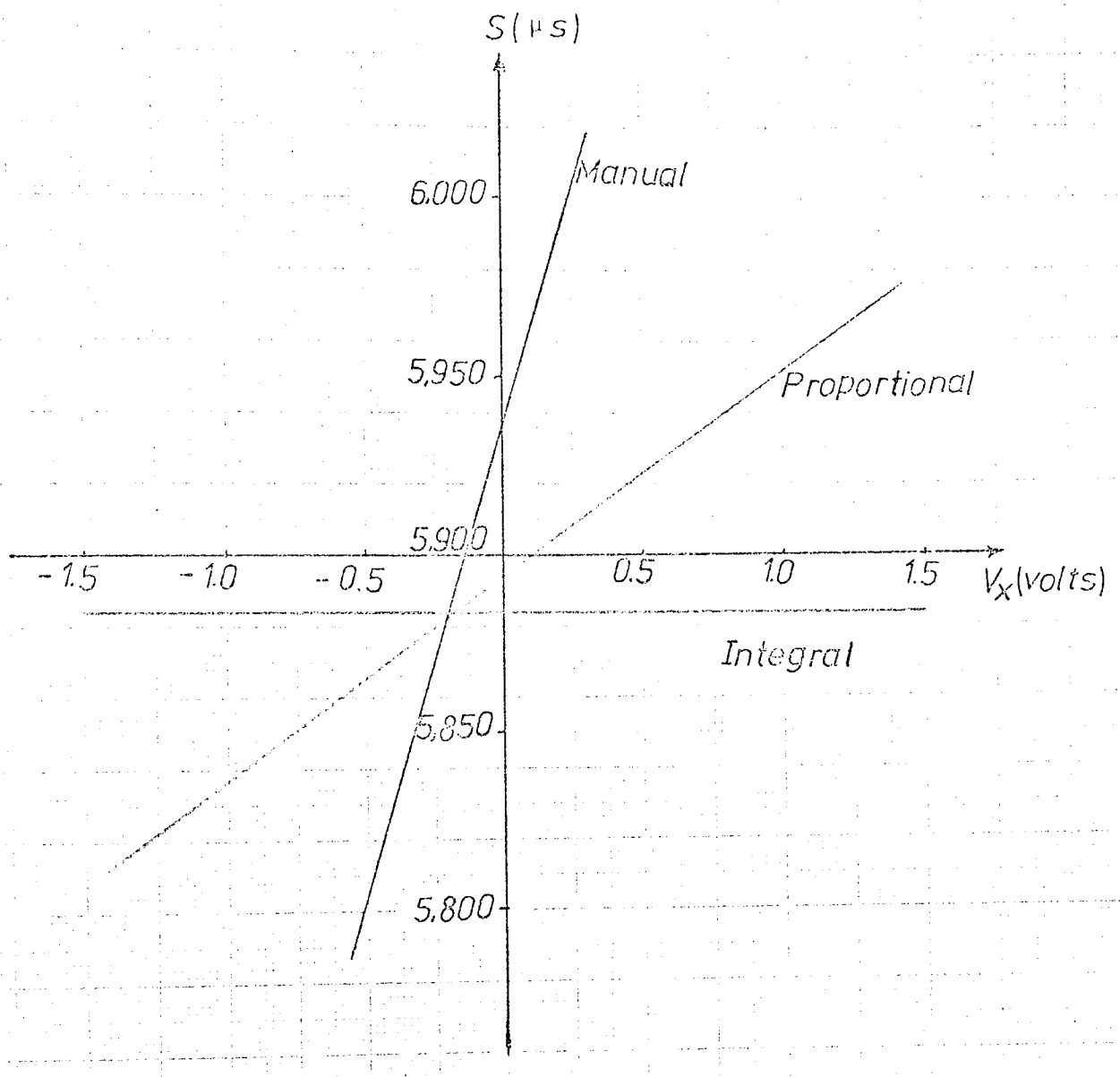

Fig·7·3

This figure shows the readout period S for the three conditions of Control. Resonance is at 5.884 μ Sec. and is maintained at this value on integral control. On switching from manual to proportional control the error in S is reduced by 4.4 i.e. 1+A. It will be noted that the same value of V_x which gave $V_{out}=0$, now gives the readout period for all three conditions.

On integral control the slop is unity ($\frac{\partial Vout}{\partial Vx} = 1$) as the feedback voltage nullifies Vx, this requires S=D.

It will be noted that, for a particular value of Vx, (-0.2V approx.), the value of Vout is zero for all the three conditions.

In Fig. 7.3 the relationship between the readout period S and Vx for the three conditions of control are shown.

Resonance is at 5.884 μsec and is maintained at this value on integral control. On switching from manual to proportional control, the error in S is reduced by 4.4 i.e. 1+A.

It will be noted that the same value of Vx which gave Vout = 0, now gives the readout period for all the three conditions.

7.2.3 Dynamic Test on the Electronic System

a) Frequency Response

Experiments were performed to measure the amplitude and phase response of the overall electronic system as a function of frequency. For this purpose the Solartron Frequency Response Analyser model 1310 was used, where a sine wave at its output terminals (sin ωt) served as the input (Vx) to the summation amplifier.

In the simple case where negligible noise and harmonics are introduced by the frequency analyser, the final output from the integrator will have the same form $A\sin(\omega t+\phi)$ where A is the gain or loss of the system and ϕ is the phase shift introduced by the electronic system. Both these quantities

are assumed to be constant for a given frequency. The function performed within the frequency analyser is to measure A and ϕ at each frequency desired. In practice the amplitude of the signal from the frequency analyser was kept constant at 1 volt and the frequency varied from 0.02 Hz up to 10 Hz, while the variations of the output components A and ϕ were taken in the record as shown in Table 7.4.

Table 7.4

Input (Reference)	Output (Quadrature)	
Frequency Amplitude=1V, ϕ=0	Amplitude	Phase
0.02 Hz	3.40 volts	+170 ^{o}lead
0.05	3.25	160
0.10	2.95	140
0.15	2.50	127
0.20	2.15	118
0.30	1.55	104
0.40	1.22	96
0.50	0.99	90
0.60	0.81	84
0.80	0.58	75
1.0	0.43	69
1.50	0.24	54
2.0	0.155	45
3.0	0.075	32
4.0	0.046	20
5.0	0.025	0
6.0	0.022	- 2 Lag
7.0	0.012	- 8
8.0	0.008	-10
9.0	0.006	-12
10.0	0.001	-20

The results are demonstrated in two forms. In Fig. 7.4

Log 6 Cycles x mm, ½ and 1 cm

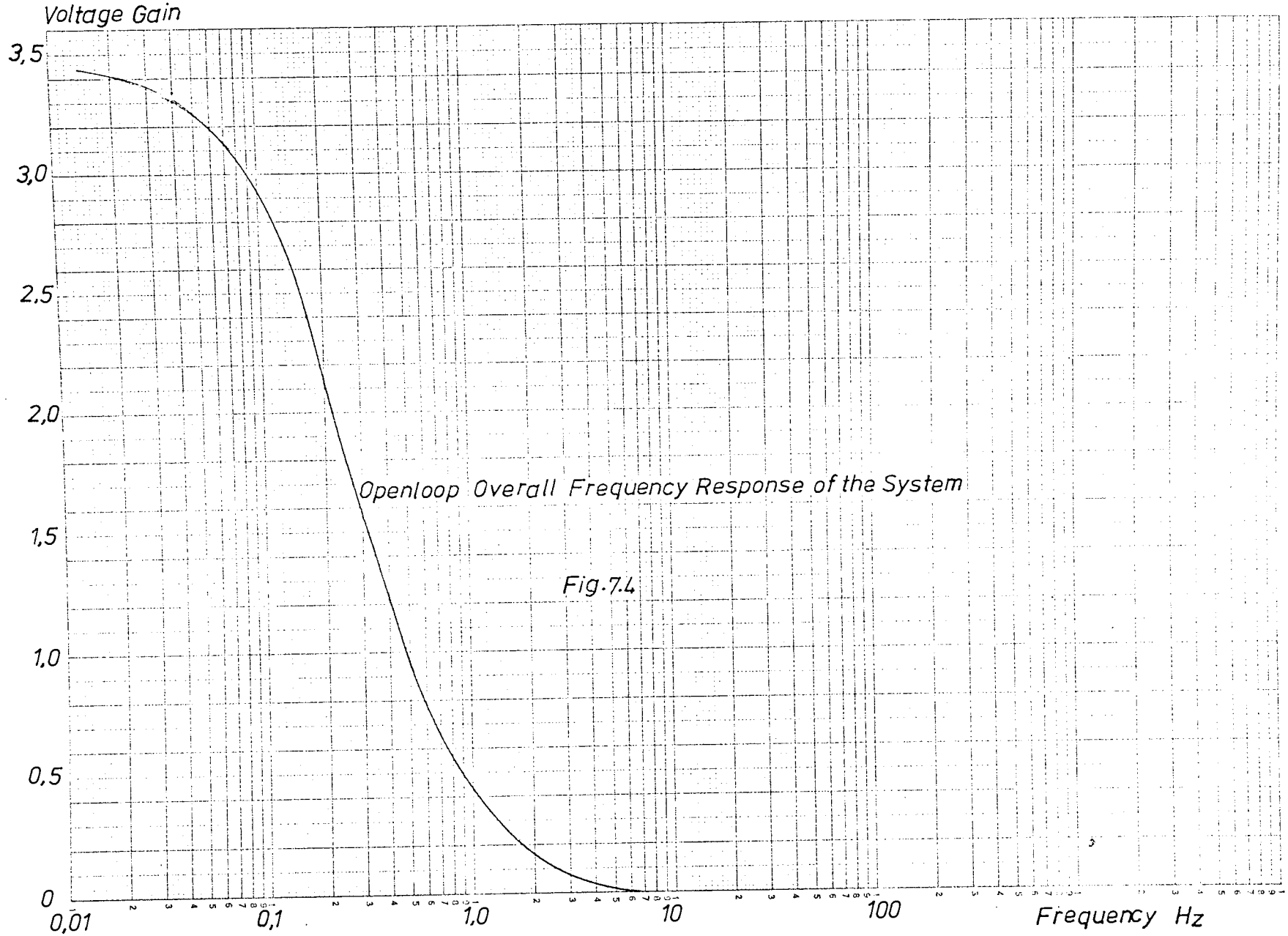

Openloop Overall Frequency Response of the System

Fig. 7.4

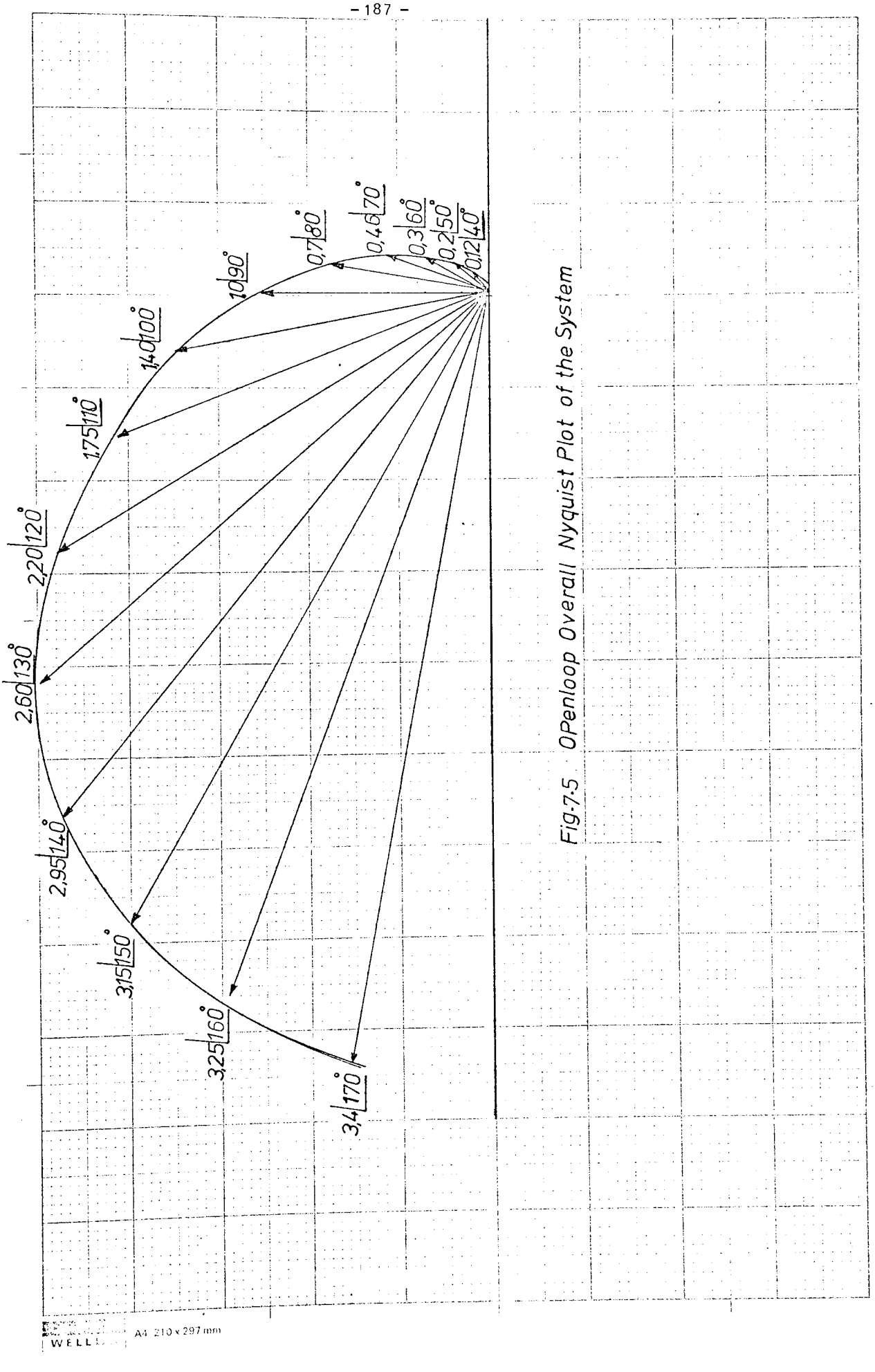

Fig.7.5 OPenloop Overall Nyquist Plot of the System

the variations of the overall gain against frequency, and in Fig. 7.5 the output gain and phase in the form of the Nyquist plot are shown.

b) Lissajous Figures

In the next experiment the output signal from the frequency analyser connected to both the electronic system and the X input terminals of a XY plotter, while the display period S of the system was connected to the Y input of the plotter. The relative Lissajous figures are shown in Fig. 7.6. It will be seen that at low frequencies the period change is very small and in quadrature with the input. As the input frequency increases, the output amplitude increase and the period and input phase are equal.

c) Step Response

The dynamic performance of the control loop which is a second order type were obtained previously by equation 7.5 in the form of

$$\frac{\partial Vout}{\partial Vx} = \frac{K}{S^2 + \frac{1}{\tau_1} S + K} \qquad (7.9)$$

where $K = \frac{k_o k_1}{\tau_1 \tau_2}$ and $k_o k_1$=open loop gain = 3.4

τ_1 = time constant of the first integrator before the difference amplifier and from Fig. 6.18

$\tau_1 = RC = 8.2 \times 10^6 \times 0.02 \times 10^{-6} = 0.164$ sec.

and τ_2 = time constant of the final integrator, where two values for the feedback capacitor were considered

if C = 11μF then $\tau_2 = 100 \times 10^3 \times 11 \times 10^{-6} = 1.1$sec, and if C = 1 μF, τ_2= 0.1 sec.

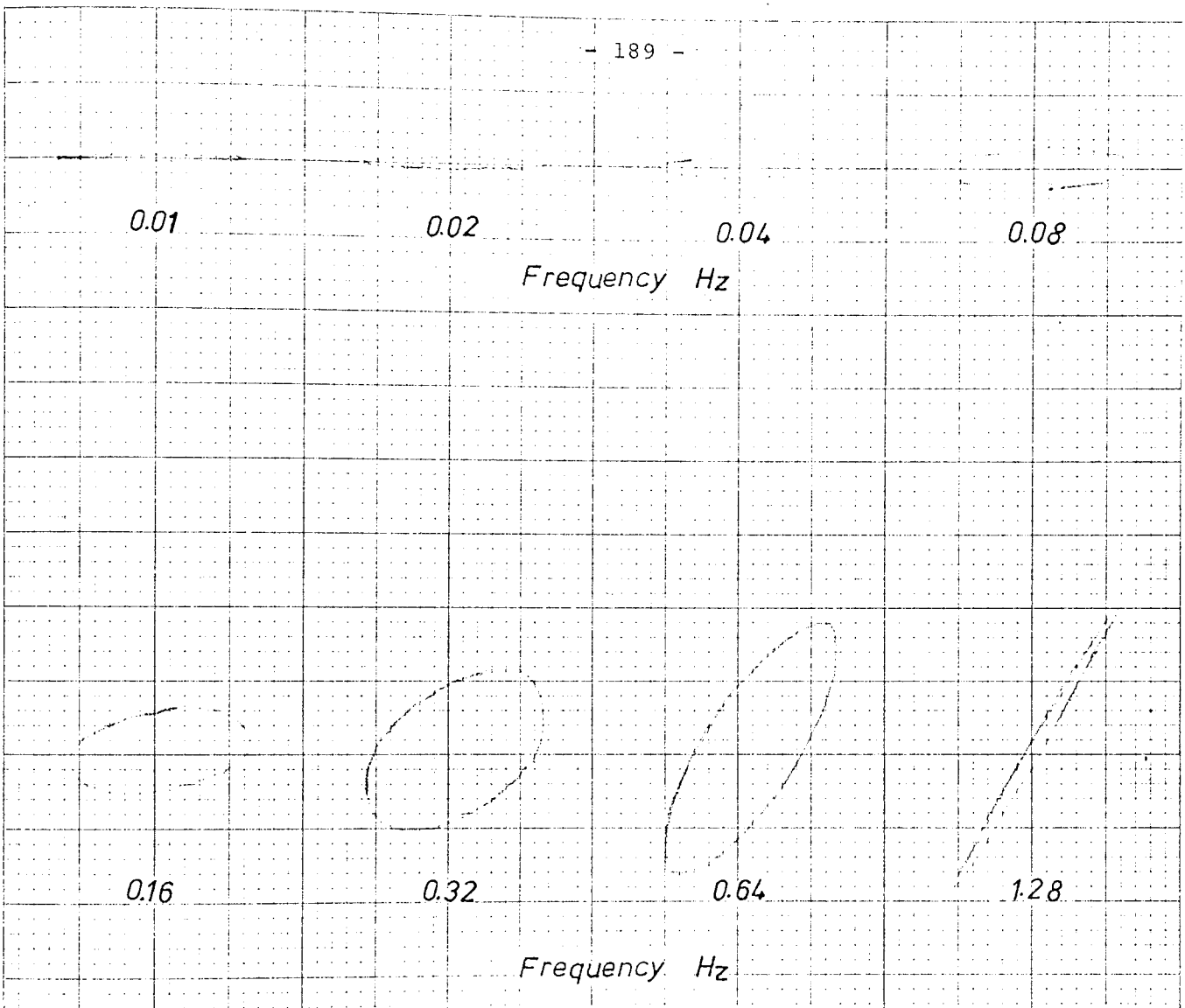

Fig.7.6 The lissajous figures relating input (X) to output Y for progressive increase in frequency. The integral loop was used. The input amplitude was held constant and the period was used as the output.

It will be seen that at low frequencies the period change is very small and in quadrature with the input. As the input frequency increases the output amplitude increases and the period and input phases are equal.

If considering $S^2+C_1S+C_2=0$, rather than $S^2+\frac{1}{\tau_1}S+K = 0$ (7.10) therefore, the factors C_1 and C_2 becomes:

$$C_1 = \frac{1}{\tau_1} = \frac{1}{0.164} = 6.10 \quad \text{and} \quad C_2 = \frac{k_o k_1}{\tau_1 \tau_2} = \frac{3.4}{0.164 \times 1.1} =$$

$$= 18.84 \text{ or } 207.31$$

Equation (7.10) is similar to (7.11) of the second order step function

$$S^2 + 2\zeta\omega_n S + \omega_n^2 = 0 \qquad (7.11)$$

where $\omega_n^2 = C_2$ therefore $\omega_n = \sqrt{C_2} = \sqrt{\frac{k_o k_1}{\tau_1 \tau_2}} = \sqrt{18.84} = 4.34$ or 14.399
and $2\zeta\omega_n = C_1$ therefore $\zeta = \frac{1}{2}\frac{C_1}{\omega_n} = \frac{1}{2} \times \frac{6.10}{4.34} = 0.702$ or 0.212
The theoretical results are shown in Figs. 7.7 and 7.8 for the two values of $\zeta = 0.702$ (overdamped) and $\zeta = 0.212$ (underdamped).

In practice the dynamic response was examined on integral control which is the normal operating mode of the instrument. A step input Vx was applied and the response of Vout and S displayed as a function of time, Fig. 7.9.

Two values of time constant were used, τ_2 = 1.1 sec when the system is overdamped ($\zeta = 0.702$) and τ_2 = 0.1 sec when it is underdamped ($\zeta = 0.212$). It will be seen that Vout goes to a new value (equal to -Vx) and S is returned to its original value.

In the next experiment response of the different stages of the system to a step input were considered. Using Y inputs of a XY plotter for connecting to the outputs which desired, enabled the relative response to be obtained as

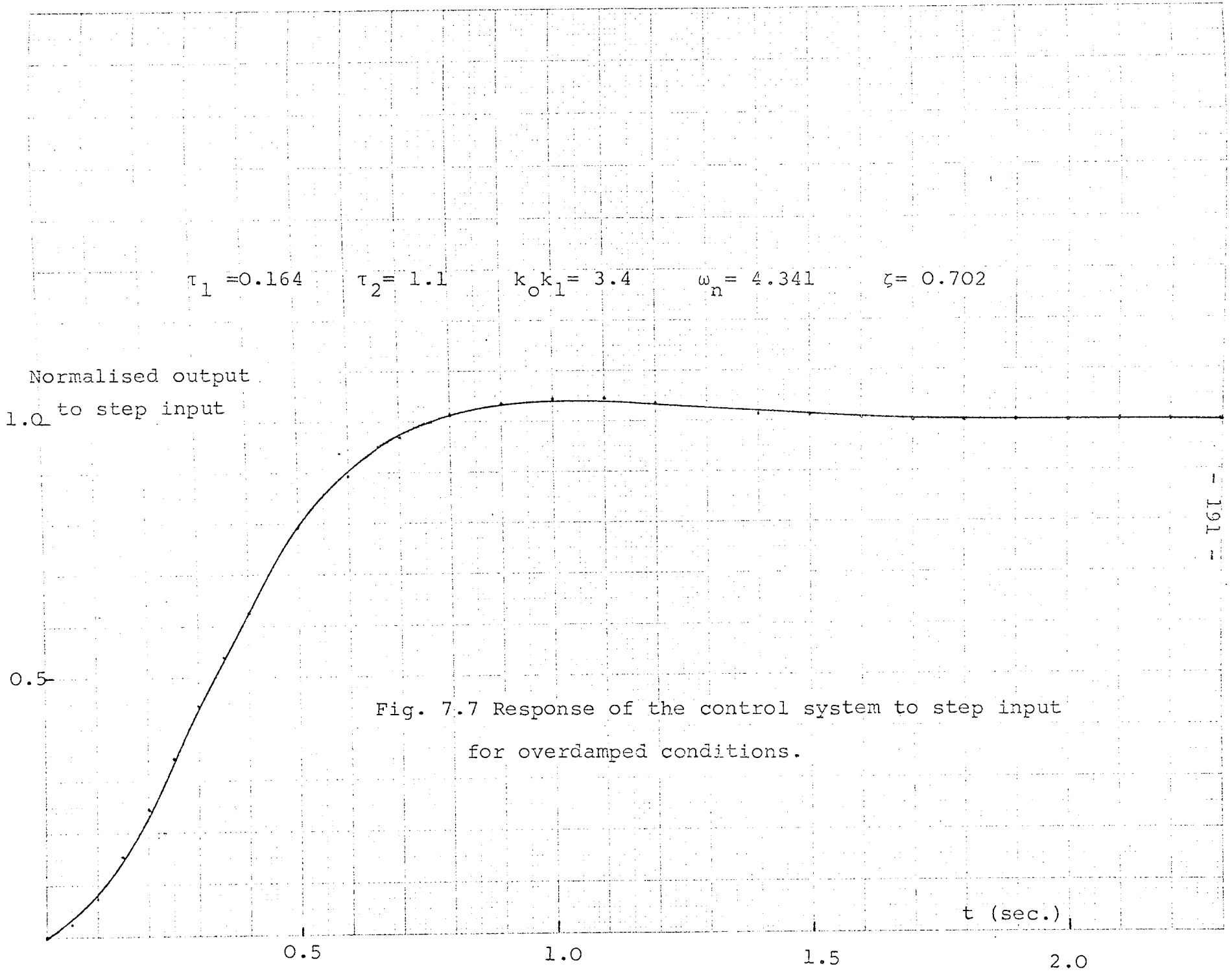

Fig. 7.7 Response of the control system to step input for overdamped conditions.

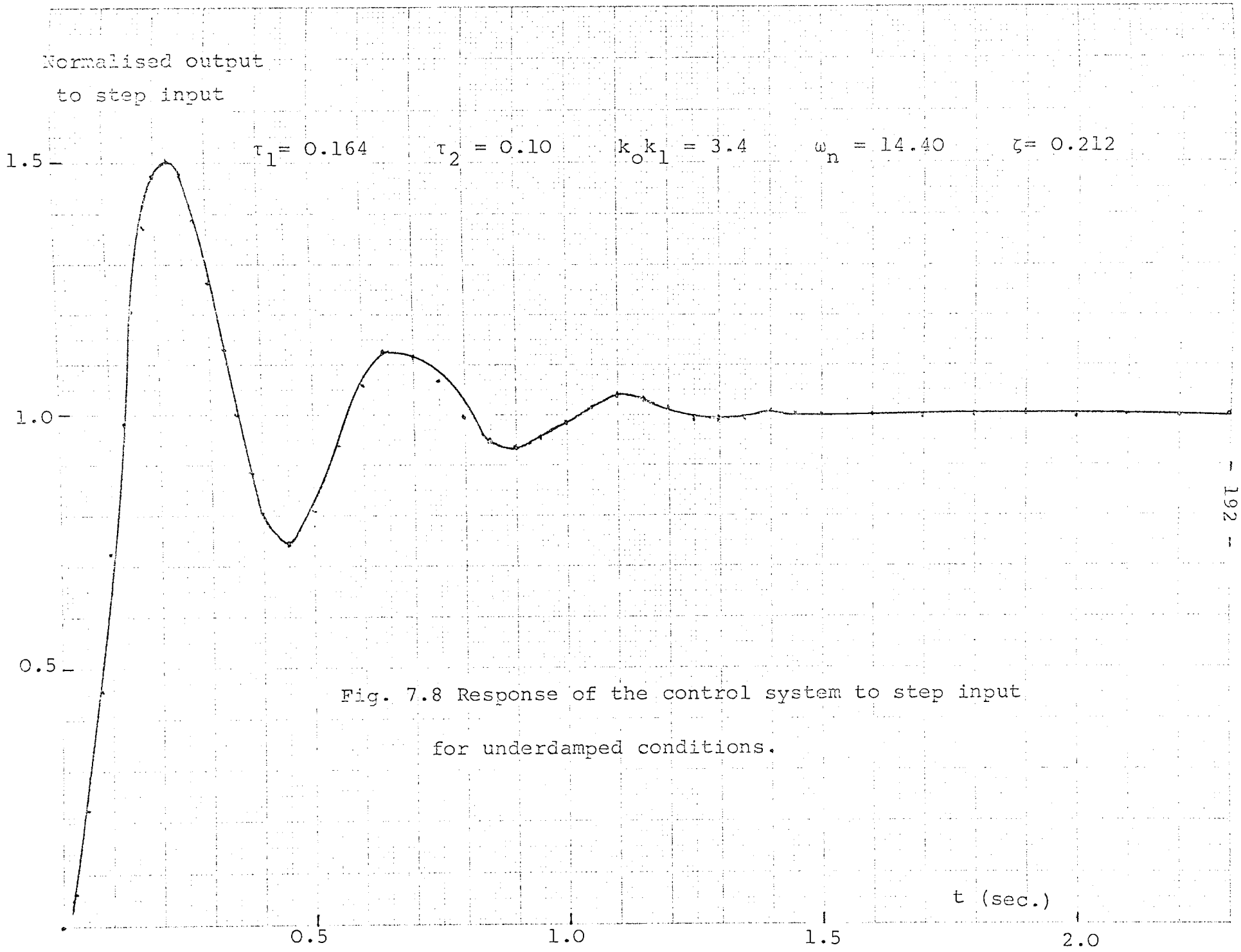

Fig. 7.8 Response of the control system to step input for underdamped conditions.

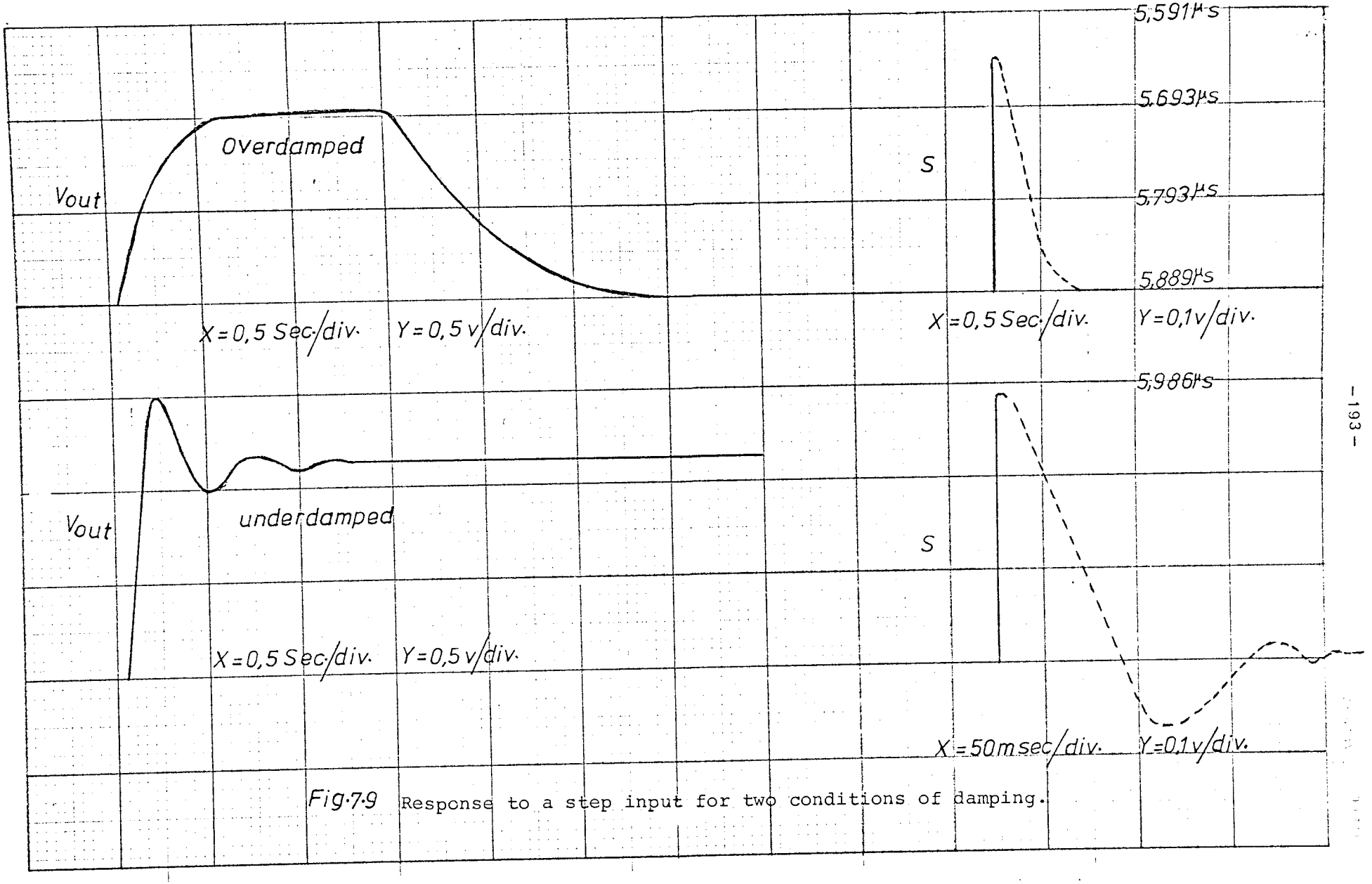

Fig·7·9 Response to a step input for two conditions of damping.

shown in Fig. 7.10.

Fig 7.11 shows the photographs corresponding to the response of the error signal (Ve) to an input step for the three values of the damping factor (ζ) while the system is on integral control and PRF = 10 msec. The interval between the points is therefore 10 msec.

In photograph a, τ_2 = 1.1 sec and system is overdamped in b, τ_2 = 0.55 sec and system is crytically damped and in C, τ_2 = 0.11 sec and system is underdamped.

Fig. 7.12 shows the photographs concerning with the response of the final integrator to an input step while the system is operating on integral mode of control. In photograph a, system is overdamped but the comparison is made between two values of the operating cycle of the instrument, for upper trace PRF = 10 msec and for lower trace PRF = 50 msec.

Photograph b, gives the same comparison while the system is underdamped.

Oscillograms of Fig. 7.13 show the response of the error signal (Ve) to an input step for overdamped conditions. In both photographs (a and b) the response are shown in integral mode of control (upper trace) and on open loop, while for a the opertaing cycle is 10 msec and for b 50 msec.

Oscillograms of Fig. 7.14 (a and b) are shown exactly the same as 7.13(a and b) but for underdamped conditions.

Oscillograms of Figs. 7.15 and 7.16 show the response of the analogue display of the period to an input step for the two conditions of damping. In a PRF is 10 msec and in

Fig. 7.10 shows response of the various stages of the automatic control system to an input step function on the XY recorder.

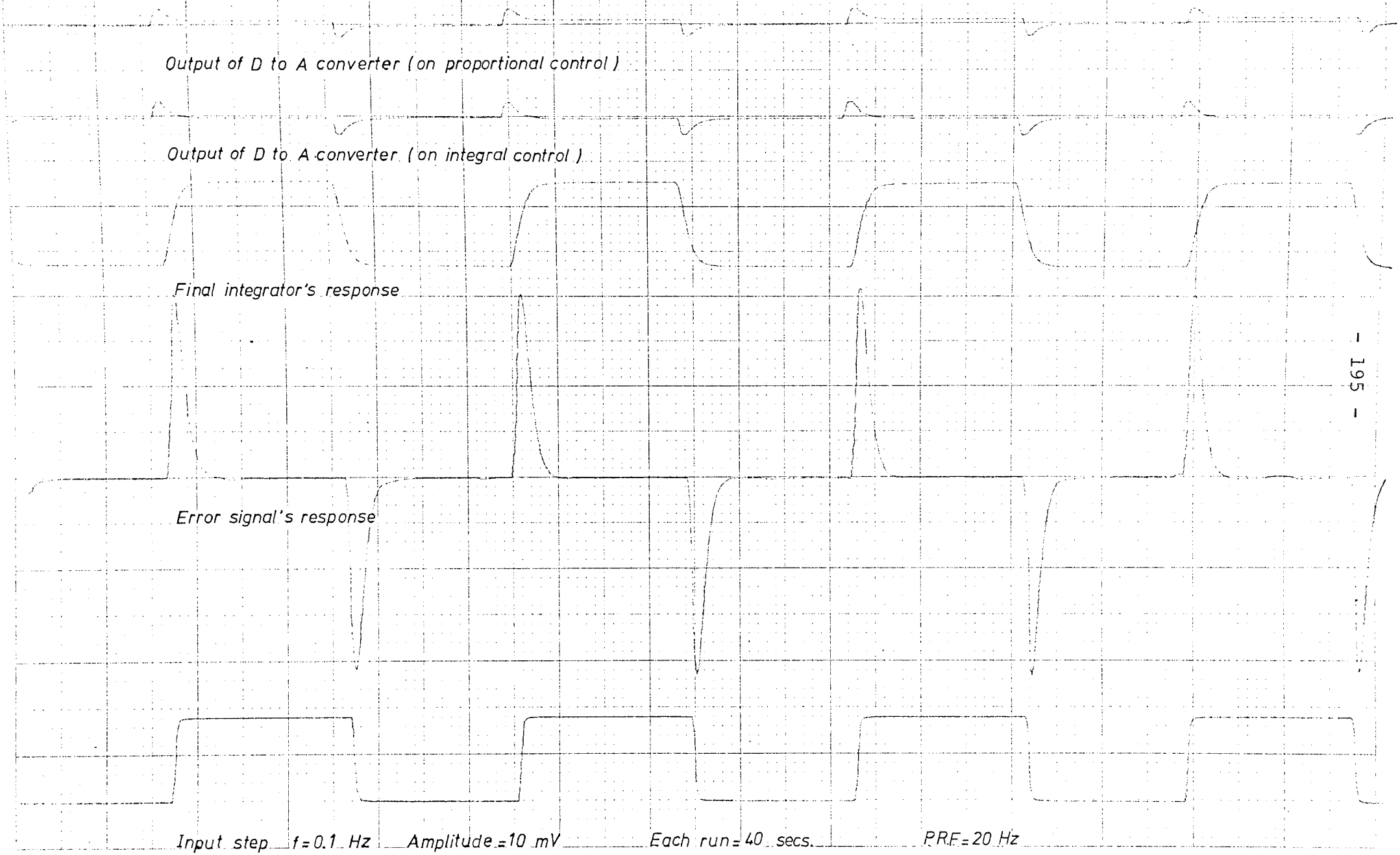

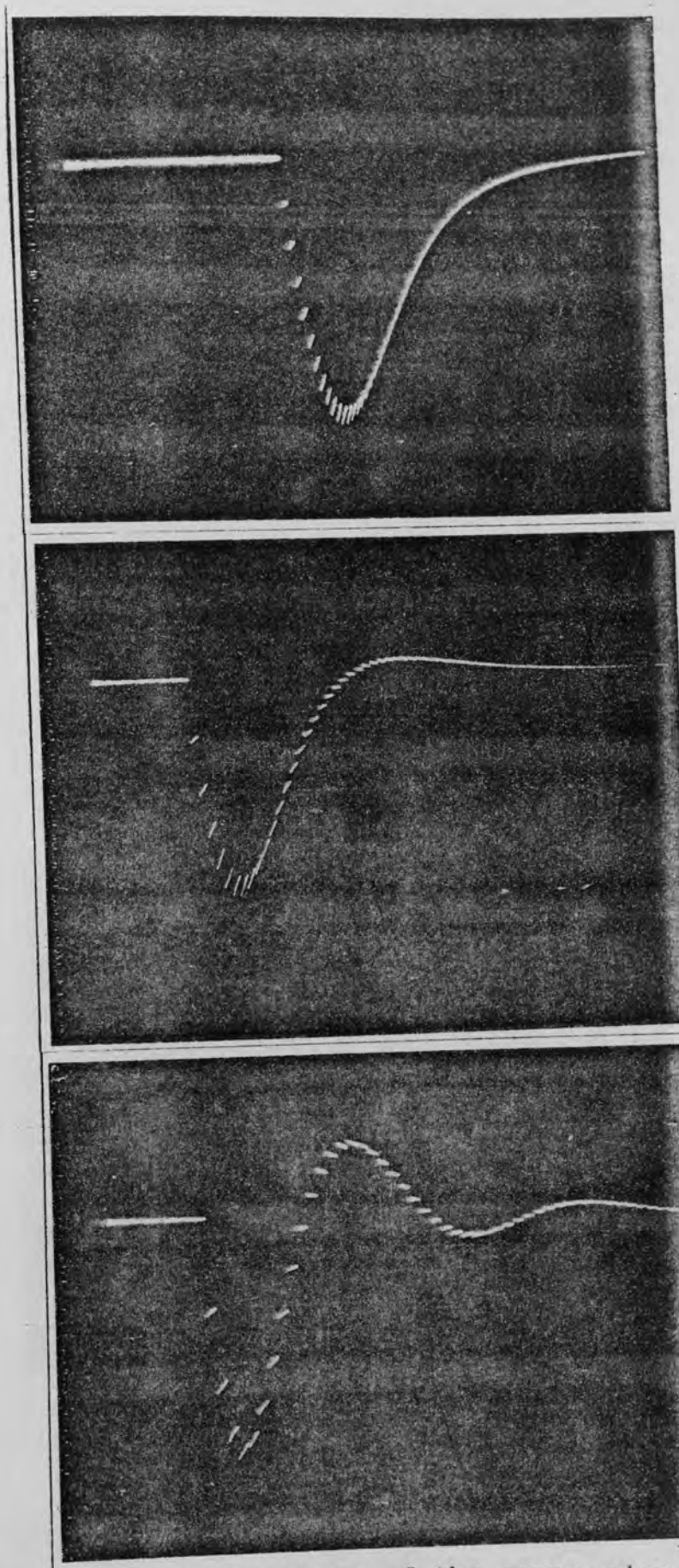

(a)

Integrator Time Constant = 1.1sec

Time Base = 100msec per cm

Sensitivity = 1V per cm

(b)

Integrator Time Constant = 0.55sec

Time Base = 100msec per cm

Sensitivity = 1V per cm

(c)

Integrator Time Constant = 0.11sec

Time Base = 50msec per cm

Sensitivity = 0.5V per cm

Fig. 7.11 Response of the error signal to step function. Mode of the control:Automatic integral with 10 oscillations in sampling and 5 oscillations in delay.
PRF = 10 msec.

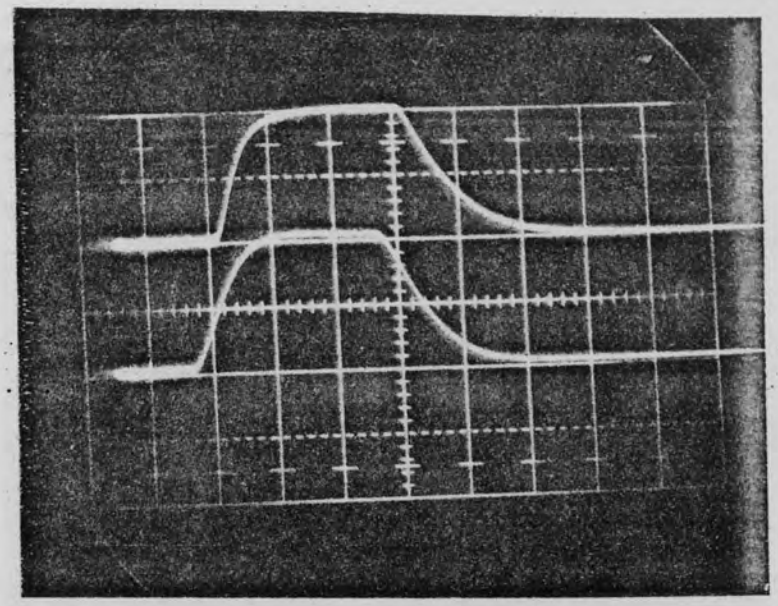

(a)

Integrator Time Constant = 1.1sec

Time Base = 0.5sec per cm.

Sensitivity = 0.5V per cm

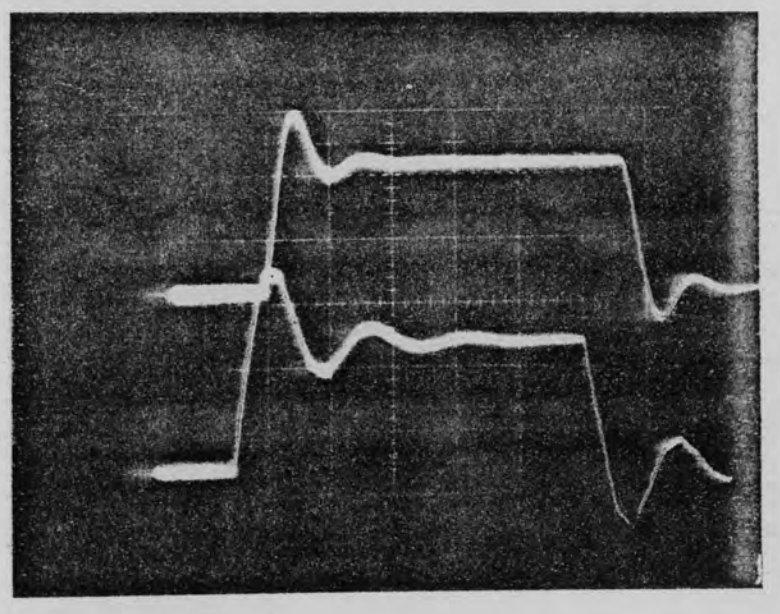

(b)

Integrator Time Constant = 0.11sec

Time Base = 0.5sec per cm

Sensitivity = 0.5V per cm

Fig. 7.12 Response of the final integrator to step function. Mode of control:Automatic integral with 10 oscillations in sampling and 5 oscillations in delay.
PRF:Upper Trace = 10 msec
Lower Trace = 50 msec.

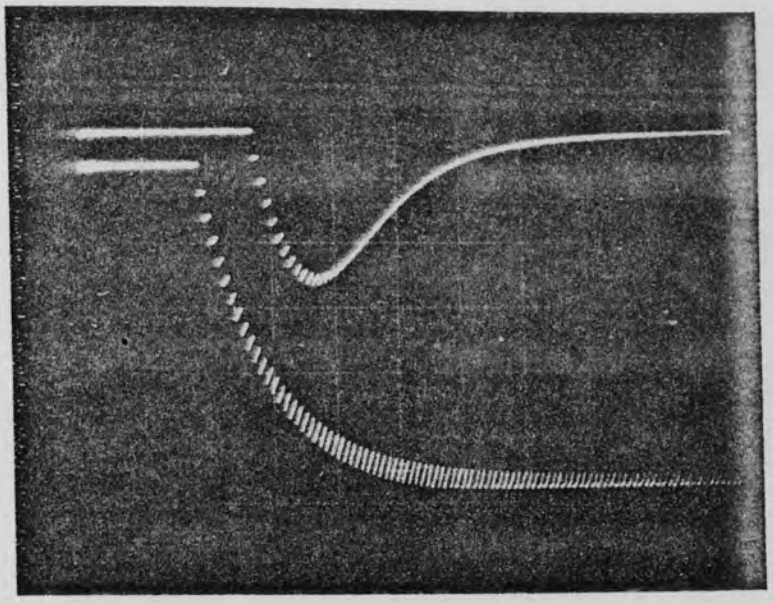

(a)

Integrator Time Constant = 1.1sec

PRF = 10 msec

Time Base = 0.1sec per cm

Sensitivity = 2V per cm

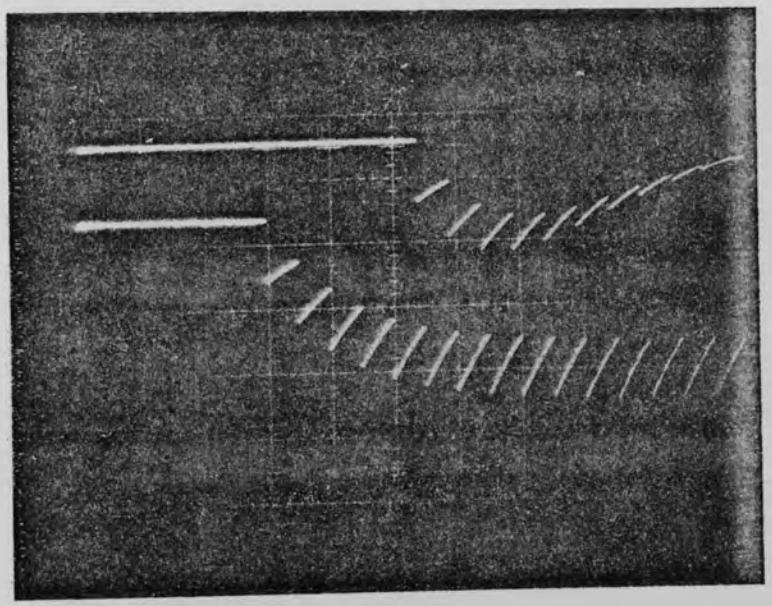

(b)

Integrator Time Constant = 1.1sec

PRF = 50 msec

Time Base = 0.1sec per cm

Sensitivity = 2V per cm

Fig. 7.13 Response of the error signal to the step function. Mode of control: Upper Trace = on automatic integral with 10 oscillations in sampling and 5 oscillations in delay. Bottom Trace = on manual.

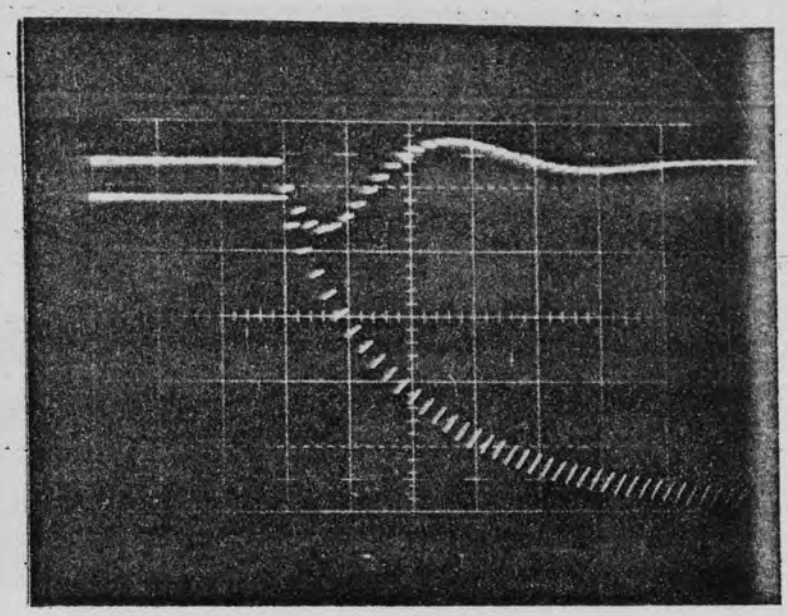

(a)

Integrator Time Constant = 0.11sec

PRF = 10 msec

Time Base = 50msec per cm

Sensitivity = 2V per cm

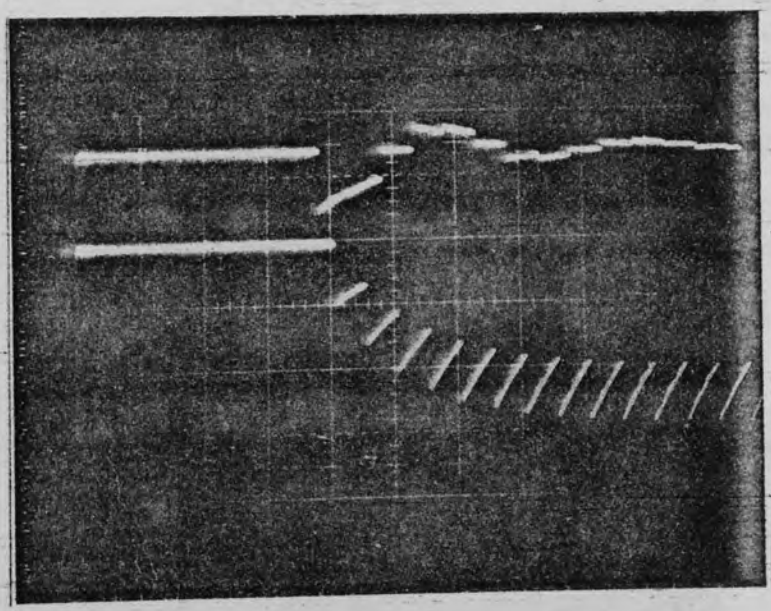

(b)

Integrator Time Constant = 0.11sec

PRF = 50 msec

Time Base = 100msec per cm

Sensitivity = 2V per cm

Fig. 7.14 Response of the error signal to step function
Mode of control: Upper Trace = on automatic integral with 10 oscillations in sampling and 5 oscillations in delay.
Bottom Trace = on manual control.

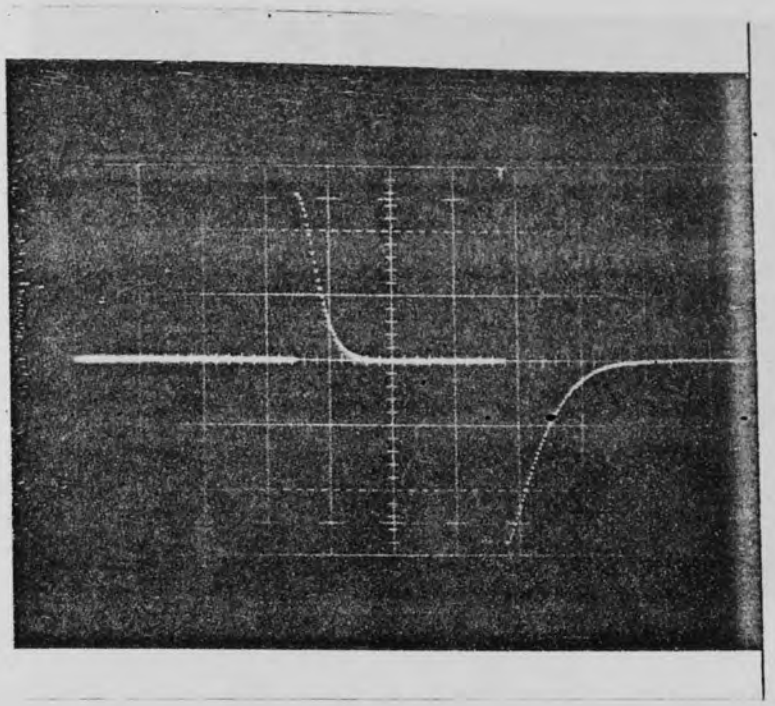

(a)

PRF = 10 msec

Time Base = 0.5sec per cm

Sensitivity = 0.1V per cm

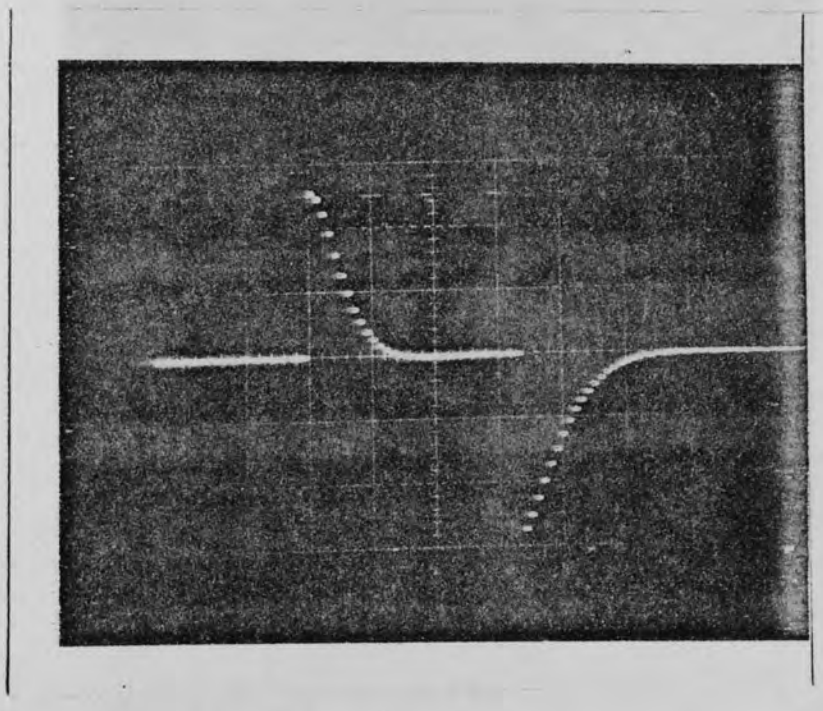

(b)

PRF = 50 msec

Time Base = 0.5sec per cm

Sensitivity = 0.1V per cm

Fig. 7.15 Response of the analogue display of the period to step function. Mode of control:Automatic integral with 10 oscillations in sampling and 5 oscillations in delay.
Integrator time constant = 1.1 sec

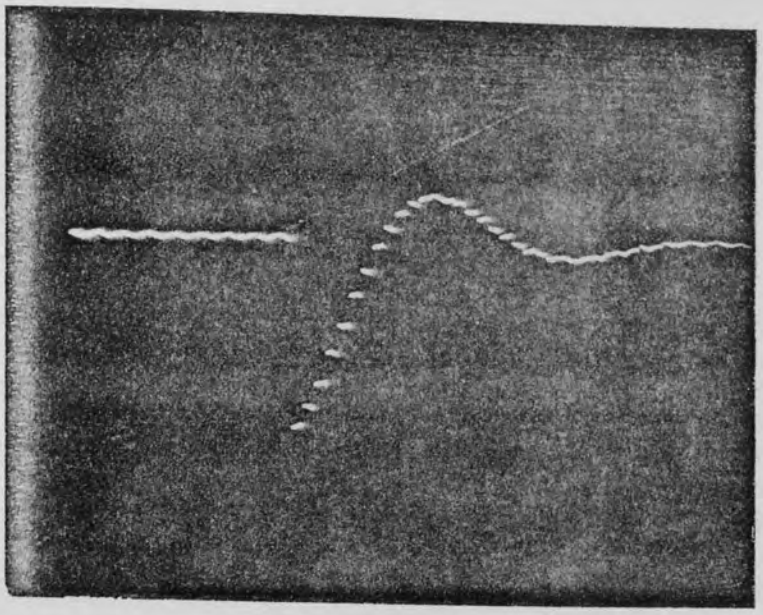

(a)

PRF = 10 msec

Time Base = 50msec per cm

Sensitivity = 0.1V per cm

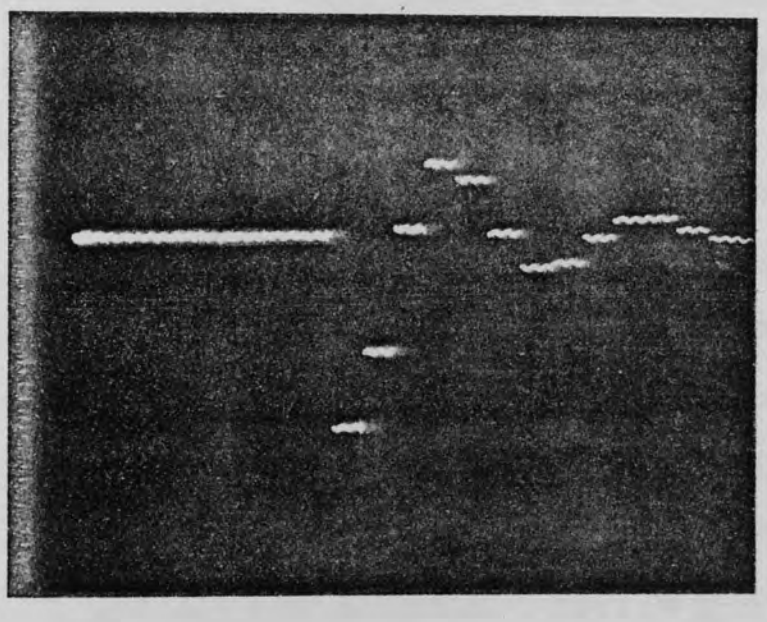

(b)

PRF = 50 msec

Time Base = 100msec per cm

Sensitivity = 0.1V per cm

Fig. 7.16 Response of the analogue display of the period to step function. Mode of the control:Automatic integral with 10 oscillations in sampling and 5 oscillations in delay.
Integrator time constant = 0.11 sec.

b 50 msec.

7.3 NOISE INVESTIGATIONS

An important feature of a well designed electronic system is that, the extraneous signals are to a great extent eliminated. There remains random effects known as noise which set one of the limits to a measurement.

The presence of these random signals in all electrical systems result in false signals, spurious triggering and other errors. The signal to noise ratio - a power ratio - is a useful criterion in a system. Equally the noise immunity of a device e.g. a monostable is a useful part of its specification. Experimental work on errors arising from noise have shown that even very good signal to noise ratios result in finite error rates.

In ultrasonic thermometry and other frequency "domain" measuring transducers the high intensity narrow band ultrasonic vibration used, gives the system immunity from vibration, shock and electrical interference, even in the extreme conditions of a jet aero-engine.

If a transducer has inherent frequency variations of 1 in 10^5 and the parameter being measured changes the frequency by a maximum of 10%, then the sensitivity is 1 in 10^4 and changes outside this limit can, with confidence, be attributed to a genuine parameter changes. It is customarily to classify the fluctuations as instrumentation or system noise and data noise respectively.

In ultrasonic thermometry, the high Q factor gives a correspondingly high frequency stability and as the

temperature coefficient is relatively large (50-500 ppm/ kelvin), the result is a highly sensitive instrument which will measure changes of ±2 kelvin. The instrumentation noise (expressed as a temperature) uncertainty is the ratio of the stability to the transducer coefficient $(\frac{1}{f}\frac{df}{d\theta})$.

In operating a complex system such as a nuclear reactor data noise can be of great value in determining the stability of performance of the system. For example, the fluctuations of coolant temperature will show a correlation with coolant flow rate and neutron density. While it is unlikely that these correlations could be calculated with any certainty, their constancy over a period of time is a good indication of the constancy of performance of the system.

For correlation to be effective the "texture" of the noise must be similar. This requires the bandwidths of the transducers to be approximately equal.

7.3.1 Experimental Work

A large number of experiments are performed to investigate the stability of the electronic system. These experiments depend upon the texture of the noise could be divided in the two groups.

a -Group one - Large and short term stability measurements of the control loop and the voltage control signal generator, where the system operates manually and automatically. The electronic system drives an ultrasonic temperature probe for the purpose of producing a measureable decrement to operate the control loop, while the probe itself is kept at the room temperature.The output signal fluctuations are genuine

instrumentation noise.

b - Group two - Long and short term stability measurement of the overall automatic system when the actual probe is measuring a temperature. The probe may either be used for temperature measurement of a gas flame (high fluctuation of data noise), or inside a silica tube furnace (low fluctuation of data noise). In both of these cases the fluctuations at the output is greater than the instrumentation noise.

To demonstrate the results of all the above experiments graphically, a XY plotter were used extensively, where any desired output voltage were plotted against the time or any other variables which required. The results are shown in the following figures.

Fig. 7.17 shows the period fluctuations for three 12 minutes samples. The resolution is the same for each sample. a) shows the very small variations in period of the V.C.O. b) and c) show the variations in period where the V.C.O is controlled by the probe resonator. The latter fluctuations are significantly greater than those of the V.C.O. and are threfore associated with the overall instrument performance.

Fig. 7.18 shows the period fluctuations for six 10 minutes samples. The probe resonator which controls the voltage control oscillator is the same as the previous probe with the difference which it is used to measure the temperature stability of a silica tube furnace. The fluctuations which increases with the temperature level are due to the data noise.

Fig. 7.19 shows the peiord fluctuations for two 12

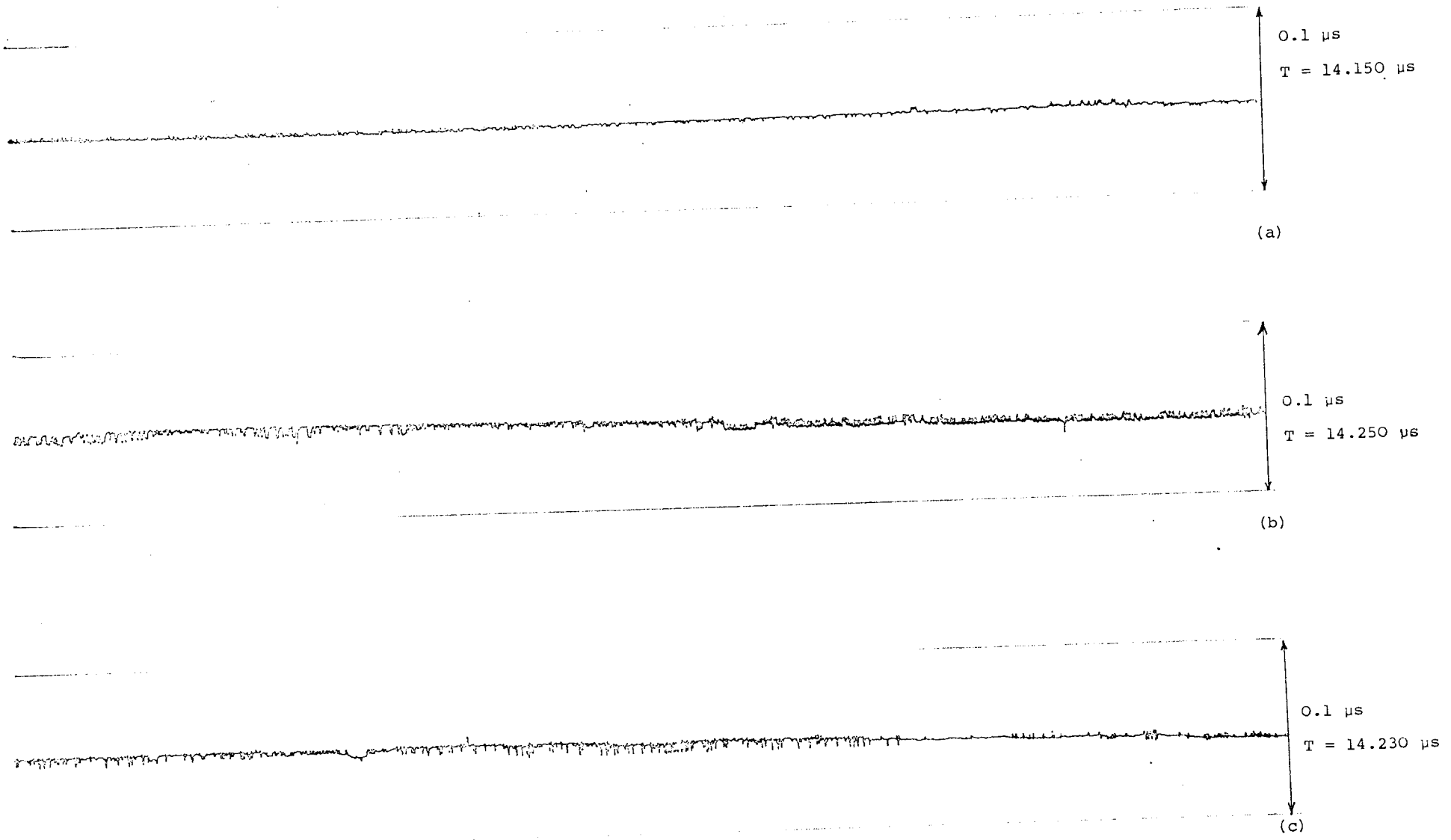

Fig. 7.17 Noise investigation of V_{C_0} at room temperature with a half wavelength steel probe fr = 70 kHz (L= 37 mm, Diameter = 10.3 mm) a - on open loop, b - closed loop integral control, c - closed loop proportional control. Each run for 12 minutes.

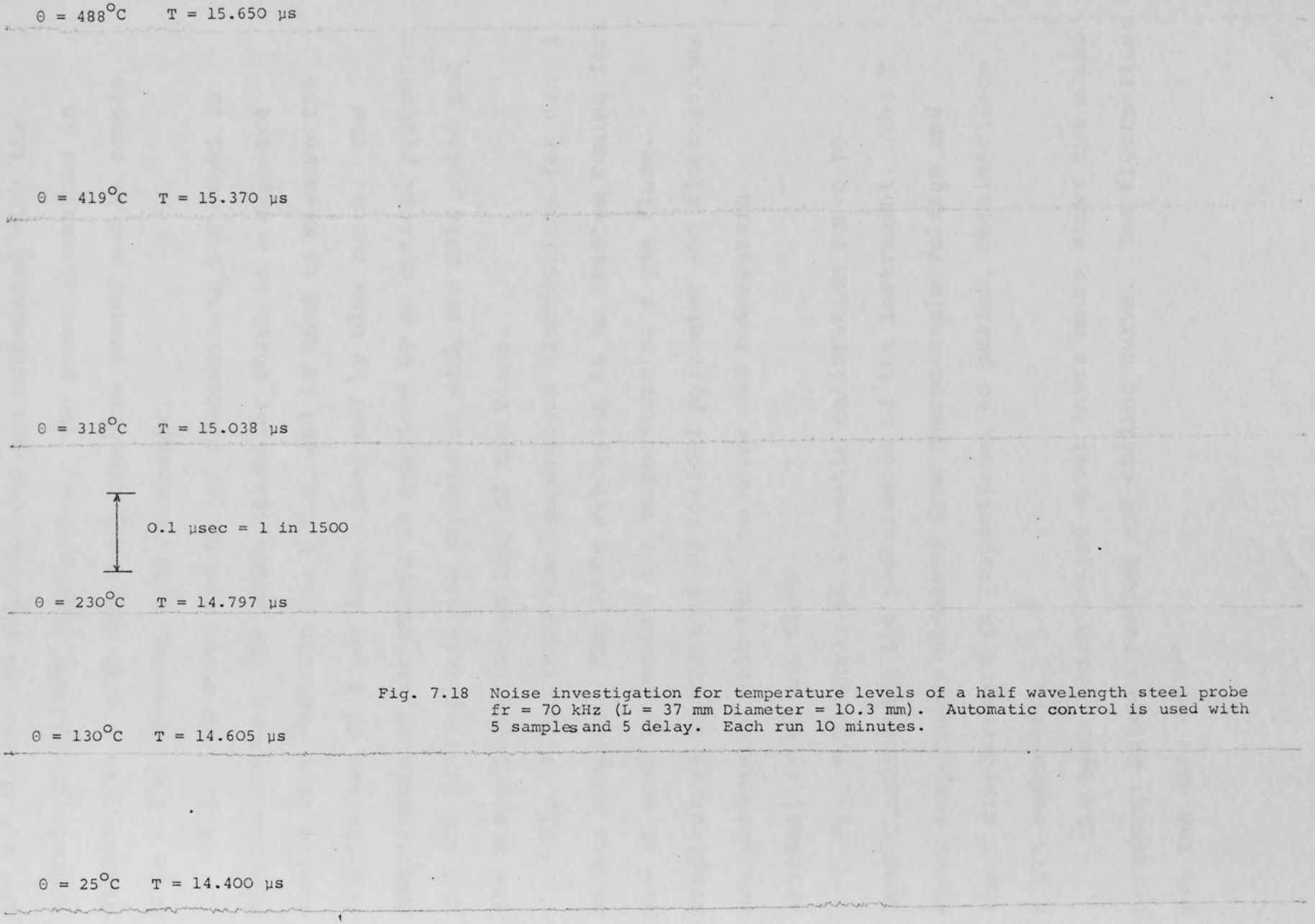

Fig. 7.18 Noise investigation for temperature levels of a half wavelength steel probe fr = 70 kHz (L = 37 mm Diameter = 10.3 mm). Automatic control is used with 5 samples and 5 delay. Each run 10 minutes.

minutes samples. In both samples the probe resonator controls the V.C.O. and the fluctuations are associated with the overall instrument performance. The probe resonators in sample a is a high frequency sapphire sensor and in sample b is a low frequency iridium sensor.

Fig. 7.20 shows the period fluctuations for eight 15 minutes sample. The probe resonator which is a sapphire tuning fork controls the V.C.O. and is used to measure the temperature of a gas flame, produced by blow torch. The temperature of the sensor is measured by an optical pyrometer and the fluctuations are associated with the data noise and the temperature instability of the flame.

FIg. 7.21. shows the temperature fluctuations for nine 1 minute samples. The probe resonator is an iridium tuning fork and is used to measure the temperature of a gas flame. Temperature is measured by optical pyrometer and fluctuations are associated with the data noise and temperature instability of the flame.

Fig. 7.22 shows an automatic calibration curve to 1000 ^{o}C,indicating the performance of the instrument. The X shows temperature obtained from thermocouple voltage and the Y displacement is proportional to period, obtained from a D/A converter.

The cycle which lasted about three hours shows the close agreement between heating and cooling curve. The fluctuations are the data noise.

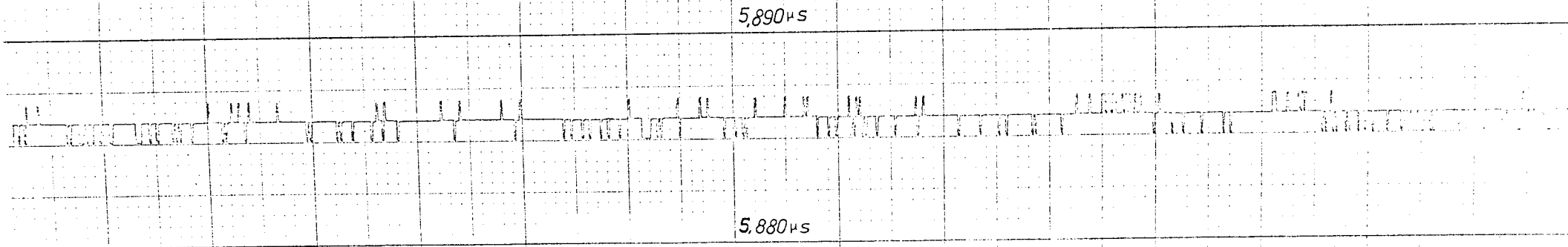

Period fluctuation due to the instrumentation noise for sapphire probe 1 part in 2500

P.R.F. = 1,25 H_z Time Base = 1 minut/inch

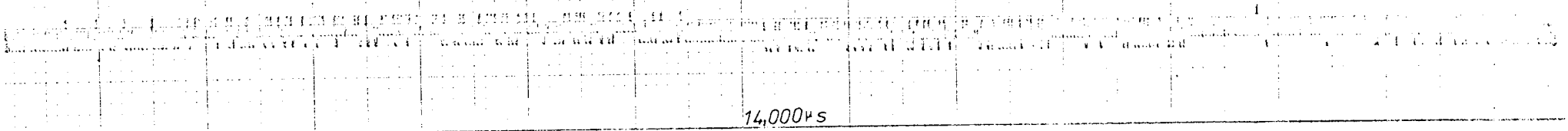

Period fluctuation due to the instrumentation noise for Iridium probe 1 Part in 3500

P.R.F. = 1,25 H_z Time Base = 1 minut/inch

Fig. 7.19

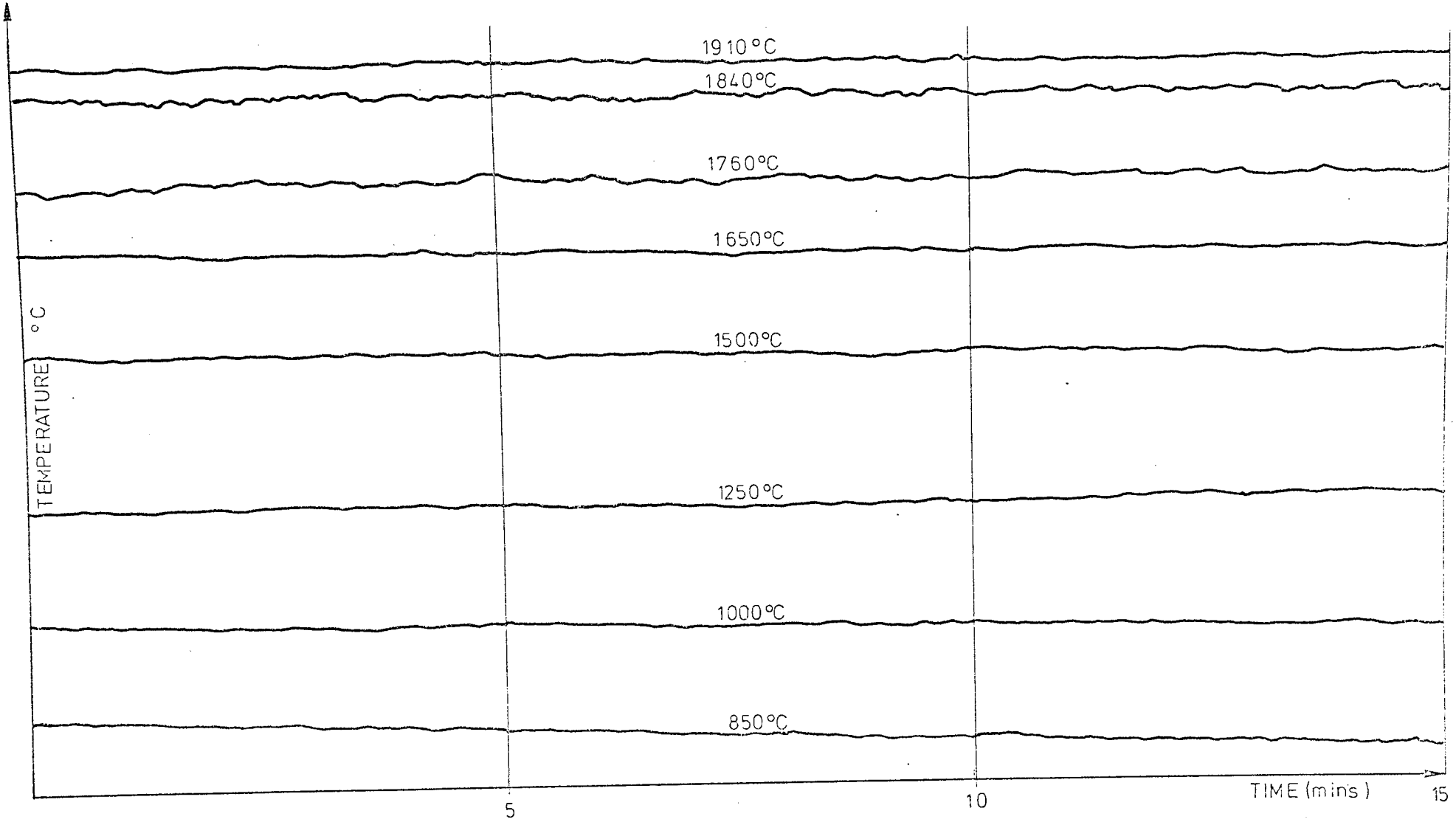

FIG. 7-20 TEMPERATURE STABILITY OF THE SAPPHIRE ULTRASONIC PROBE IN BLOW TORCH FLAME.

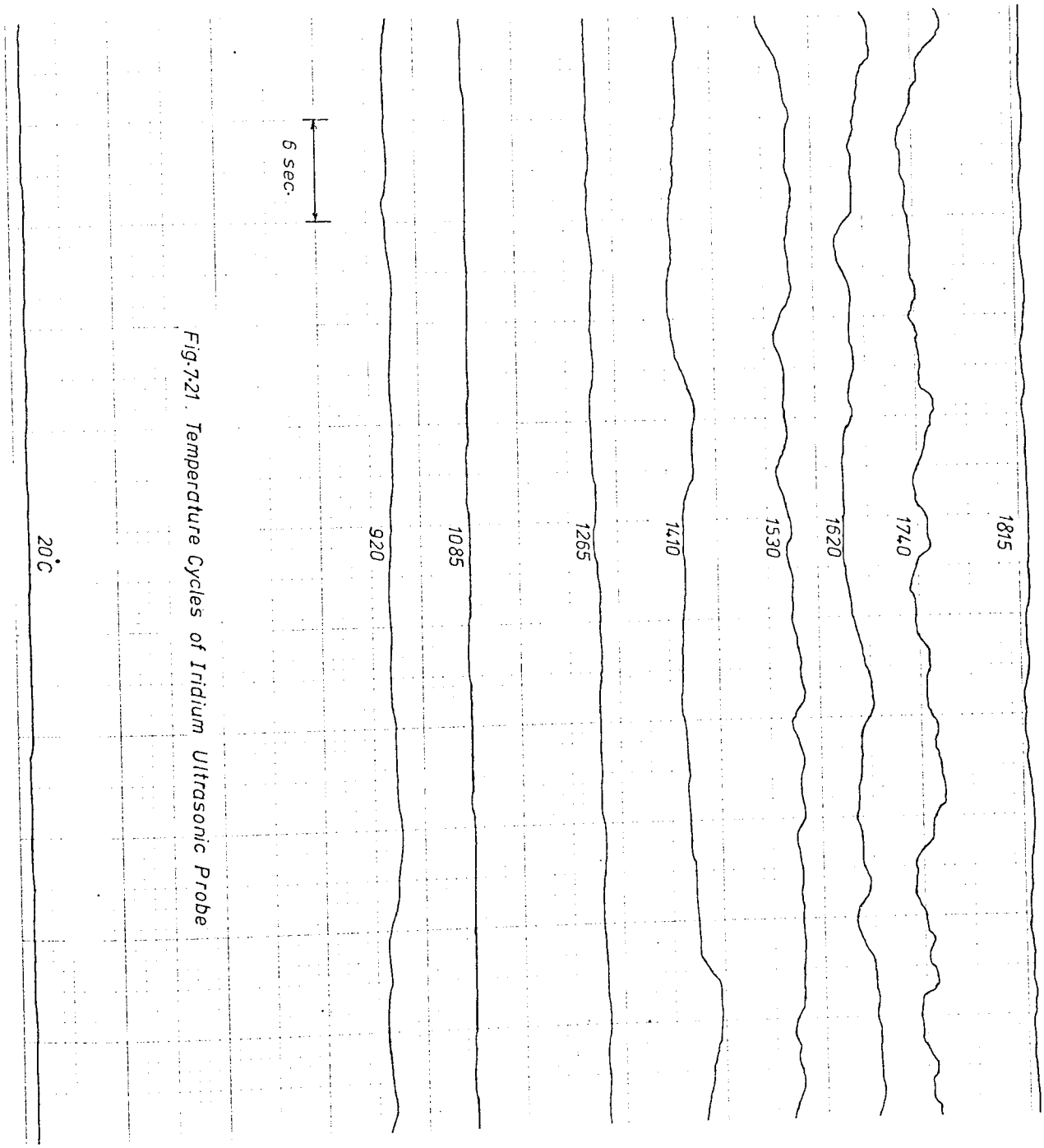

Fig.7.21. Temperature Cycles of Iridium Ultrasonic Probe

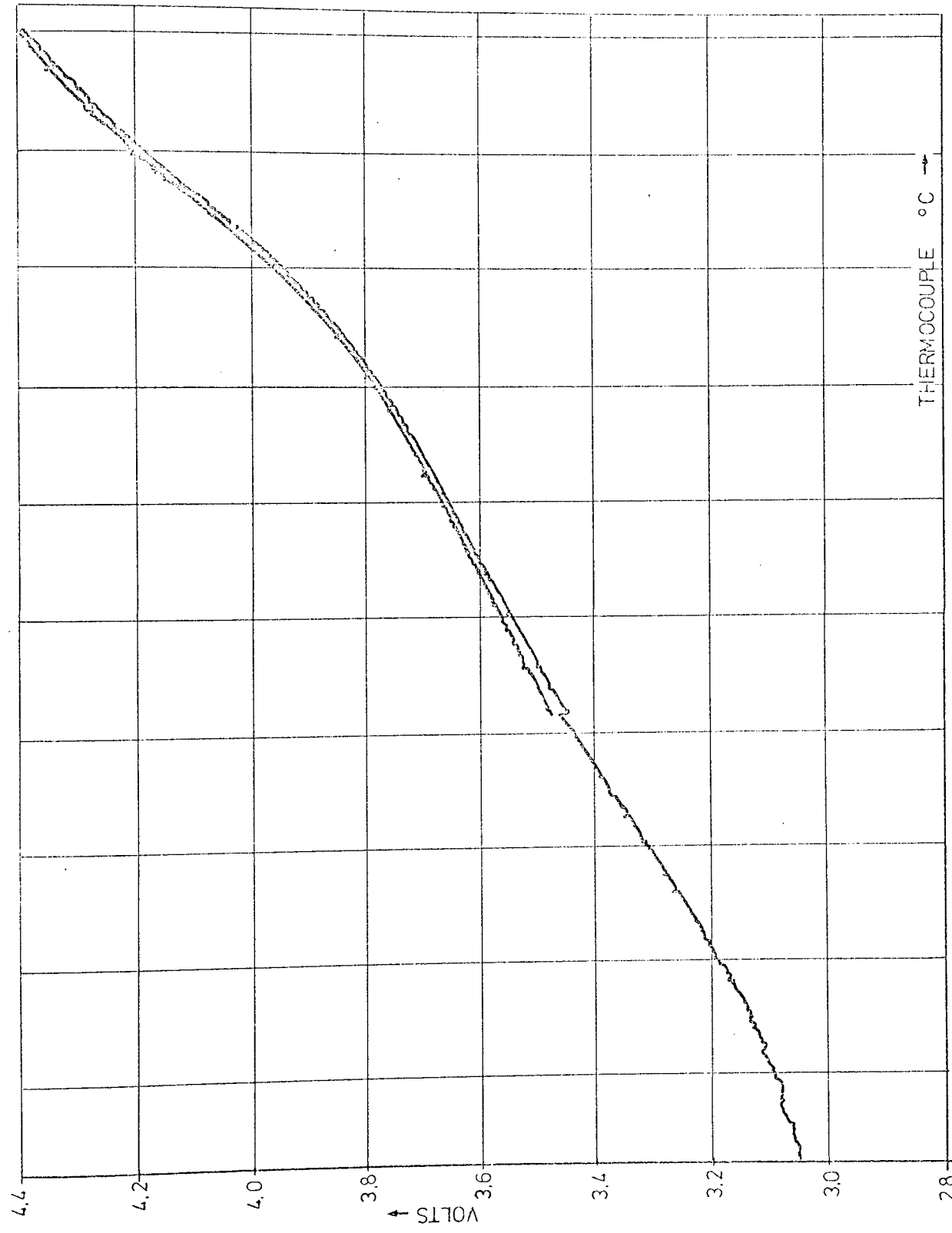

FIG. 7·22TEST ON IRIDIUM ULTRASONIC TEMPERATURE PROBE 0-1000 °C

CHAPTER 8

THE PROBE MATERIAL

8.1 INTRODUCTION

There is no limitation on the choice of material for the resonator or line other than dictated by the environment and physical properties associated with the acoustic requirements. With the integral line probe there is no stringent requirement on the high temperature properties of the transmission line, as only the end section which may be 25 to 50 cm in length needs to be at high temperature. Ideally as in the case of the tungsten probe prepared for the " Petten" experiment (1.5 mm diameter), the whole line (2 metre length) is of the probe material. Generally, three terms are used with respect to the line namely, launcher, line and probe as shown in Fig. 8.1.

Various combinations of materials can be used in the system.

The launcher must be of magnetostrictive material and joined to the lead in line. The first joint will be at low temperature but the second, while not being as high as the sensor temperature, may be quite high. The acoustic matching of the joints is particularly important in the second case where a spurious echo may be superposed on the end echo. A small mismatch on the first joint simply effects the efficiency at certain frequencies.

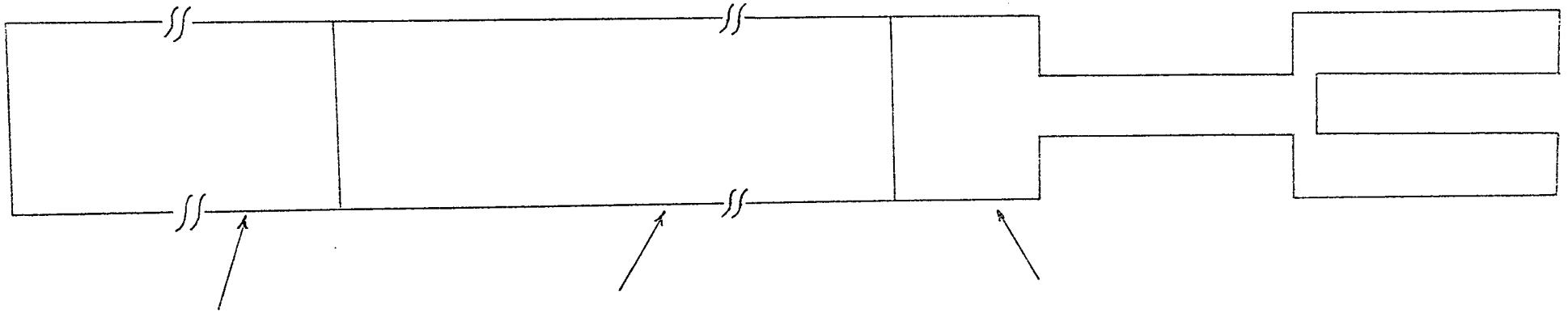

Fig. 8.1 An acoustic line with transducer and probe at the ends.

The problem of the acoustic mismatch arising from the second junction does not exist in the case of " Petten" experiments and for that of the first junction is very trivial.

8.2 CHOICE OF THE MATERIAL

Basically low velocities materials such as the tungsten and platinum presents proportionately a lower frequency, therefore providing more degrees of freedom to chose convenient dimensions for the resonator. This becomes an important factor only when the resonator size being limited for an individual experiment. Generally the selection of the probe material is based upon the following properties.

1) A sufficiently high melting point for the particular application.

2) Regular change of elastic constants with temperature without a phase change or temperature hysteresis effect.

3) Low material losses at the highest operating temperature. The above three points are essential for any probe material.

4) Machinability to the extent of cutting the resonator slots.

5) High thermal shock resistance (for certain applications).

6) Other properties. Hot strength for a horizontal application probe and high density for liquid immersion. These prop erties are desirable for a probe and improve

the performance.

7) Compatibility with the measuring environment such as oxidizing, reducing, carbonising, corrosive and nuclear radiations.

This is essential for particular application. For example, the environment within the reactor core primarily includes UO2 or other fuel alloys at temperatures upto ~2700^{o}C, intense thermal and fast neutron fluxes (~10^{15}n/cm^{2}sec, 10^{22} to 10^{23} nvt in one year of continuous operation) and gamma radiation.

8) Cost and availability.

Cost is an important parameter. Typically a rhenium probe material will cost about £100, sapphire about £20 and tungsten or molybdenum less than £2. Availability is the deciding factor. The optical and electrical properties of the materials are not important for this application.

8.3 MELTING POINT

The maximum temperature at which the material can be used for the probe is a fraction of its melting point, depending on internal friction. The materials having high melting points are referred to as refractory materials, and these can be divided into three categories: metals; ceramics; and cermets.

8.3.1 The Metals[63]

The metals which possess the highest melting points are the transition metals in the three long series in the

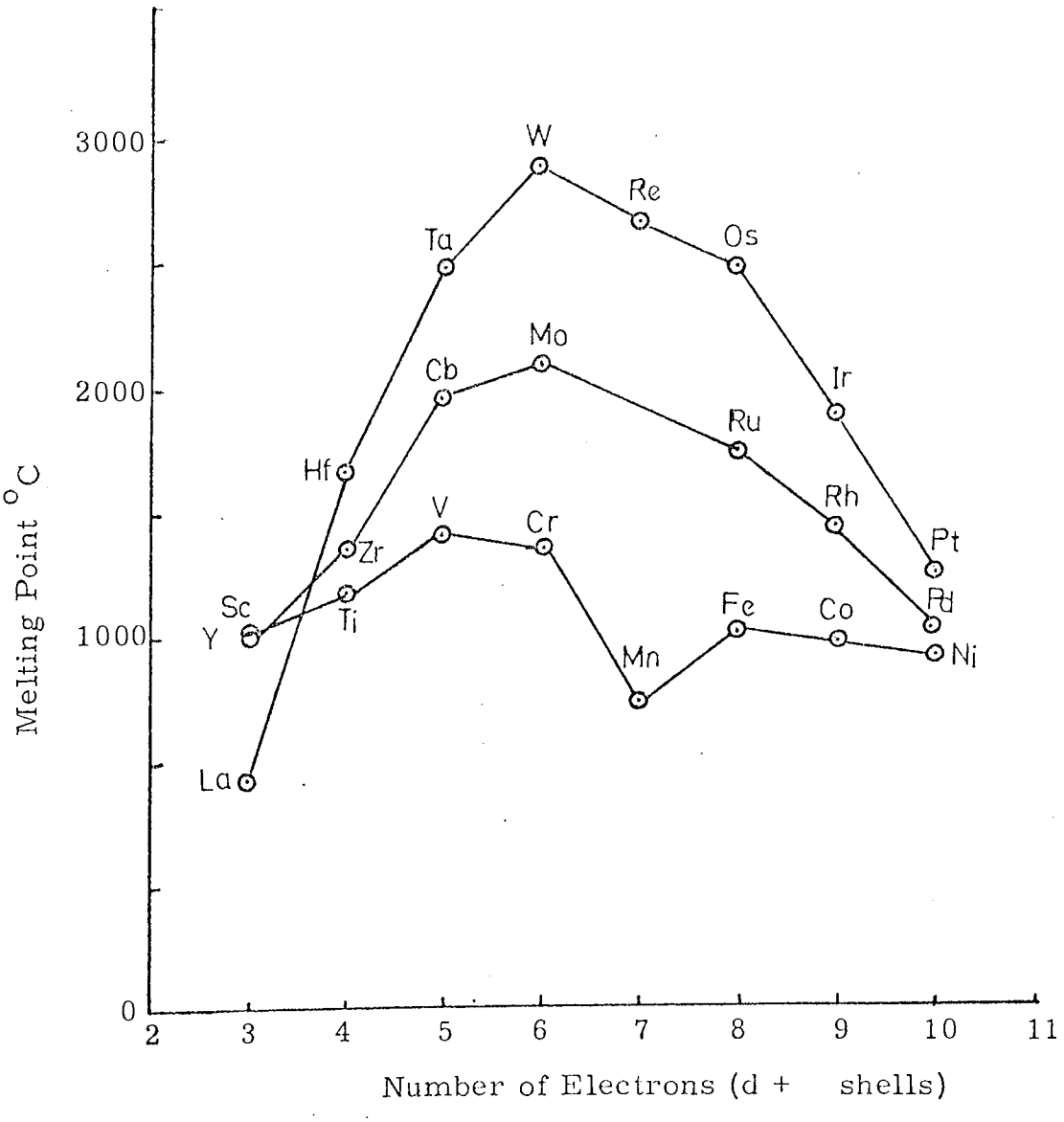

Fig. 8.2 Melting point for the transition metals in the three long series of the periodic table

Table 8.1 Physical Properties of Refractory Metals

Metal	Melting Point ^{o}C	Crystal Structure	Density $kg/m^3 \times 10^3$	Modulus of Elasticity $N/m^2 \times 10^9$	Velocity of Sound at $20^{o}C$	Conductivity Watt m^{-1} k^{-1}	Coefficient of Linear Expansion α per $^{o}C \times 10^{-6}$ near $20^{o}C$	Specific Acoustic Impedance ρc $kg\ m^{-2}\ Sec^{-1}$
Tungsten W	3410	BCC	19.3	408	4310 m/sec	202	4.5	83.1
Rhenium Re	3180	HCP	21.0	530	4980	71	8	104.9
Osmium Os	3000	HCP	22.5	570	4980	-	6.6	112.3
Tantalum Ta	2996	BCC	16.6	190	3550	54.4	6.6	58.8
Molybdenum Mo	2610	BCC	10.2	336	5700	146.5	5.4	58.2
Iridium Ir	2442	FCC	22.4	546	4790	146.5	6.5	105
Niobium Nb	2415	BCC	2.56	105	-	52.5	7.1	-
Ruthenium Ru	2250	HCP	12.2	440	5900	-	9.6	72
Hafnium Hf	1975	HCP	13.36	85	2700	22.2	6.0	36
Rhodium Rh	1960	FCC	12.4	386	5520	15.1	8.5	68.4
Vanadium V	1900	BCC	6.11	151	4940	31	9.7	30.2
Chromium Cv	1875	BCC	7.20	190	5100	67	6.2	36.7
Platinum Pt	1773	FCC	21.45	172	2800	69	8.9	60.2

HCP : Hexagonal Closed Packed
BCC : Body Centered Cubic
FCC : Face Centered Cubic

periodic table. The variation of the melting points of these metals is shown in Fig. 8.2[64]. There are twelve metals with melting points equal to or greater than that of chromium, a temperature which is commonly accepted as the lower melting point limit for defining a refractory metal. Platinum is aslo considered as a potential material for the probe. Table 8.1 by Jaffee, Maykuth and Sherwood[65] summarises the physical properties of these metals.

8.3.2 The Ceramics

The word ceramic comes from Cerami; a district of ancient Athens where potters manufactured their wares (keramos = burnt stuff)[66]. Traditional ceramics cover the raw materials and products of the pottery industry such as earthenware, china, porcelain, tiles and bricks.

The physical and mechanical properties of ceramics stem from their atomic binding and crystal structure. The binding is ionic or intermediate between ionic and covalent. The absence of free electrons is responsible for making ceramics poor conductors of electricity and normally heat, giving their important applications as thermal and electrical insulators, and, where the energy gap is small, as semiconductors. The bonds are highly stable and ceramics have very high melting points and high chemical stability. Hafnium carbide(Hfc) at 4150^{o}C has the highest melting point of any known material. Consequently ceramics are widely used as furnace linings and containers for high temperature

reactions, therefore, their ability to withstand thermal shock is of very great importance. A rapid change in temperature leads to thermal gradients and differential thermal expansion; this effect is aggravated by the low thermal conductivities of ceramics. Rapid cooling is usually more disastrous than a rapid heating as the former puts the surface into tension, where small flaws then grow to cracks. Lastly, differential effects also arise from non-uniform composition.

The term ceramics now covers a very much wider field. Besides the traditional ceramics based on clay, it embraces the new ceramics, such as very pure and dense single oxide, carbides, nitrides, graphite, cement and concrete, cermets (ceramics in a metal matrix), glass and glass ceramics.

8.3.2.1 Oxide Ceramics[67,68]

The oxides can be divided into two general groups, the single oxide and the mixed or complex oxide, only the former will be dealt with here. Out of a large number of oxide ceramics only alumina, beryllia, magnesia, thoria and zirconia are practicable and are currently available in possible probe forms. Table 8.2 by Campbell and Sherwood[67] summarises some of their properties. From the table it can be concluded that these oxides are potential materials due to their high melting points.

8.3.2.2 Graphite[69] (m.p. 3500°C)

It is a potential material having a high melting point

Table 8.2 Physical Properties of Oxide Ceramics

Material	Formula	Molecular Weight	Melting Point ^{o}C	Boiling Point ^{o}C	Density g/cm^3	Modulus of elasticity $N/m^2 \times 10^9$	Principal Limitation
Aluminium Oxide (Alumina)	Al_2O_3	101.92	2015	2980	3.65	382	
Beryllium Oxide (Beryllia)	BeO	25.02	2550	4260	3.01	310	Price Toxicity
Magnesium Oxide (Magnesia)	MgO	40.32	2800	2825	3.58	210	
Thorium Oxide (Thoria)	ThO_2	264.12	3300	4400	9.69	140	Price radioactivity
Zirconium Oxide (Zirconia) Stabilized	ZrO_2	123.22	2770 ± 80	4300	5.56	172	Price

and complete compatibility with the nuclear environment, but due to a wide thermal hysteresis loop it is not suitable for probe and further investigations were ruled out. It has not been possible to obtain pyrolytic graphite which may not have the deficiencies of the normal form.

8.3.3 Cermets[66,70]

Cermets consist of small particles of crystalline ceramic held together by a matrix of metal, typically tungsten carbide in cobalt. Some examples of cermets are $Cr\text{-}Al_2O_3$, Co-TIC, NI-TIC. The principal cermet used for high speed metal cutting tools and mining drills is composed of tungsten carbide WC and 6-20wt per cent of cobalt Co. The tungsten carbide is a hard and brittle ceramic with a simple hexagonal crystal structure and cobalt is a ductile metal with a cph structure which is able to wet the carbide phase and form a strong adhesive bond with it.

The development of cermets as high temperature structural materials has been given much effort in the last twenty years, especially for gas turbine blades. Here the thermal shock resistance, creep and inpact strength at temperature are more important than hardness and wear resistance. The proportion of ceramic to metal is accordingly moved towards a majority of the metalic[1] phase. Of the carbides, only the TiC based cermets have comparable oxidation resistance and their mechanical properties are possibly superior, if still inadequate. These are not readily available, therefore

further investigations were not made. The refractory metals, their alloys and oxide ceramics satisfy the high melting point requirements, therefore these were further investigated for other properties.

8.4 ELASTIC CONSTANTS AT HIGH TEMPERATURES

An important physical property of material for probe use is the variation of elastic constants with temperature. It is required that there should be minimum difference between the heating and cooling (thermal hysteresis) and also between subsequent heatings. In some materials hysteresis effects are originally present but are gradually reduced with temperature cycling. Another important factor is the phase change with temperature. A phase change in the operating range automatically excludes a material because of the associated recrystallization. Typically titanium and zirconium have phase changes which preclude their use.

8.4.1 The Metals

Among the refractory metals only chromium shows a phase change from BCC to FCC at 1850^{o}C (m.p. 1875^{o}C) and hafnium from CPH to BCC at 1950^{o}C (m.p. 1975^{o}C). Therefore these metals potentially can be used to a temperature near to melting point. The variation of elastic constants with temperature for certain metals are widely reported and are summarised below. The temperature coefficient of Young's modulus for tungsten, molybdenum and their alloys increases with temperature. At a

temperature of about $0.5T_{melt}$, the increases is sharp[71]. The temperature coefficients of elastic moduli for other metals also show this characteristic knee.

8.4.1.1 Tungsten (m.p. 3380°C)

Several groups of investigators have measured the elastic moduli of tungsten as a function of temperature. Peterson[72] have made a comparison between the results obtained from the different dynamic techniques of ultrsound velocities. The elastic modulus of tungsten have been reported by Koster[44], Armstrong and Brown[73], Fine[74] and Pisarenko et. al.[75], who used the resonant-bar method of measurement. Fig. 8.3 shows the effect of temperature on the modulus of elasticity of tungsten. The earlier data by Koster[44], are seen to be in excellent agreement with the data of Armstrong and Brown in the overlapping temperature zone. The hysteresis effects are very small.

Other investigators such as Bernstein[37] and Lowrie and Gonas[38] have also used pulse-echo technique for measurement of the elastic modulus of tungsten and generally there is a good agreement between the results obtained from the both dynamic methods.

The effect of impurities and alloying on the internal friction of tungsten at high temperature have been reported by Berlec[76]. It is shown that pure tungsten after a second recrystallization has an extremely high damping, where the doped material, shows rather low damping which only slowly increases with temperature.

The doping impurities accumulate at the grain boundaries and prevent metal to metal contact between the grains, this eliminates the internal friction at these boundaries.

8.4.1.2 Rhenium (m.p. 3170°C)

Sims and Jaffee[77] measured the modulus of elasticity as a function of temperature in a helium atmosphere using the resonance technique. Fig. 8.4 shows that the modulus decreases linearly from room temperature to 900°C. There is no mention of hysteresis effect. Due to its very high melting point it is a potential material for the probe. The addition of thoria to rhenium reduces the ultimate tensile strength and ductility and lowers the recrystallization temperature. Rhenium is resistant to attack by molten tin, zinc, silver, and copper; attacked slowly by aluminium; and readily dissolved by nickel and iron.

8.4.1.3 Tantalum (m.p. 3000°C)

Fig. 8.5 shows the modulus of elasticity from -196 to 900°C determined by two investigators Koster [44] and Begley[78]. The two values exclude tantalum for any but hard vacuum uses.

8.4.1.4 Molybdenum (m.p. 2620°C)

The variation of modulus of elasticity of molybdenum from 20 to 2000°C is shown in Fig. 8.6. Dynamic data shown

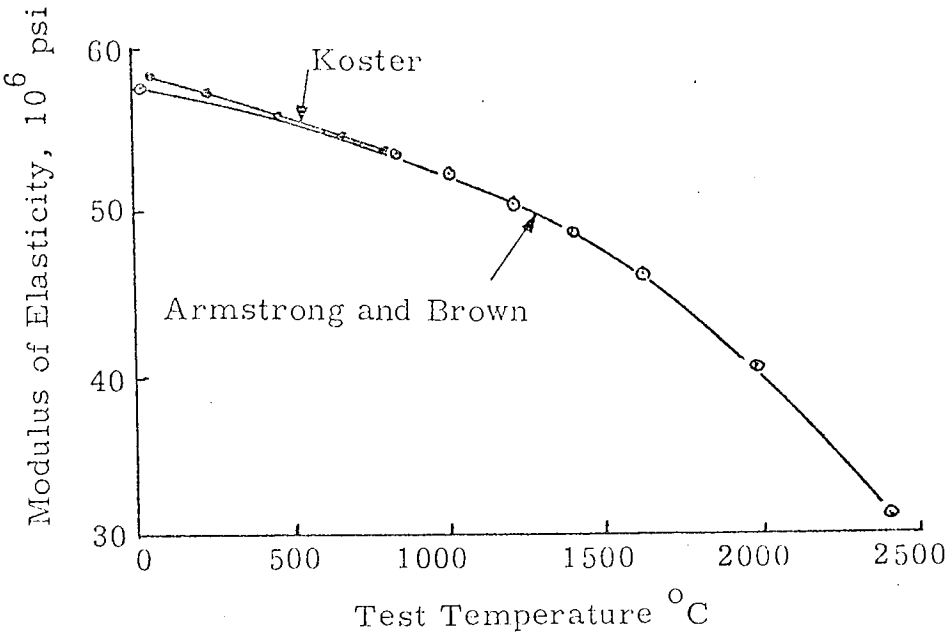

Fig. 8.3 Modulus of elasticity of Tungsten vs test temperature. Data from Armstrong and Brown and Koster.

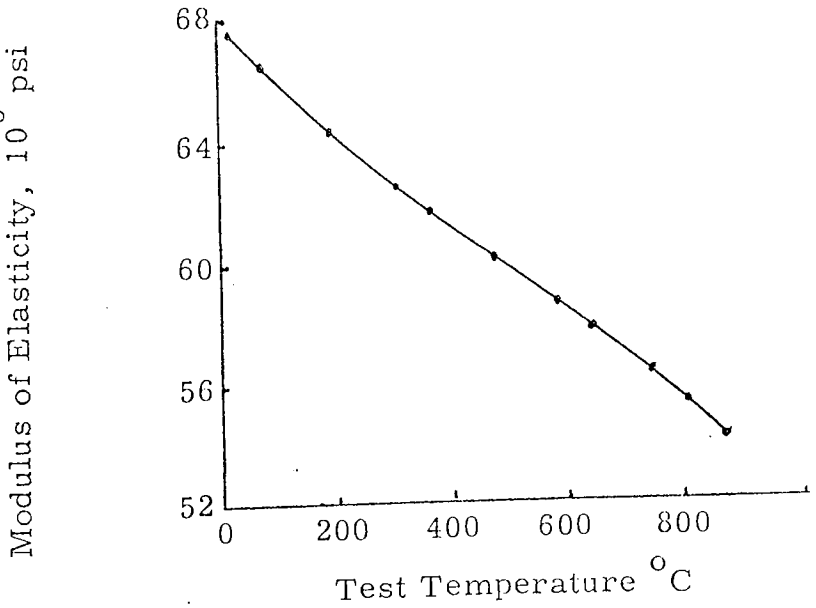

Fig. 8.4 Modulus of elasticity of recrystallized Rhenium as a function of temperature. Data from Sims and Jaffee.

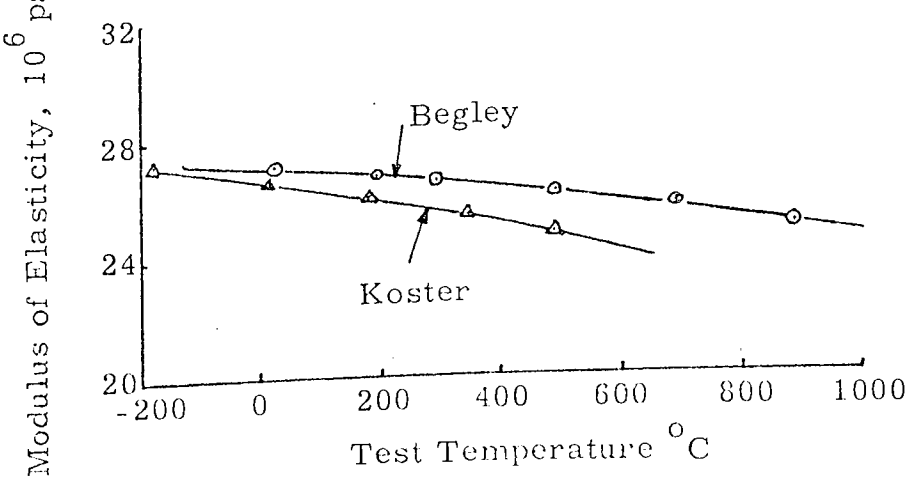

Fig. 8.5 Modulus of elasticity of Tantalum vs test temperature. Data from Begley and Koster.

by Armstrong and Brown[73], and Freeman and Briggs[79], indicate a decrease of modulus with increasing temperature and also a knee at about 1400°C.

Molybdenum is a good probe material because of its high melting point, the consistent variation of elastic constant with temperature, the absence of thermal hysteresis, the low neutron cross-section and compatibility with the alkali metals.

Ababkov and Morgunova[80], have been reported the mechanical properties of molybdenum and tungsten alloys at the elevated temperatures. It has shown that the strength of MO-W alloys at low (20 - 600°C) and high (over 1800°C) temperatures increases with the tungsten content, and at moderate temperature (600 - 1800°C) the strength is highest for alloys with the maximum alloying. Also at 1500 - 1800°C the strength to weight ratio is highest for molybdenum alloys with 80, 56 and 32.5 W, and is equal to or larger than that of unalloyed tungsten.

The strength of MO-W alloys can be increased substantially by small additions of titanium and zirconium. Molybdenum is used extensively.

8.4.1.5 Niobium (or Columbium) m.p. 2470°C

Brown and Armstrong[47], measured the modulus of elasticity of niobium from 20 to 2000°C by dynamic method with results shown in Fig. 8.7. The curve shows a knee at about 1400°C, similar to other refractory metals. The

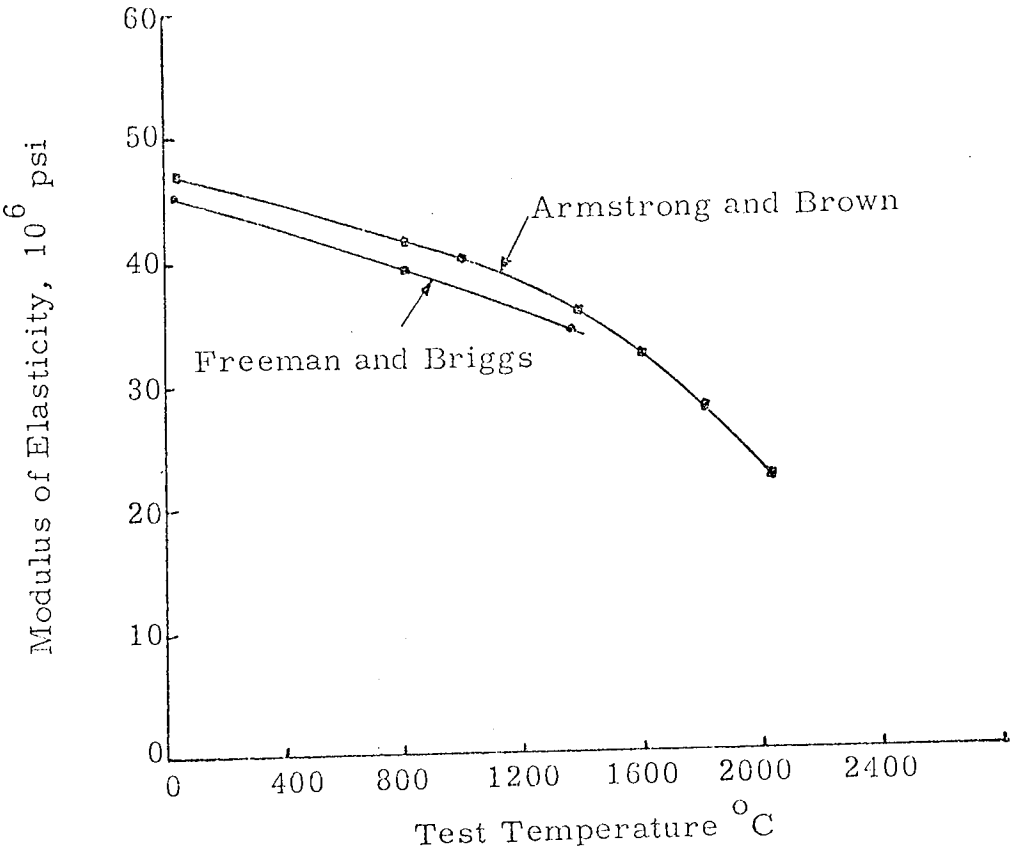

Fig. 8.6 Modulus of elasticity of Molybdenum vs test temperature. Data from Armstrong and Brown and Freeman and Briggs.

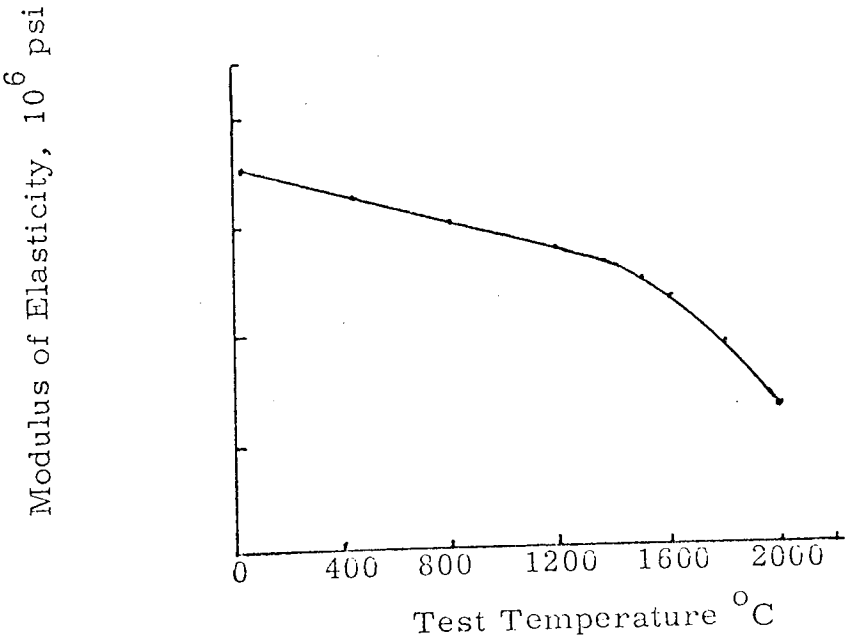

Fig. 8.7 Modulus of elasticity of Columbium vs test temperature. Data from Brown and Armstrong.

phenomenon has been associated with a grain boundary process. Dreshpak[71], has shown the addition of tungsten and molybdenum to niobium increases its modulus of elasticity, but hafnium carbide slightly decreases it.

8.4.1.6 Vanadium(m.p. 1920°C)

Similar measurements by Hill and Wilcox[81], are shown in Fig. 8.8 the decrease in modulus with temperature is 6% in 550°C. The agreement between the modulus values of the two forms, wrought and recrystallized, at all temperatures suggests that purity and structure have little effect on the modulus of elasticity. It absorbs oxygen, however, and this has an assoiciated internal friction peak, reported by my colleague Dr. Pelmore[51].

8.4.1.7 Chromium (m.p. 1880°C)

Measurements by Maykuth et.al. [82] for pure chromium and Cr-Fe and Cr-Ni alloys are shown in Fig. 8.9. The anomolous behaviour near room temperature is exhibited in the unalloyed chromium but does not appear for alloys.

8.4.1.8 Platinum (m.p. 1780°C)

Platinum is not a refractory metal as such, but its melting point and resistance to oxidation and reduction makes it an attractive material for a probe. It has low hysteresis, high calibration stability over long periods and high sensitivity. Ketova et. al.[83], have investigated

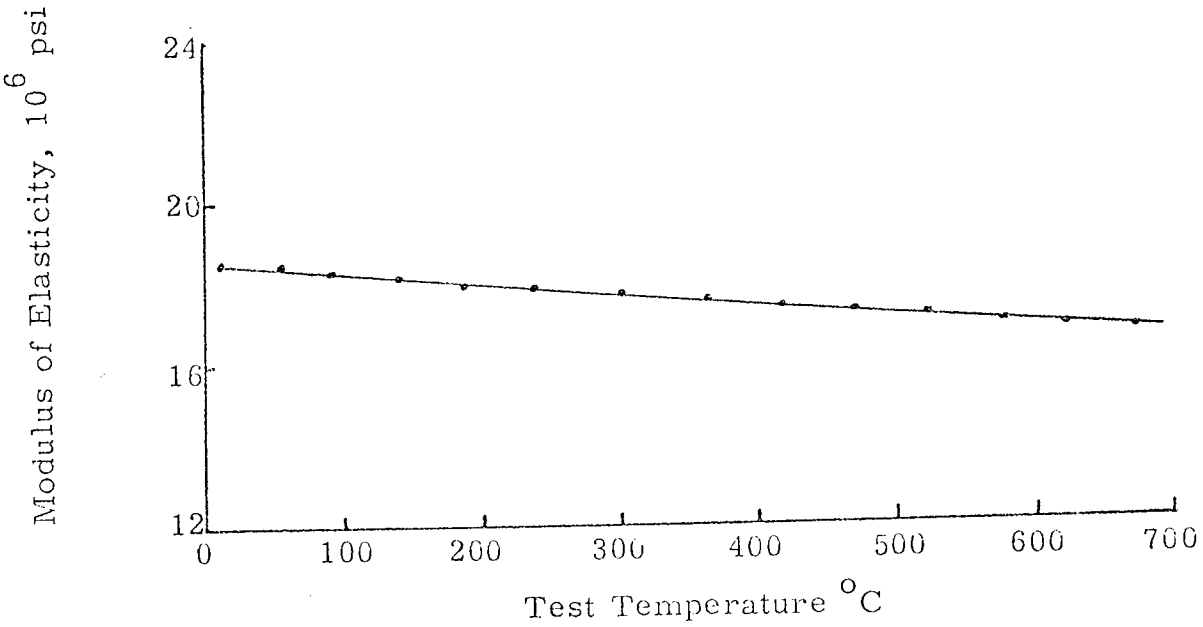

Fig. 8.8 Modulus of elasticity of Vanadium vs test temperature.
Data from Hill and Wilcox.

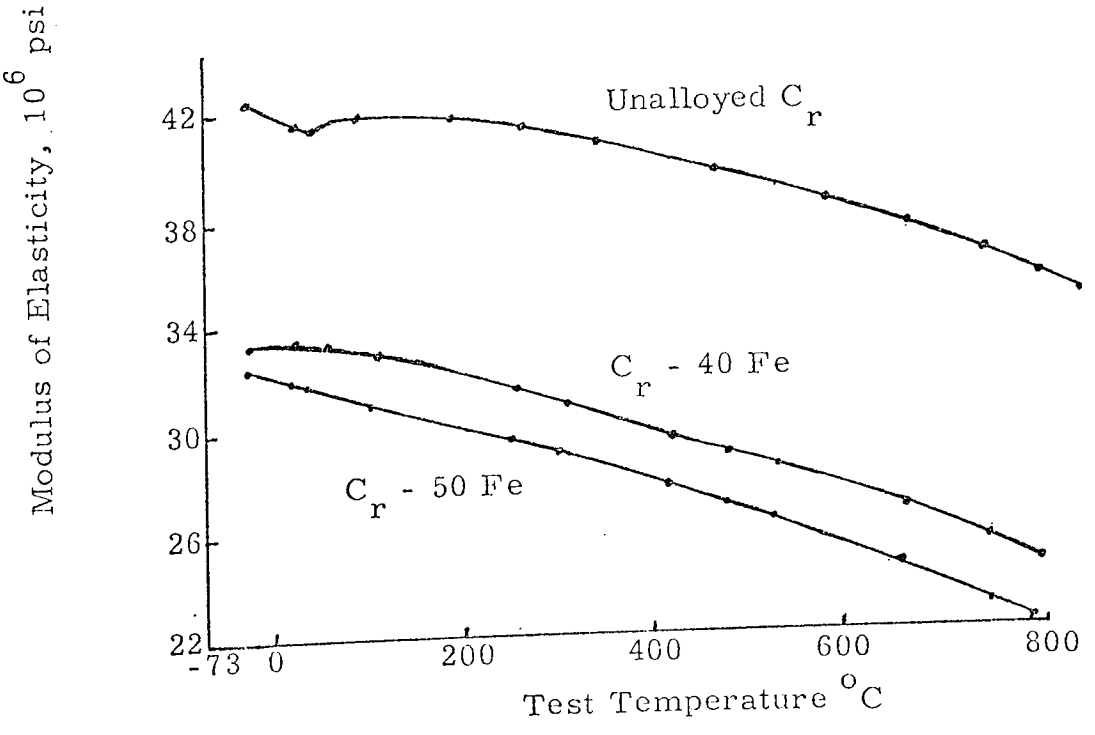

Fig. 8.9 Modulus of elasticity of Chromium and two Chromium alloys as a function of temperature.
Data from Maykuth, Jaffee and Blocher.

the effect of alloying on the modulus of elasticity of platinum alloys. They showed that when platinum is alloyed with one element (ruthenium, rhodium, palladium) the variation of the elastic modulus for the binary alloy with concentration increases with the elastic distortion in the lattice of the alloy and with the elasticity modulus and melting point of the alloying element. For the pt-pd system the elasticity modulus decreases continuously with increasing palladium concentrations up to 100%.

8.4.1.9 Iridium (m.p. 2440°C)

This metal has the highest melting point of any that is stable to oxidation. There is an internal friction peak at about 1800°C but this drops down at 2050°C. The thermal hysteresis is very good. The performance of this material is surprisingly good and shows great potential as a probe for temperatures up to 2000°C with capability of operation in oxidising or reducing atmospheres and no thermal shock problems. This is extensively used as described later.

8.4.2 Oxide Ceramics

Dynamic measurement of elastic constants over a temperature range for various oxide ceramics have been made by Wachtman and Lam [46], Soga and Anderson [84], Spriggs et. al. [85] and various other workers. Wachtman and Lam measured Young's modulus of a free-free bar vibrating in flexure at high temperature for single crystal

alumina, i.e. sapphire and ruby and polycrystalline alumina, magnesia, thoria and stabilized zirconia. Their observations shows that for single crystal ceramics the variation of Young's modulus with temperature is almost perfectly linear as shown in Fig. 8.10. For a polycrystalline alumina it is linear up to 1000°C followed by a sharp drop in the value at a higher temperature (Fig. 8.11). Magnesia and thoria are linear up to 1200°C followed by a similar drop (Fig. 8.11). Stabilized zirconia exhibits (Fig. 8.12) a complex change with temperature which excludes it as a possible material.

Single crystal oxide ceramics are conspicuously better suited for the probe application because the temperature dependence of YOung's modulus is linear almost to its melting point and most important is the absence of the high internal friction of polycrystalline materials.

8.5 MATERIAL LOSSES AT HIGH TEMPERATURE

For probes using the resonance technique, the material Qm (proportional to 1/losses) sets an upper limit to the measurement. In general Qm falls rapidly with temperature and in fact log(1/Qm) is often a linear function of 1/T, the Arrhenius plot. These plots are available for large numbers of materials. Typically, for iridium the value of Qm^{-1} ranges from 10^{-3} to 10^{-4} at room temperature, is 5×10^{-3} at 1300°C and 8×10^{-2} at 2000°C. It also shows a peak between 1800°C to 1900 °C, Pelmore[51]. It is

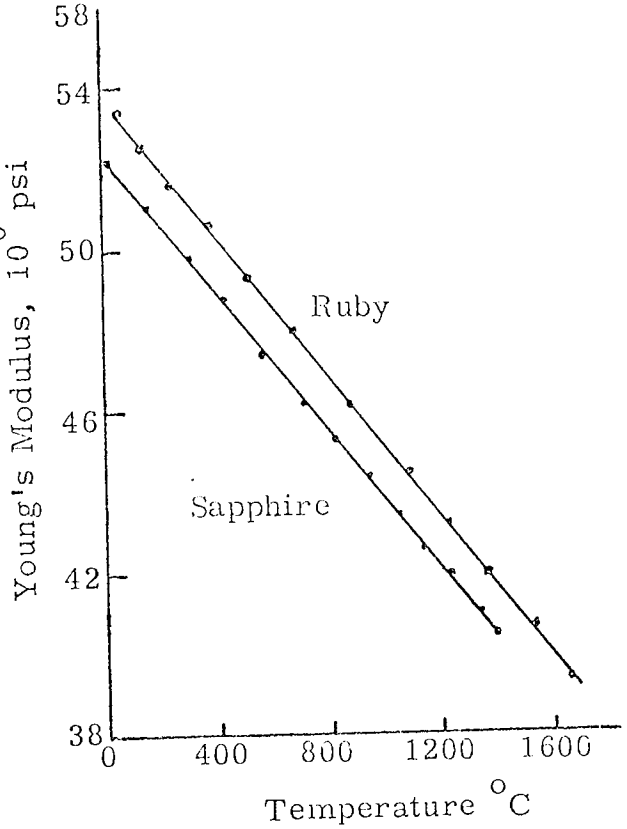

Fig. 8.10 Young's modulus of Sapphire and Ruby as a function of temperature

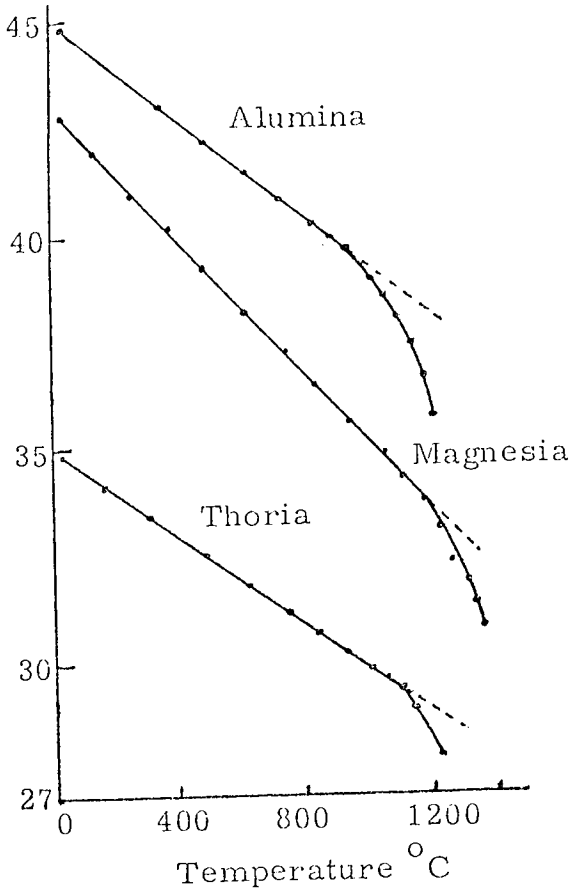

Fig. 8.11 Young's modulus of Polycrystalline Alumina, Magnesia and Thoria as a function of temperature

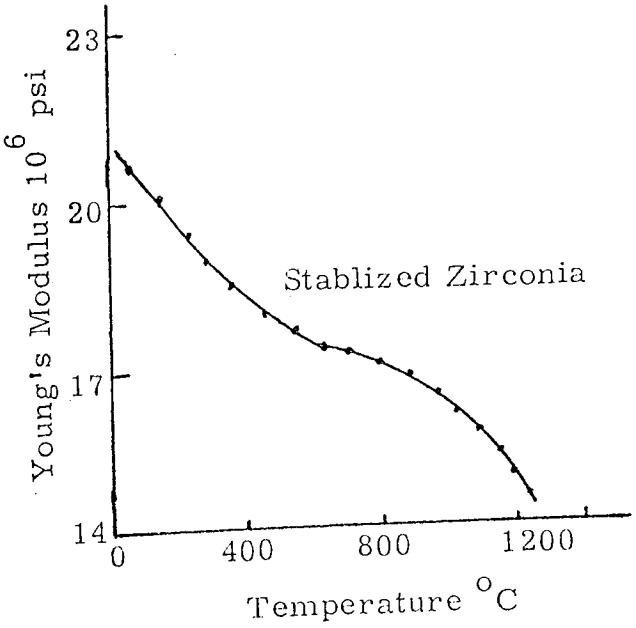

Fig. 8.12 Young's modulus of stablized Zirconia as a function of temperature

Data from Watchman and Lam for all the three figures

generally true that at room temperature, losses are small. As the temperature is increased the losses increase. Above a certain temperature the losses increase rapidly, the cross over disappears, the decrement amplitude gets very small the resonance cannot be detected. Thus losses put an upper limit on the usefulness of a material. Crystalline materials have low losses to a temperature near to melting point, a typical example is single crystal alumina with a melting point of 2050°C, which can be used up to 2000°C. Polycrystalline alumina, however, cannot be used beyond 1400°C. Molybdenum with a melting point of 2620°C is unsuitable beyond 1600°C.

8.6 MACHINABILITY

Machining of some of the material selected for the probe presented problems. Diamond wheel cutting was employed for ceramics and certain hard refractory metals. Pure tungsten was particularly difficult and iridium, which on its pure state is very brittle, must be alloyed with platinum to be used. Thoriated tungsten is much more machinable than pure tungsten. The resonator design developed required only a small amount of machining and this is possible for all the materials encountered.

8.7 THERMAL SHOCK

Thermal shock designates a condition brought about by a sudden and severe change in the temperature at the surface of a body. In most metals having a high thermal

conductivity, temperature gradients and therefore thermal stress will be small and there is no shock problem. In refractory material, however, especially ceramics, which are usually poor thermal conductors, steep temperature gradients will be set up giving dangerous thermal stresses with possible mechanical fracture. Thermal shock becomes a very serious problem where high temperature operation of such materials are involved as in the case of the probe.

Empirical formulae were obtained by Buessem[86] in terms of material properties and geometry of the object to give a maximum acceptable temperature difference. Good thermal shock properties are associated with high thermal conductivity, high fracture strength, low coefficient of expansion and low elastic constant. Geometrically thin strips and thin walled tubing are much superior to rods, spheres and other bulk forms.

Of all the temperature-resistant nonmetallic materials available, carbon and graphite have the best overall thermal-shock resistance. In practice graphite becomes stronger with increasing temperature. One variety, which breaks at 3600 Psi at room temperature, increases its strength to 6800 Psi at 2660^{o}C.

Silicon carbide refractories are noted for their heat-shock resistance.

8.8 OTHER PROPERTIES: HOT STRENGTH AND DENSITY

Hot strength is the ability to stand up under load at elevated temperatures. Loading can arise from the actual weight of the probe itself(important for horizontal use) or

from internal stresses. Above a certain temperature the material becomes susceptible to deformation and ultimately fails. Good hot strength is therefore desirable.

For liquid or molten metal measurement, the acoustic losses are proportional to the ratio of liquid to probe densities. Therefore materials of high density are desirable.

8.9 COMPATIBILITY WITH MEASURING ENVIRONMENT

The materials which have the above qualities are suitable for a probe but they must also be compatible with the measuring environment. The probe material is selected for a particular application. The measuring environments encountered are oxidizing, reducing, carbonising, corrosive and nuclear radiations and for molten metals the probe should not react or dissolve.

The refractory metals and oxide ceramics are considered for their chemical properties. For molten metal measurements these properties must be studied separately for each application. It is not possible to give here all the chemical properties of the probe material, but some of them are described here.

8.9.1 Oxidation Behaviour[65]

The refractory metals (Os, Re and Mo) which form low melting oxides have extremely high oxidation rates. Metals (Nb, Ta and W), whose oxides are solids within the temperature range 700 to 1400^{o}C, but which do not form a protective

coating, tend to have intermediate oxidation rates. Metals (Ru, Ir and Rh) with volatile oxides are better to an increasing order as named. Chromium is the only refractory metal which forms a tight oxide and is oxidation resistant. Platinum is particularly suited to this environment.

Oxide ceramics are very stable in an oxidising atmosphere even up to melting point. Table 8.5[67] summarises the behaviour of oxide ceramics in various atmospheres.

8.9.2 Reduction Behaviour

Refractory metals and oxide ceramics, because of their high chemical stability, are in general, unaffected by reducing atmosphere. Chromium, however, reacts preferentially with nitrogen, and magnesia has poor reduction resistance.

8.9.3 Other Relevant Properties

Tungsten is carburized in carbon or hydrocarbon atmospheres. Beryllia has a peculiar chemical property of acting on some human organisms, causing berylliosis, and its use is not safe without extensive precautions. Oxide ceramics are stable in corrosive atmospheres. At a sufficiently high temperature oxide ceramic reacts with carbon. There is practically no oxide stable enough to withstand the reducing action of carbon under the appropriate temperature conditions, particularly in a vacuum. Alumina reacts with carbon below 2000°C, magnesia at 1900°C, beryllia at 1800°C and zirconia at 1300°C[68].

Table 8.5 Chemical Properties of Oxide Ceramics

Material	Melting Point °C	Limit of Usefulness in Oxidizing Atmosphere °C	Thermal Shock	Reducing Atmosphere	Stability				
					Carbon	Acid	Basic	Metals	Nuclear
Alumina	2015	1950	Good	Good	Fair	Good	Good	Good	
Beryllia	2550	2400	Excellent	Excellent	Excellent	-	Fair	Good	
Magnesia	2800	2400	Fair	Poor	Good	Poor	Good	Fair	
Thoria	3300	2700	Poor	Good	Fair	Poor	Good	Excellent	
Zirconia (Stabilized)	2600	2500	Fair	Good	Fair	Good	Poor	Good	

Molybdenum, tungsten and rhenium and other refractory metals have low nuclear cross-section and are therefore suitable for use with the nuclear reactor. Practically in nuclear thermometry, high temperature thermocouples are insulated by a very pure refractory ceramics, such as Beo, Al_2O_3, ThO_2, HfO_2, and MgO and protected by a sealed refractory metalic sheath, such as Ta, Mo and Nb.

Activated tantalum is an extreme health hazard, far greater, for example, than beryllia which is often looked upon as a very lethal material at the fabrication stage.

The transmutation effects of the thermal neutrons on the temperature sensor element must be considered as being reported by Shepard et. al.[15] A progressive pattern of increasing loop resistance and indicated temperatures of many W/Re alloy thermocouples are attributed to transmutation of Rhenium to Osmium.This causes decalibration in thermo-couple, shown in Figs. 8.13 and 8.14.

8.10 CONCLUSIONS

Refractory metals, e.g. molybdenum, tungsten and rhenium are suitable for high temperatures in reducing, vacuum and nuclear environment. Molybdenum is suitable for liquid sodium and alumina for brass. Platinum is satisfactory upto 1300°C in air. Single crystal oxide ceramics can be used very near to their melting point in oxidising, reducing, corrosive and nuclear atmospheres. Materials are selected for a given temperature range measuring conditions. For the Petten experiment thoriated tungsten has been selected and this is expected to be

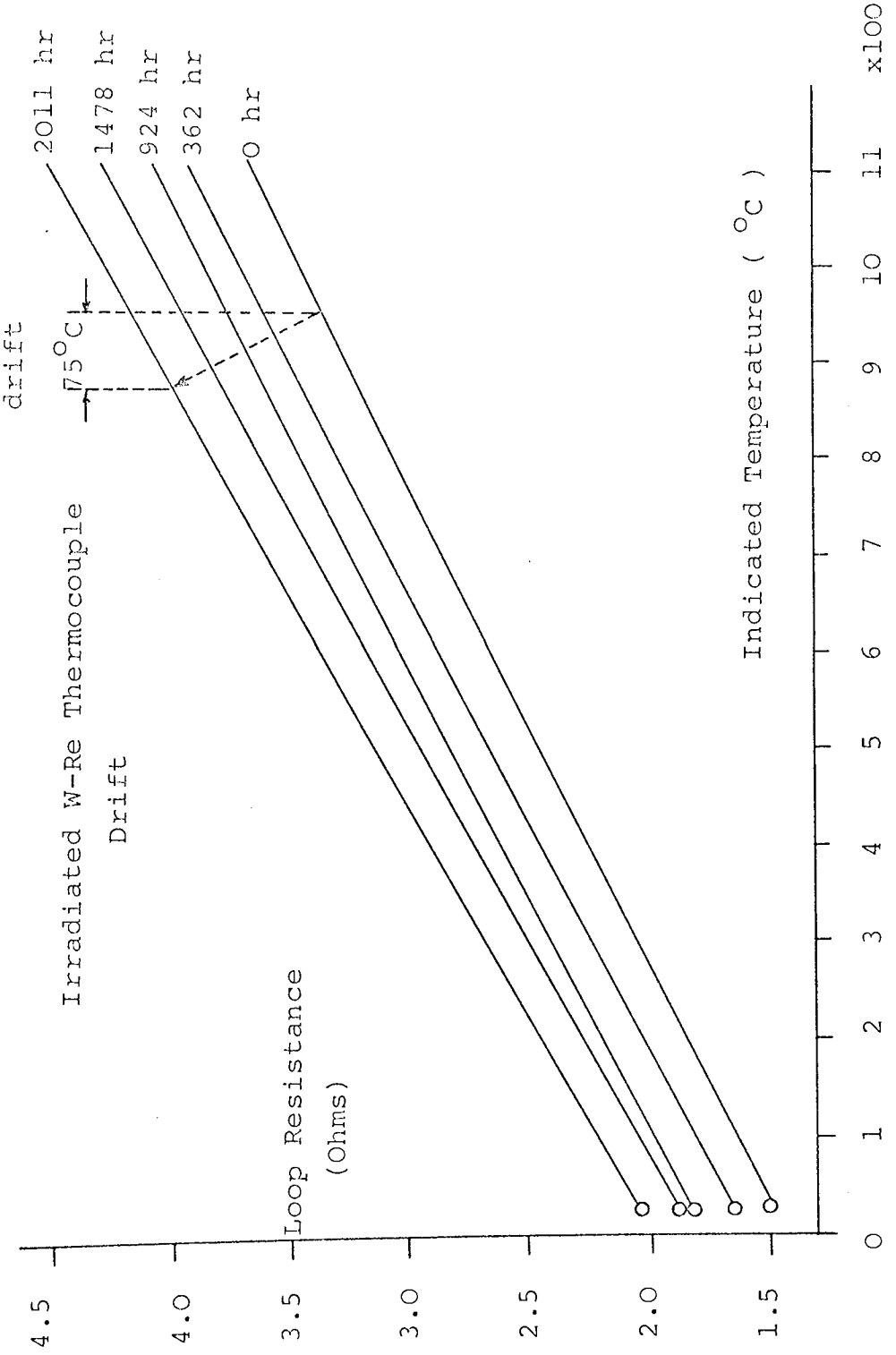
Irradiated W-Re Thermocouple
Drift
Loop Resistance
(Ohms)
4.5
4.0
3.5
3.0
2.5
2.0
1.5
0
1
2
3
4
5
6
7
8
9
10
11
x100
Indicated Temperature (°C)
2011 hr
1478 hr
924 hr
362 hr
0 hr
drift
175°C

Fig. 8.13

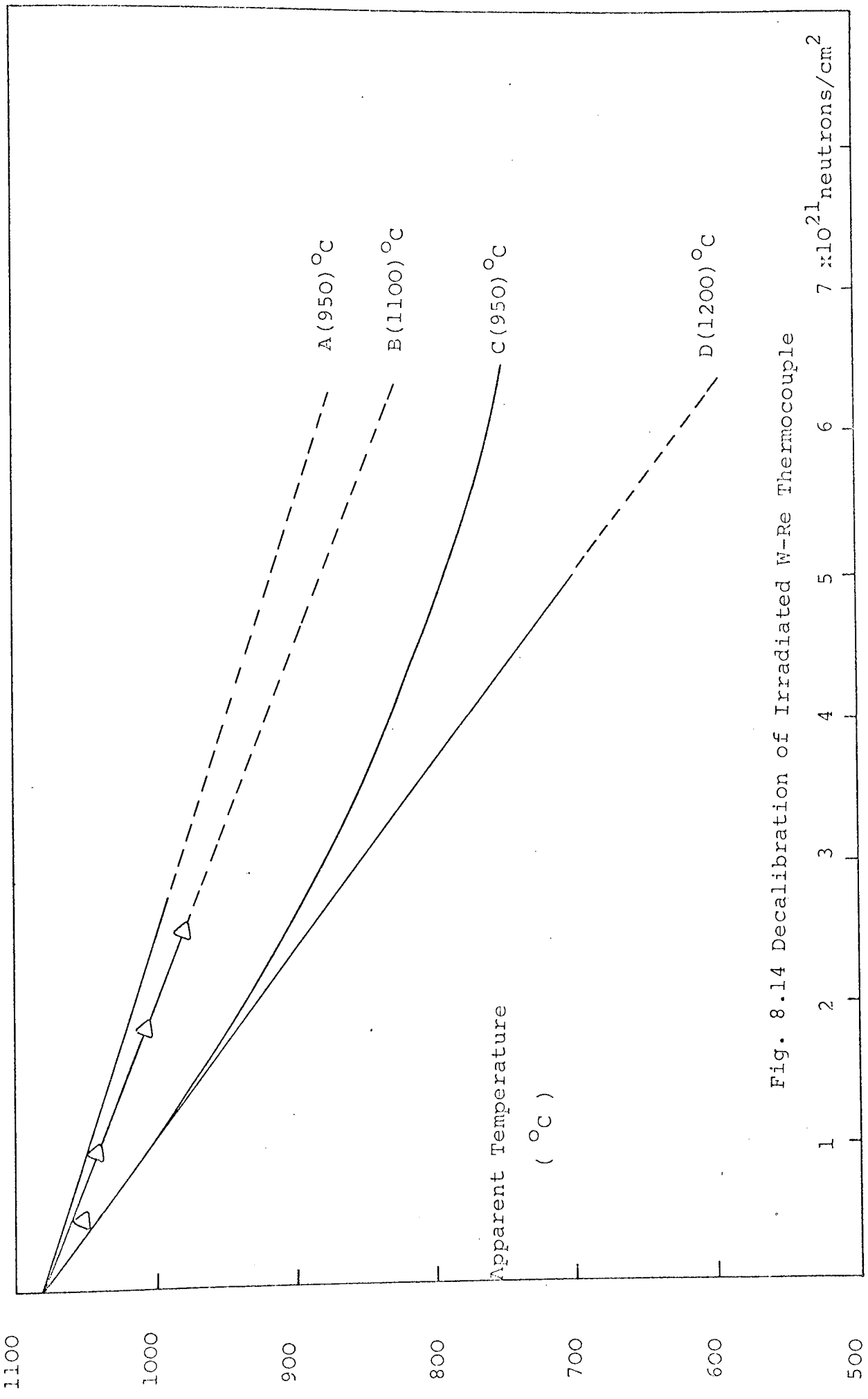

Fig. 8.14 Decalibration of Irradiated W-Re Thermocouple

satisfactory upto 1700°C. Above 2000°C, ceramics such as magnesia or silicon carbide, preferably in the single crystal form would probably function satisfactory but these are not available in the required geometry.

CHAPTER 9

TRANSDUCER DEVELOPMENT FOR NUCLEAR APPLICATION

9.1 INTRODUCTION

Engineering textbooks define transduction as the process of converting one form of energy to another, and a transducer as the device that performs the conversion. A device that simply acts upon an energy form without changing the nature of that energy is called a modifier element, not a transducer of energy.

The transducer in the probe is usually a mognetostrictive one and is non-resonant by virtue of being a matched section of the transmission line. The name magnetostriction or piezomagnetism is given to the phenomenon that, when some materials are magnetised a change in dimensions occurs[87]. This change is non-linear and can be either positive or negative in the direction of the field. The inverse magnetostrictive effect refers to the fact that if the material is subjected to a mechanical strain while immersed in a magnetic field there will be a change in the flux in the sample[59].

Magnetostriction is ideal for introducing longitudinal or torsional waves into a bar because it only requires to surround the magnetic bar with a solenoidal coil about half a wavelength long. The coil can be relatively long $\geq$ 1 cm, because for both longitudinal and torsional waves the wavelength must be much longer than the bar diameter,

typically ~2 mm.

Magnetostrictive materials must be biased with a DC magnetic field into a linear region to make them analogous to piezoelectric materials which are linear by nature. For magnetostrictive materials, the linear region occupies a portion of the curve between zero flux and saturation. With an applied DC component H_{DC} of magnetic induction H bringing it into the linear region, the magnetostrictive material will respond with an AC strain to an applied AC magnetic field H_{AC}, Fig. 9.1.

The DC magnetic bias for magnetostriction can be supplied in four ways. These are:

(1) Permanent magnetization of the bar,

(2) Magnetic biasing with an external permanent magnet,

(3) Magnetic biasing with a DC electric current in a surrounding coil which can be the same carrying the AC driving current,

(4) Magnetic biasing with a pulse of current in a surrounding coil so that the rise and fall of the pulse current is used also to provide the AC magnetic field to shock-excite the bar and give a strain pulse.

This method is useful for transmission, and provides some permanent (remanent) magnetization for reception[21].

The theory of magnetostrictive delay line is given by Williams[88], and magnetostrictive materials by Kikuchi[89].

9.2 DESIGN OF THE TRANSDUCER

A transducer assembly is shown in Fig. 9.2.

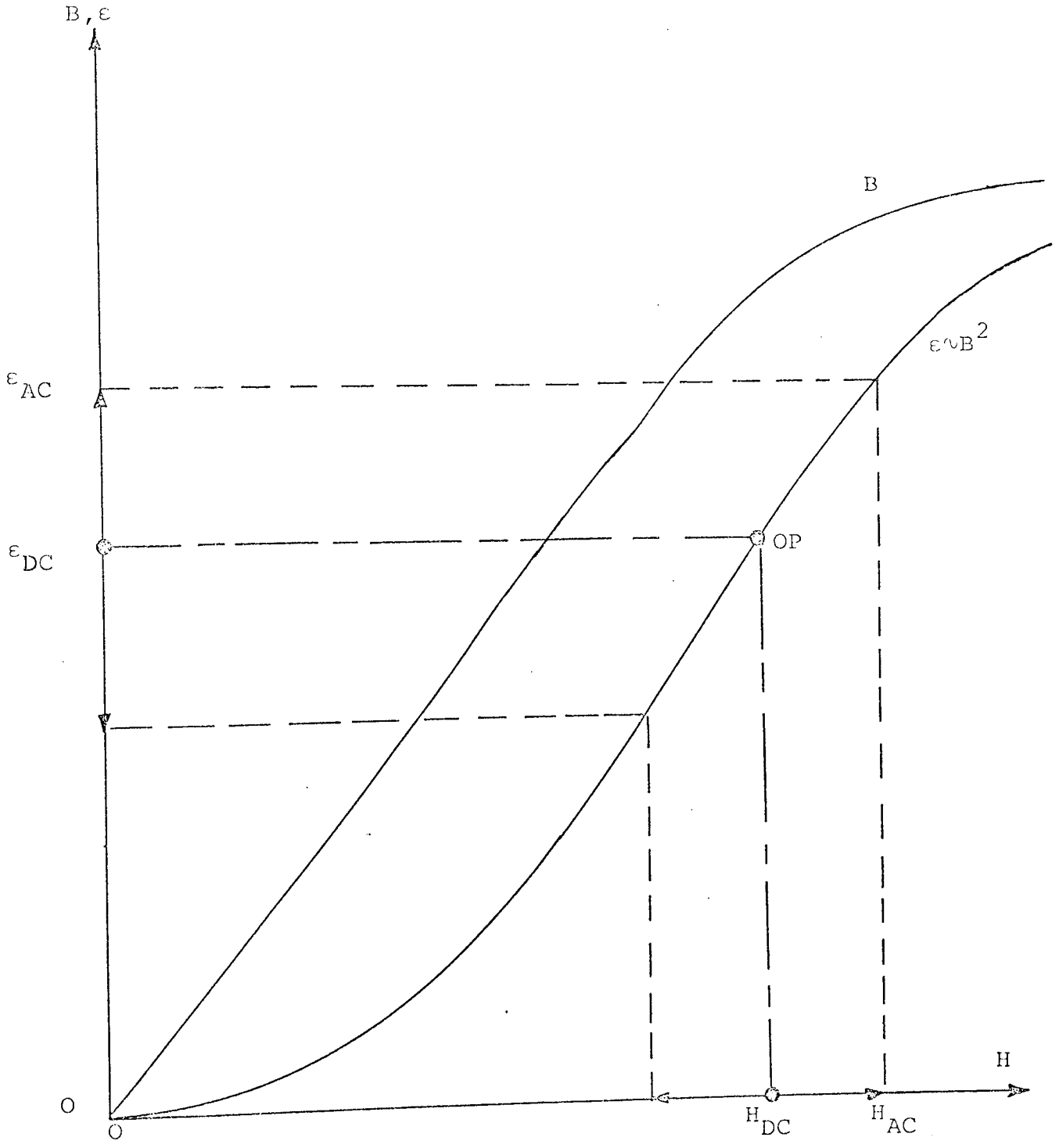

Fig. 9.1 Graph showing the operating point OP of a biased magnetostrictive material driven with an alternating field. H is magnetic induction, B is magnetic flux, and ε is strain. The change in strain per unit change in induction is greatest at the operating point, and the response is most linear there.

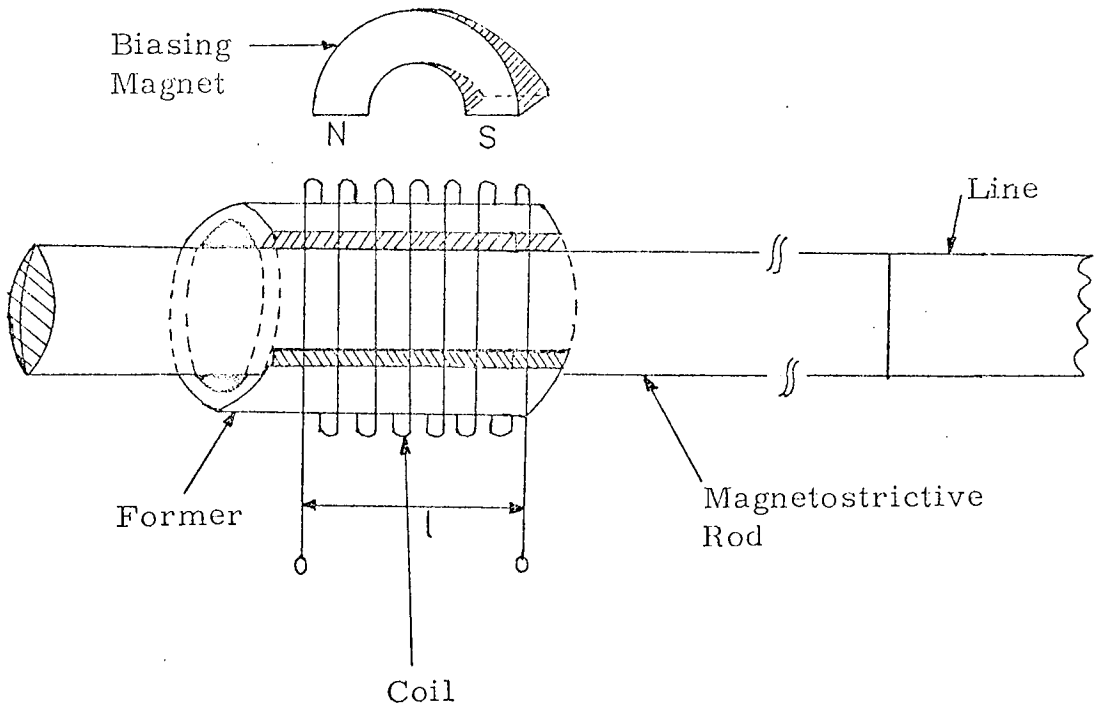

Fig. 9.2 A magnetostrictive transducer assembly

Permendur, 49% iron - 49% cobalt - 2% vanadium,[90] which is a highly efficient magnetostrictive material is used for transducer. The coils is wound on a silica or alumina tube. The magnetic bias is provided by a permanent magnet of a horse shoe or ferrite ring type.

The bias depends on the particular properties of the transducer material which are very dependent on the exact thermal history of the material in the transducer region, the optimum bias can differ for different samples of the same nominal rod.

The disadvantages of permanent magnet are that the bias is only altered by moving the magnet relative to the transducer by mechanical means, and that the magnet itself is bulky and making it unsuitable for some delicate works such as the inside of the 15 mm diameter protective tube available for this application.

An electromagnet is used for the bias, passing a DC current in a coil wound over the first coil. This is considered for the "Petten" experiment, where the probe is supported by terminating the launcher with a short heavy isolating rod which can be secured to the reactor structure. This support, the bias and launching coil and the launcher are made up into a single compact unit shown in Fig. 9.3.

9.2.1 Detail of the Design

Various design parameters are adjusted to obtain maximum efficiency and a good bandwidth.

The length of the launching coil is $\lambda/4$ = 13.5 mm at the operating frequency, 100 kHz as before, and the coil former which is a very thin glass tube (3.4 mmOD) is housed inside a 5 mm deep hole provided in the heavy metal. The 2 mm magnetostrictive rod is a good fit without constriction inside the coil former (2.4 mmID) giving a very good flux linkage from the coil to the rod hence a good efficiency.

The free end of the launcher is silver brazed inside the heavy metal in a distance of $\lambda/2$ = 27 mm from the centre of the coil, which gives the maximum reenforcement from the other end of the rod.

The launching coil has eight layers, each containing 60 turns of 0.15 mm copper wire, giving 11.9Ω D.C. resistance at room temperature and producing a high impedance at the signal frequency to give a convenient match to the output stage of the transmitter. To avoid slipping of the wires over the lower layers and to produce a strong solid coil, thermal setting araldite has been used extensively. After winding each layer, a long tip soldering iron (of the same diameter as the launcher) was inserted into the coil former, this allows the thermal setting araldite to bake at its particular temperature and a strong solid coil to be obtained. This coil is tuned with a parallel capacitor to provide maximum energy transfer from the transmitter to the transducer and back.

The magnetic bias, as before, is obtained by a D.C.

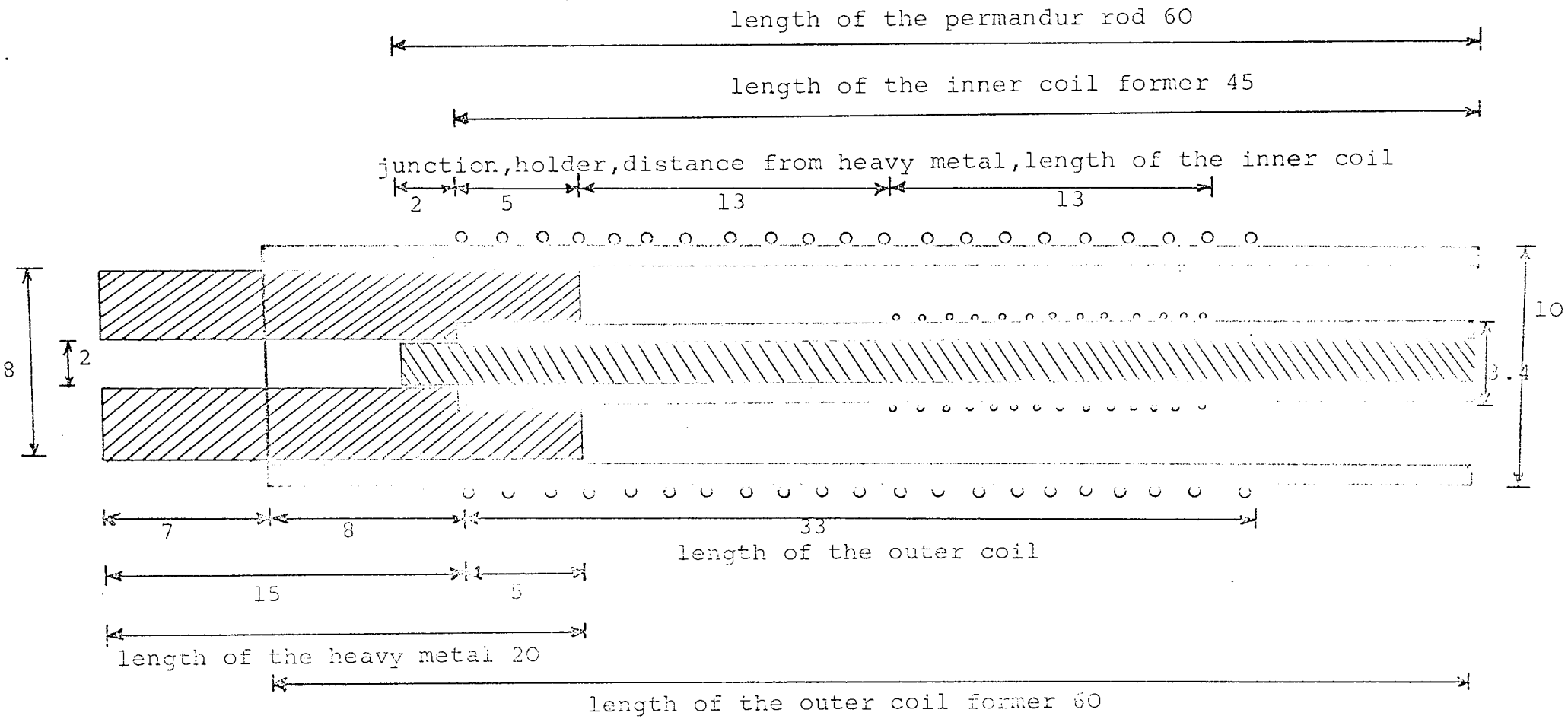

Fig. 9.3 Dimensions of the transducer design.

source. This is a wirewound coil consisting of eight layers, each containing 90 turns of 0.22 mm copper wire, giving 16.2Ω resistance at room temperature. The coil is made in the same style as the launching one and is baked to cure the thermal setting araldite. The inner diameter is 8 mm which gives a good support for the heavy metal inside and all the launching unit can be moved easily inside the D.C. coil for further tuning.

The outer diameter of the coil former is 10 mm and the total diameter of the complete D.C. coil is less than 13 mm and can be accommodated inside a 15 mm protective tube of the reactor.

The D.C. source is adjusted for maximum efficiency and finally the position of the launcher inside the heavy metal is adjusted to obtain maximum bandwidth. The length of the magnetostrictive rod (60 mm) is chosen, a) to give maximum reflection of the echo from the resonator and b) just being long enough for silver brazing to the transmission line.

A D.C. current source of 500 m.a. for magnetic biasing, gave 1.1V echo amplitude for the best condition of adjustment. This is more than adequate for signal processing. This again depends on the thermal history of the particular piece of permendur rod which is used.

9.2.2 Experimental Tests on Launcher

An experiment was performed to measure the increased

temperature of the D.C. coil due to the consumption of power, this showed an increase of 40°C after several hours operating of the ultrasonic thermometer.

In the next experiment the transducer unit was placed in a hot region of about 180°C, as this is the normal operating temperature for the "Petten" reactor structure, where the transducer will be located.

The launcher was 1.5 mm permendur line of 84 cm in length, the D.C. coil made of 6 layers of 0.15 mm copper wire, each layer of 90 turns (R_1 = 27Ω at room temperature), and the A.C. coil of 6 layers, each having 60 turns of the same wire (R_2 = 9.0Ω at r. temp.).

The amplitude of the first echo in the best conditions of tuning (period = 10μsec), together with a bias of 11V D.C. and 270 m.A. was e_1 = 0.7V.

The results are shown in Table 9.1

Table 9.1

Temperature	D.C. Current	Echo Amplitude
60°C	270 mA	0.70V
70	260	0.65
90	250	0.64
110	240	0.62
130	230	0.60
150	220	0.57
170	210	0.54
190	200	0.52
230	180	0.44

The results show that the drop in echo amplitude (≈0.3V) and increased coil temperature have no drastic effect

on operating of the system and this is quite satisfactory.

In a similar experiment the diameter of the D.C. coil wire is increased to 0.22 mm. This allowed with a small D.C. supply of 5V and 310 mA current an echo of 0.92V produced, which after replacing in the hot plate of 180^{o}C amplitude reduced to 0.8V, which is more than adequate.

9.2.3 The Heavy Metal

For final modifications an isolating rod of 2 cm in length and 8 mm in diameter is used for supporting the launcher, as shown in Fig. 9.3. The rod is a piece of heavy metal which is a generic term for a range of tungsten-rich alloys containing copper and nickel. The densities of these alloys are slightly lower than that of tungsten (from 16.2 to 18.0 gr/cc), but the alloys can be fabricated into shapes which are not possible with pure tungsten.

The alloys are easily machined and readily brazed to other metals, and have an electrical conductivity of 0.7×10^{5} ohm-cm and coefficient of linear expansion is about 6×10^{-6} inch/^{o}C. These alloys are used as radiation shields and components and vessels for the handling and transit of radio-active sources, both in medical and industry. Fig. 9.4 shows the photograph of the transducer designed in the assembly and separated forms.

Fig.9.4 This photograph shows the transducer design in the assembly and separated forms.

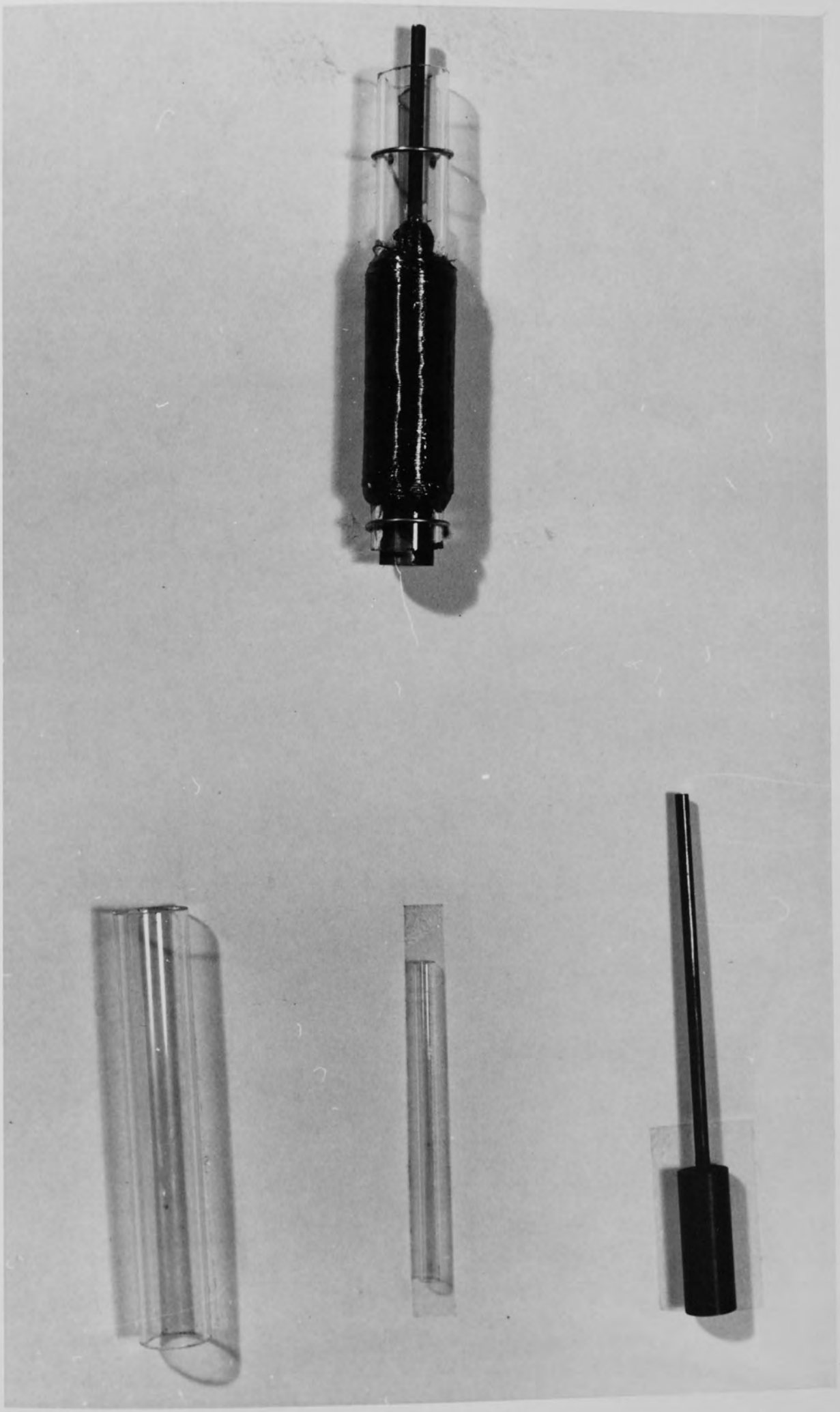

9.3 CONCLUSION

A compact magnetostrictive transducer unit has been designed for the nuclear environment applications. It is enable of operation at a hot region of about ~180^{o}C and D.C. bias is employed to produce the required magnetic field. Its main advantage over the conventional forms is that it can support the line and the temperature sensor by a short piece of heavy isolating metal.

CHAPTER 10

CALIBRATION OF THE PROBES

10.1 INTRODUCTION

An important aspect of any probe is its stability of calibration. Ideally it should indicate the same value, if the parameter being measured remains the same, whatever other parameters change. Typically a temperature sensor or probe is independent of the variation in pressure or medium density.

Deficiencies in calibration which occur in all sensors to some extent are:

(1) Ageing or calibration drift. This is a well known phenomenon particularly in the case of high temperature thermocouples employed as temperature sensors in nuclear reactor experimental equipment. The effect is notably important in thermocouples based on the tungsten and tungsten-rhenium alloys. Both the transmutation of tungsten to rhenium and rhenium to osmium have large effect on thermocouple output, although the respective effects are of opposite sign[14]. The net result is that the overall effect of transmutation on thermocouple output is uncertain and percentage error may be different for low or high temperature operation. Unirradiated thermocouples are replaced periodically in the experimental channels to re-calibrate the installed couples and thus to be able to follow the drift in output.

(2) Hysteresis. In its most obvious manifestation it gives a different reading depending on whether the value is approached from the high or low sides.

In a large number of instruments the calibration is linear, at least over a limited range, and the stability can be separated into:

a) shift of zero

b) change of slope.

Shift of zero is very common and in the setting up of many instruments the "set zero" is preliminary to their use. When the normal operating point is known it is not uncommon to set, that is, calibrate, at this point and rely on a reasonable stability of "slope"for reading near this point.

Some sensor metals, which are essentially polycrystalline, in the form of wires or rods are usually in a state of mechanical strain arising from the fabrication or drawing and the thermal treatment. Strain is relieved by holding the metal at a temperature above crystallization and cooling it sufficiently slowly to avoid strain by differential contraction. Shift of calibration will occur due to this, the extent depending on various factors such as the elastic anisotropy of the metal.

Of the various probe materials described in the Chapter 8, iridium, single crystal sapphire polycrystalline silicon carbide and tungsten were extensively studied for calibration stability and hysteresis and were calibrated against a thermocouple.

Before describing the probe calibrations, the different method for specimen heating which are available in the laboratory are discussed.

10.2 SPECIMEN HEATING

A comprehensive review of high temperature technology is given by Campbell[67]. Various systems were specially designed and constructed for specimen heating between -190°C and 2000°C by my colleagues, Pelmore[51] and Sadollah[52], as there was no suitable commercial apparatus in the laboratory. The general requirement was that the specimen temperature could be controlled to within a few degrees °C. For temperatures above 200°C the specimens generally had to be heated in an oxygen free atmosphere and below room temperature in a dry atmosphere to prevent condensation. Generally a vertical arrangement was used making support of the transmission line much easier.

Chromel/alumel thermocouples were used for the -190°C to 1200°C range and platinum - 13% rhodium thermocouples were used upto 1600°C. Above this temperature either tungsten - 3% rhenium/tungsten - 26% rhenium thermocouples or an optical pyrometer were used.

Argon is used when an inert atmosphere is required and vacuum system is used when a clean system free of contamination and a uniform temperature distribution are needed, as there are vital features for protection

of refractories at high temperatures.

10.2.1 1000°C Furnace

A Wild Barfield nichrome wound furnace was used up to 1000°C. The tube assembly which is made of a transparent silica has a length of 50 cm and internal diameter of 40 mm. The furnace is suspended from stranded cables using pulleys and counterweights, where it can be easily moved up over the work tube. This is a very convenient arrangement because the experiment can be set up and visually inspected through the walls of the work tube before the furnace is moved into position. Its advantage is it allows a rapid heating of the specimen by use of a preheated furnace and rapid cooling. The temperature profile of the furnace is known and a temperature difference of 3°C over a length of 5 cm steel specimen was found.

This furnace was always used with inert gas, usually high purity argon, sometimes nitrogen and a commercial proportional controller was used to control the temperature.

10.2.2 1800°C Furnace

A Metals Research PCA 10 furnace was kindly lent by UKAEA, Harwell - shown in Figures 10.1 and 10.2. This consists of a pure alumina 25 mm internal diameter by 45 cm long furnace tube wound with molybdenum. A 25% hydrogen-nitrogen mixture was used to protect the winding. This mixture was used, rather than pure hydrogen for

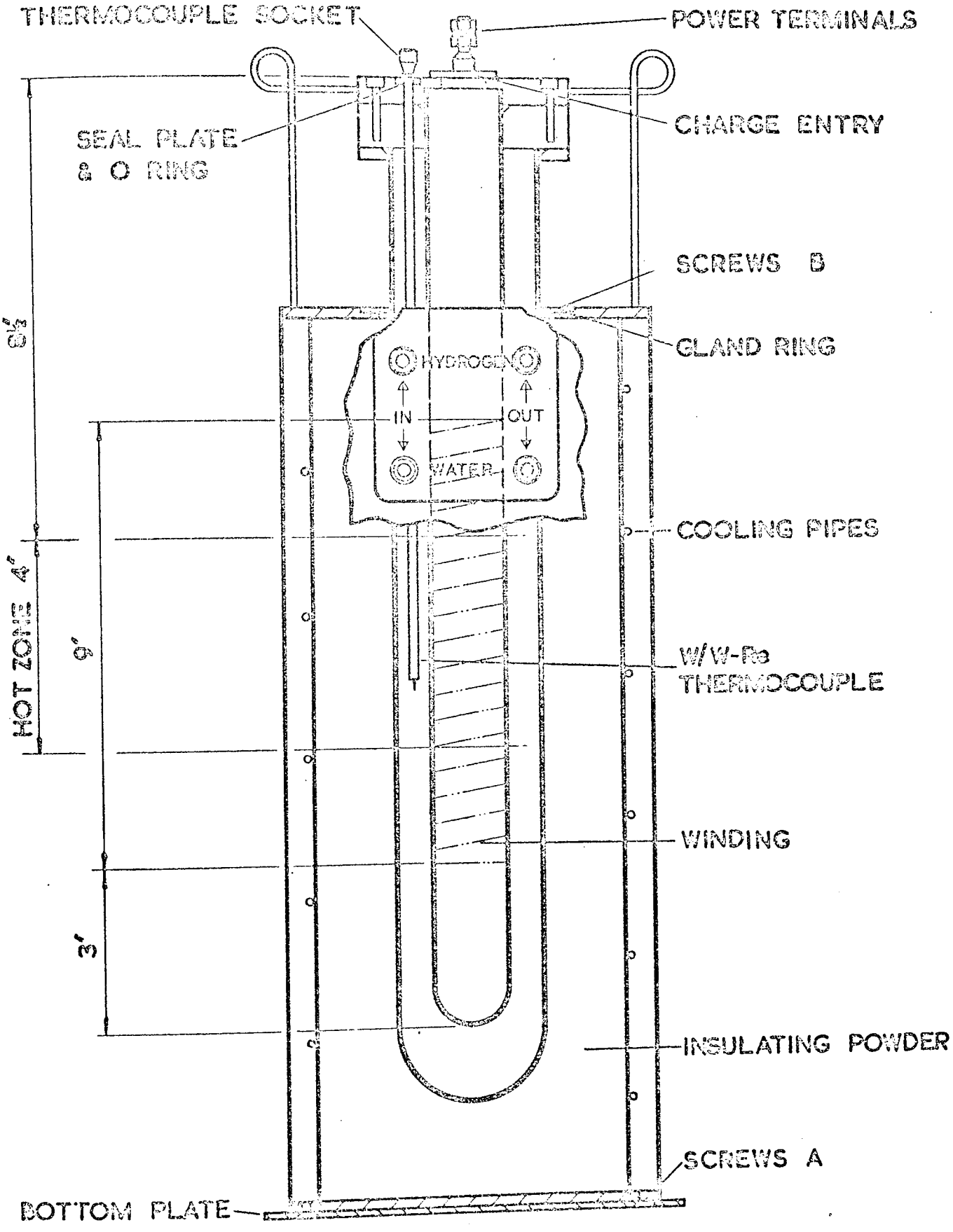

FURNACE TYPE PCA 10

Fig. 10.1 Specification of 1800°C vacuum furnace.

Fig. 10.2 This photograph shows the 1800°C vacuum furnace type PCA 10 and the temperature controller.

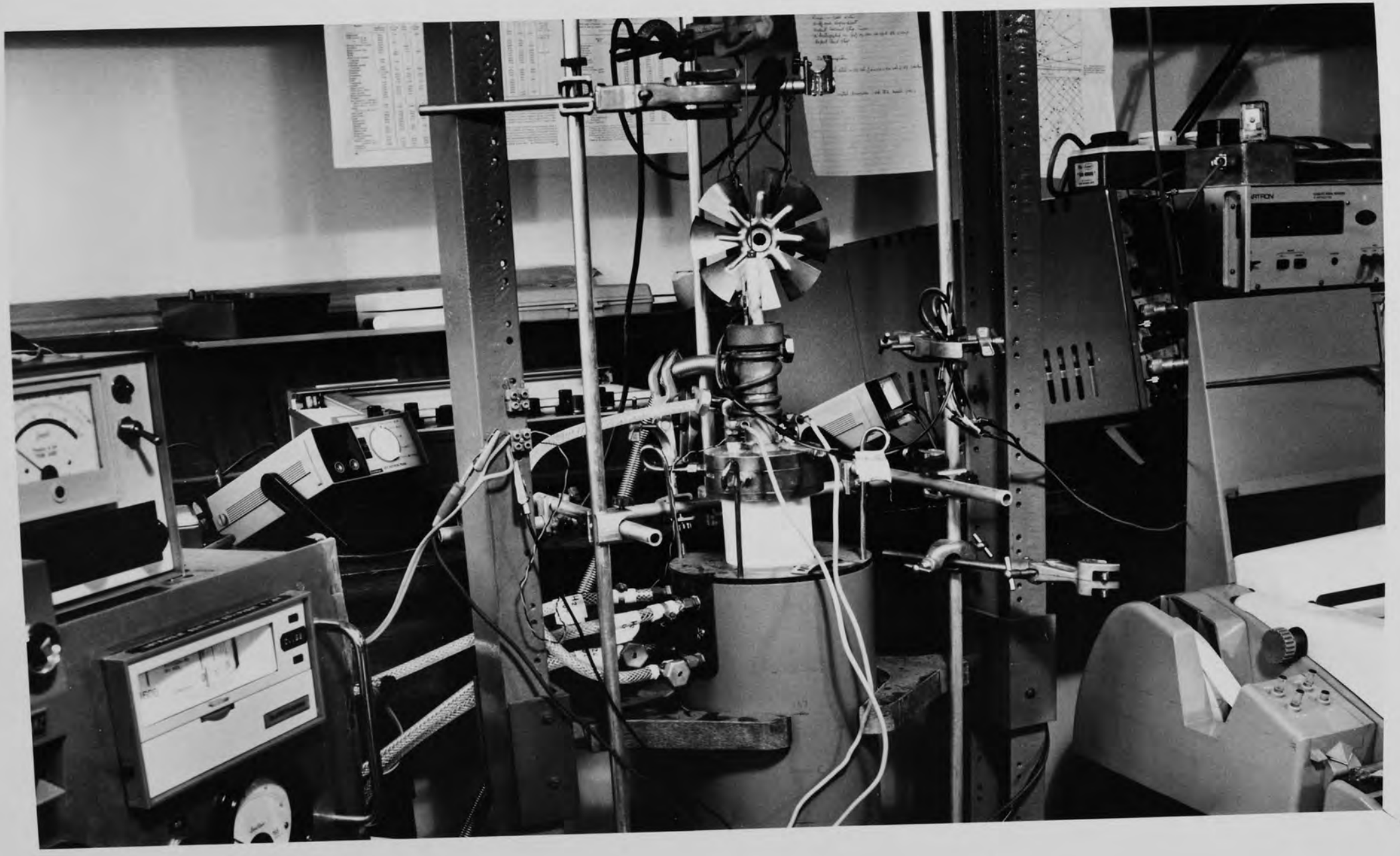

safety reasons. The outside of the furnace is water cooled.

A special brass head was designed to allow convenient operation. Because of the small bore, no work tube was used so care has to be taken to avoid damage to the furnace tube. The top of the alumina specimen tube gets hot due to thermal conduction and has to be cooled. A beaker of water, a wick and a fan were used to cool it. A standard Eurotherm three term controller type 072 was used to give very good control of temperature. As the controller used was for use with platinum thermocouples an external 15 mV source was put in series with the tungsten/tungsten rhenium thermocouple so that temperatures upto 1800°C could be controlled.

A two stage rotary pump was used to evacuate the furnace tube and the pressure was measured with a Pirani gauge. A pressure of about 10^{-2} torr was generally achieved when hot. It would have been desirable to use a diffusion pump to give pressures in the 10^{-4} range but this was not readily available. Because the furnace tube is slightly porous the residual gas will be mainly nitrogen and hydrogen giving a slightly reducing atmosphere. Normally a 200 cm long rod specimen was used with a tuning fork cut into one end. This was then joined to a 2 mm diameter, 6 cm long permendur launcher.

10.2.3 Flame 800-2000°C

Temperatures in excess of 1900°C generally require

the use of a vacuum furnace because this is the highest usable temperature of alumina refractories. As no such furnace was available an oxygen-coal gas flamemaster torch was used to heat nonoxidisable specimens upto 2050°C. Fig. 10.3 shows a photograph of an iridium specimen heated in this way. Temperature control is not very good but the hot zone is very small and experimental work is very rapid, because of the fast heating and cooling rates. Temperatures were measured using a Pyrowerk optical pyrometer (disappearing filament type). The temperature reading has to be corrected for the emissivity of the specimen and herein lies a source of error. The sapphire specimens were heated inside an alumina tube to prevent the formation of hot spots with consequent melting. The outside temperature of the tube was taken as the specimen temperature because it was assumed that the radial heat flux would be small giving a small temperature gradient.

10.3 CALIBRATION OF IRIDIUM PROBE

Iridium has the highest melting point (2440°C) of any metal that is stable in oxidation and reducing atmospheres, having desirable performances such as good thermal hysteresis and low thermal shock. For this work a 4.75 x 0.5 mm x 250 mm strip 99.95% pure supplied by Johnson Matthey was used. A Seth tuning fork was cut in one end and a 3.1 mm steel transmission line was matched and silver soldered, to the other end. The sample was heated in a torch flame as shown in Fig. 10.3

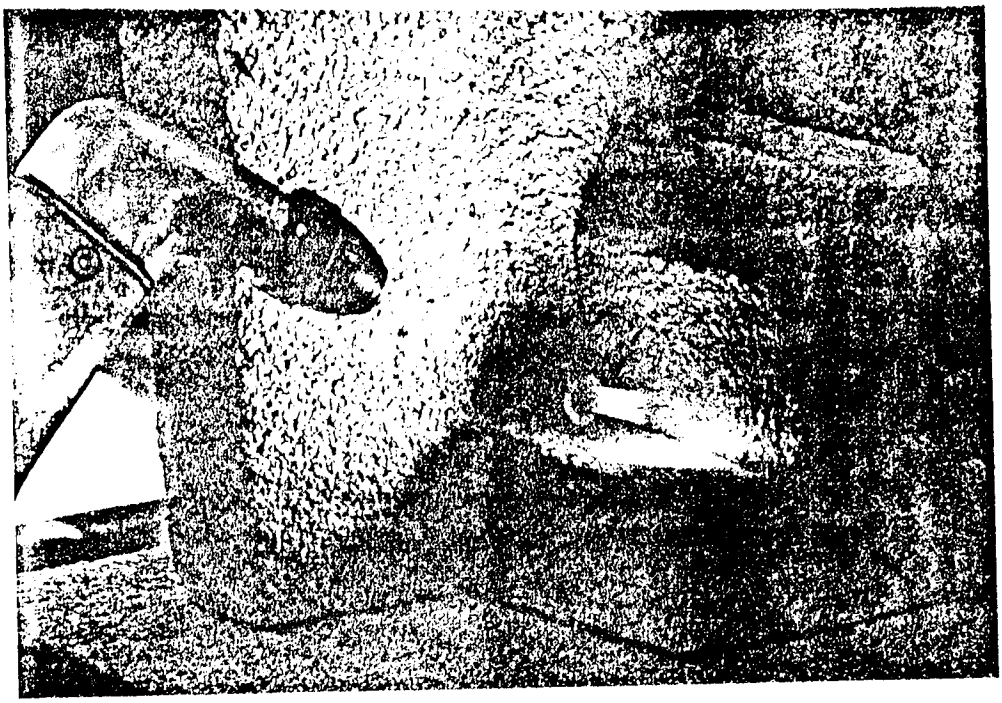

FIGURE 10.3 - An oxygen-coal gas flame was used to heat some of the specimens up to 2000°C. This was useful in attaining higher temperatures than the furnace and also for heating short specimens. The temperature was measured with an optical pyrometer. The specimen is an iridium strip with a tuning fork cut into it.

so that temperatures of 2000°C+ could be reached. Temperatures were measured with an optical pyrometer taking $\varepsilon = 0.30$. Above 1800°C slight oxidation occurs as shown by a drop in frequency on prolonged heating but this is not troublesome. Internal friction has a peak at about 1800°C, as reported by Pelmore[51], but this drops down at 2050°C which was the highest temperature that could be reached in the flame. Internal friction reduces the echo decrement drastically and makes decrement sampling, and hence automatic control, difficult.

Photographs in Fig. 10.4(a) to (c) show the echo pattern from room temperatrue to the highest temperature which the decrement signal could be tracked by the automatic control. In all the photographs the error signal is also shown on the lower trace.

The observation for one heating and cooling cycle are given in Table 10.1. Calibration curve is plotted from 950°C upto 1815°C as shown in Fig. 10.5. The slope of the curve increases with increasing temperature. The sensitivity of the probe is calculated from the slope at 1000°C, which is 177 ppm/°C. The upper limit of the measurement is set by material losses.

Table 10.1

Temperature	Heating Cycle Frequency	Number of steps
20°C	86.8 kHz	1
995	78	2
1105	75.5	3
1270	73.5	4

Temperature	Frequency	Number of steps
1410°C	71.5 kHz	5
1570	68.5	6
1680	66.5	7
1765	65.5	8
1815	63	9

Cooling Cycle

Temperature	Frequency
1740°C	64.5 kHz
1650	66.8
1590	68
1530	69
1430	70.6
1320	72.4
1240	73.6
1080	75.8
940	77.5

The temperature differential between the optical pyrometer and probe temperature in the heating and cooling cycles, is due to the large thermal time constant of the massive probe compared to the thin wire thermocouple. Therefore the hysteresis effect can be attributed to the dimensions of the probe rather than the physical properties of iridium.

Photographs in Fig. 10.4 show that by increasing temperature the cross-over moves to the right, the amplitude of the echo and the decrement falls. At temperatures above 1815°C the cross-over disappears and automatic control is lost.

In performing the above experiment, the analogue output

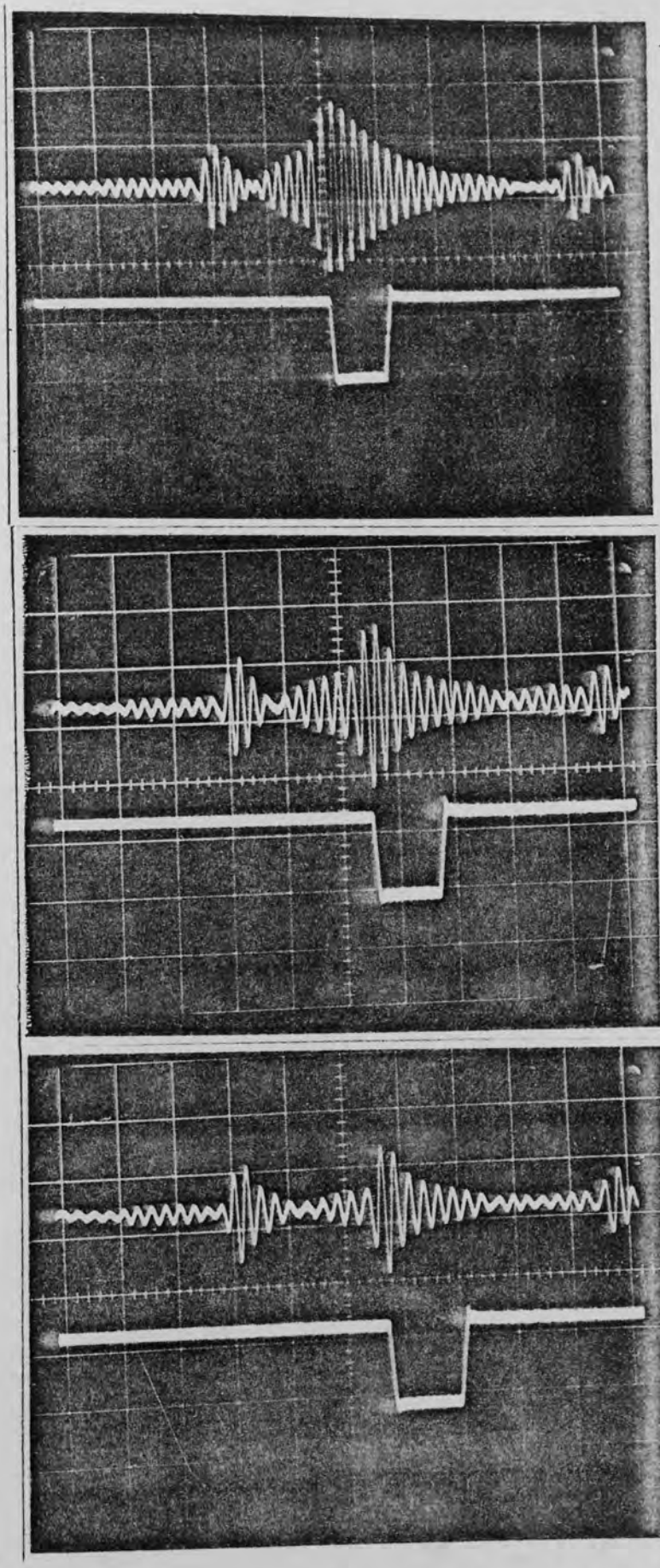

a) at room temperature 20°C
fr = 86.8 kHz
Pm = 4

b) at 1200°C
fr = 74.6 kHz
Pm = 4

c) at 1815°C
fr = 63 kHz
Pm = 4

In all photographs sensitivity for upper trace=0.1Vcm^{-1} & for lower trace = 1 Vcm^{-1}

Fig.10.4 Iridium ultrasonic temperature probe(Line length= 1.0 m). Mode of control:automatic integral with 5 oscillations in sampling. Heat treatment:blow torch flame and temperature measurement by optical pyrometer.

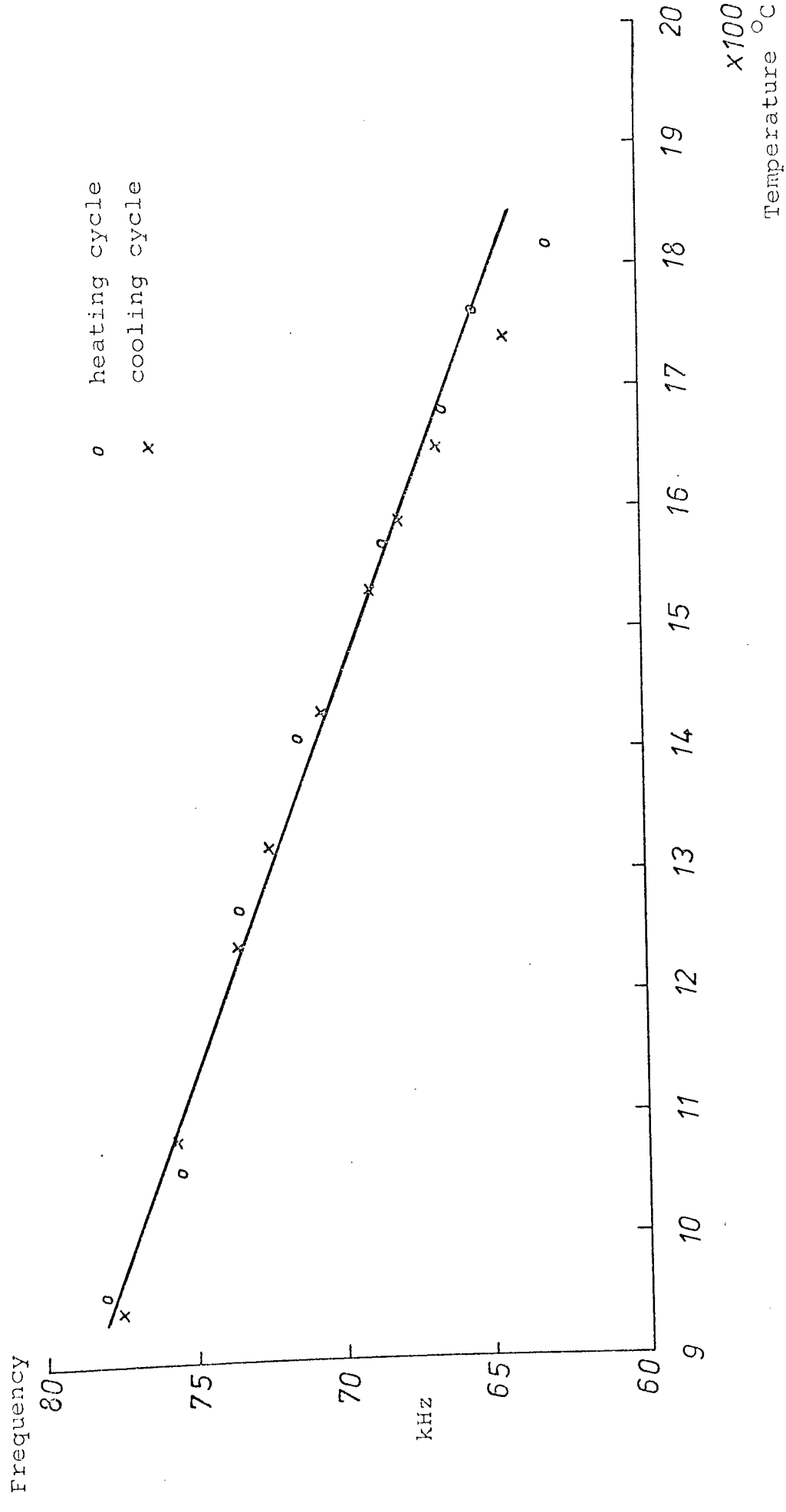

Fig. 10.5 Calibration of Iridium probe in coal-gas oxygen flame.

of the automatic system was fed to the Y input of an XY plotter. The observations were made a) to demonstrate the data noise of the system concerning with the fluctuations of the probe temperature in the torch flame, and b) to determine the response of the iridium probe to a fast thermal shock.

The results for both experiments are shown in Figs. 10.6, 10.7 and 10.8. Fig. 10.6 gives the various step positions of the probe and Fig. 10.7 shows two cycles of heating in a gas flame to the limit of the probe. Smooth curves are obtained demonstrating the stability of the instrument and the smoothness in following a very rapid temperature change. Fig. 10.8 shows a heating cycle with rapid heating and slow cooling.

After many experimental tests in the coal gas oxygen flame giving satisfacoty results, it was decided to obtain the calibration curve and sensitivity of iridium probe in the 20-1000^{o}C temperature range and compare the results to a thermocouple. To do this another tuning fork similar to the first with a slightly different frequency was used in silica tube furnace. Probe temperature(X axis) was measured with a chromel/alumel thermocouple and the analogue display of the period (using D/A converter) was fed to Y input of an XY Plotter.

From the first experiment the required calibration curve of the iridium probe in 20-1000^{o}C range is obtained automatically from the plotter as shown in Fig. 10.9.

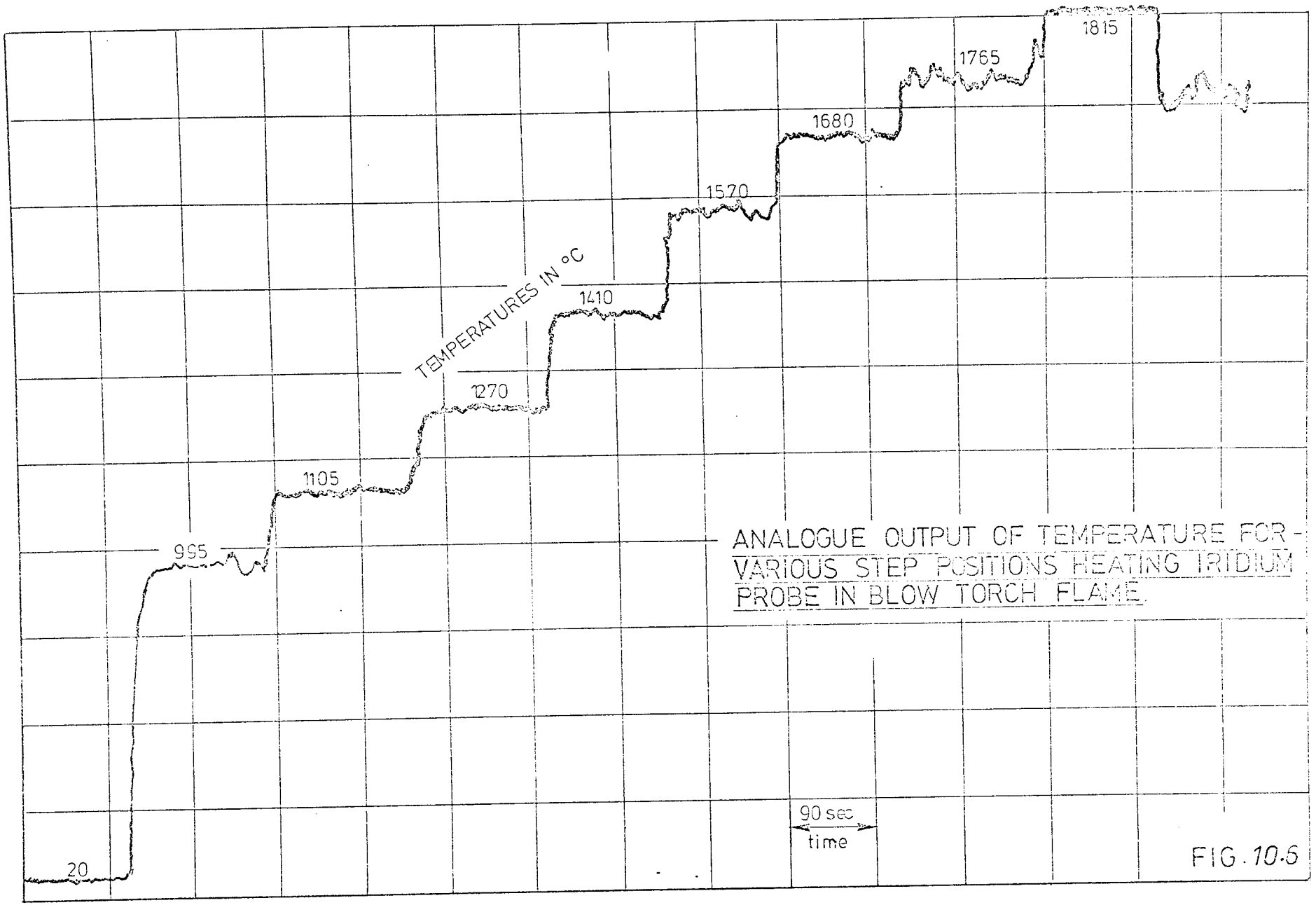

ANALOGUE OUTPUT OF TEMPERATURE FOR - VARIOUS STEP POSITIONS HEATING IRIDIUM PROBE IN BLOW TORCH FLAME.

FIG. 10.6

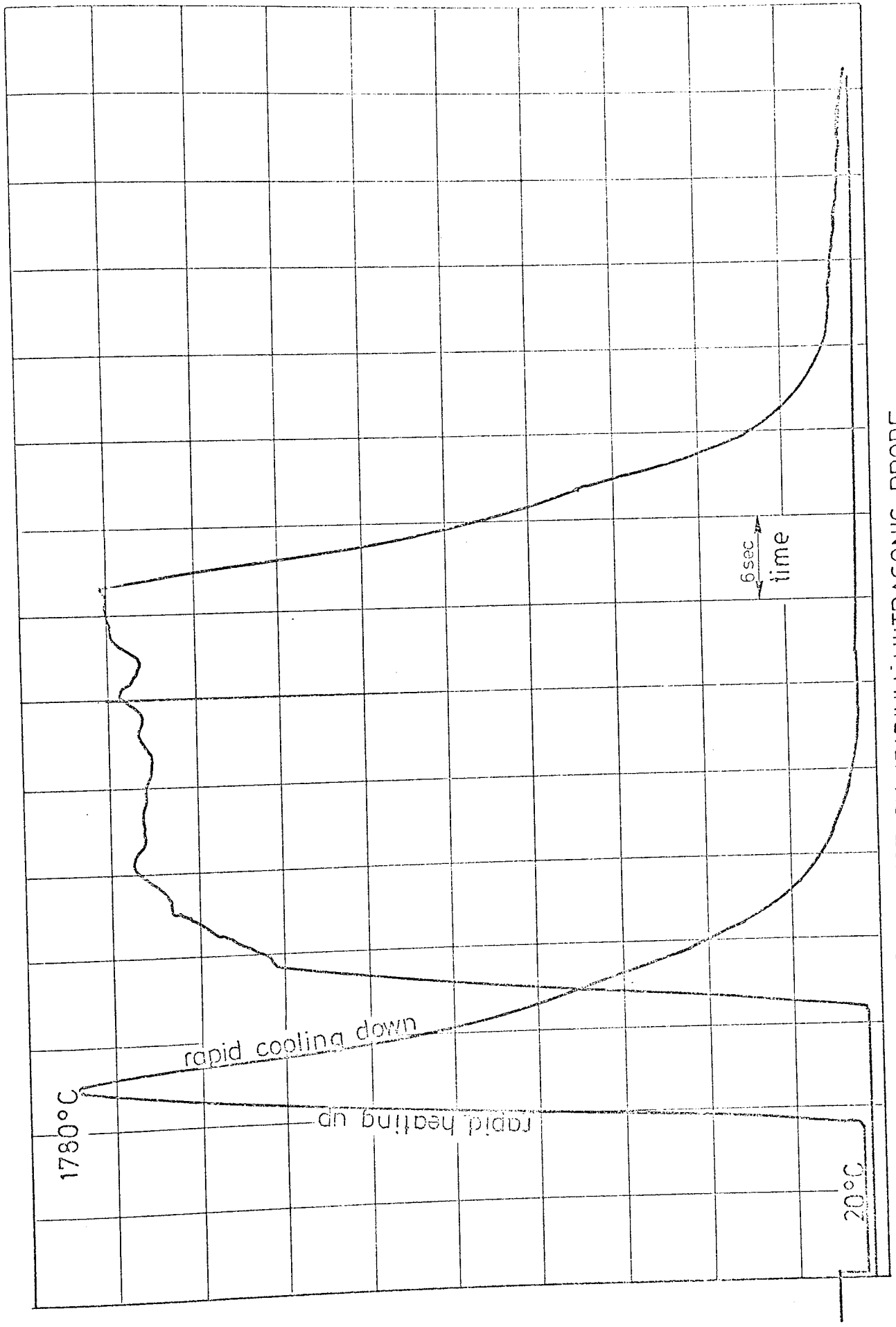

FIG. 10.7 TEST ON IRIDIUM ULTRASONIC PROBE

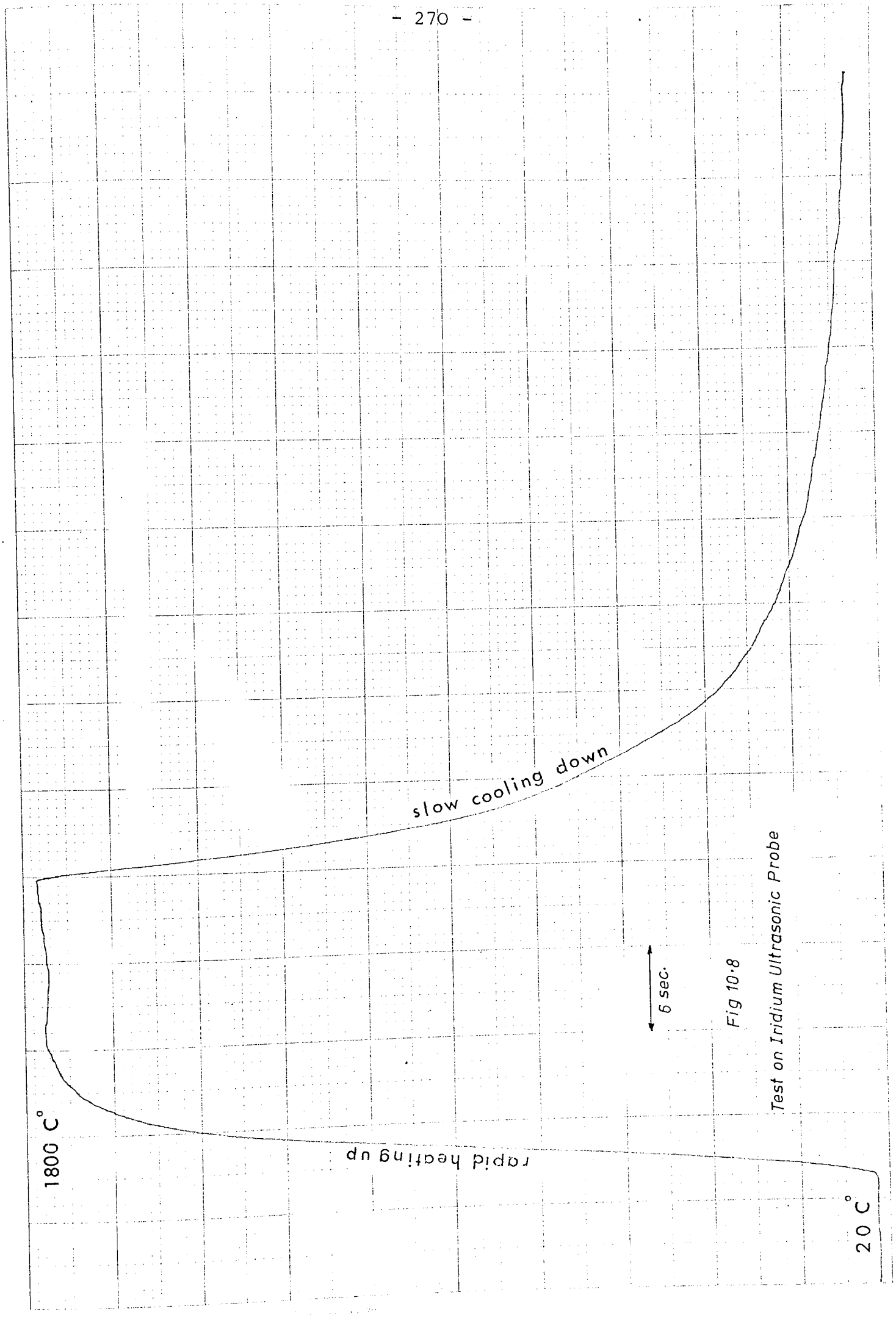

Fig 10·8 Test on Iridium Ultrasonic Probe

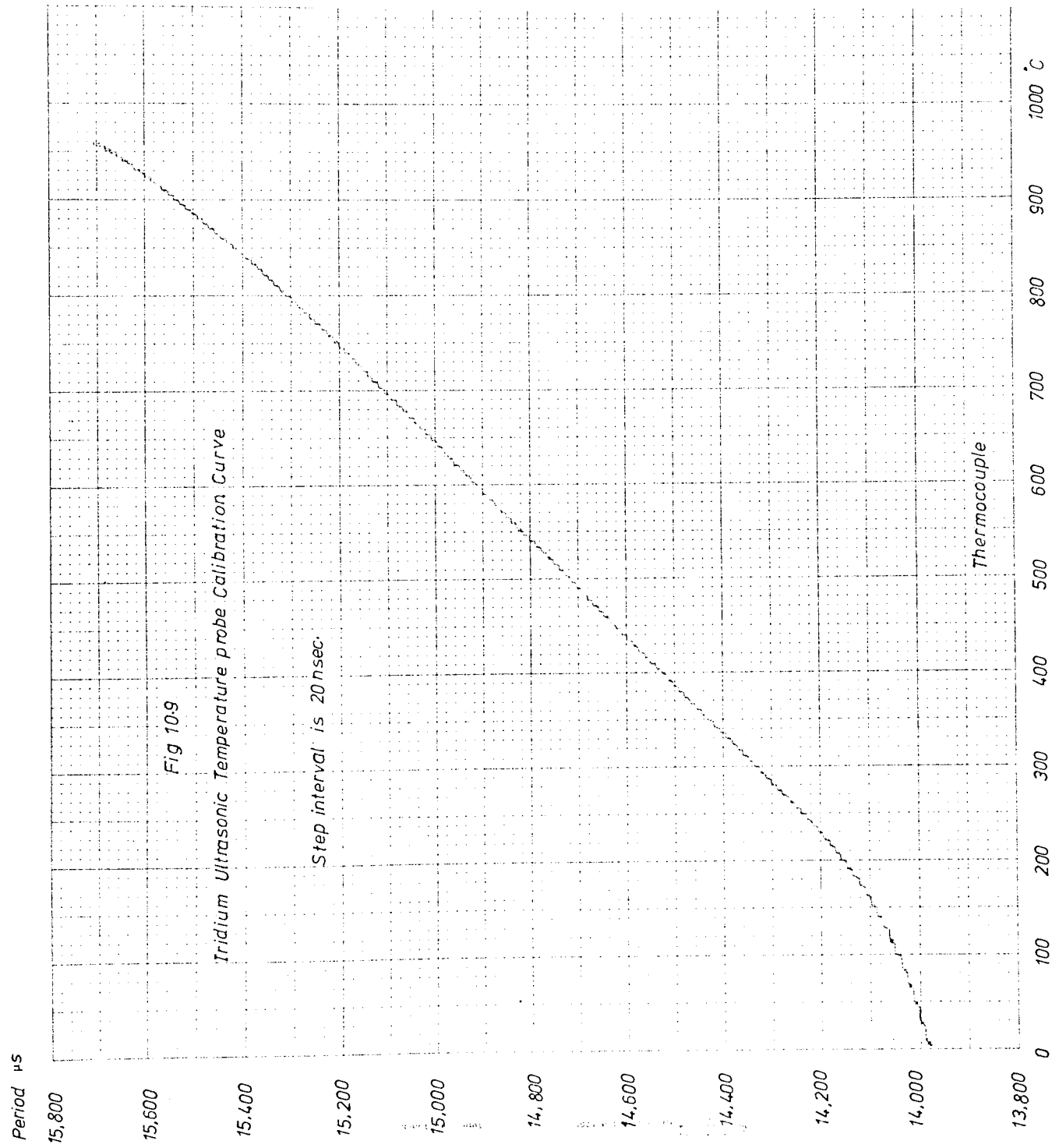
Period µS
15,800
15,600
15,400
15,200
15,000
14,800
14,600
14,400
14,200
14,000
13,800
0
100
200
300
400
500
600
700
800
900
1000 °C
Thermocouple
Fig 10.9
Iridium Ultrasonic Temperature probe Calibration Curve
Step interval is 20 nsec.

The smooth result shows stability of the electronics and agreement between the iridium probe and thermocouple, from this curve the sensitivity at 500°C is 136ppm/°C.

10.4 CALIBRATION OF SAPPHIRE PROBE

Wachtman and Lam[46] measured Young's modulus of sapphire and other oxide ceramics as a function of temperature, as was shown in Fig. 8.10. It has almost a linear variation from 100°C to 1400°C, the highest temperature of measurement. Also the material losses are very small. Qm^{-1} is about 5×10^{-4} at the highest temperature. These properties make sapphire an attractive probe material.

An integral line probe, on a 3.1 mm diameter and 25 cm long sapphire rod, of resonance frequency of 170 kHz and Q-factor of 59 was used. The other end was joined to a 3.1 mm steel transmission line using the "silver paint" technique as described in Appendix 2.

The probe was heated in an oxygen-coal gas flame in air and protected from uneven heating by a short length of 99.7% pure alumina tube. Measuring the probe temperature by an optical pyrometer presented an emissivity correction problem as the inside of the protection tube was not a black body. Again, the outside temperature of the alumina tube was measured taking $\varepsilon = 0.3$. This should closely correspond to the temperature of the sapphire, the radial temperature gradient being small.

Observations were taken from 1000°C to 2040°C, where the protective tube starts melting. The frequency

temperature characteristic is shown in Fig. 10.10. The results are given in Table 10.2. The calibration curve is notable for its almost linearity and constancy. When the specimen was heated up and cooled, the frequency returned to within 10 Hz at 170 kHz of the previous value.

Photographs in Fig. 10.11 and 10.12 are shown the echo pattern at different temperatures. The photographs show that even at 2040^{o}C the losses in sapphire are very low. The temperature sensitivity of the probe at 1000^{o}C is 45 ppm/^{o}C and at 1500^{o}C is 30 ppm/^{o}C. The good cross-over at 2040^{o}C will be noted. The very low internal friction, chemical properties and the frequency curve reproducibility over many temperature cycles, showed that the sapphire is an ideal material for an ultrasonic thermometer probe. The only drawback is its low thermal shock resistance, which in the nuclear case is not effective parameter.

A series of experimental tests were performed to obtain the calibration curve and hysteresis of sapphire probes in the 20-1000^{o}C temperature range. For this purpose a silica tube furnace was used extensively and the temperature measured using chromel/alumel thermocouple.

The results of all experiments show that the frequency curve is reproduci ble over many cycles. The result of one experiment is shown in Fig. 10.13.

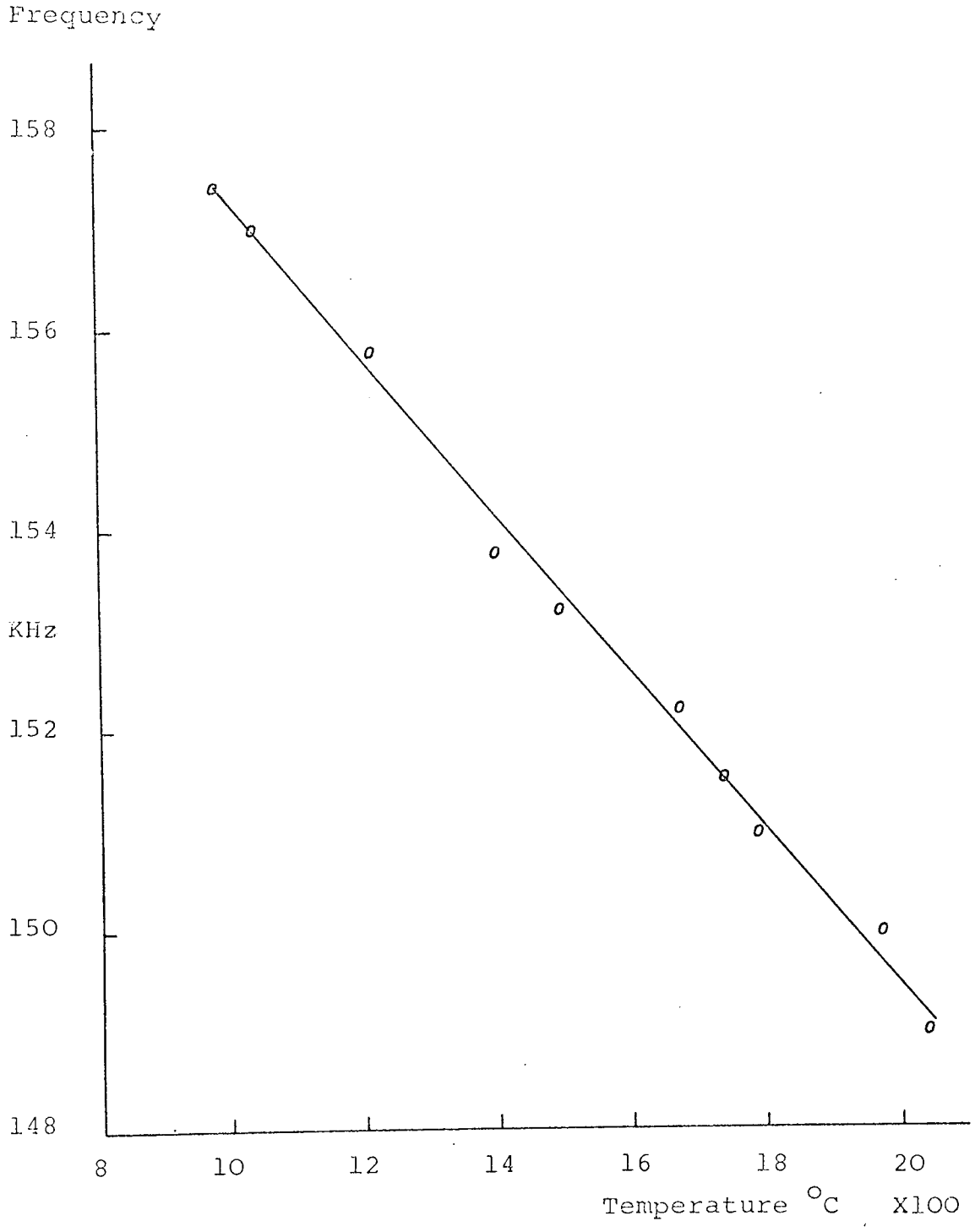

FIg. 10.10 Frequency-temperature characteristic of sapphire ultrasonic probe in coal-gas oxygen flame.

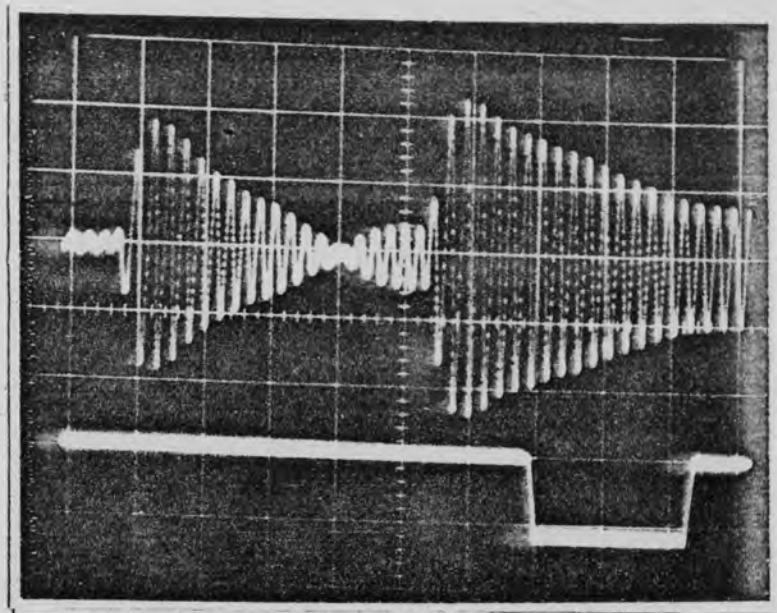

1) at 20°C
fr= 169.80 kHz
Pm = 13

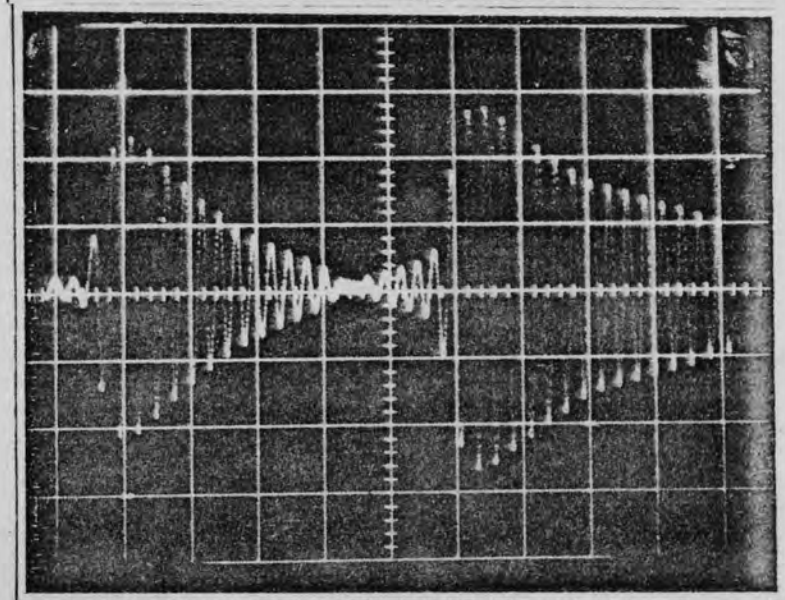

2) at 950°C
fr = 158.80 kHz
Pm = 13

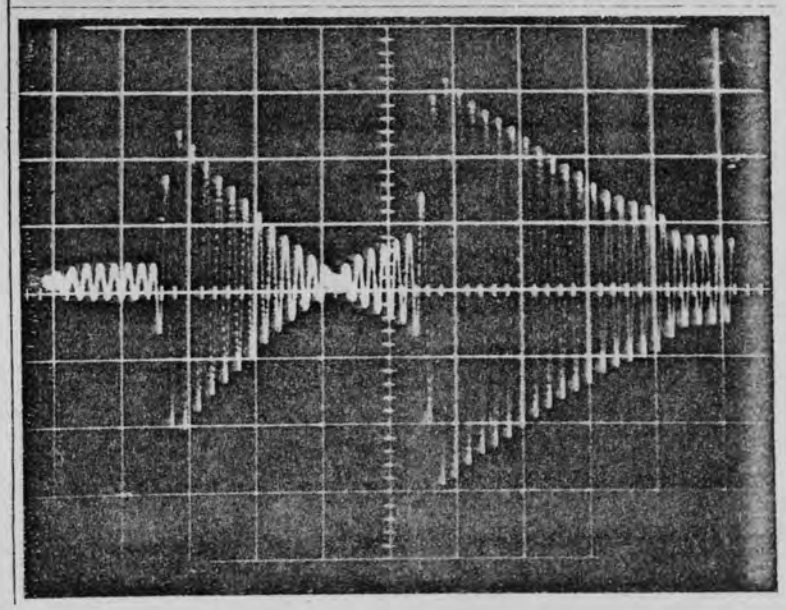

3) at 1850°C
fr = 150.6 kHz
Pm = 13

In all photographs
sensitivity = $0.05\ Vcm^{-1}$

Fig.10.11 Sapphire ultrasonic temperature probe(Line length= 0.8 m). Mode of control:automatic on integral control 10 oscillations in sampling & 5 oscillations in delay. Heat treatment:by blow torch flame & temperature measurement with optical pyrometer.

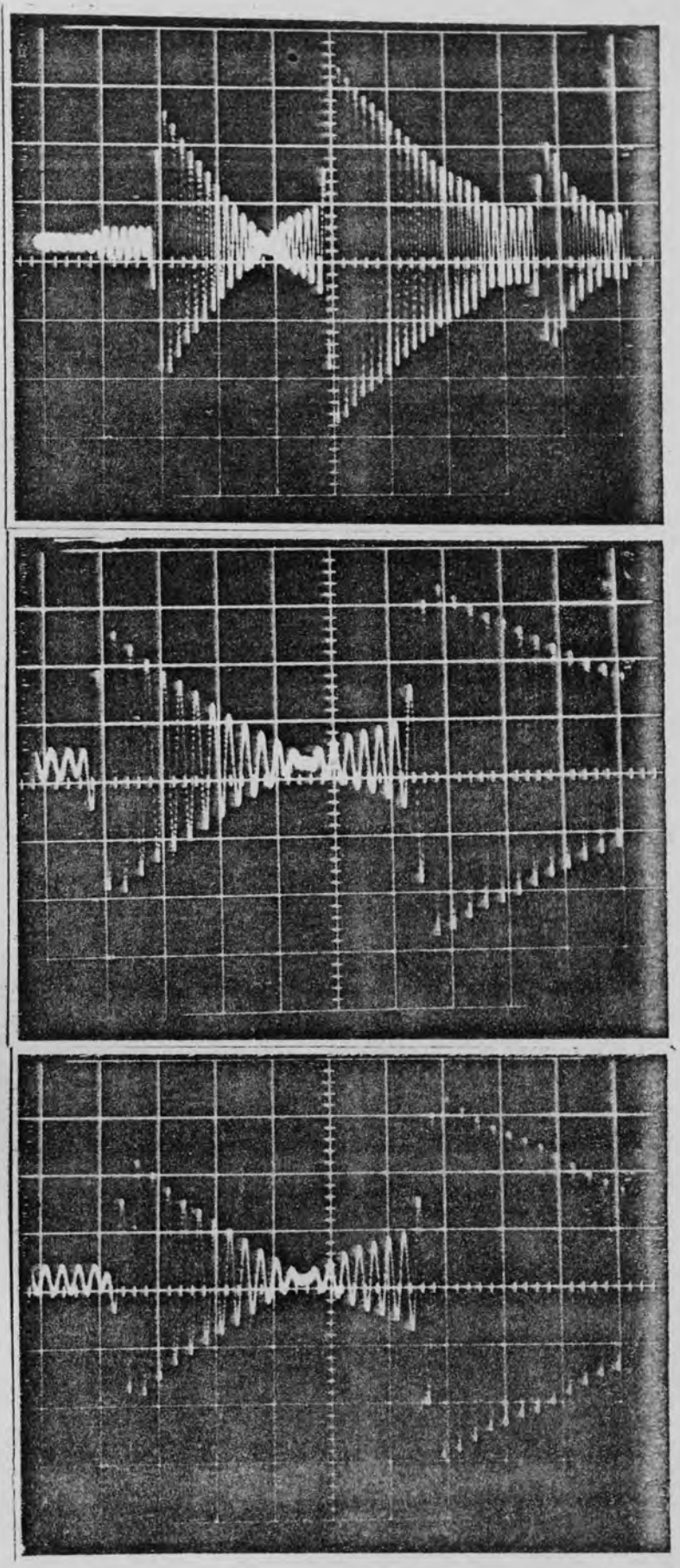

1) at 1850°C
fr=150.6kHz
Pm = 13

2) at 2010°C
fr= 149.3 kHz
Pm = 13

3) at 2040°C
fr= 148.8 kHz
Pm = 12

In all photographs
Sensitivity=0.05 Vcm^{-1}

Fig.10.12 Sapphire ultrasonic temperature probe(Line length= 0.8 m). Mode of control:automatic on integral control 10 oscillations in sampling & 5 in delay. Heat treatment:by blow torch flame & temperature measurement with optical pyrometer.

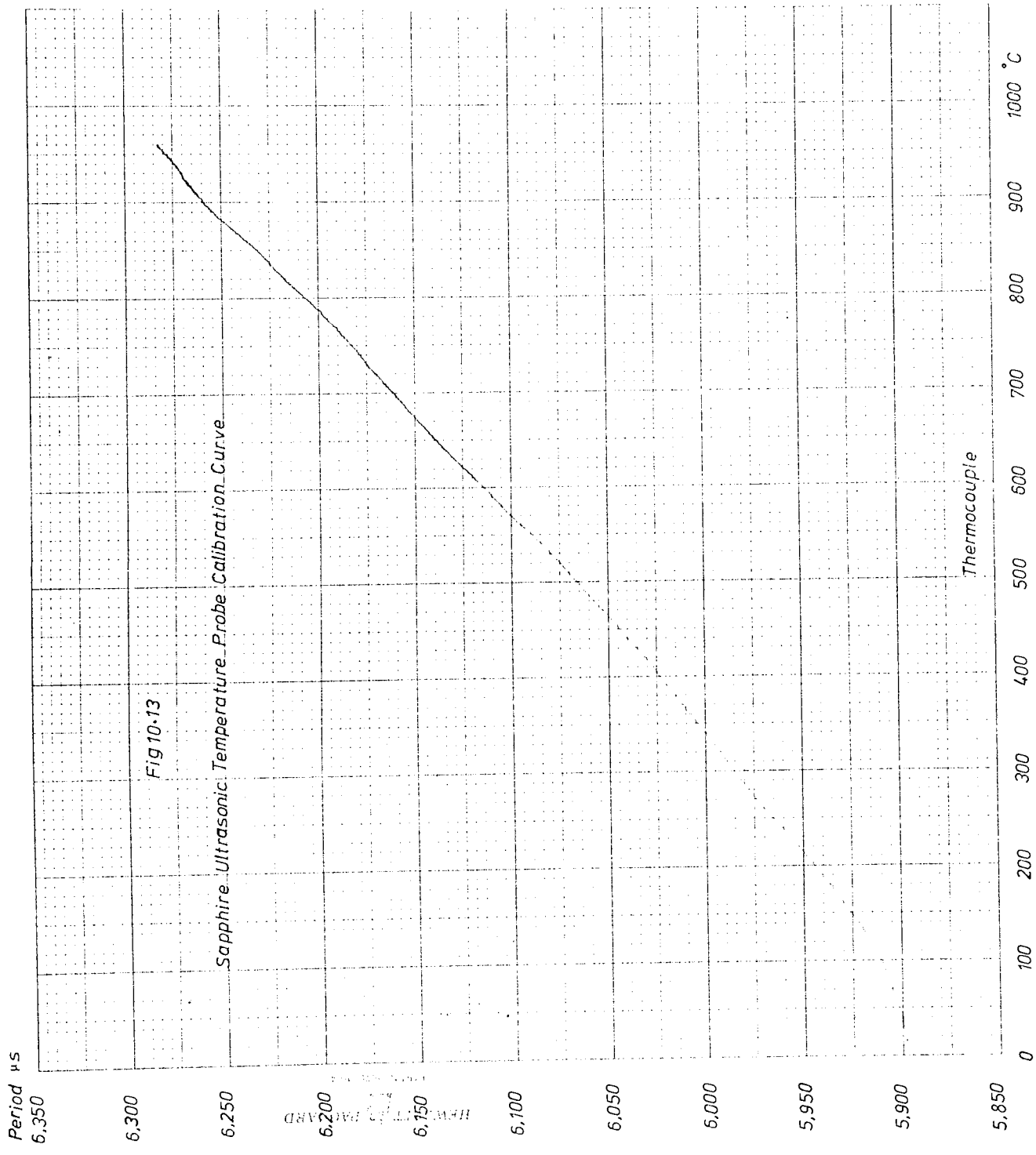

Fig 10.13

Sapphire Ultrasonic Temperature Probe Calibration Curve

Table 10.2

Temperature	Frequency
Room	169.8 kHz
980 °C	157.4
1035	157.0
1210	155.8
1400	153.8
1495	153.2
1670	152.4
1740	151.5
1790	150.9
1975	149.9
2040	148.8

In the figure, the X axis shows the thermocouple temperature and the Y displacement shows the analogue display of the period (using D/A converter). The linearity of the probe calibration against thermocouple is noteable. The probe sensitivity at 500°C is 90 ppm/°C and the fluctuation is data noise.

10.5 CALIBRATION OF SILICON CARBIDE PROBE

Polycrystalline silicon carbide (m.p. 2700°C) is one of the non-metallic inorganic materials which is attractive as a probe material. Its thermal coefficient of expansion is one third and its thermal conductivity is 3 times as that of the alumina. Silicon carbide at high temperature has shown slight superiority over other carbides and many grades of graphite. The highly resistive to the thermal shock, abrasion, corrosion and

oxidation are the particular properties of this material.

The only available 3.9 mm diameter x 10 cm silicon carbide rod had a tuning fork cut into one end with the resonance frequency 156 kHz and the Q factor 36. The other end was joined to a 3.1 mm steel transmission line using the silver paint technique. The specimen was heated in the oxygen-coal gas flame and its temperature measured by an optical pyrometer. The joint which was very close to the hot zone (9.5 cm) had to be cooled. A beaker of water and a wick were used to cool it.

Observations were taken from 900°C to 1400°C, where the internal friction reduces the decrement amplitude drastically. The results for one heating cycle is given in Table 10.3 and the calibration curve in Fig. 10.14.

Table 10.3

Temperature	Frequency
Room	155.8 kHz
904°C	155.30
950	155.0
1026	154.80
1082	154.60
1150	154.20
1232	153.80
1300	153.60
1380	153.0
1426	152.70

By increasing the temperature to above 1400°C, the frequency falls down rapidly and small decrement causes automatic control to be lost. When the specimen was cooled, the frequency returned to within a few Hz at

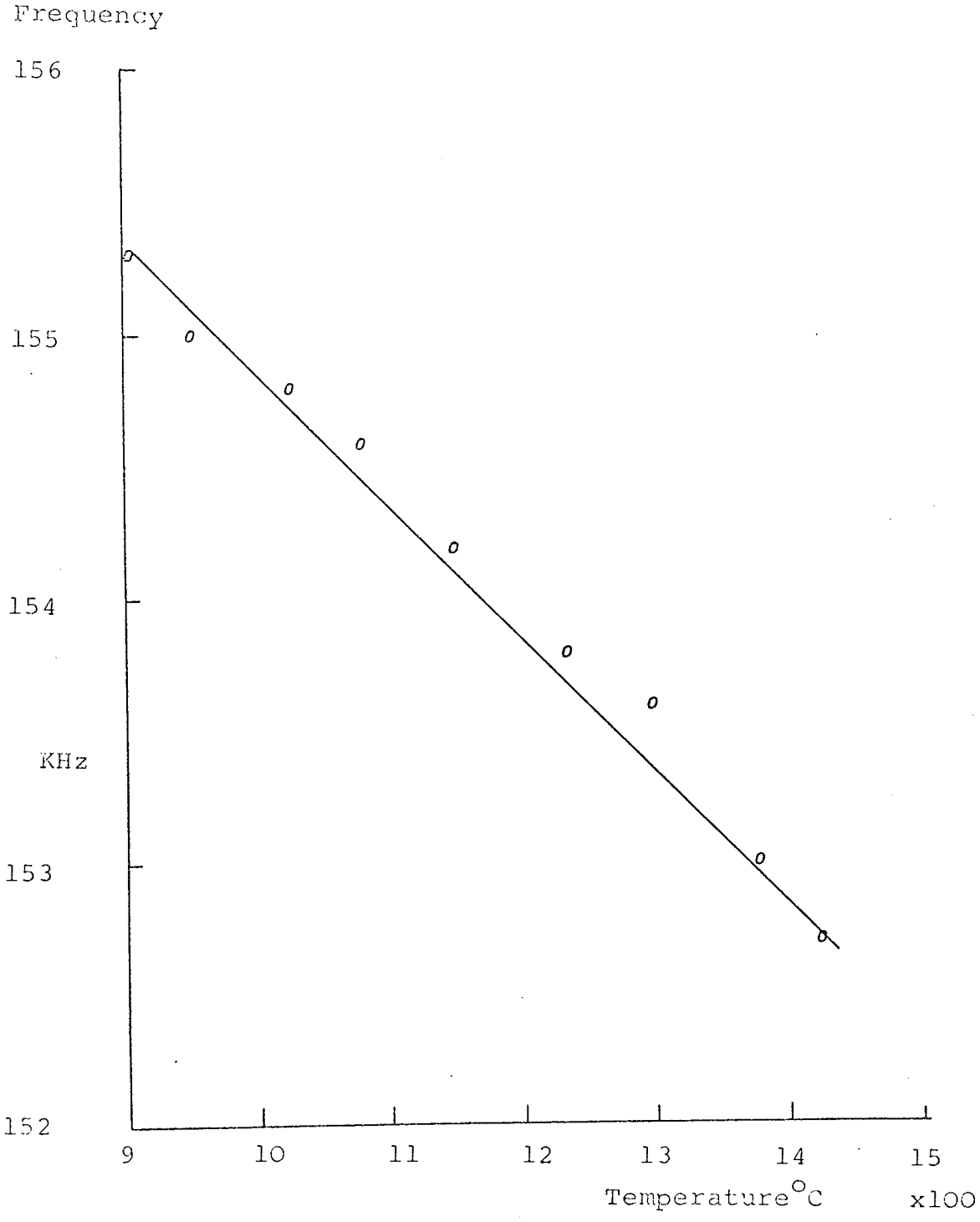

Fig. 10.14 The Frequency-Temperature characteristic of silicon carbide probe in coal-gas oxygen flame.

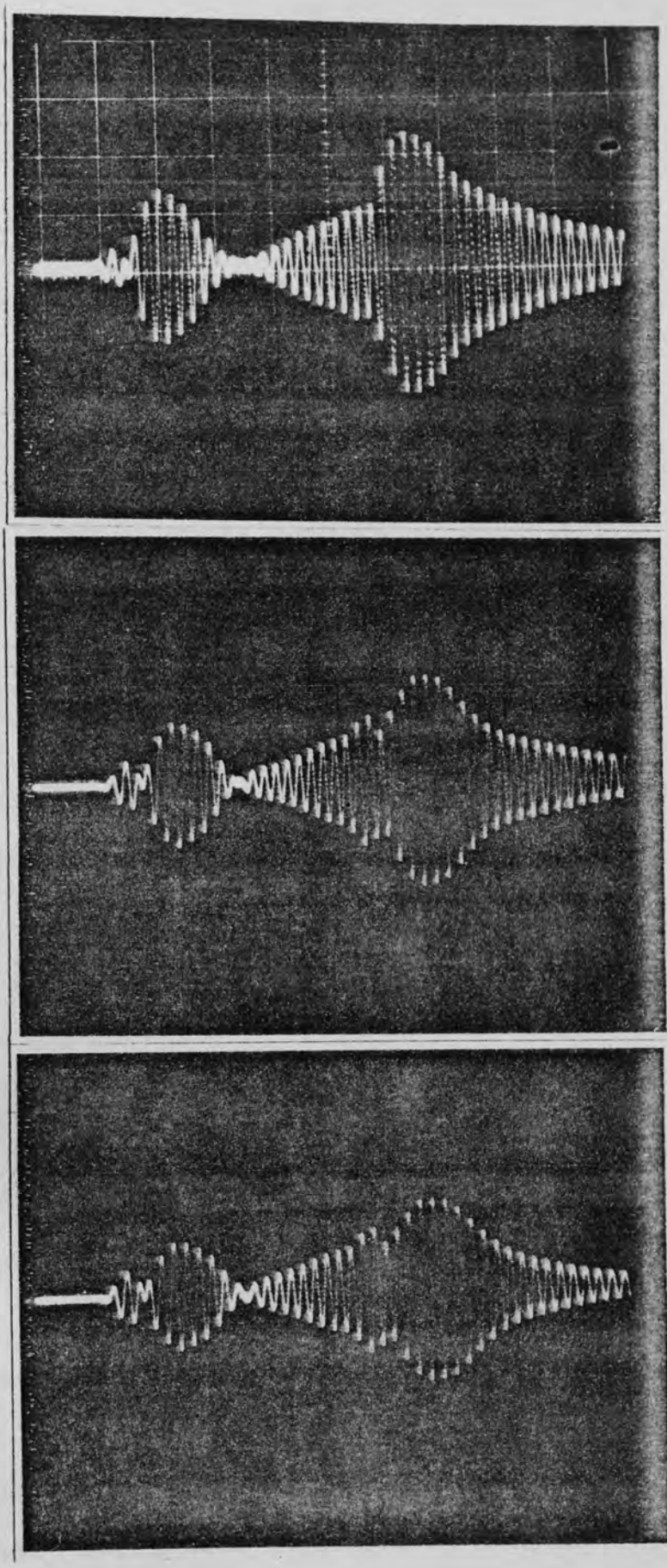

1) at room temperature 20°C
fr = 155.8 kHz
Pm = 7

2) at 1100°C
fr = 154.6 kHz
Pm = 6

3) at 1400°C
fr = 152.7 kHz
Pm = 6

In all photographs sensitivity = $0.05 V cm^{-1}$

Fig.10.15 Silicon carbide ultrasonic temperature probe (Line length = 1.0 m). Mode of control:automatic integral with 5 oscillations in sampling & 5 oscillations in delay. Heat treatment by blow torch flame & temperature measurement with optical pyrometer.

155.80 kHz of the previous value.

The echo pattern for one heating cycle are shown in photographs concerned with the Fig. 10.15. The sensitivity of this probe at 1000^{o}C is 31 ppm/^{o}C. While the calibration curve is not linear over a wide temperature range its reproducibility is overriding. To make a suitable probe of silicon carbide a specimen of length at least 25 cm is required. Regrettable single crystals are not available in a suitable form.

10.6 CALIBRATION OF TUNGSTEN PROBE

Tungsten, as discussed previously in 8.4.1.1, is one of the most attractive refractory materials for temperature probesparticularly for the nuclear environment where the atmosphere is inert. High melting point (3380^{o}C), small hysteresis, reproducibility of calibration and high modulus of elasticity are significant properties of this material.

After successful development of the 1.5 mm integral line probe (by the author), as described in the Chapter 5, the 1.5 mm tungsten probe was considered to be a suitable temperature sensor for the "Petten" experiments.

A large number of 1.5 mm and 2 mm diameter of 50 cm , 100 cm and 200 cm long tungsten rods with a purity greater than 99.9% were supplied by Tungsten Manufacturing Co. The results of experiments are classified in the below:

10.6.1 Results of Experiments

Generally two series of observations were considered. In the first series three samples of 50 cm long were calibrated in 0-1000°C silica tube furnace. The frequency-temperature characteristic for each sample was repeated upto five heating and cooling cycles. The linearity and reproducibility of all samples were quite satisfacory as shown later. In the second series four samples of 50 cm and 200 cm were calibrated in the 1800°C vacuum furnace. The probe temperature was measured using a W-26%Re/W-3%Re thermocouple which was located very close to the tuning fork. In this case, too, a few heating and cooling cycles were performed for each sample.

As long term temperature measurement and stability were important for these probes, automation for recording the results and data were considered. To do this, a Solartron Data Transfer Unit and a Teletype machine in conjunction were used to give simultaneous automatic recording of resonance period and temperature (thermocouple voltage). The DTU is controlled by an internal clock and can be set to take readings at various time intervals as required.

10.6.1.1 Results of Experiments in the 1000°C Furnace.

First sample (A) of 1.5 mm x 50 cm tungsten rod had the new model of tuning fork cut into one end (fr=97.6kHz and Q factor = 50), and was silver brazed to a 2 mm

permendur line at the other end. The specimen was heated upto the 1000°C in argon atmosphere and its temperature was measured with a chromel/alumel thermocouple. The results of the fourth heating and cooling cycle are given in Table 10.4 and the frequency-temperature calibration in Fig. 10.16. The linearity of the characteristic and small thermal hysteresis will be denoted. Photographs in Fig.10.17 are shown the successive echo pattern of the probe at different temperatures. Geometrical dimensions of the tuning fork (TIT-1) are given in Fig.10.18(a).

Table 10.4

Temperature	Heating Frequency	Cooling Frequency
Room	97.656 kHz	97.933 kHz
100°C	97.276	97.523
200	96.805	97.050
300	96.181	96.441
400	95.620	95.850
500	95.039	95.265
600	94.482	94.679
700	93.844	94.100
800	93.350	93.440
900	92.730	92.807
1000	92.123	92.123

This probe has a sensitivity of 61 ppm/°C at 900°C.

The second sample (B) of 1.5 mm x 50 cm tungsten rod had a similar tuning fork (TIT-2) with resonance frequency of 101.1 kHz and Q-factor of 59, as shown in Fig. 10.18(b). It was calibrated in the same conditions as sample A. The observation results are given in table 10.5 and the frequency-temperature characteristic in

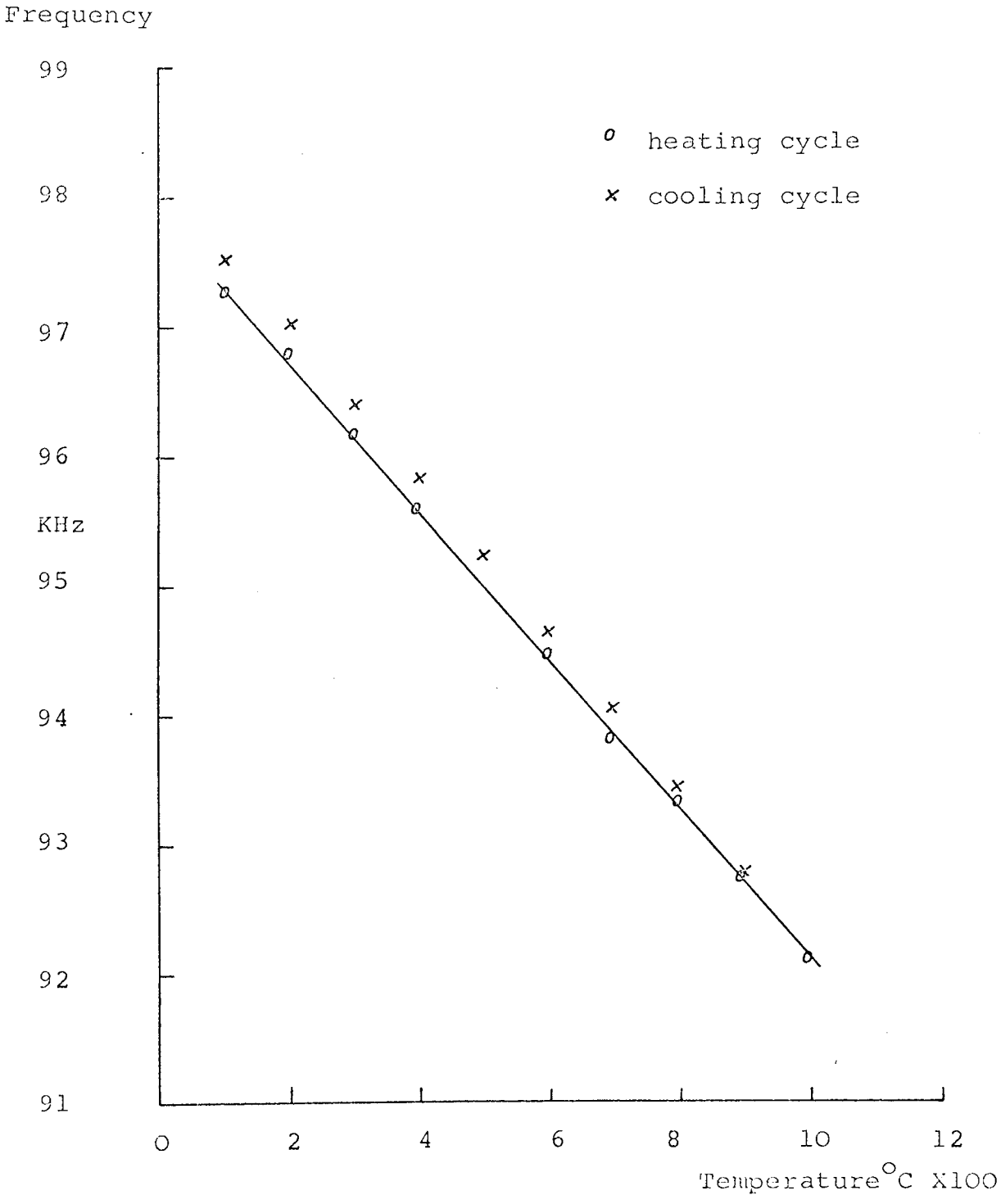

Fig. 10.16 The frequency-temperature characteristic of the first tungsten probe in 1000°C furnace.

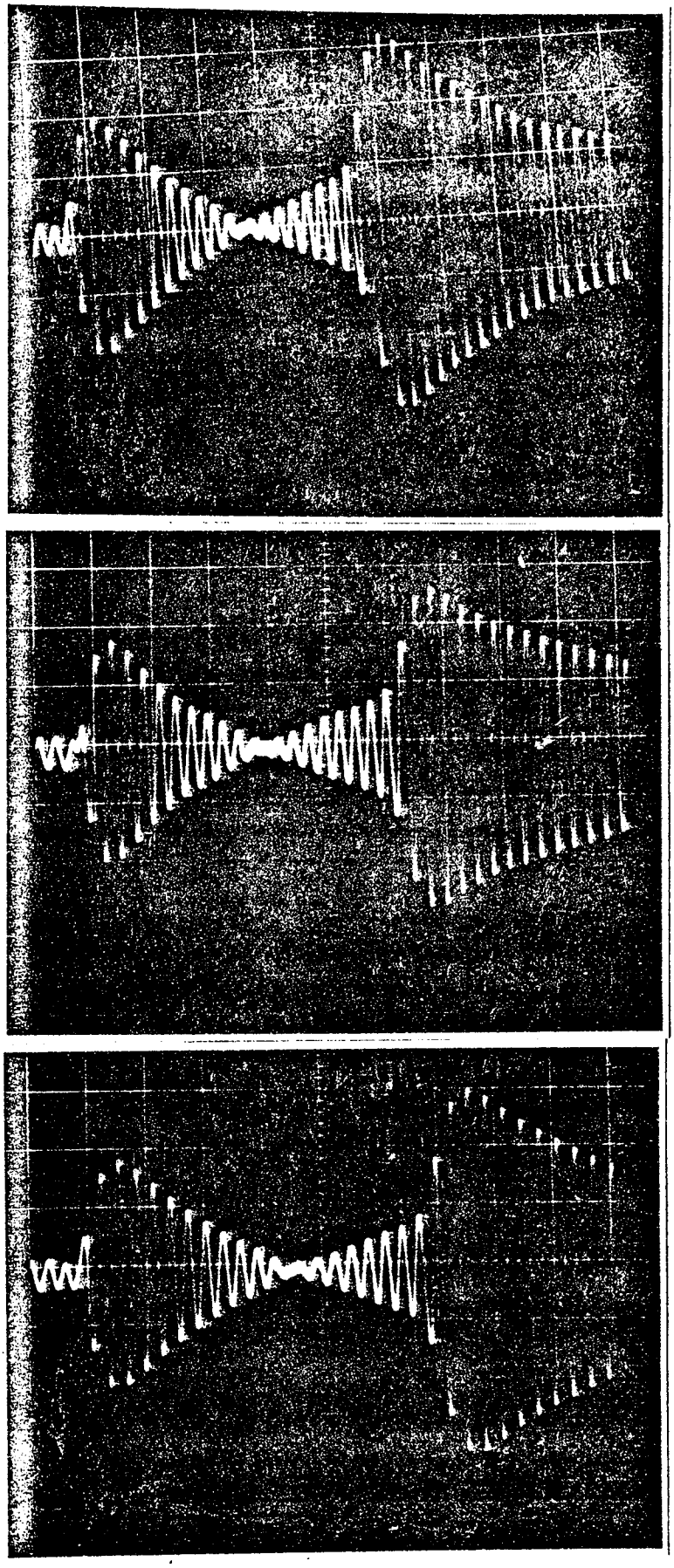

(a) at room temperature

(b) at 1000°C

(c) at room temperature after cooling down from 1000°C.
In all photographs sensitivity = 0.02V/cm.

Fig. 10.17 Successive echo pattern of the first 1.5 mm x 50 cm tungsten probe in the 1000°C furnace.

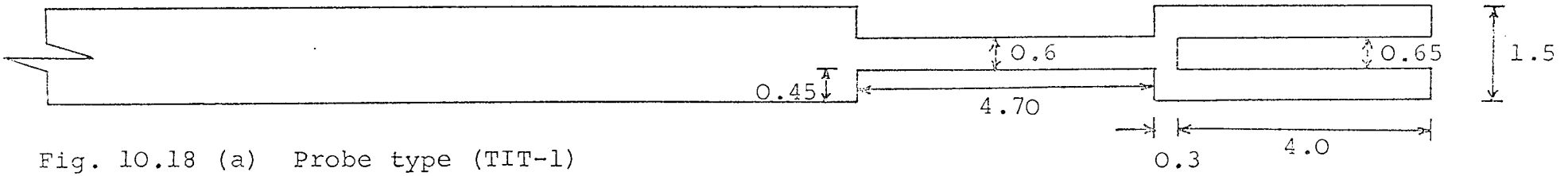

Fig. 10.18 (a) Probe type (TIT-1)

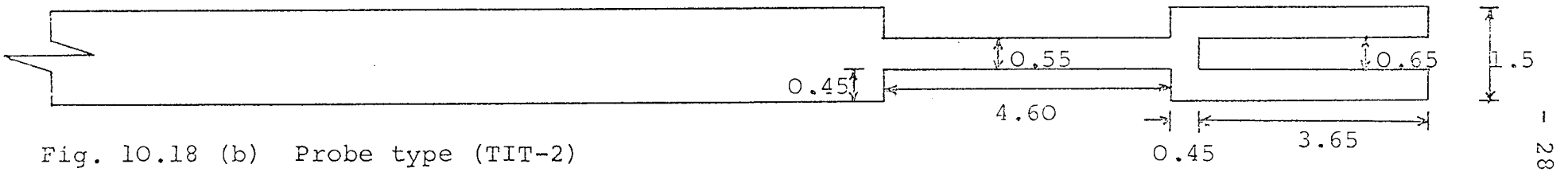

Fig. 10.18 (b) Probe type (TIT-2)

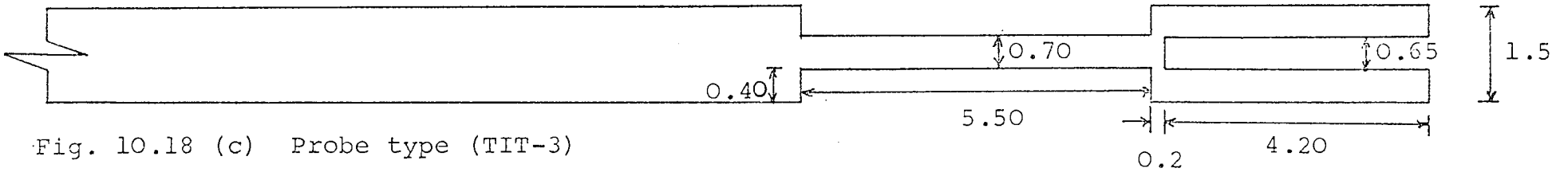

Fig. 10.18 (c) Probe type (TIT-3)

Fig. 10.18 Dimensional diagram of three tungsten integral line probes.

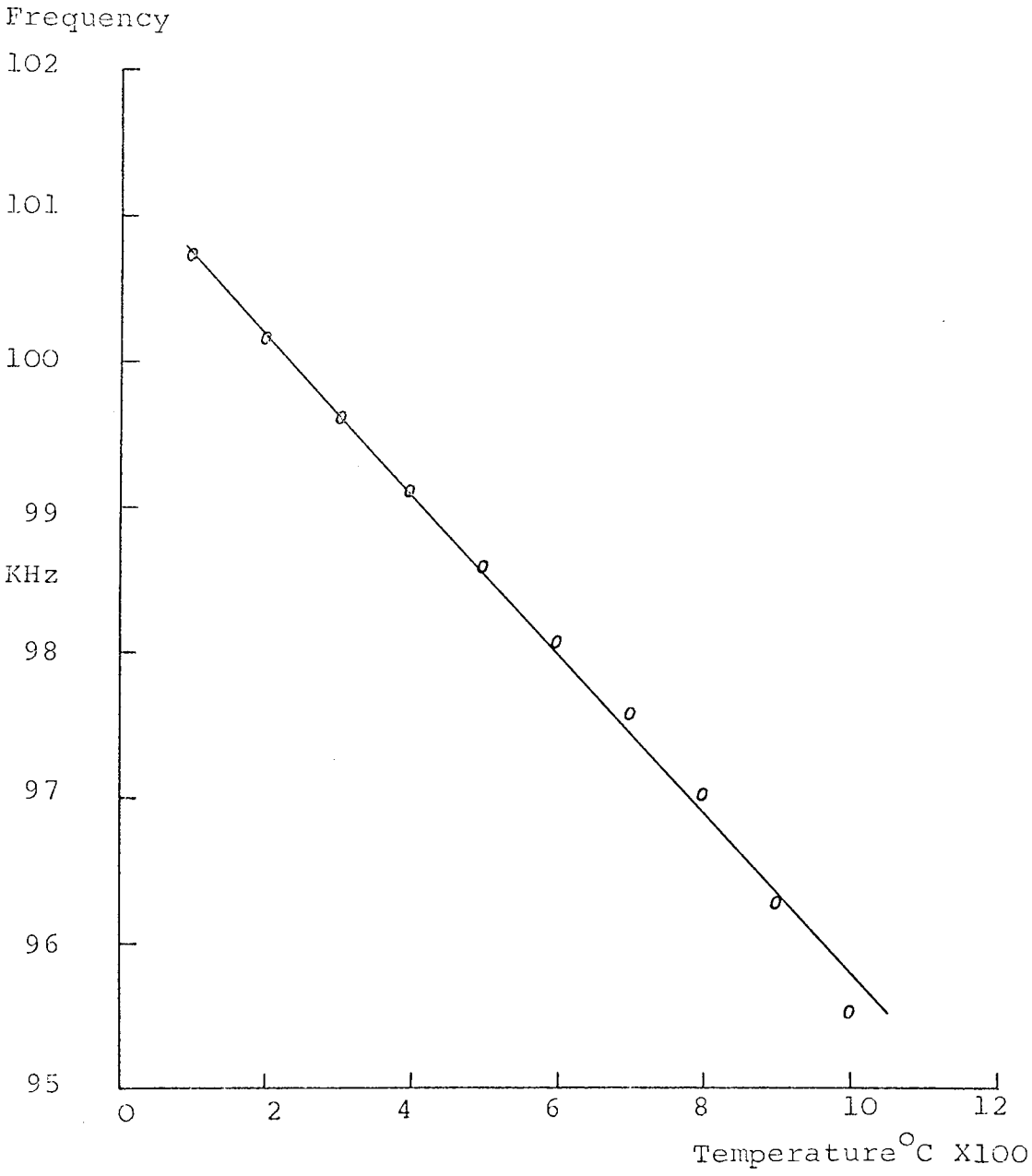

Fig. 10.19 The frequency-temperature characteristic of second tungsten probe in 1000°C furnace.

Fig. 10.19. This probe after cooling from 1000°C to the room temperature had exactly the same frequency, as before, (101.1 kHz). Photographs of the echo pattern at different temperatures are shown in Fig. 10.20.

Table 10.5

Temperature	Frequency
Room	101.163 kHz
100°C	100.705
200	100.170
300	99.621
400	99.108
500	98.600
600	98.097
700	97.570
800	97.021
900	96.274
1000	95.520
Room	101.163

This probe has a sensitivity of 56 ppm/°C at 800°C.

The third sample (C) of 1.5 mm x 50 cm tungsten rod had a tuning fork (TIT-3) with resonance frequency of 81.8 kHz and Q-factor of 45, its dimensions are given in Fig. 10.18 (C). Again, this probe was calibrated in the same conditions as the other two. The period-temperature characteristic was obtained automatically using XY plotter as shown in Fig. 10.21. The X axis is the thermocouple voltage and Y displacement is the analogue display of the period (using D/A converter).

10.6.1.2 Experimental Results in the 1800°C Furnace

For the first experiment a new sample of 1.5 x 50 cm

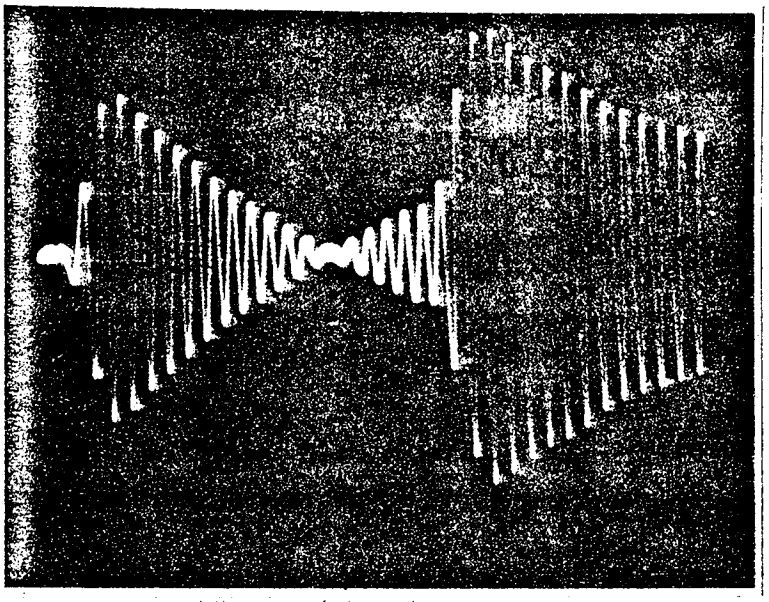

(a) at room temperature

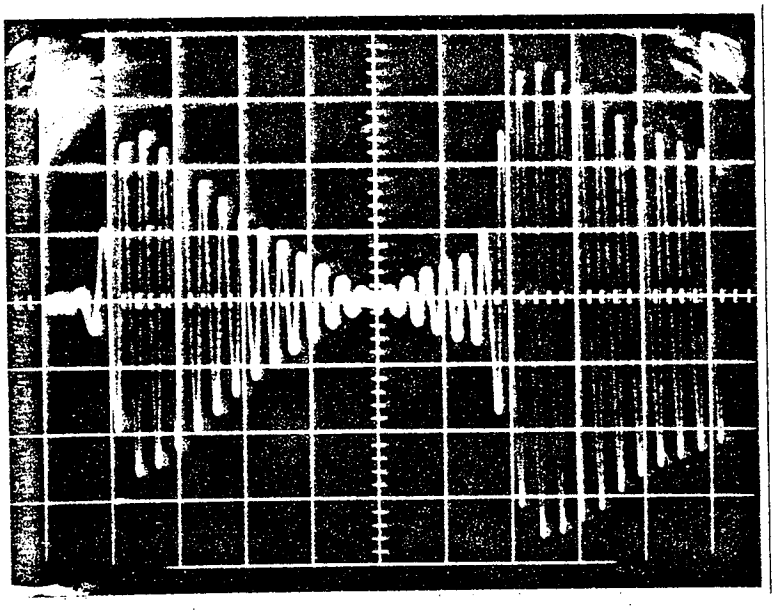

(b) at 1000°C

Sensitivity for both photographs = 0.02V/cm

Fig. 10.20 Successive echo pattern of the 2nd 1.5 mm x 50 cm tungsten probe in 1000°C furnace.

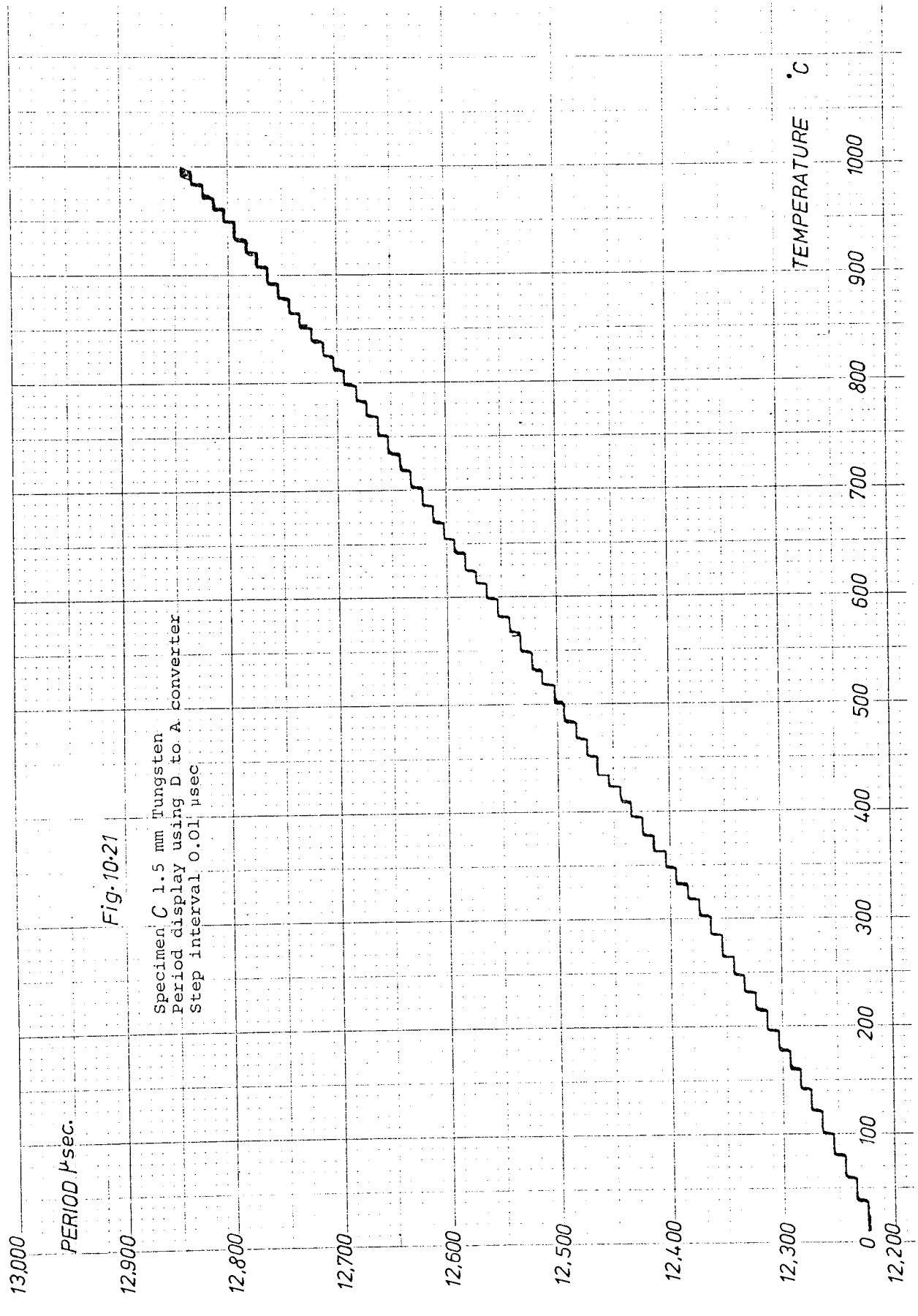
PERIOD μsec.
13,000
12,900
12,800
12,700
12,600
12,500
12,400
12,300
12,200
0
100
200
300
400
500
600
700
800
900
1000
TEMPERATURE °C
Specimen C 1.5 mm Tungsten
Period display using D to A converter
Step interval 0.01 μsec

Fig. 10.21

tungsten rod which had a precisely machined tuning fork at one end (fr = 99.8 kHz and Q factor = 59), was used. The specimen was heated upto 1750^{o}C in the vacuum furnace and its temperature measured using W-26%Re/W-3%Re thermocouple. Six heating and cooling cycles were performed for this sample and the values of the periods and temperatures were recorded automatically using DTU and teletype machines. The results of the final run are given in Table 10.6 and the frequency-temperature characteristic in Fig. 10.22. The photographs of the relative echo patterns at different temperatures are shown in Fig. 10.23. From the photographs, the effect of damping at temperatures above 1500^{o}C will be notable. This is attributed to the internal friction and the grain growth of the pure tungsten, as reported by Berlec[76].

Table 10.6

Heating Cycle

Temperature	Frequency
Room	99.810 kHz
240^{o}C	99.591
434	98.745
616	97.665
772	96.348
926	95.283
1134	93.843
1302	92.481
1440	91.232
1552	90.244
1660	89.102
1750	88.409

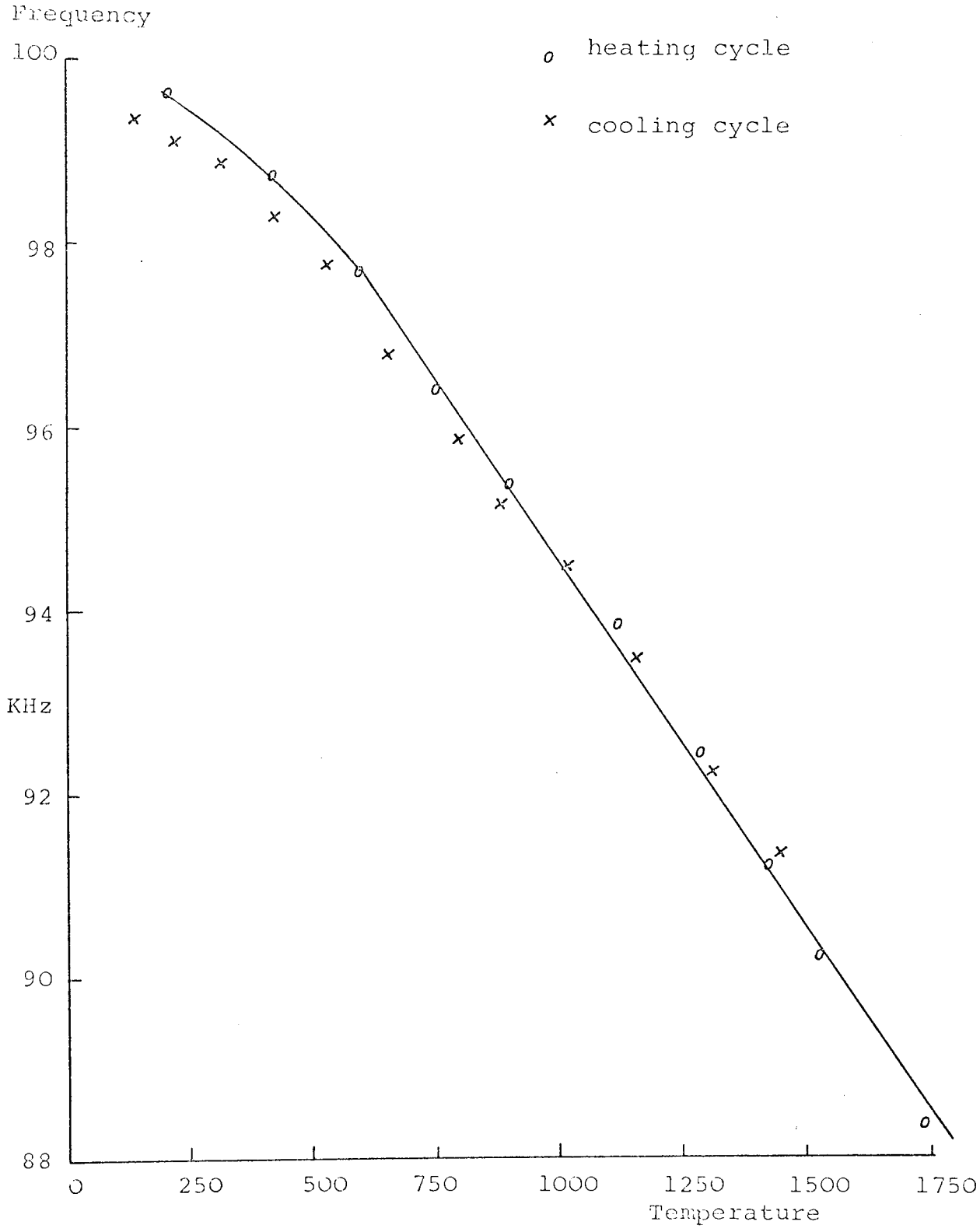

Fig. 10.22 The frequency-temperature characteristic of the first tungsten probe in 1800°C furnace.

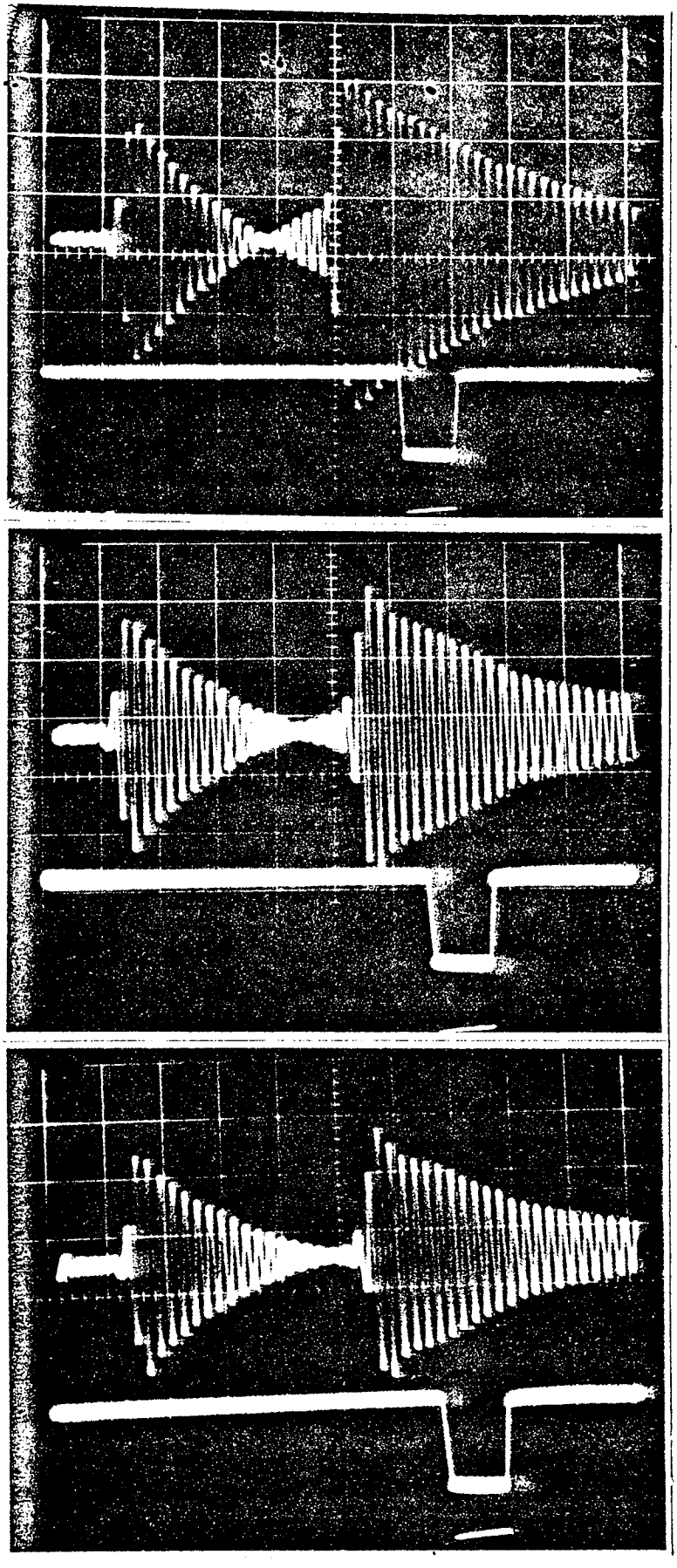

(a) at room temperature

(b) at 1500°C

(c) at 1600°C

Sensitivity in all photographs. For upper trace =0.02V/cm and for lower trace = 2V/cm.

Fig. 10.23 Successive echo pattern for a 1.5 mm x 50 cm tungsten probe in the 1800°C vacuum furnace.

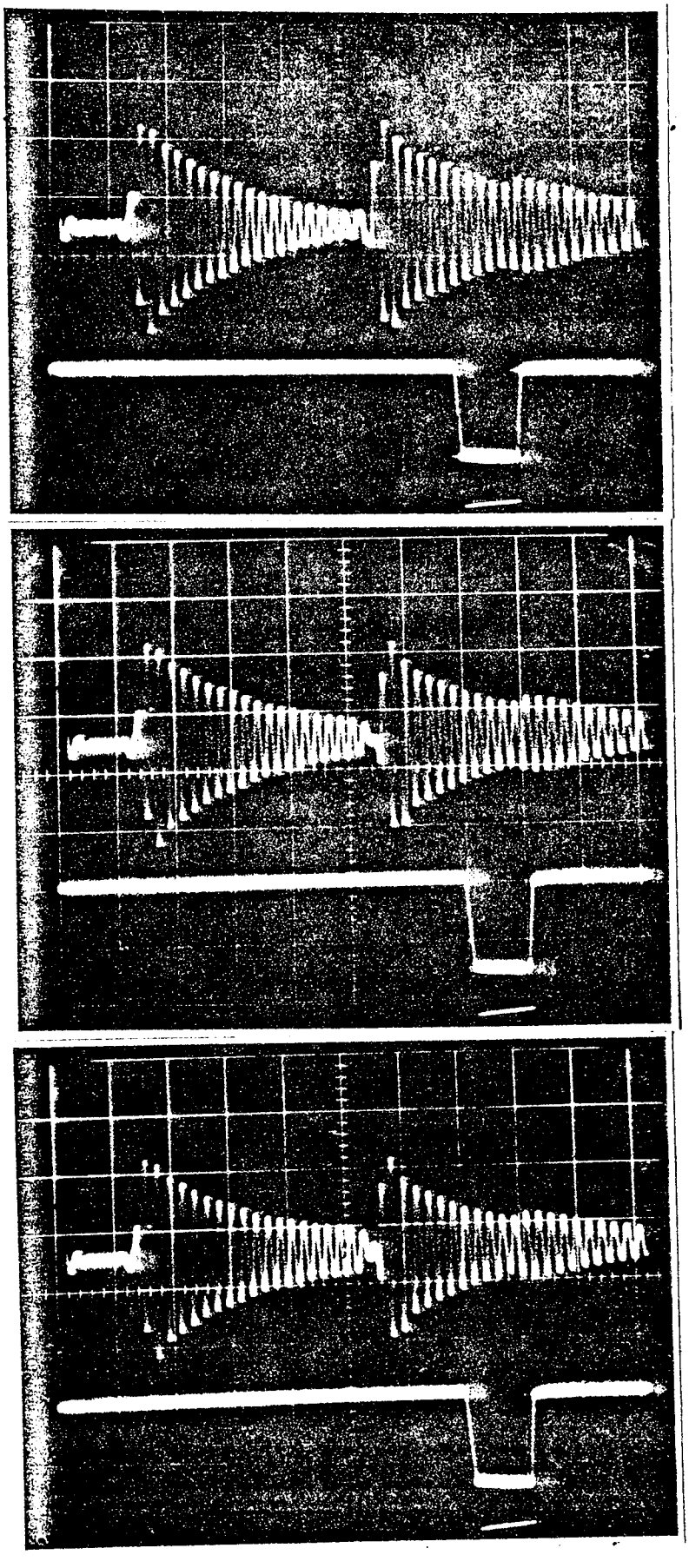

(d) at 1700°C

(e) at 1730°C

(f) at 1750°C

Sensitivity in all photographs For upper trace = 0.02V/cm and for lower trace = 2V/cm.

Fig. 10.23 Successive echo pattern for a 1.5 mm x 50 cm tungsten probe in 1800°C vacuum furnace.

Cooling Cycle

Temperature	Frequency
1464	91.349
1328	92.242
1160	93.501
1030	94.455
916	95.192
810	95.868
680	96.805
544	97.742
436	98.309
326	98.794
230	99.127
148	99.344

In the next experiment a sample of 1.5 mm x 200 cm tungsten rod, having a precisely machined tuning fork at one end and silver brazed to a short piece (6 cm long) of launcher at the other end, were calibrated in the vacuum furnace for the "Petten" reactor. The conditions were the same as the previous sample and the resultant data were recorded automatically on the teletype. The values of the periods and temperatures of the first run which took over 8 hours are given in Table 10.7.

Photographs of the relative echo pattern at various temperatures are shown in Fig. 10.24. Again the effect of the internal friction for the temperatures above 1500^{o}C will be noted.

Another experiment was performed to investigate the reproducibility of the calibration and the effect of the thermal hysteresis on this probe. For this reason the probe was calibrated in the second run under the same

Table 10.7

A.A.FATHIMANI OCT.8TH.1975

FIRST RUN ON 2.0M LONG TUNGSTEN TUNING FORK IN THE VACUUM FURNACE, HEATING UP TO 1800 C.
AUTOMATIC CONTROL IS USED TO TRACK THE RESONANCE FREQUENCY OF THE FORK.
FIVE SAMPLES OF DECREMENT USED IN CONTROL AND FIVE SAMPLES DELAYED.
READING TAKING EVERY 5 MINUTES.

TIME
TEMPERATURE PERIOD

*091001
10 +00010 1 011772
*091501
10 +00041 1 011781
*092001
10 +00124 1 011808
*092501
10 +00230 1 011842
*093001
10 +00345 1 011891
*093501
10 +00464 1 011936
*094001
10 +00580 1 011975
*094501
10 +00698 1 012016
*095001
10 +00811 1 012041
*095501
10 +00920 1 012070
*100001
10 +01024 1 0121;9
*100501
10 +01129 1 012195
*101001
10 +01225 1 012210
*101501
10 +01321 1 012239
*102001
10 +01411 1 012256
*102501
10 +01494 1 012287
*103001
10 +01575 1 012314
*103501
10 +01644 1 012347
*104001
10 +01709 1 012373
*104501
10 +01751 1 012393

Table 10.7 contd.

```
*105001
10 +01820 1 012424
*105501
10 +01874 1 012456
*110001
10 +01924 1 012486
*110501
10 +01969 1 012518
*111001
10 +02010 1 012551
*111501
10 +02045 1 012577
*112001
10 +02074 1 012603
*112501
10 +02100 1 012627
*113001
10 +02128 1 012652
*113501
10 +02144 1 012680
*114001
10 +02161 1 012707
*114501
10 +02174 1 012731
*115001
10 +02190 1 012758
*115501
10 +02204 1 012784
*120001
10 +02219 1 012810
*120501
10 +02234 1 012835
*121001
10 +02245 1 012859
*121501
10 +02255 1 012871
*122001
10 +02271 1 012980
*122501
10 +02281 1 012920
*123001
10 +02294 1 012940
*123501
10 +02305 1 012960
*124001
10 +02315 1 012979
*124501
10 +02325 1 013001
*125001
10 +02324 1 013005
*125501
10 +02340 1 01303?
*130001
10 +02349 1 013061
*130501
10 +02354 1 013082
*131001
10 +02360 1 013106
*131501
10 +02538 1 013351
*132001
10 +03171 1 013475
```

Table 10.7 contd.

```
 COOLING DOWN
 *132501
 10 +02705 1 012944
 *133001
 10 +02435 1 012766
 *133501
 10 +02254 1 012665
 *134001
 10 +02101 1 012590
 *134501
 10 +01965 1 012529
 *135001
 10 +01841 1 012473
 *135501
 10 +01724 1 012423
 *140001
 10 +01618 1 012375
 *140501
 10 +01515 1 012331
 *141001
 10 +01419 1 012288
 *141501
 10 +01328 1 012247
 *142001
 10 +01240 1 012212
 *142501
 10 +01160 1 012182
 *143001
 10 +01084 1 012154
 *143501
 10 +01015 1 012129
 *144001
 10 +00948 1 012105
 *144501
 10 +00884 1 012082
 *145001
 10 +00824 1 012061
 *145501
 10 +00769 1 012042
 *150001
 10 +00718 1 012024
 *150501
 10 +00670 1 012007
 *151001
 10 +00625 1 011991
 *151501
 10 +00581 1 011977
 *152001
 10 +00545 1 011963
 *152501
 10 +00509 1 011950
 *153001
 10 +00475 1 011939
 *153501
 10 +00444 1 011927
 *154001
 10 +00414 1 011917
 *154501
 10 +00385 1 011907
 *155001
 10 +00360 1 011999
 *155501
 10 +00339 1 011891
 *160001
 10 +00315 1 011884
 *160501
 10 +00295 1 011876
 *161001
 10 +00265 1 011871
 *161501
```

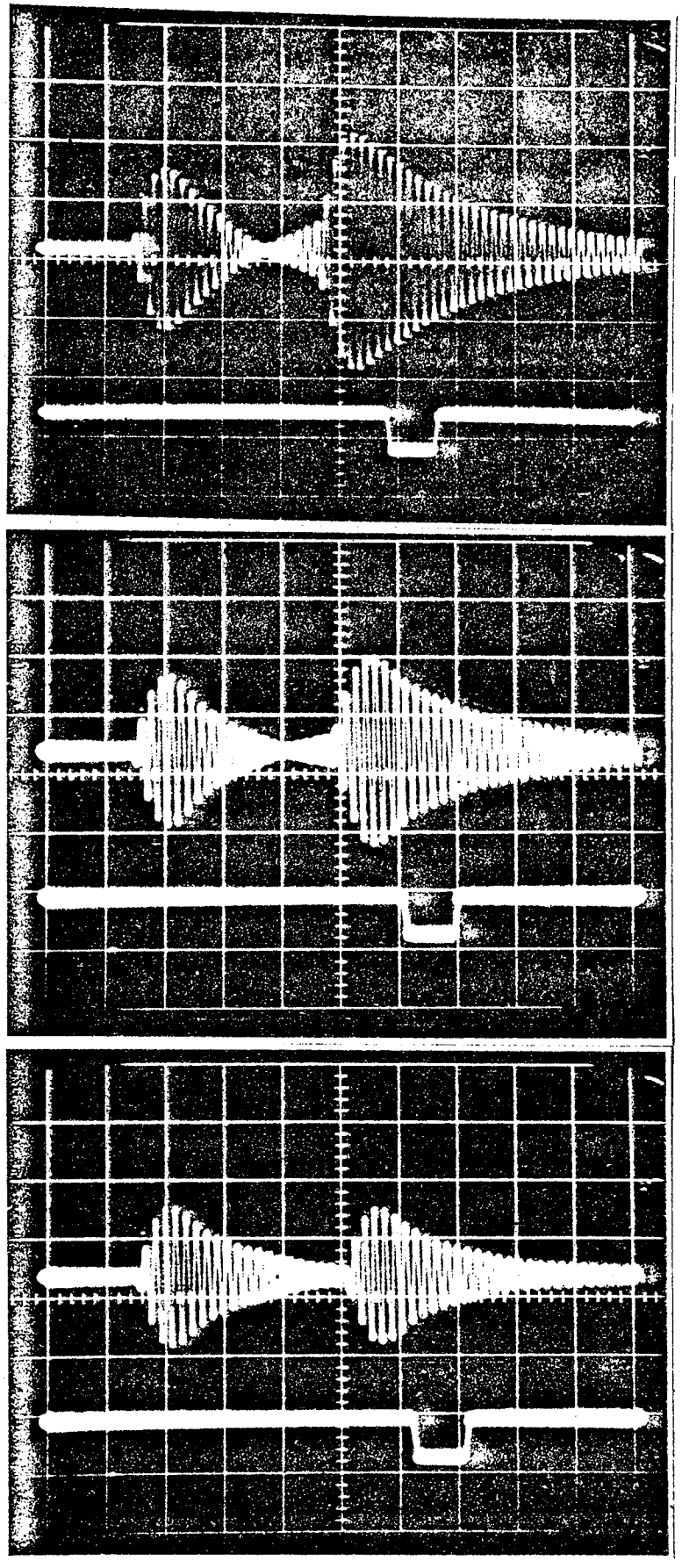

(a) at room temperature

(b) at 1480°C

(c) at 1650°C

Sensitivity in all photographs. For upper trace = 0.05V/cm for lower trace = 5V/cm

Fig. 10. 24 Successive echo pattern for a 1.5 mm x 200 cm tungsten probe in the 1800°C vacuum furnace.

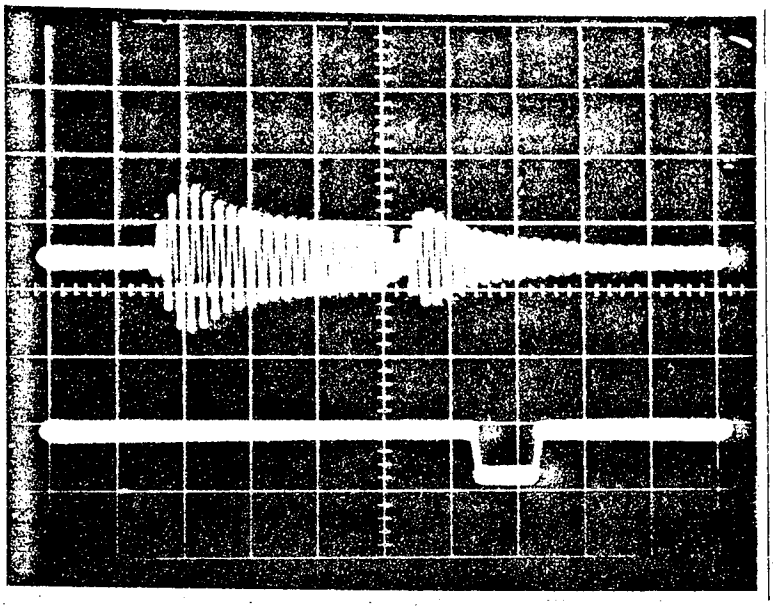

(d) at 1760°C

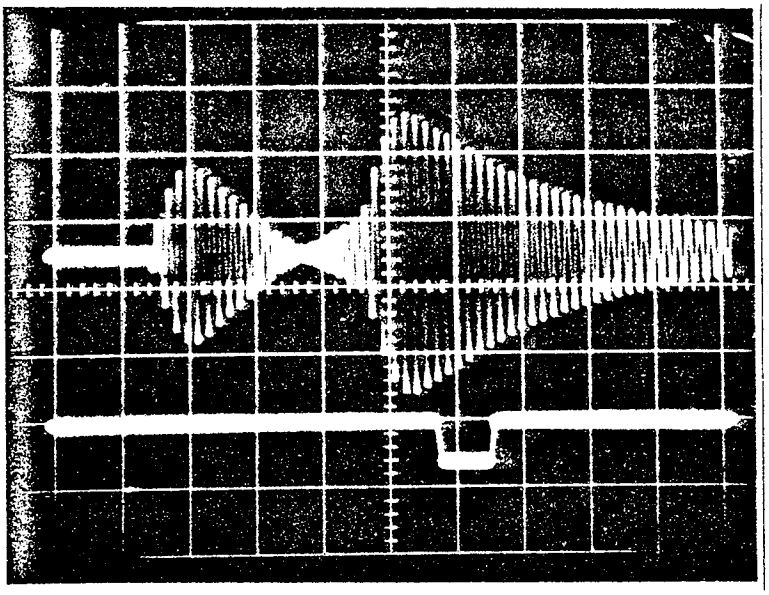

(e) at 150 °C after cooling down from 1760°C.

Sensitivity in both photographs. For upper trace = 0.05V/cm for lower trace = 5V/cm

Fig. 10.24 Successive echo pattern for a 1.5 mm x 200 cm tungsten probe in the 1800°C vacuum furnace.

conditions. The results are given in Table 10.8, the calibration curve in Fig. 10.25 and the relative echo pattern at various temperatures in Fig. 10.26. The negligible thermal hysteresis and reproducibility of the calibration characteristics are quite satisfactory upto the 1500°C. Above 1500°C, as before, damping effect due to the internal friction increase and presumably there is a grain boundaries peak at 1750°C, but as the maximum temperature for the "Petten" experiments is considered to be 1600°C, therefore the presence of the internal friction will not be serious for this application.

10.7 CALIBRATION OF THORIATED TUNGSTEN PROBE

A decision was made to move from pure tungsten to thoriated tungsten, which is commercially available as it is much easier to machine with precision. The presence of the thoria was expected to reduce internal friction at the grain boundaries and possibly improve the stability of calibration by suppressing grain growth.

An experiment was performed to calibrate a thoriated tungsten probe for the "Petten" reactor. A sample of 1.5 mm x 200 cm tungsten - 2% thoria rod had a precisely machined tuning fork at one end and silver brazed to a 6 cm launcher at the other end was used. A few heating and cooling cycles were performed in the vacuum furnace under the same conditions of the tungsten probes and the results were obtained automatically as before.

Table 10.8

A.A.FATHIMANI OCT.9TH.1975

SECOND RUN ON 2.0M LONG TUNGSTEN TUNING FORK IN THE VACUUM FURNACE, HEATING UP TO 1800 C.
AUTOMATIC CONTROL IS USED TO TRACK THE RESONANCE FREQUENCY OF THE FORK.
FIVE SAMPLES OF DECREMENT USED IN CONTROL AND FIVE SAMPLES DELAYED.
READING TAKING EVERY 5 MINUTES.

TIME
TEMPERATURE PERIOD

*090500
10 -00001 1 011782
*091000
10 +00024 1 011789
*091500
10 +00101 1 011804
*092000
10 +00205 1 011830
*092500
10 +00329 1 011869
*093000
10 +00461 1 011918
*093500
10 +00590 1 011973
*094000
10 +00721 1 012025
*094500
10 +00844 1 012072
*095000
10 +00965 1 012118
*095500
10 +01080 1 012150
*100000
10 +01190 1 012198
*100500
10 +01295 1 012232
*101000
10 +01400 1 012262
*101500
10 +01499 1 012293
*102000
10 +01594 1 012328
*102500
10 +01691 1 012368
*103000
10 +01781 1 012409
*103500
10 +01871 1 012448
*104000
10 +01954 1 012485
*104500
10 +02038 1 012533

Table 10.8 contd.

```
*105000
10 +02115 1 012591
*105500
10 +02191 1 012634
*110000
10 +02264 1 012661
*110500
10 +02425 1 012761
*111000
10 +02560 1 012848
*111500
10 +02660 1 012912
*112000
10 +02750 1 012969
*112500
10 +02828 1 013023
*113000
10 +02898 1 013077
*113500
10 +02960 1 013138
*114000
10 +03015 1 013197
*114500
10 +03071 1 013266
*115000
10 +03108 1 013344
*115500
10 +03139 1 013404
*120000
10 +03194 1 013500
*120500
10 +03160 1 013583
```

COOLING DOWN

```
*121000
10 +02720 1 013060
*121500
10 +02450 1 012908
*122000
10 +02858 1 013169
*122500
10 +02804 1 013118
*123000
10 +02820 1 013128
*123500
10 +02830 1 013133
*124000
10 +02831 1 013130
*124500
10 +02845 1 013140
*125000
10 +02854 1 013143
*125500
10 +02861 1 013144
*130000
10 +02878 1 013146
*130500
10 +02895 1 013147
*131000
10 +02931 1 013150
```

Table 10.8 contd.

```
*131000
10 +03035 1 013154
*131000
10 +03341 1 013158
*132500
10 +03741 1 013157
*133000
10 +04290 1 013155
*133500
10 +04949 1 013153
*134000
10 +05514 1 013154
*134500
10 +06014 1 013157
```

```
*135000
10 +04880 1 012908
*135500
10 +04518 1 012795
*140000
10 +04284 1 012718
*140500
10 +04030 1 012658
*141000
10 +03779 1 012607
*141500
10 +03540 1 012562
*142000
10 +03314 1 012509
*142500
10 +03104 1 012465
*143000
10 +02895 1 012420
*143500
10 +02704 1 012389
*144000
10 +02534 1 012356
*144500
10 +02375 1 012326
*145000
10 +02224 1 012301
*145500
10 +02074 1 012275
*150000
10 +01941 1 012251
*150500
10 +01815 1 012230
*151000
10 +01699 1 012211
*151500
10 +01585 1 012194
*152000
10 +01481 1 012176
*152500
10 +01384 1 012161
*153000
10 +01295 1 012146
*153500
10 +01209 1 012133
*154000
10 +01129 1 012120
*154500
10 +01051 1 012109
*155000
10 +00980 1 012099
*155500
```

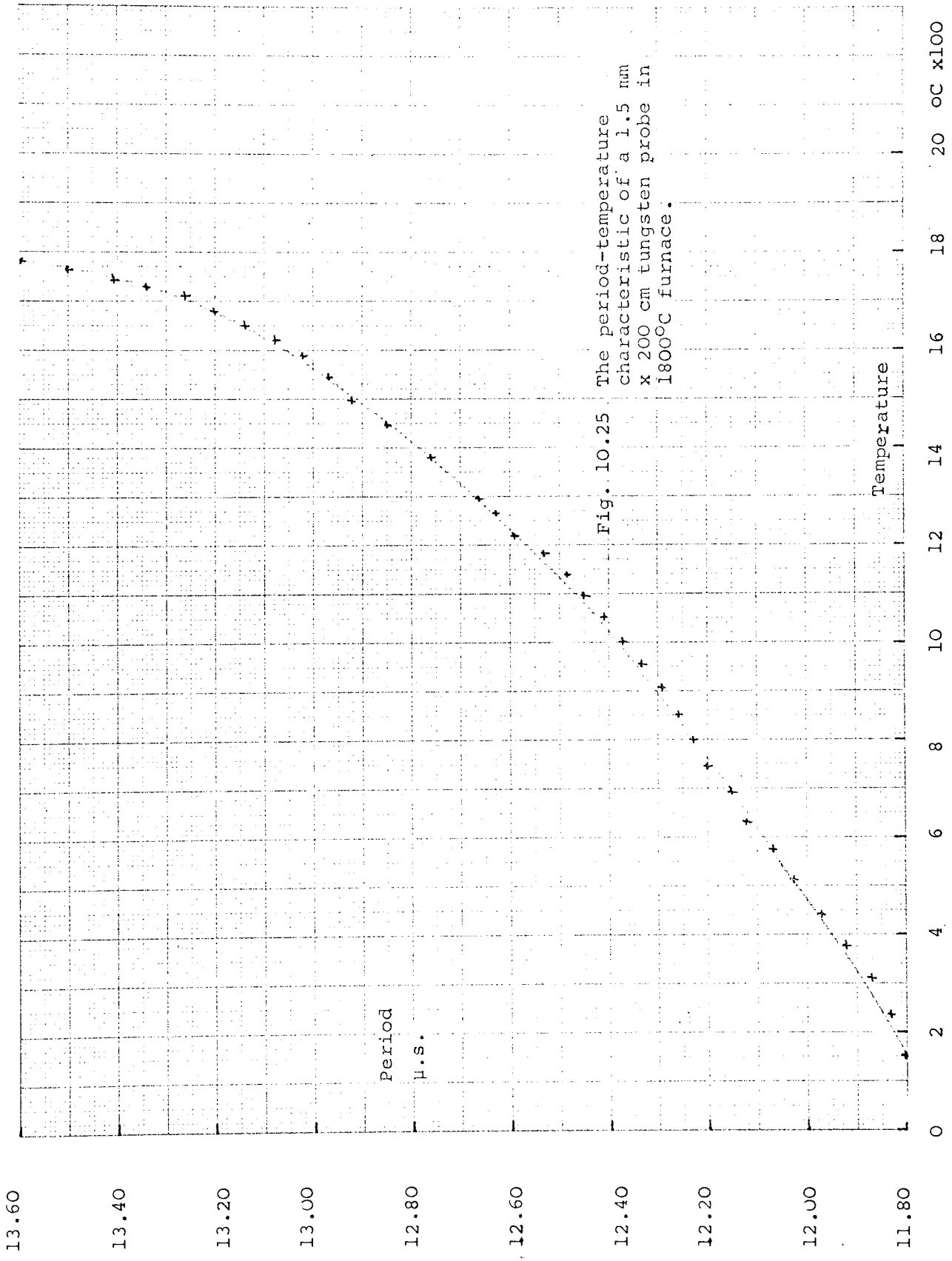

Fig. 10.25 The period-temperature characteristic of a 1.5 mm x 200 cm tungsten probe in 1800°C furnace.

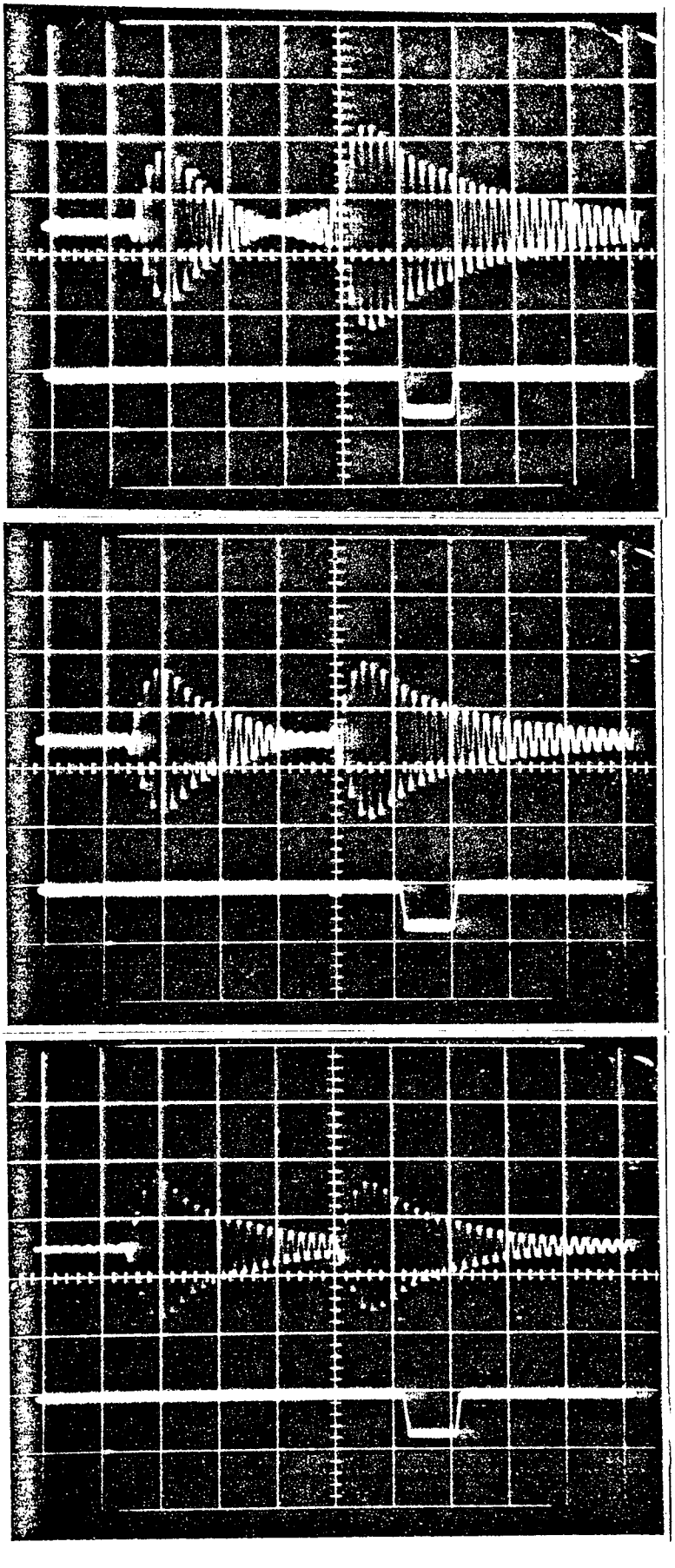

(a) at 1500°C

(b) at 1650°C

(c) at 1700°C

In all photographs sensitivity: for upper trace = 0.05V/cm for lower trace = 5V/cm.

Fig. 10.26 Successive echo pattern for a 1.5 mm x 200 cm tungsten probe at the second run in the 1800°C vacuum furnace.

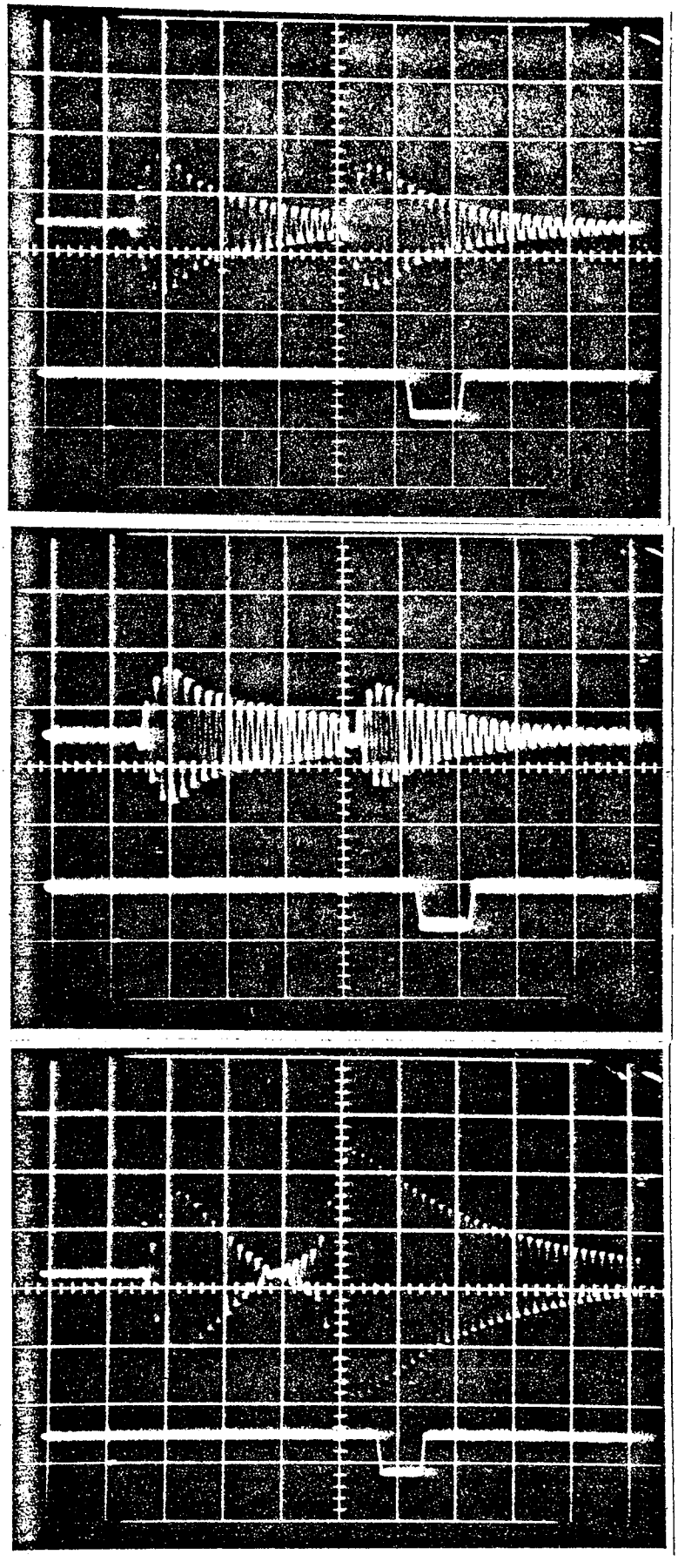

(d) at 1720°C

(e) at 1750°C

(f) at room temperature after cooling down from 1750°C.

In all photographs sensitivity: for upper trace = 0.05V/cm for lower trace = 5V/cm.

Fig. 10.26 Successive echo pattern for a 1.5 mm x 200 cm tungsten probe at the second run in the 1800°C vacuum furnace.

The period-temperature characteristic of the fourth run is shown in Fig. 10.27 and the photographs of the relative echo pattern at various temperatures are shown in Fig. 10.28. From these photographs there will be no sign of internal friction even after many hours operating at 1600^{o}C.

The stability of calibration, negligible of thermal hysteresis and undetectable internal friction of the thoriated tungsten in temperatures upto 1600^{o}C was quite encouraging. Accordingly this temperature probe was considered to be quite suitable for the "Petten" reactor.

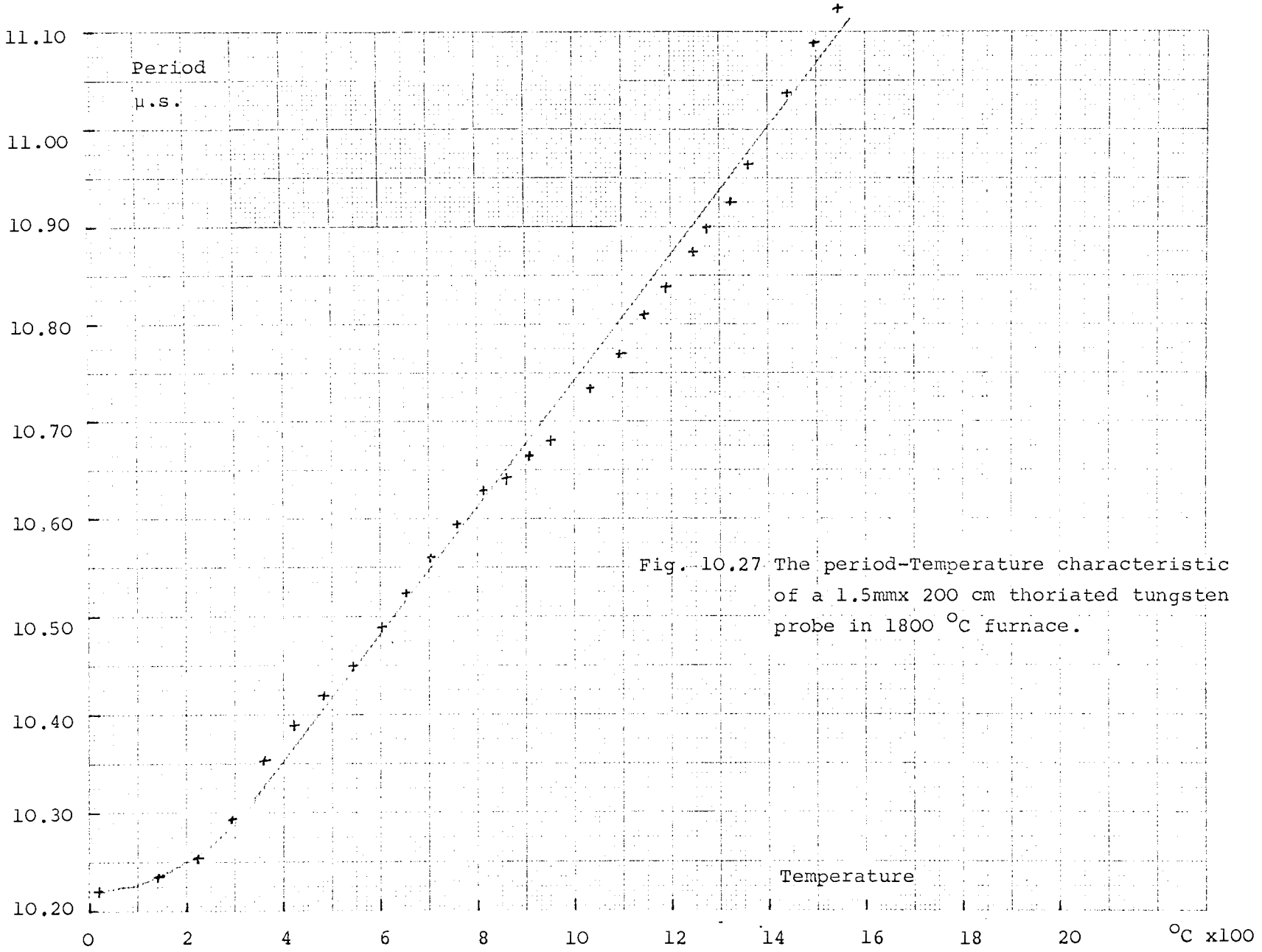

Fig. 10.27 The period-Temperature characteristic of a 1.5mmx 200 cm thoriated tungsten probe in 1800 °C furnace.

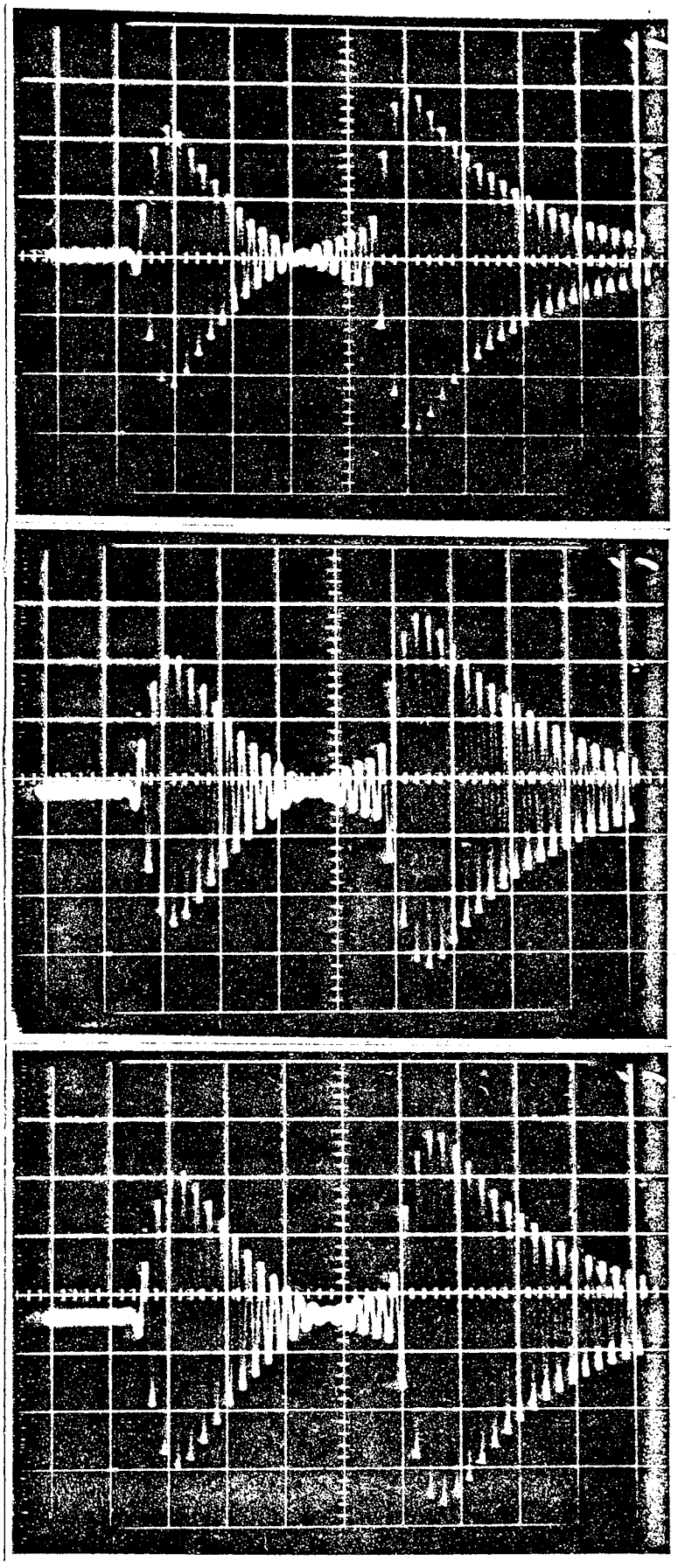

(a) at 100°C

(b) at 1000°C

(c) at 1600°C after 4 hours operation Sensitivity in all photographs 0.05V/cm

Fig. 10. 28 Successive echo pattern for a 1.5 mm x 200 cm thoriated tungsten probe in 1800°C vacuum furnace.

Fig. 10.29 This photograph shows the 3 mm sapphire integral line probe and the 3 mm iridium strip line probe used for investigation of their calibration.

Fig. 10.30 This photograph shows the new 1.5 mm tungsten integral line probe used for the Petten experiments.

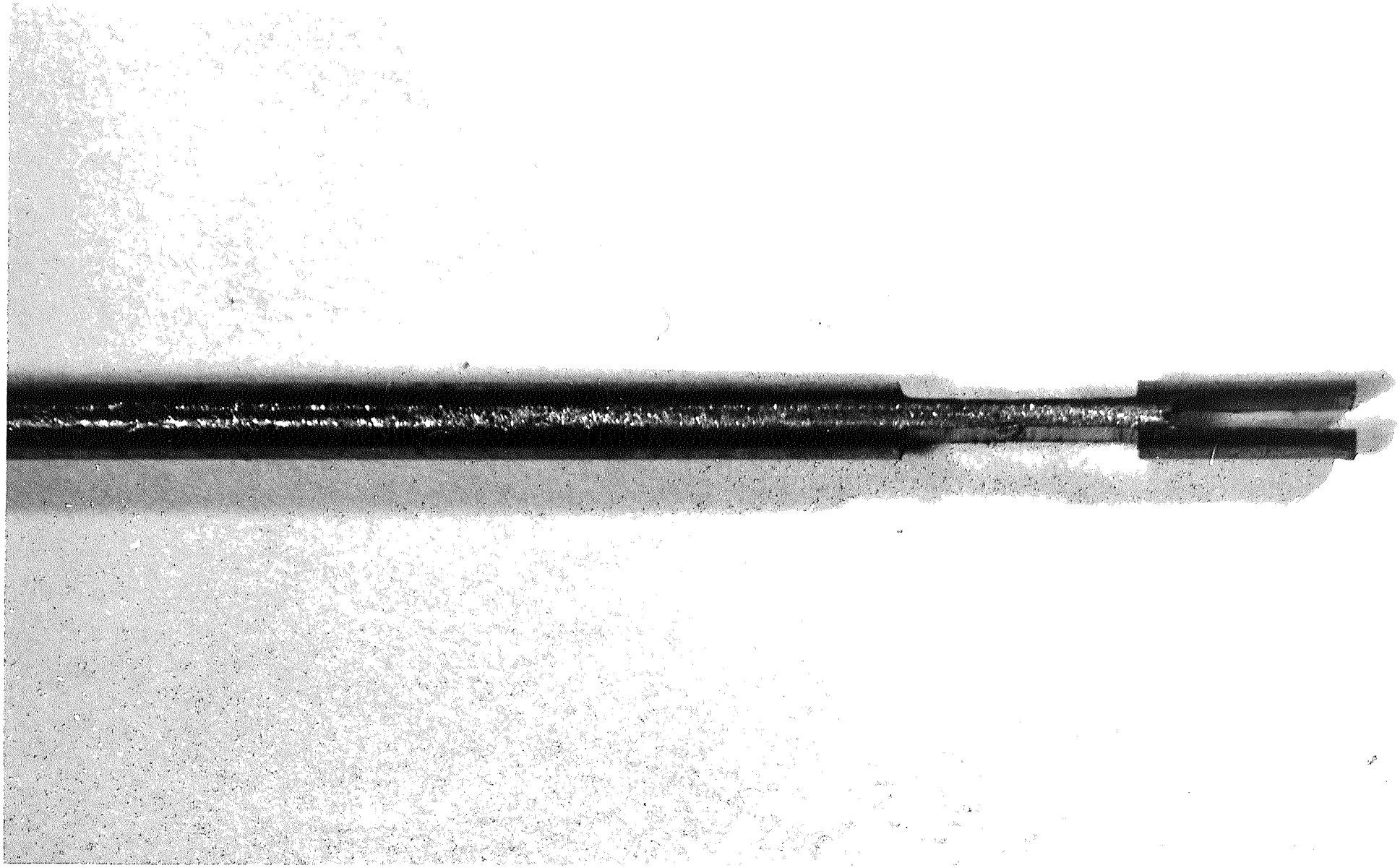

Fig. 10.31 This photograph shows the new 1.5 mm thoriated tungsten integral line probe used for the Petten experiments.

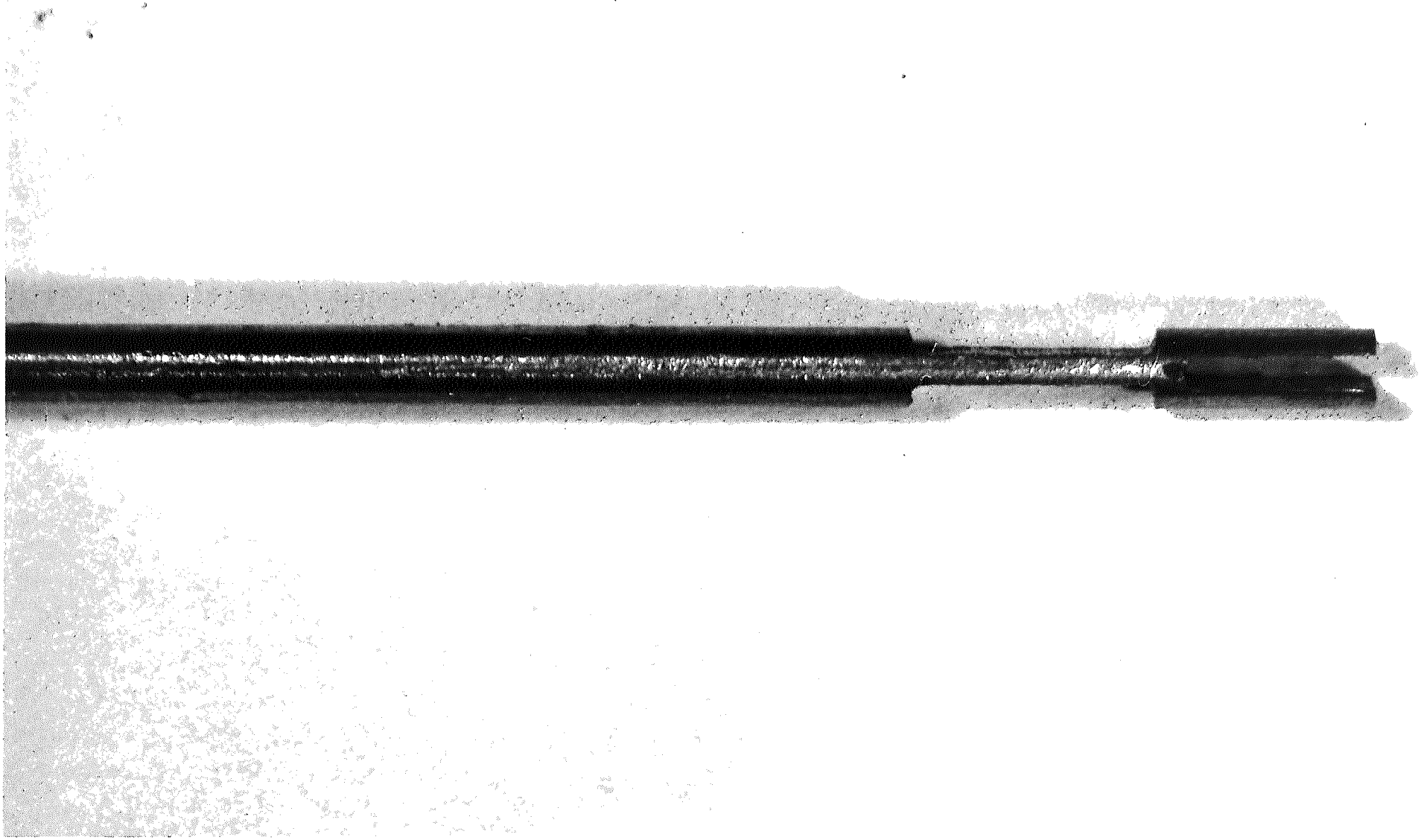

Fig. 10.32 This photograph shows an experimental set-up for the calibration of the probe.

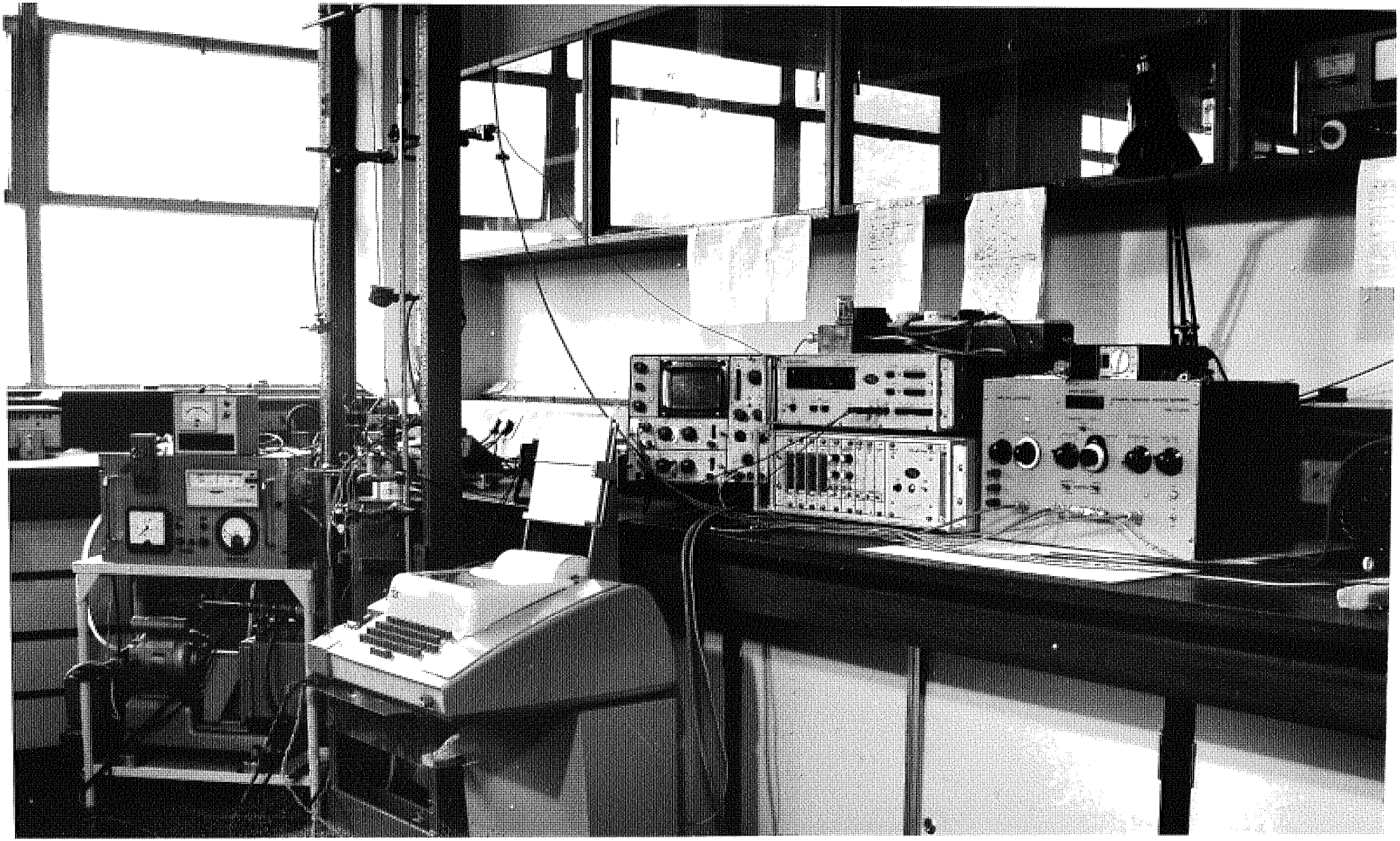

CHAPTER 11

THE CONCLUSIONS

The objective of the research work was to devise an automatic system to measure temperature in the 1000-2000^{o}C range in gaseous environment and inert atmosphere. The situations encountered are in nuclear reactors and for chemical processing industries, where a continuous monitoring of temperature is required for the control of the operation. Various methods were considered for their merits and it was concluded that the ultrasonic method offers a better choice for these cases than thermocouples and other instruments.

Various ultrasonic techniques of temperature measurement were reviewed, all of which depend on velocity measurement, and it was found that (a) the video pulse technique using wires and (b) the resonance technique using a line resonator are feasible. The thin wire method requires a long sensor of the order of 25 mm and its velocity measuring accuracy is of the order of 1%. Its range of operation extends to near 80% of the melting point of the sensor material. In the resonance method the sensor can be made as small as 2 mm long and the corresponding accuracy is as high as 0.02%.

The range of measurement, however, is limited by the high material losses for polycrystalline materials at high temperatures which reduces the sharpness of the resonance. It was decided to adopt the more accurate

resonance technique and search for materials with high melting points and low losses.

Types of resonators and their modifications available were studied as potential sensors.The resonators, namely half-wave length, quarter-wave length, disc, ring, bar and tuning forks all have their limiting features. One factor common to all these is that they require a high temperature joint between the line and the resonator. It is not possible to obtain adhesion which can withstand temperatures above 1500^{o}C for any length of time. A second less critical feature is the size of the resonator, which in general is too big. This led to the design of a resonator integral with the line, which overcomes these difficiences.

The study of various resonators resulted in the selection of the tuning fork which, vibrating in flexure, is small and of a convenient shape. The fork was made integral with a circular rod line by machining a longitudinal slot at the end. Various designs of the resonator and coupling section were investigated to obtain an optimum design producing a given frequency and adequately tight coupling. The performance of the probe was studied for the effect of all the design parameters. From these analyses a new model of integral line tuning fork based on 1.5 mm tungsten rod was established. The resonator has low frequency (100 kHz) together with low coupling Q which is obtained on a small diameter line. The shape of the probe is convenient for machining and the joint between the main

line and the probe if necessary at all can always be kept at a low temperature. The limiting feature of the probe is suceptibility to thermal shock in the case of ceramic probes, but this is not effected for the nuclear application, as this was the main object of the probe development.

Having established the design of the probe a literature study of elastic properties, phase change, thermal shock at high temperatures of potential probe materials, the refractory metals and oxide ceramics, was made. It was established that high melting point metals e.g. tungsten, rhenium, molybdenum, iridium, rhodium and platinum are satisfactory. Among oxide ceramics, polycrystalline alumina, magnesia, zirconia, thoria, single crystal alumina i.e. sapphire appear attractive. Among these sapphire is the best due to its low material losses very near to the melting point. From carbides single crystal silicon carbide has a remarkable properties but is not readily available.

From all these materials, iridium, sapphire, polycrystalline silicon carbide, tungsten and thoriated tungsten were selected for investigation of their calibration stability and thermal hysteresis. It was found that iridium, a very costly material, after annealing above 1700^{o}C for a long period has very low hysteresis and high calibration stability. Losses above 1700^{o}C set this as an upper temperature limit. Sapphire has low thermal hysteresis, high stability, linear variation of elastic constant with

temperature and low losses even above 2000°C and near to the melting point. These properties make it the most attractive probe material so far studied, tungsten and thoriated tungsten are very suitable material for temperature probe particularly for the nuclear environment but are limited to about 1700°C. They were selected for the "Petten" reactor and are commercially available in the desired dimensions, preferably in 1.5 mm diameter x 200 cm in length.

Thoriated tungsten is expecting to have a better performance than the pure metal. It is more machinable and the addition of 2% thoria seems to reduce the internal friction at the grain boundaries, and imporves the stability of calibration.

The electronic system designed to automate the temperature measurement is based on comparing the periods of the echo decrement pulses, which are at the frequency of the resonator, with the periods of the transmitted pulses. The range of control is approximately ±30% from the centre frequency. The resonant period is displayed and is available for data logging and automatic recording. The analogue value of the display is also available for plotter and chart recorder.

The frequency range over which the electronic circuits operate is sufficient for all foreseeable probes, the overall limitation being the probe materials. Iridium and sapphire operate to about 2000°C in air and tungsten, which must be protected, operates to 1700°C.

Possible future work can be classified into three areas, the probe geometry, the probe material and the electronic system.

The design of the new integral line probe is complete but its analysis is only empirical at this stage. The empirical results obtained to date are adequate for probe design and while a mathematical analysis is desirable the problem is rather complex and a formal solution is unlikely.

The refractory metals and oxide ceramics have been studied, to extend the range of measurement, various alloys of these metals, other ceramics and possibly cermets should be investigated. For liquid metal measurements a search for materials compatible with the measuring metals and environments should be made. Attention should primarily be focused on single crystal materials since they have low losses at the highest temperature of operation.

The present electronic system operates perfectly and no further modification will be required. In this system display the period is the parameter obtained. The temperature can be shown on a pen recorder by using D/A converter and the known calibration of the probe. A digital readout of temperature could readily be provided using a Read Only Memory holding the probe calibration.

To summarise, a satisfactory probe geometry has been developed, the overriding advantages of single crystal materials have been uncovered and the identification of the use of the electronic control via the decrement has been established.

APPENDIX 1

TRANSMISSION LINES

A1.1 ELECTRO-ACOUSTIC-MECHANICAL ANALOGY

Transmission of plane sound wave through a pipe or a rod is analogous to the propagation of an electromagnetic wave through a concentric cable. The theoretical analysis of electrical systems are applicable to mechanical and acoustical systems and vice versa. There exists a complete analogy between the three systems as given in Table A1.1. Any acoustical or mechanical system may be transformed into the analogous electrical system, and the problem is then solved by the analysis of the electrical system.

Table. A1.1 Analogy between Electrical, Acoustical and Mechanical Quantities.

Electrical		Acoustical		Mechanical	
Quantity	Symbol	Quantity	Symbol	Quantity	Symbol
Self inductance	L	Inertness	$M=\frac{m}{A^2}$	Mass	m
Electrical charge	q	Volume displacement	X	Linear displacement	x
Current	$i=\frac{dq}{dt}$	Volume current	$\dot{X}=\frac{dX}{dt}$	Linear velocity	$\dot{x}=\frac{dx}{dt}$
Electromotive force	$e=L\frac{di}{dt}$	Pressure	$p=M\frac{d\dot{X}}{dt}$	Force	$f=m\frac{d\dot{x}}{dt}$
Electrical resistance	$r_E=\frac{e}{i}$	Acoustical balance	$r_A=\frac{P}{X}$	Mechanical resistance	$r_m=\frac{f}{x}$
Electrical capacitance	$C_E=\frac{q}{e}$	Acoustical capacitance	$C_A=\frac{X}{P}$	Compliance	$C_m=\frac{x}{f}$

A is the area over which the mass (m) is distributed.

A1.2 TRANSMISSION LINE EQUATION[96]

In the analysis of the electrical transmission line, the line is considered to consist of small sections of lines of lumped series impedance and shunt admittance. The series impedance of the section consists of resistance R and reactance $j\omega L$ per unit length. The shunt admittance consists of conductance G and susceptance $j\omega C$ per unit length. The quantities R and G represent the line losses.

In steady state conditions, propagation constant ν and characteristic impedance Z_o determine the performance of the line. In terms of primary parameters of the line and Z_o are given by

$$\nu = (R + j\omega L)\ (G + j\omega C) \tag{A1.1}$$

and

$$Z_o = \frac{R + j\omega L}{G + j\omega C} \tag{A1.2}$$

The propagation constant ν can be written as

$$\nu = \alpha + j\beta \tag{A1.3}$$

where α = attenuation constant

and β = phase constant.

When the line is lossless R = G = O and α = O, then the values of ν and Z_o are given by

$$\nu = j\ = j\omega\sqrt{LC} \tag{A1.4}$$

$$Z_o = \sqrt{\frac{L}{C}} \tag{A1.5}$$

The phase velocity or the propagation velocity from

(Al.4) is given by

$$v = \frac{\omega}{\beta} = \frac{1}{\sqrt{LC}} \qquad \text{(Al.6)}$$

and

$$\beta = \frac{2\pi}{\lambda} \qquad \text{(Al.7)}$$

Consider a line of length l, the input impedance for

(i) open circuited at the end is:

$$Z_{oc} = Z_o \cot j\ \beta\ l \qquad \text{(Al.8)}$$

This is equivalent to an acoustic line with a massive termination, i.e. end a node,

(ii) short circuited at the end is:

$$Z = Z_o \tan j\ \beta\ l \qquad \text{(Al.9)}$$

This is equivalent to an open acoustic line, i.e. end is an antinode.

In the steady state a half wave resonator has an antinode at the ends and a node at the centre. Thus a half wave resonator at the end of a line presents an antinode and hence an open circuit.

Similarly a quarter wave resonator presents a node and hence a short circuit.

N.B. A node represents a high impedance and an antinode a low impedance.

If a line of characteristics impedance Z_o is terminated in an impedance Z_L or connected to another line of impedance Z_L then the reflection coefficient, R, defined as "the fraction of the incident wave amplitude reflected at the

load end" is given by

$$R = \frac{Z_L - Z_o}{Z_L + Z_o} \qquad \text{(A1.10)}$$

and the transmission coefficient, T, defined as "the fraction of incident wave amplitude transmitted through the junction" is given by

$$T = \frac{2Z_L}{Z_L + Z_o} \qquad \text{(A1.11)}$$

These expressions for R and T are derived in any textbook on transmission lines.

A1.3 ACOUSTIC IMPEDANCE[59]

In dealing with the acoustic materials and lines the term acoustic impedance is used. Three acoustic impedances are defined.

(1) Specific acoustic impedance Z_s (pressure/particle velocity), a material property primarily useful in calculations involving the transmission of acoustic waves from one medium to another is given as $Z_s = \rho C$.

(2) Characteristic acoustic impedance Z, (pressure/volume velocity), a line property electrical analogue of impedance, is given as $Z = \rho C/A$. Primarily it is useful in the calculation of the transmission of acoustic radiation through pipes and horn.

(3) Radiation impedance Z_r (force/particle velocity), an alternative definition is given as $Z_r = \rho CA$, it is used in calculating the coupling between acoustic

waves and driving the source or driven load. This definition is used extensively in this work. The three impedances are related by the expression shown below

$$Z_r = AZ_s = A^2Z$$

The characteristic acoustic impedance of a line can be obtained by using primary acoustical parameters and the analogous equation (A1.5).

$$Z_A = \sqrt{\frac{M}{C_A}} = \sqrt{\frac{m/S^2}{X/\rho}} \qquad \text{(A1.12)}$$

$$Z_A = \frac{\rho C}{A} \qquad \text{(A1.13)}$$

$$Z_r = A^2 Z_A = \rho CA \qquad \text{(A1.14)}$$

It can be shown that for acoustic matching between the two media the radiation impedances given by equation (A1.14) should be equal. For example a line of specific acoustic impedance $Z_1 = \rho_1 C_1$ of area A_1 can be matched to another line of specific impedance $Z_2 = \rho_2 C_2$ of area A_2 if

$$\rho_1 C_1 A_1 = \rho_2 C_2 A_2 \qquad \text{(A1.15)}$$

or

$$Z_{r_1} = Z_{r_2}$$

Also, radiation impedance is used to calculate the coupling between the two media and the reflection and

transmission coefficients.

The propagation velocity and the resonant frequency of a half wave resonator can be obtained by equations (A1.6), (A1.7) and the electromechanical analogy.

The particle velocity is given by

$$C = \frac{1}{\sqrt{mCm}} = \frac{1}{\sqrt{mx/f}} = \sqrt{\frac{E}{\rho}} \qquad \text{(A1.17)}$$

and the resonant frequency by

$$\omega = 2\pi f = C\beta \quad C. \frac{2\pi}{\lambda}$$

$$= \sqrt{\frac{E}{\rho}} \frac{2\pi}{2l}$$

$$\text{or} \quad f = \frac{1}{2l} \cdot \sqrt{\frac{E}{\rho}} \qquad \text{(A1.18)}$$

Thus it can be inferred that the acoustic line problems can be solved by analysing the equivalent electrical line and using the electroacoustical analogies.

APPENDIX 2

ACOUSTIC MATCHING TECHNIQUES

Matching techniques are described for making joints between lines of various cross-sections and materials used in the system. The objective has been to obtain good acoustic matching with good mechanical strength. The problems of adhesion are also discussed.

A2.1 JUNCTION THEORY

At the junction of two lines of impedances Z_1 and Z_2 (Fig. A2.1) the coefficients of reflection and transmission are given by equations (A1.10) and (A1.11) respectively.

$$R = \frac{Z_2 - Z_1}{Z_2 + Z_1} \qquad \text{(A2.1)}$$

$$T = \frac{2Z_2}{Z_2 + Z_1} \qquad \text{(A2.2)}$$

where $Z_1 = \rho_1 C_1 A_1$ and $Z_2 = \rho_2 C_2 A_2$, the parameters ρ, C and A are defined in Appendix 1.

In a pulse-echo system all the boundaries are traversed twice and T^2 appears in all equations where

$$T^2 = \frac{4Z_1 Z_2}{(Z_1 + Z_2)^2}.$$

For a perfect match, i.e. $Z_1 = Z_2$ or $\rho_1 C_1 A_1 = \rho_2 C_2 A_2$ as given by equation (A1.15), all the signal is transmitted. For $Z_2 < Z_1$ the reflected signal is in reverse phase. This

can be visualised by thinking of a pulse of compression reaching the end of a rod, it will be returned as a pulse of refraction. Similarly for $Z_2 > Z_1$ the end of the rod is fixed and the returned pulse is compressional. The phase of the signal transmitted is always continuous with the incident wave.

The major effect of a discontinuity in a line is from its echo rather than the drop in power transmitted. In Fig. A2.1 the discontinuity is taken as arising from a small impedance mismatch. The fraction of signal reflected is R and the fraction returned from the remote end is T^2 where R and T^2 in terms of impedance ratio $r = \frac{Z_1}{Z_2}$ is

$$R = \frac{1 - r}{1 + r} \quad \text{(A2.3)} \quad \text{and} \quad T^2 = \frac{4r}{(1 + r)^2} \quad \text{(A2.4)}$$

Numerically if r = 1.1, R is 5% of the incident signal while the end echo is reduced by less than ¼%. The spurious echo might, depending on the position of the discontinuity, combine with the desired signal and give false phase and amplitude signals and hence errors in resonant frequency and loss measurement.

A2.2 MATCHING

When lines are of the same material they must be of the same area and can be keyed together as convenient. For good acoustic contact they must be welded together, ideally by a braze of similar impedance to the material. For different

materials the impedance match is given by equation (A1.15)

$$\rho_1 C_1 A_1 = \rho_2 C_2 A_2$$

or

$$\frac{A_1}{A_2} = \frac{\rho_2 C_2}{\rho_1 C_1} \qquad \text{(A2.5)}$$

For rods, the diameter ratio is given as

$$\frac{d_1}{d_2} = \left(\frac{\rho_2 C_2}{\rho_1 C_1} \right)^{\frac{1}{2}} \qquad \text{(A2.6)}$$

A graphical display of acoustic properties of solids is given by, Bell, Noble and Seth[95]. Young's modulus is plotted against density on a Log-Log graph with lines of constant velocity and specific acoustic impedance (at room temperature). From the nomogram the materials can be selected to have approximately equal specific acoustic impedance.

A2.3 LINE MATCHING SECTIONS

To join different shapes of the lines, e.g. a) two rods of (i) equal diameters (ii) different diameters b) a rod to a strip, requires different matching sections as being described by Seth.

For the case (i) if material is the same in both rods, the simplest joint is a butt joint, shown in Fig. A2.2. Where good adhesion is obtainable, as with a silver braze, this is satisfactory for most applications. In Fig. A2.2, Z_2 represents the impedance of the adhesive. The impedance

ratio for a typical silver braze to steel is approximately 0.7. The resulting mismatch at the junction gives a reflected signal from the junction, the amplitude of which is directly proportional to the adhesive thickness and the frequency. For the case (i) if material is not the same in both rods, (different specific acoustic impedance) e.g. steel and alumina, therefore a butt joint with araldite is not sufficient. The keyed joint shown in Fig. A2.3 with silver solder has a much greater contact area.

To join two rods of different diameters and materials, matching is achieved by making the impedances of the joining ends equal. A typical example is steel to tungsten. A matching section is machined down by a few steps on one rod as shown in Fig. A2.4 and A2.5, and then a butt joint gives satisfactory contact. The strip to rod matching requires a particular strip width for a given rod diameter. To obtain a good match between a strip and a rod, the strip may being slotted into the rod as shown in Fig. A2.6.

A2.4 ACOUSTIC JOINTS

A number of adhesives have been found to be satisfactory.

A2.4.1 Thermal setting Araldite and Glazes

It is very convenient for making quick joints and when properly cured it can withstand temperatures up to 180°C. Mechanically, it tends to be weak. Its acoustic impedance is very low and the finite width of the adhesive section consequently becomes significant. It can be used with both

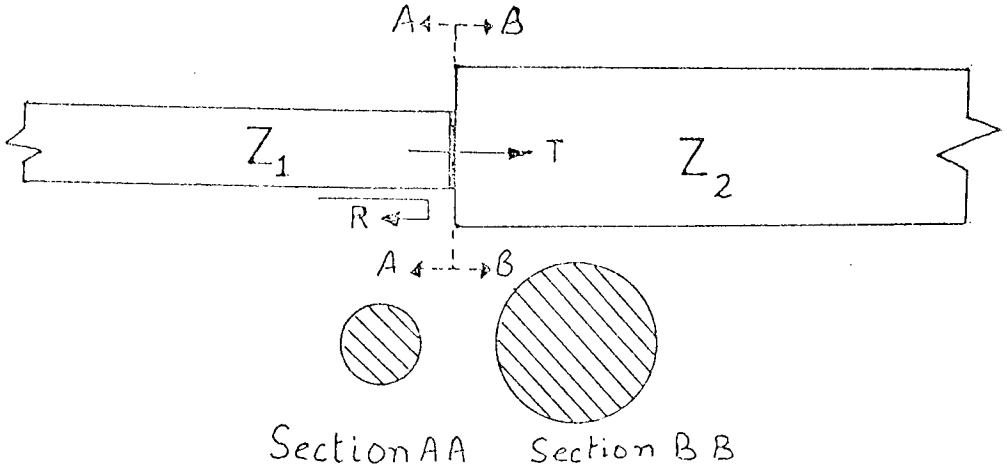

Fig. A2.1 Joint between two rods of impedance Z_1 and Z_2 respectively, showing a junction mismatch.
R, the reflected fraction and T, the transmitted.

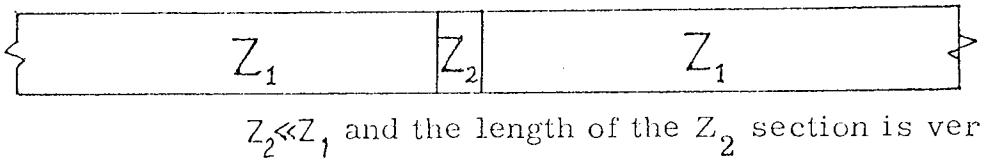

Fig. A2.2 A butt joint between two rods of equal impedance, Z_2 represents the impedance of adhesive section.

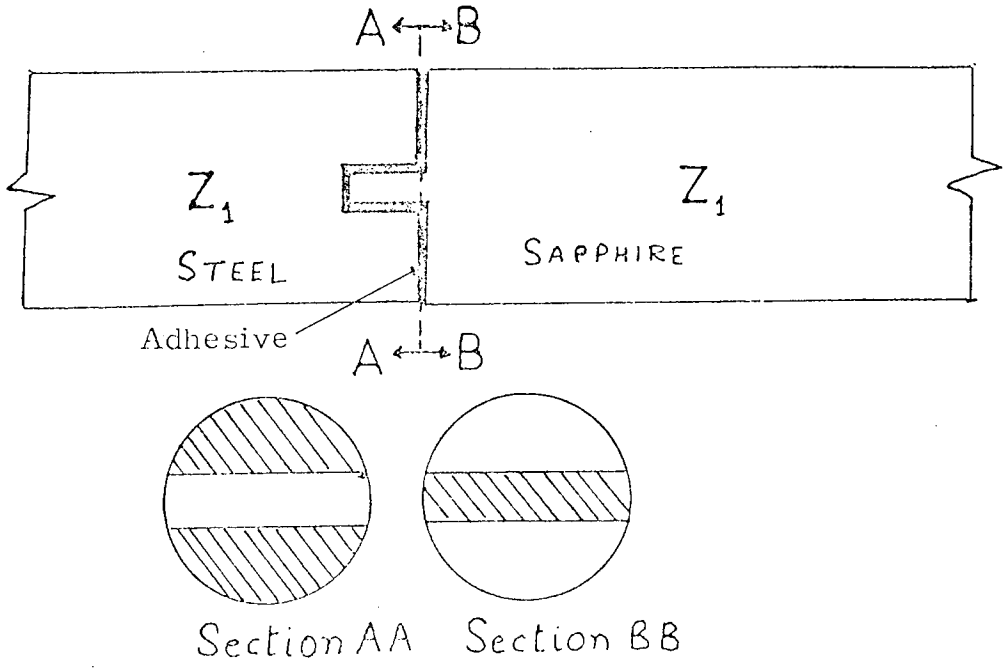

Fig. A2.3 A keyed joint between steel and sapphire rods.

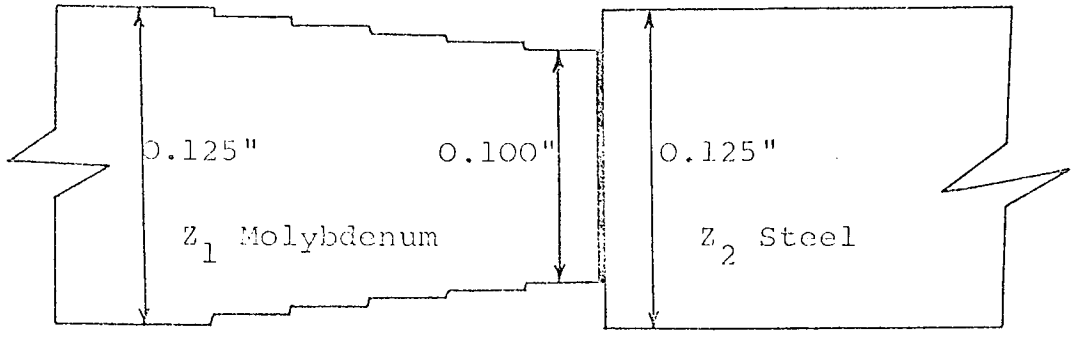

Fig. A2.4 A matching section on a molybdenum rod to match the impedance of an equal diameter steel rod.

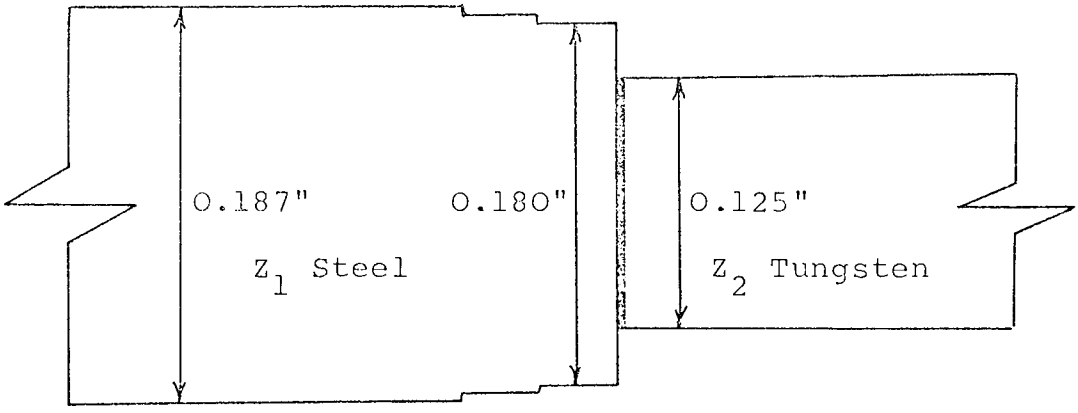

Fig.A2.5 A matching section on a steel rod to match the impedance of a smaller diameter tungsten rod.

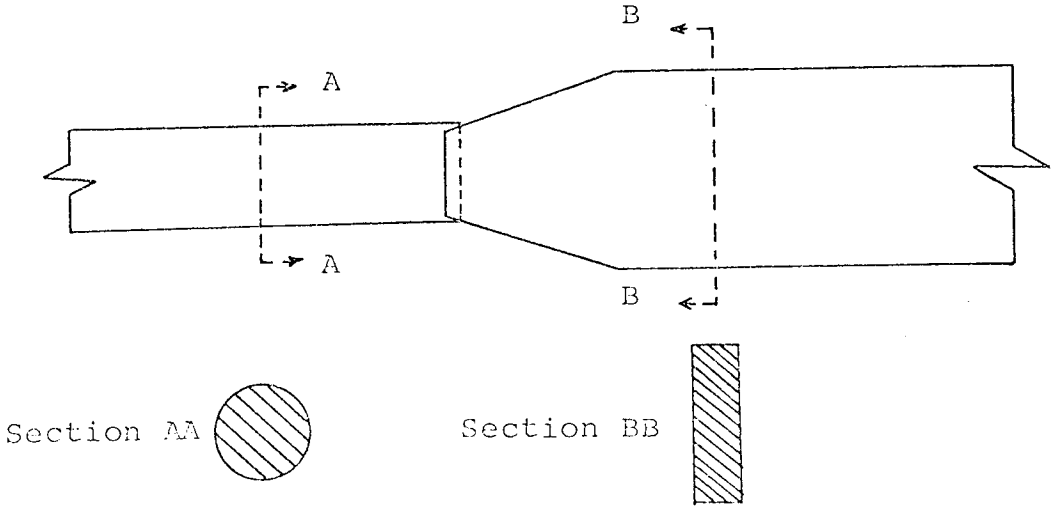

Fig.A2.6 A joint between a rod and strip of matched impedances.

metals and ceramics. A superior thermosetting glazing flux made by Pyrotenax Ltd. can be easily used to join alumina to steel and can withstand temperatures up to 300°C.

A2.4.2 Silver Solder Braze[97,98,99]

This, along with the usual silver brazing flux consisting of boric acid, alkaline borides and fluorides, commercial name, easy flow flux, is the most commonly used adhesive and can withstand temperatures up to 700°C. Mechanically, the joint is very strong.

Silver brazing alloys may be used to join practically all metals except aluminium and magnesium base alloys and those alloys, melting below the temperature range at which the silver alloy flows. There are, however, a number of metals and alloys which for various reasons are difficult to braze with standard procedures.

A primary requisite for obtaining a strong band is that the brzing alloy must wet and at least superficially alloy with the base metals. The failure to wet may result from films, usually oxides, on the base metal or it may be the incompatibility of the brazing alloys with the metal being joined. In the first instance, the problem is to develop a flux capable of removing the film so that the brazing alloy is in direct contact with a clean base metal surface. The second case may involve the addition to the brazing alloy of constituents which will promote alloying with the base metals.

For brazing aluminium an addition of 0.15% zinc chloride to the standard flux permits the making of a strong joint. Molybdenum is also difficult to braze by the usual brazing alloys. Jacobson and Martin[99] investigated sixteen high temperature brazing alloys. Cobalt and nickel alloys give good results. An addition of 0.25% of phosphorus[97] to the brazing alloys permits molybdenum to be brazed. In the laboratory molybdenum was brazed by first alloying it with nickel after which the silver solder braze and standard flux could be used. By this technique, good joints between molybdenum and steel rods were obtained. For tungsten, nickel and manganese base brazing alloys[98] give good strength. Tantalum can be brazed with silver brazing alloys using a special flux.

A2.4.3 Brazing of Ceramics[100]

The ceramic is extensively used as a probe material, the joint between steel and ceramics presents a problem. The type of joint used is shown in Fig. A2.3. This type of joint keeps the ceramic under compression. The ceramic is machined on a diamond wheel and the sockets in the steel adjusted to fit. An attempt was made to increase the acoustic impedance of the adhesive. To do this it was decided to put a metal coating on the surface which could then be soldered to the steel line. After considering evaporation, it was decided to try Johnson Matthey silver paint preparation, which was extremely successful, giving an echo

of 5% at 150 kHz. The process takes some time to care, to be successful and works with most ceramics materials. The ceramic is carefully cleaned after machining and degreasing. It is then painted with FSP/411 (see the Johnson Matthey Data Sheet for full details) and allowed to dry. It is then painted with FSP/412 allowed to dry, slowly heated and fired at 700^{o}C in air. Careful use of a flame was found to be satisfactory for 3mm rod but the most reliable way is to use a furnace. Next the steel and the ceramic were tinned with silver-tin-lead ceramic solder using a resin flux. Finally, the parts were put on guides, heated and pushed together.

A2.4.4 FLASH WELDING

For rods of up to 2 mm diameter, flash butt welding techniques have been used. Typical joints between platinum to permendur, and tungsten to permendur have been successfully made.

LIST OF SYMBOLS

A	Area; amplifier
B	Bistable flip-flop, magnetic flux density
C	Clock pulse, comparator, coupling section, counter
C_A	Acoustic capacitance
C_m	Compliance
D	Diameter of rod; width of strip; D-type flip-flop; diodes, decrement pulse duration
E	Modulus of elasticity; energy; echo amplitude; efficiency; enable pulse
E^X	Modulus of elasticity for constant flux
G	Rigidity modulus, gate
H	Magnetic field intensity
K	Constant, Boltzmann constant
L	Length of resonator; length of tuning fork; latch pulse
LL	Lead-in line
M	Inertness; mangetostrictive constant; monostable multivibrator
N_t	Neck thickness
P	Pressure amplitude
Pm	Number of oscillations of cross-over
Q	Q-factor
Q_C	Coupling Q-factor
Q_M	Material Q-factor
Q_T	Total Q-factor
R	Reflaction coefficient; thermal-stress resistance factor; resonator

S	Strain; fracture strength; signal pulse duration
T	Transmission coefficient; temperature
U	Potential function
V	Noise voltage
W_s	Width of longitudinal slot of probe
W_n	Width of the neck
Z	Characteristic acoustic impedance = $\rho c/A$
Z_s	Specific acoustic impedance = ρc
Z_r	Radiation impedance = ρcA; resonator impedance
Z_L	Line impedance
a	Radius of disc
an	Antinode
b	Base length
c	Velocity of sound
c_l	Longitudinal velocity of sound
c_m	Shear velocity
c_p	Plate velocity
d	Neck depth; diameter of rod
f	Frequency
f_s	Signal frequency
f_r	Resonator frequency
f_i	Incident signal frequency
g	Voltage gain of the transducer
h	Half thickness of a plate or a bar; heat transfer coefficient
k	Thermal conductivity; gyration constant wave number $= \omega/c$

l	Tine length; length of coil
m	Mode of vibration
n	Node; number of turns in a coil; number of oscillations number of harmonic
r	Impedance ratio
t	Thickness of bar or tine; time
w	Width of transverse slot of probe
α	Attenuation constant
α_E	Temperature coefficient of elasticity
α_L	Temperature coefficient of linear expansion
β	Phase constant
ν	Propagation constant; intrinsitic loss in magnetostrictive transducer
ε	Emissivity
δ	Attenuation constant per wave length
θ	Temperature
λ	Wave length
μ_r	Reversible permeability
ξ	Displacement
$\dot{\xi}$	Velocity
ρ	Density
σ	Poisson's ratio
ϕ	Phase constant; flux linkage
ω	Angular frequency
Ω	$\frac{\pi f l}{c}$ frequency response factor in radians
τ	Time constant

REFERENCES

1. Kostkowski, H. J.:"The accuracy and precision of measuring temperatures above 1000^{o}k," Proceeding of an international symposium on high temperature technology, California Oct. 6-9, 1959.
2. Weller, A. E. and Bagby, F. L.:"Demands for high temperature technology," in "high temperature materials and technology," Ed. Campbell, I.E. and Sherwood, E.M., (Wiley New York, 1967).
3. Marmer, E.N.:"Measurement of high temperature" in "high temperature materials," 1971.
4. Bedford, R. E.:"High temperature thermometry (A review)," The third European Conference on thermophysical properties, Turin, 20-23 June, 1972.
5. Bell, J. F. W.:"Ultrasonic thermometry using resonance techniques," 5th Symposium on temperature, Washington D.C., 1971.
6. Shepard, R. L. et.al.:"Ultrasonic and Johnson noise fuel centerline thermometry," International colloquium on high temperature in-pile thermometry, JRC Petten, Netherlands, 12-13 Dec. 1974.
7. Brixy, H. G.:"Temperature measurement in nuclear reactors by noise thermometry," Nucl. Instr. Methods, Vol.97, 1971, (75-80).
8. Caldwell, F. R.:"Thermocouple materials," N.B.S., monograph 40, March, 1962.

9. Slaughter, J. I. and Margrave, J. L.:"Temperature measurement," in "High temperature materials and technology," Ed. Campbell, I.E. and Sherwood, E.M., (Wiley New York 1967).

10. Bauchede, J. (CEN, Saclay), and Haange, R.(A.E.E. Winfrith): "Behaviour of Pt/Pt-13% Rh thermocouples in a high temperature fuel irradiation experiment," International Colloquium on high temperature in-pile thermometry, JRC Petten, Netherlands, 12-13 Dec. 1974.

11. Rohne, B.:"High temperature thermocouple application in the R_2-reactor, Studsvik ," International Colloquium on high temperature in-pile thermometry, JRC Petten, Netherlands, 12-13 Dec.1974.

12. Evans, J. P. et.al.:"The production of reactor grade high temperature thermocouples at A.E.R.E. Harwell," International Colloquium on high temperature in-pile thermometry, JRC Petten, Netherlands, 12-13 Dec. 1974.

13. Evans, J. P. and Mardon, P. G.:"Preparation and calibration of W-5%Re V. W-26%Re thermocouples for irradiation in H.F.R. Petten," International Colloquium on high temperature in-pile thermometry, JRC Petten, Netherlands, 12-13 Dec. 1974.

14. Johnson, F. A. et.al.:"Tungsten Rhenium thermocouple drift under irradiation," International Colloquium on high temperature in-pile thermometry, JRC Petten, Netherlands, 12-13 Dec. 1974.

15. Shepard, R. L. and Kollie, T. G. :"Correction of irradiation

produced drift in W-Re fuel centerline thermocouples," International Colloquium on high temperature in-pile thermometry, JRC Petten, Netherlands, 12-13 Dec. 1974.

16. Borkowski, C. J. and Blalock, T. V.:"A new method of Johnson noise thermometry," Rev. Sci. Instru. 45[2], Feb. 1974, (151-62).

17. Seth, T. N.:"Ultrasonic pyrometer for industrial applications," Ph.D. Thesis, University of Aston, 1974.

18. Arave, A. E.:"Use of tungsten-2% thoria ultrasonic transmission line and sensor to improve the performance of high temperature ultrasonic thermometry," International Colloquium on high temperature in-pile thermometry, JRC Petten, Netherlands, 12-13 Dec. 1974.

19. Bell, J. F. W.:"A solid acoustic thermometer," Ultrasonics, Jan. 1968, (11-14).

20. Lynnworth, L. C. et.al.:"Nuclear reactor applications of new ultrasonic transducers," IEEE Trans. on Nuclear Science, Vol. NS.18[1], Feb. 1971, (351-62).

21. U.S.A.E.C.Report on:"Ultrasonic thermometry for LMFBR system," no. NYO-3906-13, by Panametrics Inc., Mass. U.S.A. June, 1972.

22. Mobsby, E. G.:"Practical ultrasonic thermometer," Ultrasonics, Jan. 1969, (39-42).

23. Tasman, H. A. and Schmidt, H. E.:"The ultrasonic thermometer - construction, application and operating experience," Third European Conference on thermophysical properties at high temperature, Turin, 20-23 June, 1972.

24. Tasman, H. A. and Schmidt, H. E.:"In-pile ultrasonic thermometry experiment treson," International Colloquium on high temperature in-pile thermometry, JRC Petten, Netherlands, 12-13 Dec. 1974.

25. Spinner, S.:"Elastic moduli of glasses at elevated temperatures by a dynamic method," J. Am. Ceram. Soc., 39[3], 1956, (113-118).

26. Ault, N. N. and Ueltz, H. F. G.:"Sonic analysis for solid bodies," J. Am. Ceram. Soc., 36[6], 1953,(199-203).

27. Pickett, G.:"Equations for computing elastic constants from flexural and torsional resonant frequency of vibration of prisms and cylinders," Am.Soc. Testing Materials, Proc., 45, 1945, (846-65).

28. McSkimin, H. J.:"Notes and references for the measurements of elastic moduli by means of ultrasonic waves," J. Acoust. Soc. Am. 33[5], 1961, (606-14).

29. Frederick, J. R.:"Ultrasonic measurement of the elastic properties of polycrystalline materials at high and low temperatures," J. Acoust. Soc. Am. 20, 1948, (586).

30. Bell, J. F. W.:"The velocity of sound in materials at high temperatures," Phil. Mag. 2[8], 1957, (113-20).

31. Bell, J. F. W.:"Dynamic and static elasticities of solids," Nature, 181, 1958, (1330).

32. Thorn , E. A.:"The measurement of high temperatures by the determination of the velocity of sound waves in materials," Fourth ICA, Copenhagen, Aug.1962.

33. Bell, J. F. W. and Doyle, B. P.:"Sound pulses in thin non-uniform rods," Ultrasonics, Jan. 1964, (39-42).

34. Bell, J. F. W. et. al.:"An instrument for the measurement of acoustic pulse velocity and attenuation in a solid probe," J.Sci. Instru., 43, 1966, (28-31).

35. Lynnworth, L. C. et. al.:"Ultrasonic thermometry for nuclear reactors," IEEE Trans. on Nuclear Science, vol. NS. 16[1], Feb. 1969, (184-87).

36. Eros, S. and Reitz, J. R.:"Elastic constants by ultrasonic pulse echo method," J. Appl. Phys. 29[4], 1958,(683-86).

37. Bernstein, B. T.:"Elastic properties of polycrystalline tungsten at elevated temperatures," J. Appl, Phys. 33[6], 1962, (2140).

38. Lowrie, R. and Gonas, A. M.:"Dynamic elastic properties of polycrystalline tungsten, 24-1800^{o}C," J. Appl. Phys. 36[7], July, 1965, (2189-92).

39. McSkimin, H. J.:"Pulse superposition method for measuring ultrasonic wave velocities in solids," J. Acoust. Soc. Am. 33[1], Jan 1961, (12-16).

40. Holbrook, R. D.:"A pulse method for measuring small changes in ultrasonic velocity in solids with temperature," J. Acoust. Soc. Am. 20, 1948, (590).

41. Myers, A. et. al.:"Modifications to standard pulse techniques for ultrasonic velocity measurements," J. Acoust. Soc. Am. 31[2], 1959, (161-62).

42. McSkimin, H. J.:"Measurement of ultrasonic wave velocities and elastic moduli for small solid specimens at high temperatures," J. Acoust. Soc. Am. 31[3], 1959, (287-95).

43. Williams, J. and Lamb, J.:"On the measurement of ultrasonic velocity in solids,"J. Acoust. Soc. Am. 30[4], 1958, (308-13).

44. Forster, F. and Koster, W.:"Modulus of elasticity and damping in relation to the state of the materials," The Engineer, 166[4325], 1938, (626-28).

45. Roberts, M. H. and Nortcliffe, J.:"Measurement of Young's modulus at high temperature," J. Iron Steel Inst. (London), 157[3], Nov. 1947, (345-48).

46. Wachtman, Jr.,J. B. and Lam, Jr., D. G.:"Young's modulus of various refractory materials as a function of temperature," J. Am. Ceram. Soc. Vol. 42[5], 1959, (254-60).

47. Brown, H. L. and Armstrong, P. E.:"Young's modulus measurements above 2000^{o}C," Rev. Sci. Instru., Vol. 34[6], 1963, (636-39).

48. Spinner, S.: "Elastic moduli of glasses by a dynamic method," J. Am. Ceram. Soc., 37[5], 1954, (229-34).

49. Bell, J. F. W., Fathimani, A. A.and Seth, T. N.: "Ultrasonic thermometry using resonance techniques," International Colloquium on high temperature in-pile thermometry, JRC Petten, Netherlands, 12-13 Dec. 1974.

50. Sharp, J. C. K.:"A theoretical and experimental investigation into the spectra of selected resonators," Ph.D. Thesis, University of Aston, 1974.

51. Pelmore, J. M.:"Internal friction and high temperature measurement on refractory materials," Ph.D. Thesis, University of Aston, 1975.

52. Sadollah, M. A.:"Study of internal friction of polymers using ultrasonic resonance method," M.Sc. Thesis, University of Aston, 1974.

53. Mahil, K. S.:"The development of a fluid consistency transducer," Ph.D. Thesis, University of Aston, 1975.

54. Morse, P. M.:"Vibration and sound," (McGraw Hill, New York, 1948).

55. Wood, A. B.:"A textbook of sound," (G. Bell & Sons, London, 1960).

56. Rayleigh, Lord.:"Theory of Sound," Vol. 1.(McMillan & Co., London, 1929).

57. Lamb, H.:"Dynamic theory of sound," (Arnold, London,1925).

58. Stephens, R. W. B. and Bate, A. E. :"Acoustics and vibrational physics," (Arnold, London, 1966).

59. Kinsler, L. E. and Frey, A. R.:"Fundamentals of acoustics," (Wiley, New York, 1962).

60. Texas Instruments Semiconductor Components Data Book-2. Digital Integrated Circuits, July, 1971.

61. The TTL Data Handbook for Design Engineers (Texas Instruments, 1973).

62. Semiconductor Circuit Design Vol. 2.(Texas Instruments, 1973).

63. Smithells, C. J.:"Metal reference book," Vol. 1 and 2, (Butterworths, London 1962).

64. Tietz, T. E. and Wilson, J. W.:"Behaviour and properties of refractory metals," (Arnold, London 1967).

65. Jaffee, R. I., Maykuth, D. J. and Sherwood, E.M.: "Refractory metals and metalloids," in "High temperature technology and materials," Ed. Campbell, I.E. and Sherwood, E. M., (Wiley, New York 1967).

66. Wyatt, O. H. and Hughes, D. D.:"Metals, Ceramics and Polymers," in "An introduction to the structure and properties of engineering materials," 1974.

67. Campbell, I. E. and Sherwood, E. M.:"Oxide Ceramics," in "High temperature technology and materials,".

68. Ryskewitch, E.:"Oxide Ceramics," (Academic Press, 1960).

69. Losty, H. H. W. and Orchard, J. S.:"The strength of Graphite," Proc. Fifith Carbon Conference.

70. Redmond, J. C.:"Cermets" in "High temperature technology and materials,".

71. Dreshpak, V. A.:"Characteristics of elasticity of tungsten, molybdenum and their alloys at 20 to 2700°C," AD-704010, FTD-HT-23-305-69, March, 1970.

72. Peterson, R. G.:"Elastic moduli and ultrasound velocities of tungsten as a function of temperature," U.S.A.E.C. report ANL-7272, Dec. 1967.

73. Armstrong, P.E. and Brown, H. L.:"Dynamic Young's modulus measurement above 1000°C on some pure polycrystalline metals and commercial alloys," A.I.M.E. Trans. Vol. 230, Aug. 1964.

74. Fine, M. E.:"Apparatus for precise determination of dynamic Young's modulus and internal friction at elevated temperatures," Rev. Sci. Instru., Vol. 28[8], 1957, (643-45).

75. Pisarenko, G. S. et. al.:"The effect of temperature on the hardness and modulus of elasticity of tungsten and molybdenum (20-2700^{o}C)," SOV. Powder Met., 371, 1962.

76. Berlec, I.:"The effect of impurities and heat treatment on the internal friction of tungsten at high temperature," Metallurgical Trans. Vol. 1, Oct. 1970, (2677-83).

77. Sims, C.T. and Jaffee, R. I.:"Further studies of the properties of rhenium metal," A.I.M.E. Trans. Vol. 206, Aug. 1956, (913-17).

78. Begley, R. T.:"Development of Columbium base alloys," Westinghouse Research Lab. report in "Behaviour and properties of Refractory metals," by Tietz, T. E. and Wilson, J. W. (arnold, London, 1967).

79. Freeman, R. R. and Briggs, J. Z.:"Molybdenum at high temperature,"Jet Propulsion, Vol. 27, Feb. 1957.

80. Abakov, V. T. and Morgunova, N. N.:"Mechanical properties of MO-W alloys," Sov. Metals, No. 5., May, 1973.

81. Hill, W. H. and Wilcox, B. A.:"Elevated temperature dynamic moduli of vanadium, titanium and V-Ti alloys," Metals and Ceramics Laboratory report in "Behaviour and Properties of Refractory Metals,".

82. Maykuth, D. J., Jaffee, R. I. and Blocher, Jr., J. M.: "The effect of metals purity on chromium base alloys," in "Behaviour and properties of refractory metals,".

83. Ketova, V. P. et.al.:"Effect of alloys on the modulus of elasticity of platinum alloys," Sov. Metals No. 7, July, 1970.

84. Soga, N. and Anderson, O. L.:"High temperature elastic properties of polycrystalline MgO and Al_2O_3," J. Am. Ceram. Soc., Vol. 49, July, 1966, (335-59).

85. Spriggs, R. M., Mitchell, J. B. and Vasilos, T.: "Mechanical properties of pure, dense aluminium oxide as a function of temperature and grain size," J. Am. Ceram. Soc. Vol. 47, July, 1964, (323-27).

86. Buessem, W. R.:"Thermal Shock" in "High temperature Technology," Ed. Campbell, I.E. (Wiley, New York,1956).

87. Gooberman, G. L.:"Ultrasonics, Theory and Application," (English Universities Press, London, 1968).

88. Williams, R. C.:"Theory of magnetostrictive delay lines for pulse and continuous wave transmission," IEEE Trans. on Ultrasonic Engineering, Vol. UE-7, Feb. 1959.

89. Kikuchi, Y.:"Magnetostrictive materials and applications," IEEE Trans. on Magnetics, Vol. Mag-4, No. 2, June, 1968.

90. Bozorth, R. M.:"Ferromagnetism," (D. Van Nostrand Co. Inc. New York, 1951).

91. Bell, J. F. W.:"Elastic properties of graphite," Dragon Report No. 5, Oct. 1960.

92. Bell, J. F. W.:"The elastic constants of solids over a wide temperature range," Proc. 3rd ICA, Netherlands.

93. Bell, J. F. W.:"U.K. Patent No. 54637/66,"

94. Bell, J. F. W., Johnson, A. C. and Sharp, J. C. K.: "Pulse-echo method of investigating the properties of mechanical resonators," J. Acoust. Soc.Am., Vol.57 ,No.5, May, 1975, (1085-93).

95. Bell, J. F. W., Noble, A. E. and Seth, T. N.: "Graphical displays of acoustic properties of solids," Ultrasonics, No. 11, July, 1973, (178-181).

96. Royal Signals:"Handbook of line communication," War Office, 1949.

97. Chatfield, C. H.:"Silver brazing of refractory metals," The Welding Journal, Sept. 1954.

98. Albom, M. J.:"Welding and brazing of tungsten and molybdenum," Metal Progress, Vol. 83, March, 1963.

99. Jacobson, M. I. and Martin, D. C.:"Brazing molybdenum for high temperature service," Supplement to the Welding Jr., Feb. 1955.

100. Fox, C. W. and Slaughter, G. M.:"Brazing of Ceramics," Welding Jr., July, 1964.

101. Widdis, F. C. and Golding, E. W.:"Electrical measurements and measuring instrument," 5th Ed. London, Pitman, 1963.

102. Bhatia, A. B.:"Ultrasonic absorption," An introduction to the theory of sound absorption and dispersion in gases, liquids and solids, Oxford University Press, Ely House, London, 1967.

103. Johnson, A.C.J.:"An apparatus for ultrasonic measurement," M.Sc. Thesis, University of Aston, 1971.